The endothelial glycocalyx: recovery, stability and role in electric field-directed cell migration *in vitro*

By Weiqi Li

Supervisors: Professor Wen Wang

Dr Yiling Lu

Submitted for the Degree of Doctor of Philosophy

Institute of Bioengineering

Queen Mary University of London

2014

I, Weiqi Li, confirm that the research included within this thesis is my own work.

I accept that the College has the right to use plagiarism detection software to check the electronic version of the thesis.

I confirm that this thesis has not been previously submitted for the award of a degree by this or any other university.

Weiqi Li

25-11-2014

Conference:

W.Li, Y.Lu and W.Wang. Contribution of endothelial glycocalyx to electric field directed cell migration. Bioelectrochemistry (Gordon Research Seminar). Biddeford, USA. July 5-6, 2014. (Oral presentation)

W.Li, Y.Lu and W.Wang. Contribution of endothelial glycocalyx to electric field directed cell migration. Bioelectrochemistry (Gordon Research Conference). Biddeford, USA. July 6-11, 2014. (Poster presentation)

Acknowledgement

Foremost, I would like to thank my supervisor, Professor Wen Wang, for his encouragement, guidance and support to me throughout my PhD projector. Without his patience, I can't finish my work in time.

I am grateful to my co-supervisor, Dr Yiling Lu, now at University of Derby. I appreciate his detailed and constructive comments on my work.

I would like to thank Dr Julien Gautrot in School of Engineering and Materials Science for his help on micropatterning studies and Dr Ann Wheeler in Blizard Institute of Cell and Molecular Science for the training on time-lapse microscopy.

I thank engineering technicians Mr Vince Ford and Ms Jun Ma for their help on designing and manufacturing the EF and flow chambers.

I thank Professors Qian Wang and Lei Zheng at Southern Medical University, China for their help and support that ensured my PhD studentship award from QMUL and the China Scholarship Council (CSC).

I would also like to thank colleagues in the Biofluids and Cell Mechanics Laboratory, Dr Yankai Liu, Dr Ke Bai, Dr Lin Qiu, Dr Devendra Deo, Ms Miao Lin and Mr Xia Chen. Thank you very much for the warmth and happiness you have given me.

My deepest gratitude goes to my parents and my wife Shuchen Zhang. I couldn't have done my PhD without your understanding and support.

Finally, I would like to thank all who have supported me during my PhD study.

Abstract

Cardiovascular disease is the leading cause of unnatural death worldwide. Damage to the endothelial glycocalyx impairs endothelial functions and thereafter leads to the development of cardiovascular diseases. Despite this, many issues remain to be explored in our understanding of the metabolism and vasculoprotective potential of the glycocalyx. This study focuses on the recovery and structural stability of the glycocalyx, and its role in electric field-directed cell migration *in vitro*.

The integrity of the glycocalyx is compromised following trypsin treatment during cell passages. Results from our study show that cell seeding density affects the recovery speed of the glycocalyx in the first 48h. Higher cell density results in more rapid recovery of the glycocalyx. Regardless of the initial cell seeding density, a well-developed glycocalyx layer is observed when cell confluence is reached.

Micropatterning is used to study effects of the cell shape on the recovery of the glycocalyx. Elliptical patterns have been used to conform endothelial cells to torpedo shapes, mimicking their morphology under a shear flow. More rapid development of the glycocalyx on elliptical cells is observed than that on circular shaped cells during the early stage of recovery.

Effects of the actin cytoskeleton on the stability of the glycocalyx are investigated, following our interest in shedding of the glycocalyx in abnormal vascular microenvironment. Rapid depolymerisation of the actin cytoskeleton leads to cell retraction within 10mins, with the glycocalyx preserved on the cell surface. This is also seen during 24h persistent actin disruption under static conditions. However, when endothelial cells are subjected to 24h steady laminar shear stress, the glycocalyx is seen to

shift to the downstream of the cell surface in the control group, and with actin depolymerisation, significant shedding of the glycocalyx from the luminal surface of the cell is observed. This happens together with the loss of focal adhesions on the basal membrane.

Using a custom designed electric field (EF) chamber, I demonstrate that the cell migration speed increases by 30~40% following 5h of EF exposure. Cells also show preferred movement towards the anode. However, both are abolished after the enzymatic removal of the glycocalyx, indicating that the speedup and the directional cell migration in applied EF require the presence of the glycocalyx. Even distribution of the glycocalyx on the cell surface at the end of the EF stimulation suggests that EF-directed cell migration is not related to the polarization of the glycocalyx on the cell membrane.

All these findings provide a better understanding of the glycocalyx, which will help to develop new strategies for protection of the glycocalyx, restoration of endothelial functions and finally prevention of cardiovascular diseases.

Table of contents

List of abbreviations

Acrylonitrile butadiene styrene	ABS
Bovine aortic endothelial cells	BAECs
Bovine serum albumin	BSA
Cell tracker red	CTR
Chondroitin sulphate	CS
Concanavalin A	Con A
Cyclic guanosine monophosphate	cGMP
Cytochalasin D	CD
Dense peripheral actin band	DPAB
Electric field	EF
Endothelial cell growth factor	ECGF
Endothelial NO synthase	eNOS
Epidermal growth factor receptor	EGFR
Epithelial sodium channel	ENaC
Focal adhesions	FAs
Glycosaminoglycans	GAGs
Guanylyl cyclase	GCase
Heparan sulphate	HS
Human umbilical vein endothelial cells	HUVECs
Hyaluronic acid	HA
Inositol trisphosphate	IP3
Micro-particle image velocimetry	micro-PIV

Na, K-ATPase	NaKA
Na+/H+ exchanger isoforms	NHE3
N-acetyl-D-glucosamine	GlcNAc
Neuraminidase	Neu
Nitric oxide	NO
Parafomaldehyde	PFA
Phosphoinositide 3-kinase	PI3K
Phospholipase C	PLC
poly[2-(methacryloyloxy)ethyl dimethyl-(3-sulfopropyl)ammonium hydroxide]	PMEDSAH
Polydimethylsiloxane	PDMS
Polymethylmethacrylate	PMMA
Polytetrafluoroethylene	PTFE
Reactive oxygen species	ROS
Region of interest	ROI
Shear stress	SS
Sialic acid	SA
Stress fibres	SFs
Stretch-activated cationic channel	SACC
Transendothelial potential	TEP
Vascular endothelial growth factor	VEGF
Voltage-gated calcium channel	VGCC
Voltage-gated sodium channel	VGSC
Wheat germ agglutinin	WGA

List of tables

List of figures

1. Introduction

The vascular endothelium is the thin layer of cells that lines the luminal surface of blood vessels, forming an interface between circulating blood and the rest of vessel wall (Fig 1-1.A). It is critically involved in many vascular events such as the exchange of materials between blood and tissues, inflammatory response, coagulation, vasodilatation and angiogenesis. The luminal side of the endothelium is covered by a brush-like structure called the glycocalyx (Fig 1-1.B) (Gouverneur et al., 2006a). The presence of the endothelial glycocalyx has been shown to determine physiological functions of the endothelium. Damage to the glycocalyx layer leads to endothelial dysfunction and thereby contributes to the development of cardiovascular diseases such as atherosclerosis (Reitsma et al., 2007). Therefore, a sound understanding of the metabolism and functions of the glycocalyx is of great importance, as it will lead to better approaches to protect the glycocalyx, restore endothelial functions and finally prevent cardiovascular diseases. In this review, the composition and dimensions of the glycocalyx are described, followed by the highlight of the functional importance of the glycocalyx and those factors involved in the perturbation of the glycocalyx. In addition, this study also aims to couple the glycocalyx with electric field-directed cell migration. This directional cell migration and the potential mechanisms are thus described.

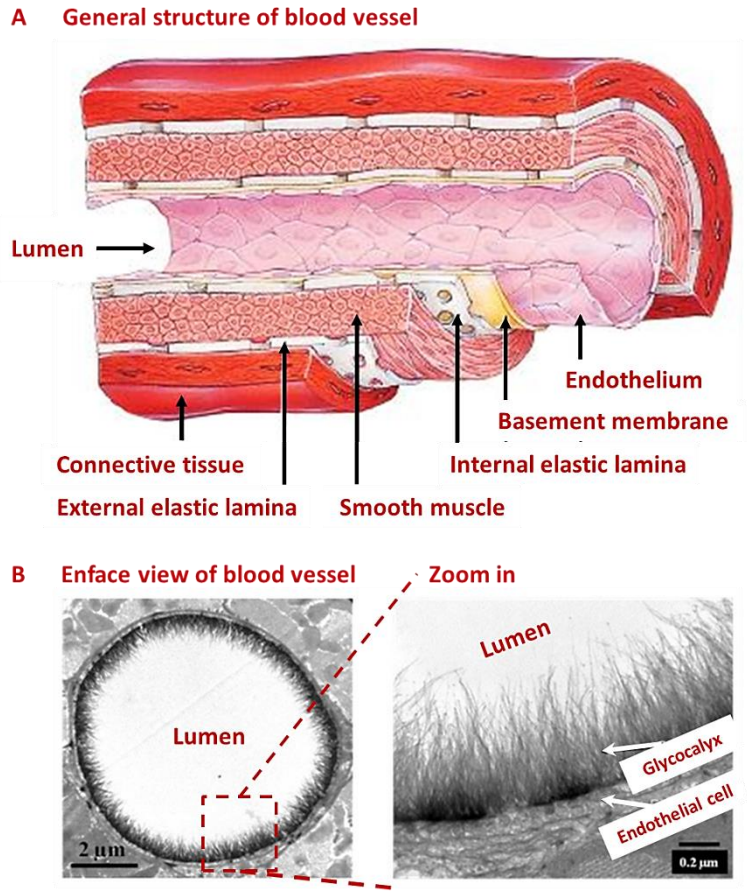

Figure 1.1 General structure of blood vessel and the glycocalyx.

(Adapted from Gouverneur et al., 2006a)

1.1. Composition of the endothelial glycocalyx

The endothelial glycocalyx is a delicate network of membrane-bound macromolecules that comprises glycoproteins and proteoglycans (Fig 1-2) (Weinbaum et al., 2007). The glycoproteins are characterized by short, carbohydrate side-chains (2~15 sugar residues) with branching while the proteoglycans are decorated with long, unbranched side-chains (~200 sugar residues) (Carney, 1986, Montreuil et al., 1986).

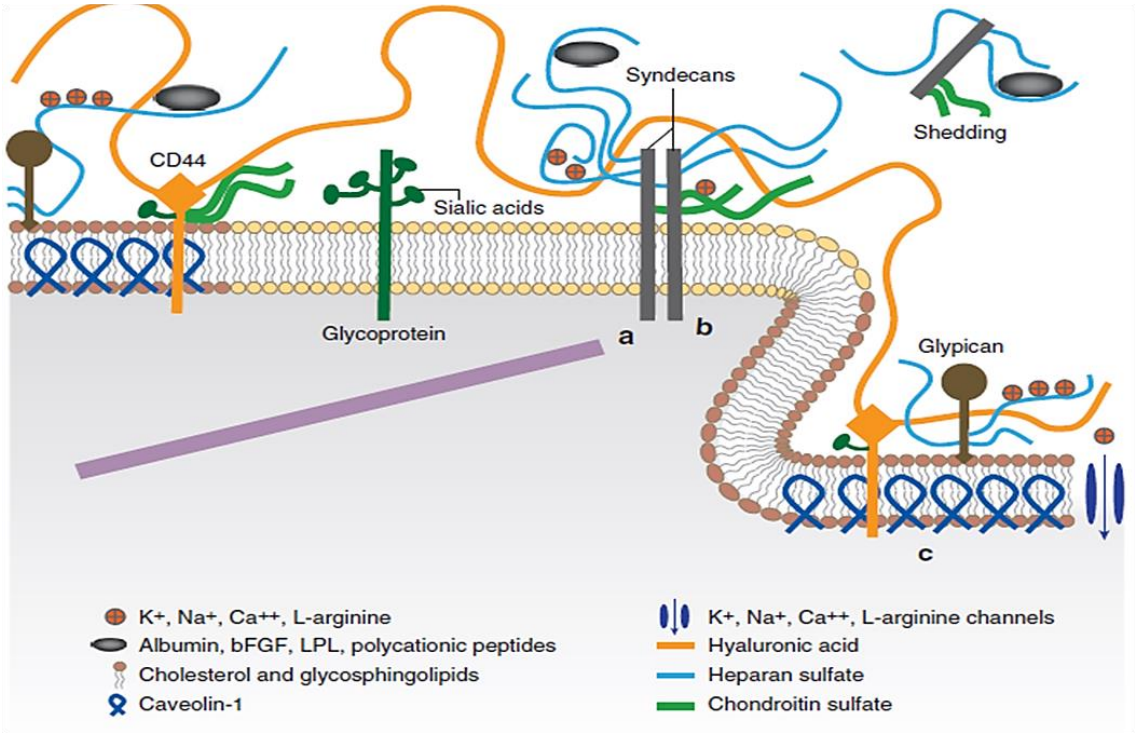

Figure 1.2 Composition of the endothelial glycocalyx.

(Weinbaum et al., 2007)

1.1.1. Proteoglycans

The proteoglycans consist of core proteins to which one or more glycosaminoglycans (GAGs) are covalently anchored. The GAGs are linear polysaccharides with a variable extent of sulphation and/or (de)acetylation, which in turn gives rise to different GAG families (Carney, 1986). In vascular systems, heparan sulphate (HS) dominates over other types of GAGs, accounting for 50%~90% of the total GAG pool (Oohira et al., 1983). The HS chain initially polymerizes from a repeating disaccharide unit, which is composed of a glucuronic acid (GlcA) and N-acetyl-glucosamine (GlcNAc). After a series of modification in cis- and trans-Golgi, the units close to the C-terminal end of the chain are preserved whereas the rest of the units are increasingly sulphated towards the N-terminal end (Fig 1-3)

(Bernfield et al., 1999). Due to the assembly of sulphated residues, the mature HS bears highly negative charges at physiological pH.

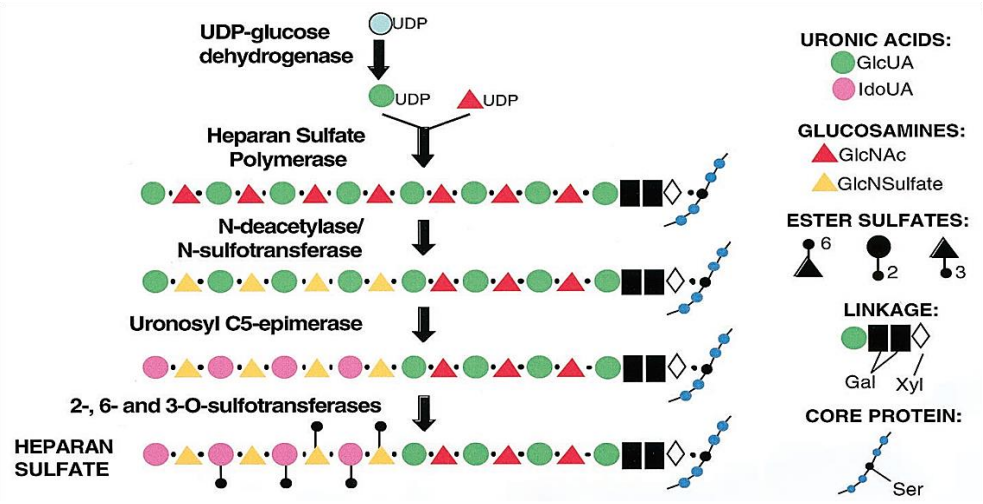

Figure 1.3 Steps for heparan sulphate biosynthesis.

(Bernfield et al., 1999)

A number of HS lyases, most of which selectively cleave the α-1, 4-glycosidic bonds between uronic acid and glucosamine, have been successfully purified and commercialized (Fig 1-4) (Fux et al., 2009, Lopes et al., 2006, Nader et al., 1990). For example, heparitinase I from *Flavobacterium heparinum* is specific to the unmodified domain rich in N-acetyl-glcuosamine. But heparitinase II preferentially acts upon the link between N, 6-sulfo-glycosamine and iduronic acid. The total degradation of HS chains is only achieved by the combination of both heparitinase. In addition, nonspecific proteases have been found to be involved in the full release of HS chains from the cell surface. The underlying mechanism for this occurs through the proteolytic cleavage of core proteins (Ihrcke et al., 1993).

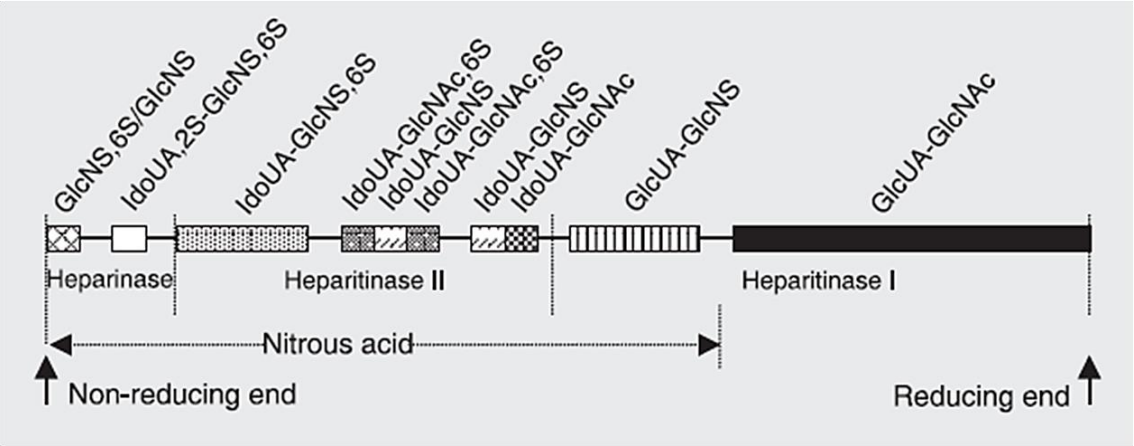

Figure 1.4 Cleaving sites of heparan sulphate chain.

(Lopes et al., 2006)

Chondroitin sulphate (CS) is the second most common GAG in vasculature, although at a ratio of 1:4 with respect to HS (Rapraeger et al., 1985). The CS is classified into three types according to the sulphation sites. The type B is known as dermatan sulphate. Chondroitinase ABC from *Proteus vulgaris* is widely used for cleaving the CS at β-1, 4-galactosaminic bonds. However, due to the structural analogy between CS and HA, chondroitinase ABC inevitably acts on the HA chains. As a result, its specificity for CS is compromised (Yamagata et al., 1968, Hamai et al., 1997).

The syndecans, glypicans, and perlecan are the three major core protein families found on the vascular endothelium. The syndecans (19-35kDa) firmly anchor to the cell membrane via a membrane-spanning domain. At the extracellular domain, the GAG attachment sites are primarily substituted by HS and occasionally reserved for CS (Bernfield et al., 1999). There are also potential proteolytic sites located proximally to the surface membrane,

making it possible for a complete cleavage of HS chains to occur under proteolytic conditions, for example, tissue digestion and trypsinization (Ihrcke et al., 1993). On the other hand, the cytoplasmic domain is associated with the actin cytoskeleton and is involved in its reorganization, which enables the syndecans to function as a mechanotransducer for shear flow (Lopes et al., 2006). Glypican-1 (64kDa) is the only subtype of glypicans expressed on the endothelium. The GAG binding sites are exclusively for the use of HS (Weksberg et al., 1996). Different from the anchorage of syndecans, the glypican-1 has a stable connection to the cell membrane via a glycosylphosphatidylinositol (GPI) anchor (Fransson et al., 2004, Zeng and Tarbell, 2014). This GPI anchor facilitates the transport of HS to lipid rafts, thereby contributing to the adaption of the glycocalyx to shear flow. Glypican-1 is insensitive to proteases. It strongly responds to the phospholipases (e.g., phospholipase C), which can cleave bonds using a GPI anchor (Ihrcke et al., 1993). Perlecan (400kD) has the largest size among core proteins for GAG (often HS). It is secreted after its assembly and GAG modification and deposited in the extracellular matrix (Iozzo, 1994).

Hyaluronan (HA) is the unique class of GAGs that is unsulphated (Reitsma et al., 2007). Additionally, there are other distinct features when comparing them to sulphated GAGs. 1) HA can reach up to 25,000 disaccharide repeats in length (Meyer et al., 1940), which is much longer than any sulphated GAGs; 2) despite the lack of sulphation, HA still carries negative charges, owing to the carboxyl residues in glucuronic acid; 3) the synthesis of sulphated GAGs exclusively occurs in the Golgi apparatus whereas synthesis of HA takes place in cytoplasm. HA is lengthened and subsequently extruded to the extracellular space through integral membrane proteins namely HA synthases (Weigel et al., 1997); 4) unlike

sulphated GAGs linking to core proteins, the exact link of HA to the cell membrane is unknown. It has been suggested that HA either directly binds to the receptor CD44 (Nandi et al., 2000) and the HA synthases (Weigel et al., 1997), or simply forms highly viscous solutions surrounding the cell membrane (Scott, 1989). In contrast to the HA synthases, hyaluronidase catalyses the hydrolysis of the β-1, 4 bond between N-acetyl-glucosamine and glucuronic acid, yielding mainly oligosaccharides.

1.1.2. Glycoproteins

Many important receptors on the endothelial cell surface, such as selectins, integrins and members of the immunoglobulin superfamily, are classified as glycoproteins and also part of the glycocalyx (Reitsma et al., 2007). Glycoproteins are proteins that are variably glycosylated with oligosaccharides. Glycosylation occurs exclusively in the Golgi apparatus and diverges according to the link between the oligosaccharides and the core proteins (Walsh, 2006). Adding the oligosaccharides on a serine or threonine residue of a peptide chain is termed O-glycosylation, while assembling the oligosaccharides with an asparagine residue of a peptide chain is called N-glycosylation. Despite the differential forms of glycosylation, the oligosaccharides are typically terminated by a nine-carbon monosaccharide, i.e., sialic acid (SA) (Fig 1-5) (Varki and Varki, 2007). The density of SA is extremely high on the endothelium, accounting for $24\sim51\times10^6$ molecules/μm^2 endothelial surface (erythrocytes, 0.15×10^6molecules/μm^2 and platelets, 15×10^6molecules/μm^2) (Born and Palinski, 1985).

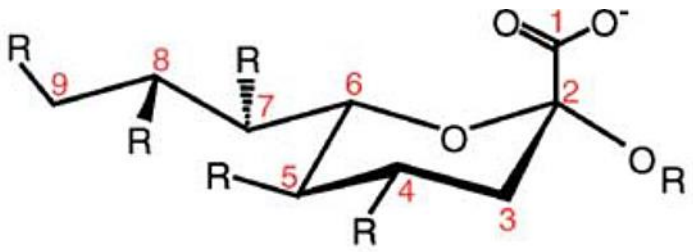

R2 = H in free Sia; alpha linkage to Gal(3/4/6), GalNAc(6), GlcNAc(4/6) or Sia (8/9)
R4 = H or *O*-acetyl
R5 = Amino, *N*-acetyl, *N*-glycolyl or Hydroxyl
R7 = H, *O*-acetyl
R8 = H, *O*-acetyl, *O*-methyl, *O*-sulfate or Sia
R9 = OH, *O*-acetyl, *O*-lactyl, *O*-phosphate, *O*-sulfate or Sia

Figure 1.5 Nine-carbon backbone of sialic acid.

(Varki and Varki, 2007)

SA is diverse in linkage and substitutions (Schauer, 2000). The first level of diversity stems from the α-linkage between its C-2 position and the underlying newly synthesized glycoconjugates, which is determined by the linkage-specific sialyl-transferases. The second level is due to a variety of modifications (e.g. acetylation, methylation and phosphorylation) from C-4 to C-9 positions. In particular, the acetylation or hydroxylation on C-5 position generates two primary SAs, N-acetyl-neuraminic acid (Neu5Ac) and 2-keto-3-deoxynononic acid (Kdn). The Neu5Ac can be further derived into N-glycolylneuraminic acid (Neu5Gc) and neuraminic acid (Neu) through hydroxylation and de-acetylation at 5-N-acetyl groups. This remarkable diversity of SA eventually contributes to a variety of glycan structures on cell surfaces. Despite this complexity, the C-1 position is conserved. The carboxyl group on it endows SA with negative charge at physiological pH. The number of negative charge carried by a carboxyl group is

theoretically less than those carried by a sulphated group. However, due to the higher expression of SA on the endothelial cell surface, SA is dominant in the overall contribution to the negative charges of the glycocalyx (Born and Palinski, 1985).

Releasing the SA from glycoconjugates requires linkage-specific sialidases (also call neuraminidase, Neu). It has been reported that the sialidases distribute in various cell compartments (Schauer, 2000, Varki et al., 2009). In the cell interior, glycoconjugates are desialylated by endosomal/lysosomal sialidases during their recycling in endosome/lysosome. The cleaved SA residues can either return to the Golgi apparatus for re-sialylation or undergo degradation in the cytoplasm. There are also cytoplasmic sialidases and mitochondrial sialidases, but their involvements in SA metabolism are poorly understood. In addition, mammalian cells have sialidases that localize on the cell surface. Cell surface sialidases abruptly shed the SA from the anchored glycoconjugates, which is thought to be the consequence of cellular responses to the environment. A number of sialidases expressed on microorganisms have been cloned and characterized. For example, Neu from *Clostridium perfringens* cleaves N-acetyl SA, which is α-2, 3- α-2, 6- or α-2, 8-linked to the glycoconjugates. The relative rate of cleavage decreases in this order: α-2-3 > α-2-6 > α-2-8. Applying Neu extracellularly enables us to demonstrate the structural and functional importance of SA in vascular pathophysiology.

Unlike GAGs, SA is recognized by SA-binding lectins rather than monoclonal antibodies (Mandal, 1990). In comparison to the high specificity of monoclonal antibodies, SA-binding lectins sometimes cross-react to underlying sugar chains, likely due to the

structural diversity of SA. Despite this, some of the SA binding lectins have been proven as powerful tool for studying the glycocalyx. For example, wheat germ agglutinin (WGA) from *Triticum vulgaris* has a high selectivity for the 5-N-acetyl group of Neu5Ac, although it is accompanied by a partial reaction to N-acetyl-glucosamine (<30%) (Peters et al., 1979). It is the most common lectin used in the visualization of the glycocalyx. Limulus polyphemus agglutinin (LPA) from *horseshoe crab* is the only lectin that specifically binds to Neu5Ac and Neu5Glc (Muresan et al., 1982). However, due to purification difficulties, the application of LPA is limited to only a few chemical labs. The density of SA varies in different states of endothelial cells. For example, the amount of SA is greater in fetal tissue than in adult tissue, indicating that SA is critical for early mammalian development. More SA is detectable in tumor cells and the tumour-associated endothelial cells. This implies the significant role of SA in enhancing tumorigenesis and/or metastasis. A regional reduction of SA has been found in the branched region of blood vessels, which is thought to be involved in degenerative diseases such as artherosclerosis and diabetes (Varki and Varki, 2007, Varki et al., 2009).

1.2. Dimensions of the endothelial glycocalyx

1.2.1. Thickness of the endothelial glycocalyx varies within blood vessels

The vascular system consists of various types of blood vessels. The lumen diameter gradually decreases from elastic artery to muscular artery, arteriole, capillary and then rebounds from venule to vein and vena cava (Wiedeman, 1963). In an early study based on electron microscopy (EM), Haldenby et al. demonstrated that the thickness of the glycocalyx in rabbit carotid was 81±2nm, nearly two-fold thicker than that in the coronary artery (Haldenby et al., 1994). The difference in thickness was also observed in the vessels of rat mesentery using dye-exclusion and immunostaining. For the former technique, the estimated thickness of the glycocalyx was 463.1±146.1nm in post-capillary venules (diameter~15μm) (Gao and Lipowsky, 2010) and reached up to 2.6±0.5μm in small arteries (diameter~150μm) (van Haaren et al., 2003). The latter technique was used to probe the functional components of the glycocalyx. For example, the labelled HS layer was slightly increased from 0.9±0.1μm in capillary to 1.2±0.3μm in post-capillary venules, and was dramatically elevated to 2.5±0.1μm in the aorta (Yen et al., 2012). All these data suggest that the thickness of the glycocalyx is not invariable along the blood vessels but that the glycocalyx thickens with an increase in lumen diameter.

Not only the lumen diameter, but also vessel types potentially alter the thickness of the glycocalyx. Smith et al. (Smith et al., 2003) first introduced hydrodynamic properties to the thickness estimation of the glycocalyx by making use of near-wall fluorescent micro-particle image velocimetry (micro-PIV) in a study that especially compared the glycocalyx

thickness in mouse cremaster muscle venules and arterioles, which share a similar range of 20~70μm in diameter (Savery and Damiano, 2008). The results showed that the glycocalyx was estimated to be thicker in venules than in arterioles (venules 0.51±0.15μm vs. arterioles 0.38±0.11μm, $p<0.01$). As the study did not find any significant difference in any of the hemodynamic parameters (e.g. velocity and viscosity) between these two types of vessels, the researchers suggested that the hydrodynamically relevant glycocalyx thickness was not strongly dependent on the hemodynamic environment. The different phenotypes of cells in venules and arterioles may therefore be determinant for the glycocalyx thickness (Kume, 2010, Swift and Weinstein, 2009). Similarly, Yen et al. reported a significant difference in glycocalyx thickness between post-capillary venules and arterioles in mouse cremaster muscle (Yen et al., 2012). The thickness of the glycocalyx in post-capillary venules was deduced as 1.5±0.2μm according to immunostaining. However, the glycocalyx was barely detectable in arterioles (only 13.5~29.8nm in thickness). A number of factors such as labelling dyes and labelling procedures have been ruled out for the rareness of the glycocalyx in arterioles. Consistent with the micro-PIV data, the phenotypical difference between arteriolar and venular endothelium can explain this spatial difference in the glycocalyx thickness.

Furthermore, the blood flow pattern has a pronounced impact on the dimension of the glycocalyx. Gorog and Born investigated SA density at different parts of the aorta as early as 1983 and found that SA density was lower on the aortic arch in comparison to the thoracic and abdominal aorta (Gorog and Born, 1983). The arch area is a flow-disturbed area that is easily deposited with lipoprotein. These observations correlated the lower amount of SA with the development of atherosclerosis. Laminar shear flow is also

disturbed at regions of bifurcation. In the work of van den Berg et al. (van den Berg et al., 2006), the glycocalyx at three distinct regions of the murine carotid artery was compared using EM. Differing from the common region (Fig 1-6.I) and flow divider region (Fig 1-6.III) in terms of laminar flow, the sinus region (Fig 1-6.II) is exposed to disturbed flow. The thickness of the glycocalyx was 399±174nm at the common region and 308±185nm at the flow divider region, whereas it dropped to 73±36nm at the sinus region. The difference in the glycocalyx thickness between atheroprotective and atheroprone regions was confirmed by the data acquired from confocal microscopy (van den Berg et al., 2009) and two-photon microscopy (Reitsma et al., 2011). In particular, in the two-photon microscopy study, although no difference was found between the glycocalyx thickness on the common carotid artery (2.3±0.1μm) and internal carotid artery (2.5±0.1μm), the surface area devoid of the glycocalyx was much larger on the internal carotid artery than on the common carotid artery (internal carotid artery 27.4±5.5% vs. common artery 8.9±4.2%, $p<0.01$), supporting the notion that the glycocalyx was diminished at these vessels where abnormal flow was easily developed.

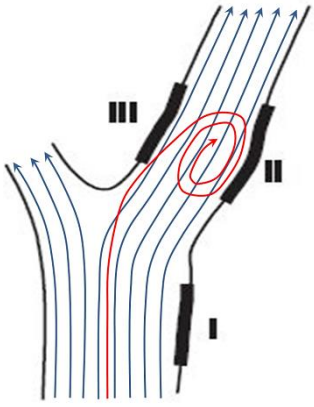

Figure 1.6 Schematic drawing of three different regions in carotid artery.

I. Common region. II. Sinus region. III. Flow divider region. Blue arrows indicate laminar flow and red arrow refers to disturbed flow. (Adapted from van den Berg BM et al, 2006)

1.2.2. Thickness of the endothelial glycocalyx varies according to detection methods

Although the difference in the glycocalyx thickness was notable, the order of magnitude in these differences varied according to different methods. EM was the earliest method to visualize the negatively charged glycocalyx (according to the binding of cationic molecules). Since it requires the slicing of vessels, this method is applicable to all vessels irrespective of the lumen diameter. However, processing the slicing involves an essential step, i.e., dehydration. It is widely believed that the dehydration of samples inevitably damages the glycocalyx. As a result, the integrity of the glycocalyx is compromised. The glycocalyx thickness determined by EM ranges from within the tens to a hundred nanometres.

A number of techniques have been developed to minimize/avoid the artefact effect induced by dehydration. These techniques include not only the improvement of sample preparation (e.g., fixation), but have also yielded new visualization methods. One of the important breakthroughs in this context is the dye-exclusion technique (Gao and Lipowsky, 2010, van Haaren et al., 2003). In this technique, the blood vessel is perfused with fluorescent micro-particles such as FITC-dextran (70 ~150kD). The size of FITC-dextran is much larger than the spacing between each unit of the glycocalyx, so that the dextran cannot penetrate into the glycocalyx. The thickness of the glycocalyx is thus determined according to the exclusion zone of FITC-dextran from the endothelial cells. The estimated value of the glycocalyx thickness can be several times greater than that measured by EM. This technique is particularly suitable for small vessels ranging from 10~15μm but fails to

provide adequate resolution for larger ones (20~40μm). Gaining insight into the atheroprone region of large vessels is rather difficult and requires additional correction procedures for estimating the dimension of the glycocalyx (van Haaren et al., 2003).

Another approach for detecting the glycocalyx *in vivo* is micro-PIV (Savery and Damiano, 2008, Smith et al., 2003), where a small volume of fluorescent micro-particles are injected into the blood vessels. The particles, following the flow dynamics, are recorded and then converted to a velocity profile. This velocity profile consistently reveals the hydrodynamic properties of the glycocalyx. Since it can provide details near the vessel wall, the resolution for both small and large vessels is improved. The estimated thickness of the glycocalyx is less than 1μm.

The glycocalyx can be detected by targeting its components with the use of immunostaining, an antibody-based method that is always combined with the use of a confocal microscope or two-photon microscope. Different from EM, dehydrating the sample is not necessary for these two direct visualization methods. The glycocalyx is largely preserved during staining. The thickness indicated by the fluorescence is usually greater than 1μm and can reach up to several microns. Although the confocal microscope and two-photon microscope both provide sufficient resolution for visualizing the glycocalyx on blood vessels, they vary in terms of penetration depth. The confocal microscope employs a pinhole to improve optical resolution and the contrast of images but still utilizes single-photon excitation. Penetration depth is not sufficient for getting through the vessel wall, so that blood vessels need to be cut open to allow imaging. This method

cannot be applied in the measurement of the glycocalyx *in vivo*. The two-photon microscope, however, is operated on the basis of two-photon excitation. The excitation of fluorophore depends on the simultaneous absorption of two low-energy photons. The out-of focus signal is thus effectively suppressed even without the pinhole. Owing to the use of a wider wavelength of excitation (700-1000nm), which doubles the common range (400-500nm) used by the confocal microscope, scattered excitation light is also reduced. As a result, penetration depth is increased (up to 1mm) and subsequently allows for imaging within intact, viable blood vessels (Megens et al., 2007, Reitsma et al., 2011).

1.2.3. Discrepancies between natural endothelium and cultured endothelial cells

The *in vitro* model is commonly used to investigate the functional importance of the glycocalyx and is accompanied by the assessment of glycocalyx thickness on cultured endothelial cells. However, discrepancies in the glycocalyx thickness between natural endothelium and cultured endothelial cells had not been fully grasped until the work demonstrated by Potter and Damiano (Potter and Damiano, 2008). In their study, the micro-PIV technique was extended from microvessels to an endothelialized microchannel, which enabled comparing the thickness of the glycocalyx on cultured endothelial cells under similar conditions. The hydrodynamically relevant glycocalyx (0.52±0.28μm) in mouse cremaster muscle venules was absent from cultured human umbilical vein endothelial cells (HUVECs, 0.03±0.04μm) and bovine aortic endothelial cells (BAECs, 0.02±0.0.04μm). In this instance, the species and vessel types of cultured cells were clearly different from the *in vivo* model. This was unlikely to induce a nearly-absent glycocalyx

layer on HUVECs and BAECs because endothelial cells from larger vessels normally possess thicker glycocalyx. In addition, one of their subsequent studies (Potter et al., 2009) demonstrated that the production of hydrodynamically relevant thickness of glycocalyx was not increased on cultured HUVEC even after seven days post-confluence, despite that the passage and culture time of endothelial cells involved in the restoration of the hydrodynamic properties of glycocalyx. Furthermore, this discrepancy was reproduced by an EM study based on the same source of endothelial cells. Chappell et al. presented a dramatic difference in the glycocalyx thickness between *ex vivo* and *in vitro* model (Fig 1-7) (Chappell et al., 2009c). The glycocalyx indicated by the dense-zone was as thick as 878±612nm in human umbilical veins whereas HUVECs displayed a layer of only 29.4±5.8nm. Even though the outer filaments emanating from dense-zone were added to the measurement, the thickness of the glycocalyx on HUVECs was averaged at 119±39.1nm, which was apparently shorter than the results found on blood vessels. It should be noted that this study also demonstrated via immunostaining that HS and syndecan-I were both detectable on blood vessels and cultured endothelial cells. However, the thickness or amount of the glycocalyx was not quantitatively compared and as such, it was unclear whether or not the order of magnitude was approximate.

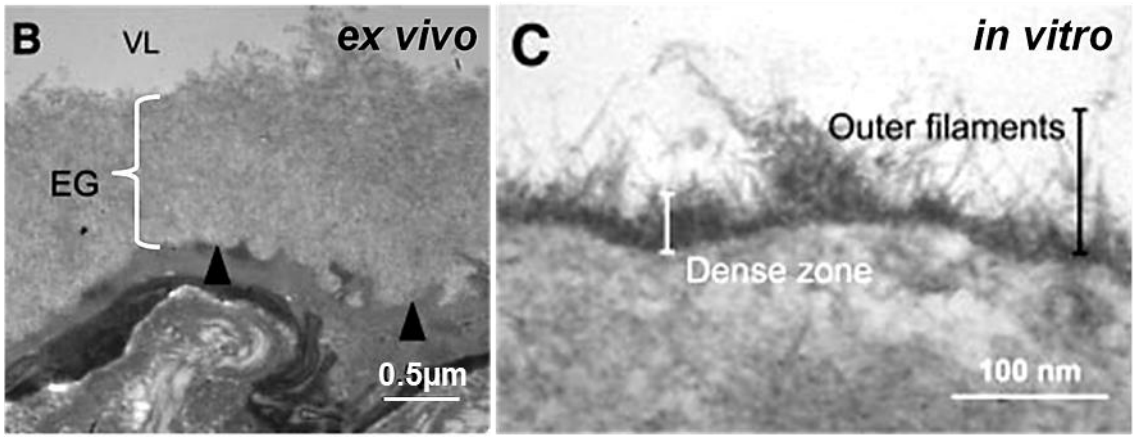

Figure 1.7 Thickness of the glycocalyx on natural endothelium and cultured endothelial cells.

EG, endothelial glycocalyx; VL, vascular lumen. (Adapted from Chappell et al., 2009)

Given that the micro-PIV and EM data revealed a difference in the glycocalyx thickness under the same detection conditions, it is suggested that the detection method is not a strong determinant for the discrepancy between natural endothelium and cultured endothelial cells. The vulnerability of the samples to the detection procedure was conceivably involved and the glycocalyx was less stable on cultured endothelial cells than on the natural endothelium of blood vessels. Another explanation for the discrepancy is the changed phenotype of endothelial cells *in vitro*. Immediately after dissection, the blood vessels were directly adapted for micro-PIV recording or perfusion-fixed for EM. The endothelial cells embedded within the luminal side of the blood vessels were preserved at the same state as those in the live condition. However, the cultured cells, they were grown under static condition until confluence. The glycocalyx was compromised due to the long-term loss of the original phenotype of endothelial cells. Although the confluent cells were detected under flow condition for micro-PIV or perfusion-fixed for EM, the glycocalyx

could not be restored in such a short period (<15mins) of stimulation. Eventually, the glycocalyx remained as a thin layer *in vitro*. It is therefore suggested that maintaining the intact nature of the glycocalyx on cultured endothelial cells requires a hydrodynamic and/or mechanical environment.

1.2.4. Glycocalyx formation on cultured endothelial cells

Shear exposure vs. static culture

The presence of shear flow has been suggested to be responsible for discrepancies in the glycocalyx thickness. No study has experimentally verified this effect using micro-PIV or EM. Such insight can only be gained from other studies, in which glycocalyx components were targeted via the incorporation of a substrate or the immunostaining. These methods were preferentially indicated by the change of component amount instead of its thickness. An early study conducted by Arisaka et al. showed that the formation of sulphated GAGs (including HS and CS), which was indicated by the incorporation of [^{35}S] sulphate, increased when the porcine aortic endothelial cells was subjected to relatively high magnitudes (15dyn/cm^2 and 40dyn/cm^2) of laminar shear stress for 24h (Arisaka et al., 1995). This was concomitant with a decrease of 44% in DNA synthesis and an increase of 50% in protein synthesis, suggesting that the proliferation was arrested to facilitate synthesis of the protein and sulphated GAGs under shear conditions. In a similar study, Gouverneur et al. did not find any difference due to the incorporation of [^{35}S] sulphate between static and shear conditions (24h, 10dyn/cm^2) (Gouverneur et al., 2006b). Instead, they found that more [^{3}H] glucosamine was detectable in the medium and trypsinized fraction of the human EC-RF24 cell line under shear condition. Due to a larger amount of

HA and stronger expression of HA-binding proteins detected at shear condition, the researchers concluded that the net increase in the amount of glucosamine-containing GAGs could be attributed to the increased production of HA. Although Arisaka et al. and Gouverneur et al. showed differential production of GAGs subtypes on the endothelial cell surface, both studies accepted that shear stress promoted the formation of GAGs by inducing a robust release of GAGs after a period of 24h rather than shortening its production time.

By microscopically imaging the HS on porcine aortic endothelial cells, Barkefors et al. showed that the HS appeared as a prominent, continuous layer on the cell surface at the end of 24h stimulation (11dyn/cm^2), whereas it distributed over the cytoplasm under static culture (Barkefors et al., 2007). The uptake of HS into the cells was largely prevented by incubating with an endocytosis inhibitor e.g., Phenylarsine oxide or by reducing the temperature to a level that suited endocytosis. In a recent study, Giantsos-Adams et al. systematically presented a HS growth profile in response to laminar shear stress (Giantsos-Adams et al., 2013). They agreed that the HS level was increased (by 40%) by exposing the HUVECs to 15dyn/cm^2 shear stress for 48h. They also evaluated the HS regrowth following 10mins heparinase III degradation and found: 1) the HS level at static and shear conditions began to rise immediately after discarding heparinise III, but the time constant for the restoration of HS was 20h for static-cultured cells and 11.8h for shear-exposed cells, indicating that the regrowth of HS at shear condition was faster than at static condition; 2) the failure of HS recovery on heparinase-treated cells at 4 degrees strongly suggested that a low temperature completely abolished the energy-dependent exocytosis of nascent HS. Collectively, Giantsos-Adams et al. proposed a kinetic model describing HS turnover on

the cell surface (Fig 1-8). This dynamic process involves five major steps: 1) transport of HS from the Golgi to the intracellular membrane; 2) shedding of HS from the cell surface; 3) endocytosis; 4) exocytosis; 5) lysosomal degradation within the cell. In this model, the differential formation of HS between shear exposed cells and static cultured cells was determined by the equilibrium of exocytosis, endocytosis and shedding, which strictly occurred at the cell membrane rather than the cell interior. The shear exposed cells exhibited faster exocytosis but slower endocytosis compared to the static cultured cells. The model also predicted a faster shedding rate under shear conditions, which was in agreement with the previous findings of Arisaka et al. (Arisaka et al., 1995). More interestingly, the faster shedding rate under shear conditions seemingly counteracted the increased ratio (3:1) of exocytosis to endocytosis. This implied that other unidentified HS stores, either in the cytoplasm or outside it, are involved in contributing to the net increase of HS production under shear conditions.

Model-derived rate constants

Name	Process	Rate constant (h^{-1}) Shear	Static
k_{Golgi}	*de novo* HS production from Golgi apparatus	0.96	0.96
k_{exo}	HS exocytosis from recycling vesicles	0.075	0.05
k_{endo}	HS endocytosis	0.025	0.05
k_{le}	HS trafficking to late endosome	0.01	0.01
k_{lys}	HS trafficking to lysosome	0.01	0.01
k_{shed}	HS cell surface shedding	0.10	0.033
k_{deg}	HS release from lysosome	0.005	0.005

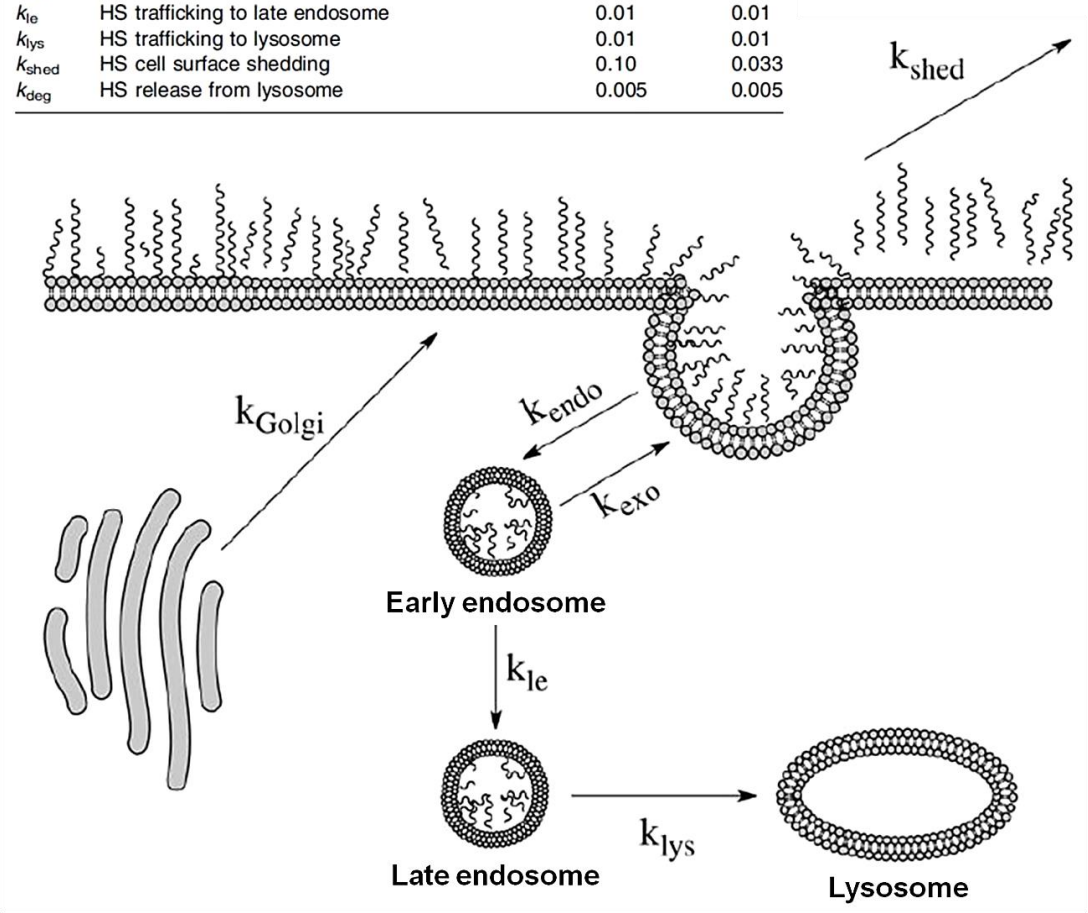

Figure 1.8 Kinetic model of heparan sulphate turnover on the cell surface.

(Adapted from Giantsos-Adams et al., 2013)

Atheroprotective flow vs. atheroprone flow

Glycocalyx formation *in vitro* was investigated with a rising interest in the effect of shear stress waveforms. This was extrapolated from the *in vivo* data and in turn provided further evidence in support of the effect of flow profiles on the glycocalyx and its special role in

atherosclerosis. The waveforms were pulsatile and derived from their regional susceptibility to atherosclerosis. It included an atheroprone profile with shear stress between -8.9 and 3.7dyn/cm^2 (mean shear stress -0.15dyn/cm^2) and an atheroprotective profile with shear stress ranging from 13.3 to 43.7dyn/cm^2 (mean shear stress 20dyn/cm^2). Maroski et al. showed that the expression of Hyaluronan synthase 2 (HAS2) on HUVECs was enhanced only after 24h atheroprotective shear stress (Maroski et al., 2011). The corresponding elevation of HA content suggested that the atheroprotective profile promoted HA synthesis by increasing the activity of HAS2. However, the failure of cell response to other flow profiles required careful consideration: 1) cells lost responsiveness to the laminar constant flow at 24h, which was contradictory to results previously reported. Because a lower level of laminar shear stress (6dyn/cm^2) was applied in the present study, further experimentation was necessary to determine the threshold of 24h shear stress in HA production; 2) the atheroprone profile did not inhibit the expression of HAS2. The influence of atheroprone flow on net HA production was clarified by the most recent, comprehensive study undertaken by Koo et al. (Koo et al., 2013). In this particular study, the amount of surface HA was maintained at a static level even after prolonged exposure to atheroprone flow for seven days. More importantly, the formation of HS differed according to distinct shear stress waveforms. The coverage of HS on HUVEC surface increased to 66.7% under atheroprotective flow, whereas coverage was reduced to 22.9% under atherprone flow. The opposite tendency was observed for the expression of syndecan-I, a major HS carrier, rather than the expression of exostosin I and II, two key enzymes for the elongation of HS, suggesting that the differential responses to atheroprotective and atheroprone flow depended on the regulation of HS carrier as opposed to HS biosynthesis. This was further confirmed by the observation that the silencing of syndecan-I completely

blocked atheroprotective flow-induced HS expression. The causal relationship between the shear stress waveforms and the formation of glycocalyx components was accordingly established, once more documenting that the hydrodynamic environment in glycocalyx formation *in vitro* is of significant importance.

Nutrients

Previous study has reported that blood plasma can modify the glycocalyx on microvessels by separating the cationized ferritin-binding layer from the apical membrane (Adamson and Clough, 1992). The total glycocalyx thickness, which is defined as the CF-binding layer plus the separation layer (Fig 1-9), was greater in the presence of whole plasma (56.2±13.7nm) than in the albumin alone (30.9±5.4nm) or in the protein-free solution (28.0±9.1nm), indicating that albumin is not an indispensable nutrient for glycocalyx formation. Similar results can be reproduced *in vitro* by subjecting rat fat-pad endothelial cells to DMEM only, DMEM+10% serum or DMEM+1% albumin for 5h. (Thi et al., 2004). Doing so indicated that cells cultured in DMEM+10% serum presented a more continuous layer of HS on the surface. When the serum was discarded, the expression of HS was significantly decreased by 27.4 ±1.1%. This reduction was not restored by DMEM+1% albumin. DMEM+1% albumin contains a sufficient amount of nutrients including inorganic salts, glucose, amino acids and vitamins, the supplement of FBS is more likely to provide additional nutrients (e.g. growth factors) for stimulating the formation of the glycocalyx *in vitro*.

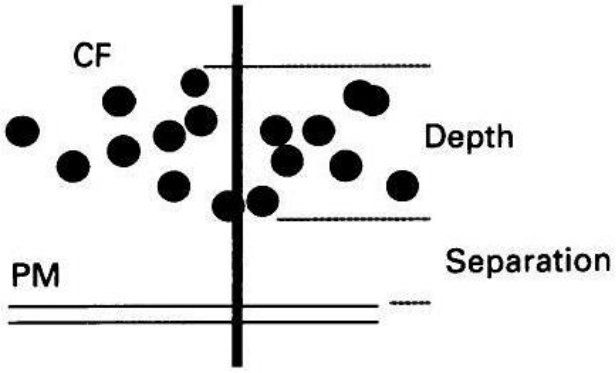

Figure 1.9 Schematic drawing of the separation of CF-binding layer.

CF, cationized ferritin; PM, plasma membrane; Depth, the depth of CF-binding layer.

(Adapted from Adamson and Clough, 1992)

1.3. Functional importance of the endothelial glycocalyx

1.3.1. Glycocalyx functions as a molecular sieve

The exchange of oxygen/carbon dioxide, nutrients and the chemical waste between the blood stream and the tissues occurs primarily in microvessels. The equilibrium between filtration and the adsorption of solutes was first described as the Starling principle, where the filtration rate was thought be proportional to the net pressure difference between the hydrostatic and oncotic pressures across the vessel wall (Starling, 1896, Levick, 1991). However, due to the observation of the glycocalyx emanating from the endothelial surface to the lumen, the Starling principle was revised by Michel (Michel, 1997) and Weinbaum (Weinbaum, 1998), who proposed that the starling forces are determined by the hydrostatic and oncotic pressure across the endothelial glycocalyx only. This was further refined as a spatially heterogeneous micro-structural model that involved the endothelial glycocalyx, inter-endothelial cleft and tight junction (Hu and Weinbaum, 1999).

Since the endothelial glycocalyx is acknowledged as the primary determinant for the balance of Starling forces, the next question concerns how the glycocalyx is involved with the regulation of transvascular transport. Henry and Duling first utilized FITC-dextrans with different molecular mass to demonstrate the permeability of the glycocalyx and found that FITC-dextran ≥70kDa was excluded from the endothelial membrane on hamster cremaster muscle microvessels (diameter<15μm) after 90mins of dye infusion (Henry and Duling, 1999). They also showed that the exclusion of 70kDa and 145kDa FITC-dextran was reduced after 1h treatment of *Streptomyces* hyaluronidase. This indicated the following digesting HA matrix generated large pores in the glycocalyx, which in turn

allowed for better access of large dextran. Nevertheless, the exclusion of 580kDa and 2000kDa FITC-dextran was not influenced by the cleavage of HA. The filtering structure glycocalyx was sustained owing to the interaction of the remaining components (e.g., HS, CS). The size-dependent exclusion of FITC-dextran was also observed in small arteries (diameter~150μm). van Haarren et al. compared 4.4kDa, 50kDa and 148kDa FITC-dextran and showed that 50kDa dextran partially penetrate the glycocalyx over time (van Haaren et al., 2003). Due to the relatively large size difference between 50kDa and 70kDa FITC-dextran, the critical pore size of the glycocalyx in small arteries was not clearly defined.

Interestingly, the size-dependent mode does not apply to all plasma molecules. Vink and Duling reported that the fibrinogen (340kDa) and albumin (67kDa), both of which carried negative charges owing to a low isoelectric point (pI4.7~5.2), showed obvious penetration with a halftime at 40mins (total exposure time=3h) (Vink and Duling, 2000). A similar result was observed when 70kDa dextran was bound to the albumin (molecular mass reached up to ~140kD). The permeation of these large proteins or protein conjugates strongly indicated that there was structural interaction between plasma proteins and the glycocalyx, which eventually facilitated the uptake of plasma proteins into the cells.

Vink and Duling also demonstrated a charge-dependent mode based on the charge modification of dextran, which showed that anionic dextran slowly diffused into the glycocalyx with halftime at 60mins, whereas the neutral dextran permeated the glycocalyx immediately following dye injection (Vink and Duling, 2000). The importance of electric repulsion was further confirmed by the charge modification of the glycocalyx (van Haaren

et al., 2005). In this particular study, the glycocalyx on rat mesenteric small arteries (diameter~190μm) were modified by altering the ionic strength of infusate. The high ionic strength (323mM, HI-MOPS) neutralized the glycocalyx while the low ionic strength (81mM, LO-MOPS) endowed the glycocalyx with higher negative charge. Due to the loss of electric repulsion at high ionic strength, the 50kDa FITC-dextran permeated the glycocalyx after the onset of infusion. Contrarily, the permeation time of FITC-dextran was further increased from 20mins at normal ionic strength to 26mins at low ionic strength. Even though the fibrinogen and albumin were allowed to penetrate the glycocalyx, neutralizing the glycocalyx increased further uptake of fibrinogen and albumin, supporting the notion that electric repulsion was involved in the hindrance of fibrinogen and albumin penetration (Gorog and Born, 1982, Ueda et al., 2004).

Taken together, the above evidence suggests that the permeability of the glycocalyx is jointly determined by pore size, the affinity with plasma molecules and negative charge. Damage to the glycocalyx facilitates the accumulation and/or uptake of plasma molecules, and thereafter gives rise to various vascular diseases.

1.3.2. Glycocalyx functions as an immuno-modulator

Leukocyte extravasation occurs mainly in post-capillary venules. This process involves chemoattraction, rolling, firm adhesion and transendothelial migration. Degrading the glycocalyx components (e.g. HS) markedly stimulated the immobilization of leukocyte on the endothelial surface and thereafter exacerbated the inflammation (Mulivor and Lipowsky, 2002, Constantinescu et al., 2003, Schmidt et al., 2012, Voyvodic et al., 2014).

This indicated that endothelial glycocalyx also serves as a barrier to prevent margination of leukocytes to the vessel walls. The leukocyte-endothelial cell adhesion depends on the coordination of molecules on the cell surface. The glycocalyx likely modulated adhesion by disturbing the communication between cellular adhesion molecules (CAMs). For example, the initial step for cell-cell adhesion, also known as rolling, requires binding between P-selectin on activated endothelial cells and ligand on leukocytes. The extracellular domain of P-selectin contains nine consensus domains for ligand bindings. Patel et al. reconstructed consensus domains at different length and demonstrated that the binding domain of P-selectin needed to be sufficiently ($n \geq 5$) exposed (Patel et al., 1995). Given that the extracellular domain of P-selectin was 38nm in length (Ushiyama et al., 1993), the researchers suggested that the critical length for effective binding was 19nm. At least half of the binding domains were masked by the glycocalyx (≈20nm) (Simionescu et al., 1981). Moreover, in order to provide a better understanding of glycocalyx thickness, some argue that the mask effect of the glycocalyx has been underestimated (Reitsma et al., 2007). Glycocalyx thickness was averaged at 1μm and could reach up to 5-10μm (Ebong et al., 2011). This was greater at least by an order of magnitude than that of P-selectin (38nm) combined with its ligand (50-60nm), suggesting that P-selectin is completely shielded within the glycocalyx network. The mask effect was also applied to intercellular adhesion molecule-1 (Mulivor and Lipowsky, 2002, Schmidt et al., 2012) and MAdCAM-1 (ligand for L-selectin) which only extended 10-15nm from the endothelial surface (Briskin et al., 1993). To establish well contact between CAMs, either an extension of microvilli from leukocytes (Sasaki et al., 1998, Zhao et al., 2001) or degradation of the glycocalyx is required.

Although the above data highlights the anti-inflammation properties of the glycocalyx, recent reports have presented conflicting perspectives on the role of HS in inflammation. These contradictions arise from the HS binding domains identified in chemokine (e.g., IL-8/CXCL8) and the CAMs (e.g., L-selectin) on leukocytes (Lortat-Jacob et al., 2002, Handel et al., 2005). Wang et al. demonstrated for the first time that neutrophil infiltration was decreased *in vivo* when the sulphation of HS was genetically abolished in endothelial cells (Wang et al., 2005). The impaired neutrophil infiltration was particularly attributed to the reduced L-selectin-mediated rolling, chemokine-activated firm adhesion and the transcytosis of chemokines across endothelial cells. Similarly, Hayashida et al. cleaved the entire HS chains on endothelial cells by silencing the syndecan-1 ectodomains *in vivo* (Hayashida et al., 2009). This demonstrated that syndecan-1 deficiency prevented the neutrophils infiltration in multi organs by scavenging proinflammatory chemokines such as CXCL1 and CXCL12. These data, along with others, clearly indicate that HS participates in almost every stage of inflammatory responses (Parish, 2006). The exact mechanism for directing the glycocalyx towards pro-inflammation and anti-inflammation is poorly understood. As such further experiments are urgently needed to clarify the dual role of glycocalyx components in inflammation.

1.3.3. Glycocalyx functions as a mechano-sensor and -transduer

Endothelium on the luminal side of blood vessels is exposed to the mechanical forces stemming from blood flow. It has long been recognized that these mechanical forces, particularly shear stress, modulate endothelial cell morphology and functions (e.g., NO production) and thereafter play a role in vascular regulation, remodelling and disease.

Mechanotransduction refers to the mechanism by which biomechanical forces are transduced to biochemical signals. The effect of the glycocalyx on the transmission of mechanical forces was initially predicted by theoretical models (Secomb et al., 2001, Weinbaum et al., 2003). When the glycocalyx is intact, it completely absorbs the shear stress exerted on the endothelial membrane. The cell membrane itself barely senses the shear stress. Contrarily, if the glycocalyx is degraded, its thickness is decreased and/or its continuity is disrupted, thereby leading to a greater fraction of shear force directly being imposed on the cell membrane.

Centralized mechanism

The primary evidence that supports the glycocalyx as having a crucial role in mechanotransduction comes from experiments in which enzymes were used to selectively degrade glycocalyx components. Pohl et al. reported that flow-dependent vasodilation in perfused rabbit mesenteric arteries was abolished by neuraminidase pretreatment (30mins, 0.2U/ml) (Pohl et al., 1991). Since flow-dependent vasodilation is modulated by NO and PGI_2 release, the study suggested that SA contributed to shear-induced vasodilators production. This was confirmed by a subsequent study in which preincubation of neuraminidase (40min, 2U/ml) significantly inhibited shear-induced NO release, but had no effect on the release of PGI_2 in rabbit femoral arteries (Hecker et al., 1993). The GAGs have also been found to be involved in shear-induced NO production. Mochizuki et al. (Mochizuki et al., 2003) demonstrated that shear-induced NO production in canine femoral arteries decreased by 80% as a result of hyaluronidase treatment (20min, 14μg/ml). On the other hand, Florian et al. utilized heparinase III (2h, 15mU/ml) to degrade HS on bovine

aortic endothelial cells (BAECs) *in vitro* and showed that shear-induced NO production was completely suppressed within 3h (Florian et al., 2003). More interestingly, they found that oscillatory shear stress (10±15 dyn/cm^2) induced a greater release of NO than steady shear stress (20dyn/cm^2). The NO production enhanced by oscillatory flow was also highly sensitive to heparinase III. In a more recent study, the effect of different glycocalyx components on the release of NO was systematically compared in BAECs *in vitro* (Pahakis et al., 2007). Consistent with previous studies, the authors presented significant inhibitions of NO production in shear-exposed BAECs with neuraminidase, hyaluronidase and heparinise III treatment but did not show any alteration in those pretreated with chondroitinase (Fig 1-10). All these data illustrated the specificity of glycocalyx components in mechanotransduction. The similar decrements found in shear-exposed cells after enzymatic treatments indicated that these functional components (except CS) evenly contributed to the mechanotransduction.

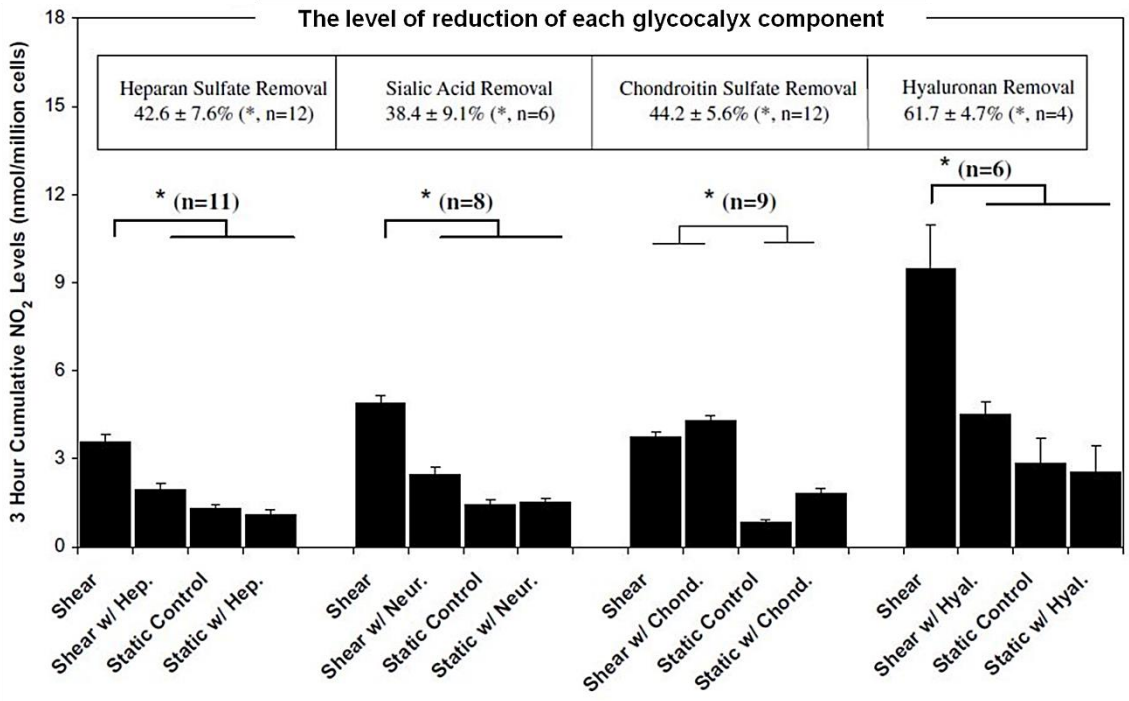

Figure 1.10 Effect of glycocalyx component degradation on shear stress-induced NO_2 production.

(Adapted from Pahakis et al., 2007)

Endothelial NO synthase (eNOS) is the unique machinery that generates NO in blood vessels. Its activity is not only regulated by shear flow, but also adapts to agonist stimuli. It should be noted that most of the above studies were executed concomitant with the test pertaining to agonist-induced NO production. Failure of enzymatic inhibition on acetylcholine- or bradykinin-induced NO production indicated that the activity of eNOS was not impaired following the removal of the glycocalyx. The glycocalyx was more likely to couple with upstream signals of eNOS. In light of the anchorage of glypican-1 in caveolae (Fransson et al., 2004, Tarbell and Pahakis, 2006) and the colocalization of eNOS with caveolae (Goligorsky et al., 2002, Shaul, 2002), it was suggested that the glycocalyx modulated the eNOS activation through a glypican-caveolae-eNOS pathway. Recently,

Ebong et al. (Ebong et al., 2014) provided direct evidence in support of this hypothesis. In this particular study, HS combined with its major core proteins (syndecan-1 and glypican-1) were investigated on BAECs under 15dyn/cm^2 shear flow. The study showed that removal of HS and knockdown of glypican-1 completely blocked eNOS phosphorylation, whereas knockdown of syndecan-1 failed to deactivate eNOS. Membrane fractionation further confirmed that glypican-1 presented as a pool in caveolae. These findings supported the fact that the glycocalyx mediates mechanotransduction through a centralized mechanism (Davies, 1995) which refers to the activation of a biochemical cascade for NO production.

As previously stated, prostacyclin (PGI_2) also participates in flow-dependent vasodilation. The fact that none of the enzyme had an inhibitory effect on shear-induced PGI_2 production (Hecker et al., 1993, Pahakis et al., 2007) suggested that the release of NO and PGI_2 relies on distinct transduction machinery. In other words, the glycocalyx was not a single mechanotransducer. Other structures were responsible for mechanotransduction in cells. For example, focal adhesions (FAs) on osteoblasts sensed the same mechanical stress due to a mechanical equilibrium between the apical surface and basal surface (Norvell et al., 2004, Ponik and Pavalko, 2004). If this principle is applied to the endothelial cells, we can infer that this process occurs regardless of the intactness of the glycocalyx. Shear-induced PGI_2 production was likely due to the FAs-mediated mechanotransduction on the basal surface, rather than the presence of the glycocalyx on top of endothelial cells.

Decentralized mechanism

Numerous studies have shown that the cytoskeleton (microfilament and microtubules) and cytoskeleton-associated structures (cell-cell junctions and focal adhesions) in endothelial cells are reorganized in response to shear stress. Attention had not been focused on the glycocalyx-mediated mechanotransduction until Squire et al. demonstrated the glycocalyx to be a quasi-periodic substructure that anchored to a scaffold of hexagonally arranged actin filaments (Squire et al., 2001). Thi et al. exposed rat fat-pad endothelial cells to 10dyn/cm^2 shear stress for 5h and carefully explored the intracellular distribution of F-actins, vinculin, paxillin, ZO-1 and Cx43 in the absence or presence of glycocalyx component (Thi et al., 2004). The study showed that in the presence of the glycocalyx, dense peripheral actin bands (DPABs) were severely disrupted and substituted with newly formed stress fibres (SFs). Tight junctions (indicated by ZO-1) and gap junctions (indicated by Cx43) were apparently discontinued. In addition, vinculin was redistributed to the cell periphery, whereas paxillin remained randomly distributed. All these responses (except paxillin) were suppressed when the glycocalyx was compromised by heparinase III, demonstrating that the glycocalyx was responsible for shear-induced cytoskeleton reorganization.

More importantly, Thi et al. proposed a "bumper-car" model for describing the transmission of shear force into cells through the glycocalyx (Thi et al., 2004). Static cells containing the glycocalyx are shown in Fig 1-11.A. The DPABs localized close to the adherens junction and served as the base for the actin cortical web (ACW) anchored by the intact glycocalyx. The DPABs functioned as rubber bumpers that were held in a lateral

register with the DPAB in neighbouring cells by the weak links of VE-cadherin. These links effectively prevented collisions between neighbouring cells in the unprotected regions behind the DAPBs. When the cells were subjected to shear stress above a critical magnitude for a certain period (Fig 1-11.B), the drag on the core proteins produced an integrated torque on the ACW, which in turn resulted in a clockwise rotation of DAPBs. Subsequently, this rotation generated a disjoining torque on the cadherin linkages between cells. When the corresponding disjoining force exceeded the binding strength of VE-cadherins, for example, 70-120pN as measured by Baumgartner et al. (Baumgartner et al., 2000), the adherens junction was disconnected and the DPABs began to fragment. To maintain a confluent configuration, new FAs and SFs needed to be assembled in the junctional region at the basal surface. It should be noted that this reorganization was transient. Once a new configuration had been stabilized, the DPABs were reformed while the SFs and FAs in the junctional region were disassembled. In contrast, the events described above never occurred if the glycocalyx was compromised (Fig 1-11.C). When the glycocalyx degraded, the shear stress acted directly on the apical membrane and was transmitted through the SFs from the apical surfaces to basal FAs. These SFs bypassed the ACW and failed to create a torque on the adherens junction. As a result, the adherens junction was stable and the DPAB remained intact. As proposed by Davies (Davies, 1995), transmitting shear force and spreading it to multiple sites within the cell (i.e. nucleus, organelles, FAs and adherents junction) reflected a decentralized mechanism on the part of the glycocalyx in mechanotransduction.

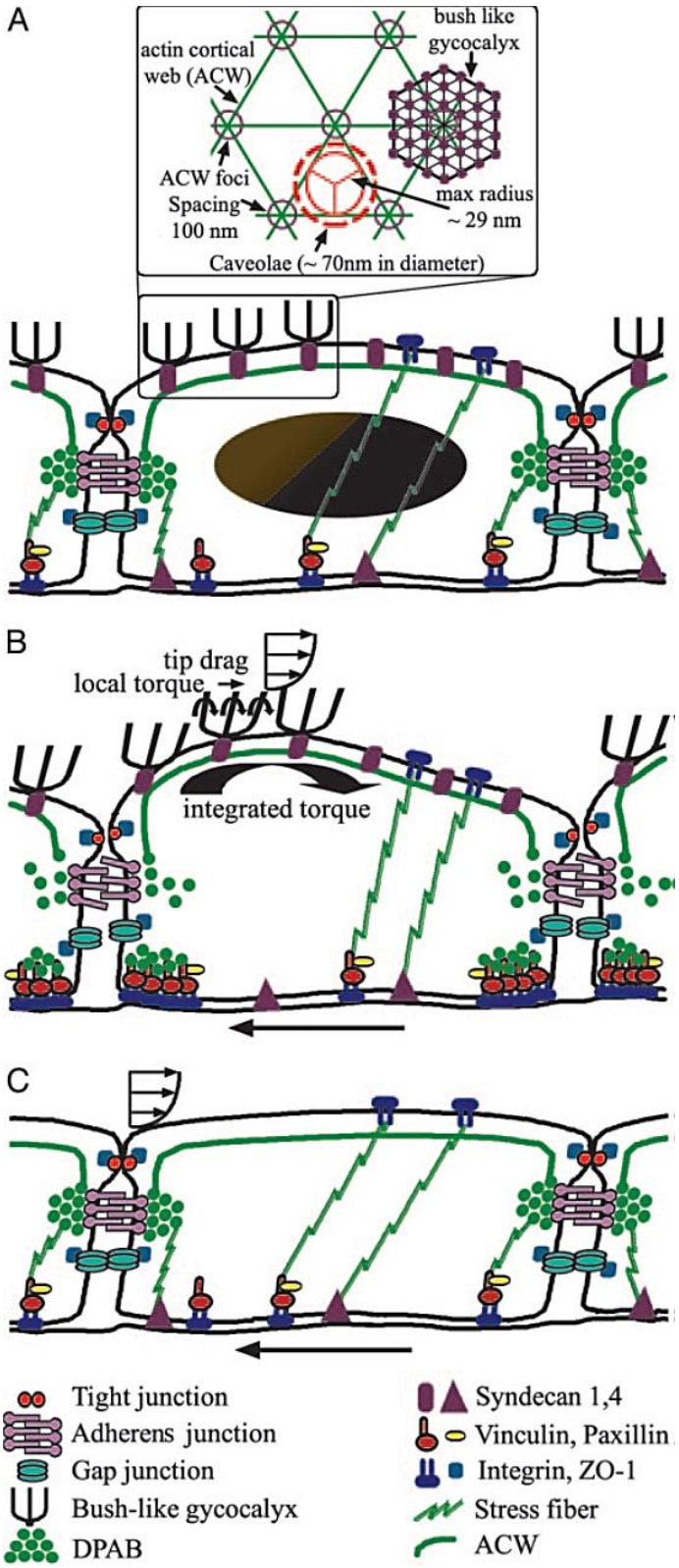

Figure 1.11 A "bumper-car" model for the structural reorganization under flow.

(Thi et al., 2004)

One of the striking cellular events controlled by cytoskeleton reorganization is endothelial cell remodelling. According to the "bumper-car" model (Thi et al., 2004), the aligned cell elongating along the shear vector renders the DPABs with longer lever arms. This leads to a reduction of disjoining force on the adherens junction and thereafter produces greater stability in response to shear flow. Yao et al. first reported that degrading the glycocalyx by heparinase III suppressed the cell alignment at the end of 24h and with 15dyn/cm^2 shear stress stimulation (Yao et al., 2007). Although they did not quantify cell elongation, the images presented in this study clearly indicated that the shear-exposed cells failed to elongate after enzymatic treatment. More recently, Ebong et al. presented complete inhibition of cell alignment and elongation in response to shear stress concomitant with heparinase III (Ebong et al., 2014). In particular, they prompted knockdown of syndecan-1 and glypican-1 separately in order to identify the HS-coupled mechanism for cell remodelling. They found that cell remodelling in response to shear stress was attenuated by HS-removal and syndecan-1 silencing, but was sustained in the absence of glypican-1. These findings confirmed that the decentralized mechanism of the glycocalyx initiated from HS and required syndecan-1 for shear force transmission.

Endothelial cell migration, a crucial step for wound healing and angiogenesis, is another event that depends on cytoskeleton reorganization. The first evidence of the role of the glycocalyx in cell migration was provided by Moon et al. who subjected sparse BAECs to 12dyn/cm^2 for 5h to show that heparinase II treatment completely abolished shear stress-directed migration (Moon et al., 2005). The key role of the glycocalyx in sensing flow direction complied with the "bumper-car" model, where there was a clockwise rotation of core proteins and ACW along the shear vector. Surprisingly, they found that heparinase II

treatment enhanced cell migration speed, not only under flow conditions, but also under static conditions. The non-specific effect of HS on migration speed was likely due to the "unusual" HS removal procedure. The BAECs were trypsinized and suspended in a heparinase II solution for glycocalyx degradation prior to reseeding for the migration test. It was reported that an amount of HS was localized in the basal surface and contributed to cell-matrix interaction. When the treated cells reattached, no HS participated in the interaction to form firm adhesion. The cells easily released from the substrate for robust migration. Hence the study proposed that "HSPGs-matrix interaction on the abluminal surface regulates EC migration speed through an adhesion-dependent manner" (Moon et al., 2005). On the other hand, Yao et al. recorded the confluent BAECs and HUVECs migration under a 15dyn/cm^2 flow condition for 24h (Yao et al., 2007). The migration speed for BAECs and HUVECs was reduced by 40% and 20%, respectively, for 1h and then recovered to the basic level. Cells short of HS maintained a regular migration speed at all times. As explained in Yao et al.'s study, the inhibited migration at the early stage may be due to an increase in cell-cell adhesion strength. This appeared to contradict the "bumper-car" model, where the cell-cell junctions would have been disjointed. However, it should be noted that the "bumper-car" model had been proposed based on 5h shear stress stimulation. Whether "bumper-car" model can explain the cellular response at an earlier stage (e.g., 1h) remained unclear.

Adaptive remodelling

In addition to the centralized and decentralized mechanism in mechanotransduction, growing evidence suggests that the glycocalyx also has an adaptive mechanism for reorganizing itself under flow condition. This was first proposed by Yao et al. in 2007

based on their observation concerning the distribution pattern of the glycocalyx (Yao et al., 2007). They noted that under static conditions, endothelial cells displayed a relatively uniform distribution of HS across the entire surface. Following 24h flow stimulation, HS was more prominent in the junctional region than the central region. Based on the notion that the shear stress gradient along the cell surface is reduced in aligned endothelial cells (Satcher et al., 1992), they hypothesized that the glycocalyx relocating from the central region to the junctional region may help to reduce the shear gradient imposed on cells (Fig 1-12). Consistently, Bai and Wang provided quantitative data based on WGA labelling (Bai and Wang, 2014). By calculating the coverage of WGA labelling on the cell membrane and the intensity ratio between the central (indicated by nucleus) and peripheral regions (indicated by the surrounding cytoplasm), they found that both parameters were decreased by roughly 30% following 24h flow stimulation, and then rebounded at 24h after the removal of shear stress. Despite these two studies presenting glycocalyx redistribution under flow, at least two issues were not addressed: 1) the glycocalyx components were labelled at the end of stimulation and the temporal redistribution of the glycocalyx was not determined; 2) the mechanism underlying the redistribution remained unidentified. Whether redistribution was due to the shedding of the glycocalyx on the apical surface or the pure movement of the glycocalyx over the surface was unclear.

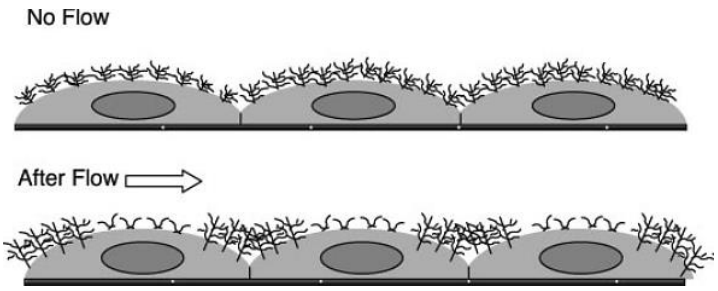

Figure 1.12 A model for the redistribution of the glycocalyx under flow.

(Yao et al., 2007)

More recently, Zeng and Tarbell et al. compared the reorganization of the glycocalyx at the early stage and late stage of stimulation, and presented a conflicting perspective on the adaptive remodelling of the glycocalyx (Zeng et al., 2013, Zeng and Tarbell, 2014). At the initial 30 min of exposure, they observed that glypican-1, rather than syndecan-1, accumulated towards cell junctions with HS. Although glypican-1 localized in caveolae and lipid rafts, the caveolae (indicated by caveolin-1) remained immobilized while the lipid rafts (indicated by ganglioside GM1) were clustered. It was therefore suggested that shear stress induced the clustering of HS via the mobility of glypican-1 in lipid rafts. In addition, the study demonstrated that no reduction was found for HS, glypican-1 or lipid rafts, excluding that HS clustering to junctions was attributed to HS shedding on the central region of cell surface. However, redistribution at the early stage was not sustained over the entire period. The study found that the expression of glycocalyx components, including HS, glypican-1 and syndecan-1, was enhanced after 24h exposure to shear stress. This in turn overwhelmed the initial polarization of HS and resulted in a nearly uniform layer close to the baseline. Meanwhile, the caveolae and the lipid rafts were also increased, which was thought to be as a result of the anchoring base for the newly-synthesized components on the surface. Despite the distribution pattern, it was speculated that the adaptive remodelling of the glycocalyx would couple with the centralized and decentralized mechanism to modulate the mechanotransduction.

1.4. Perturbation of the endothelial glycocalyx

Intact endothelial glycocalyx determines vascular permeability, mediates blood cell-vessel wall interaction and modulates the vasodilatation in healthy blood vessels. When it is disrupted, these vasculoprotective properties are lost, which in turn contributes to the development and progression of numerous diseases, for example, atherosclerosis. The previous section showed that the spatial difference in the glycocalyx thickness is related to local variations in flow profiles. Disturbed flow formed at arterial bifurcation negatively modified the glycocalyx. In this section, the perturbation of the endothelial glycocalyx under different pathological stimuli is discussed.

1.4.1. Metabolic disorder

Metabolism refers to the chemical reactions involved in the digestion and the transport of substances into cells. Disrupting this process (also known as metabolic disorder) results in an excessive or insufficient amount of substances circulating in the blood plasma. Diabetes mellitus is a well-defined metabolic disease connected with insulin absence or resistance and subsequent hyperglycaemia. It has long been recognized that hyperglycaemia can induce endothelial dysfunction such as increased vascular permeability, enhanced leukocyte-endothelial cells adhesion, and impaired eNOS activity (Morigi et al., 1998, Du et al., 2001, Algenstaedt et al., 2003). Recent studies have demonstrated that short-term and long-term hyperglycaemia adversely affected the glycocalyx intactness (Vogl-Willis and Edwards, 2004, Zuurbier et al., 2005, Kelly et al., 2006, Nieuwdorp et al., 2006a, Nieuwdorp et al., 2006b, Perrin et al., 2007, Lopez-Quintero et al., 2013). One of the structural changes that occurred was the degradation of gel-like HA matrix. This was

supported by the observation that plasma HA and hyaluronidase concentration were both increased under hyperglycaemic condition (Nieuwdorp et al., 2006a, Nieuwdorp et al., 2006b). High glucose levels also provoked the endothelial secretion of heparanase (Wang et al., 2010). The resultant reduction of HS content was associated with hyperglycaemia-impaired vasodilatation (Kelly et al., 2006, Lopez-Quintero et al., 2013). Another possible mechanism for the thinning of the glycocalyx was the glucose itself. Glucose deposited on the cell surface may occupy the GAG-attachment sites and produce fake GAG chains (Nieuwdorp et al., 2006b). When this happens, negative feedback is activated to suppress the biosynthesis of GAGs (Vogl-Willis and Edwards, 2004). Atherosclerosis is a large-artery disease that initiates from endothelial barrier dysfunction at flow-disturbed regions. This is followed by the sub-endothelial retention of low density lipoproteins, cholesterol and monocytes, and subsequent plaque formation. Hyperlipidaemia is an atherogenic risk factor that involves abnormally elevated levels of lipids and/or lipoproteins in the blood. It has been reported that oxidized low density lipoproteins and a high-fat, high-cholesterol diet (also known as a 'Western' diet) severely disrupts the glycocalyx (Vink et al., 2000, van den Berg et al., 2006). The underlying mechanism for this is not yet well understood. The degradation of the glycocalyx may be due to the production of reactive oxygen species (ROS) during hyperlipidaemia (Vink et al., 2000).

1.4.2. Ischaemic/Reperfusion

Damage to tissues during a period of absent or decreased blood flow (ischaemia) can be paradoxically exaggerated by the restoration of blood flow (reperfusion). A common pathological change for these damaged tissues is endothelial dysfunction, which occurs

preferentially in the heart and post-capillary venules. Accumulating evidence indicates that ischaemic/reperfusion (I/R) induces rapid shedding of the endothelial glycocalyx (Beresewicz et al., 1998, Platts et al., 2003, Mulivor and Lipowsky, 2004, Platts and Duling, 2004, Rubio-Gayosso et al., 2006, Rehm et al., 2007). The disruption effect on the glycocalyx can be attenuated by the blocking of xanthine-oxidoreductase (an enzyme for yielding ROS) and ameliorated by the addition of superoxide dismutase-catalase (an enzyme for scavenging ROS). It is strongly suggested that the mechanism by which I/R perturbs the glycocalyx occurs through the ROS pathway (Rubio-Gayosso et al., 2006). ROS is derived from various activated cells during I/R. This includes Kupffer cells, neutrophils, palettes and even endothelial cells. The formation of ROS initiates from the reduction of oxygen to superoxide and ends with the production of different forms of tertiary effector species (e.g. hydroxyl radical and hypohalous acids) (van Golen et al., 2012). These species are capable of fragmenting all the GAGs at the β-1, 4-glycosidic bond between uronic acid and glucosamine (Kennett and Davies, 2007, Kennett and Davies, 2009), and can shed core proteins (e.g. syndecan-1 and perlecan) by oxidizing their conformation (Kliment et al., 2009, Kennett et al., 2010, Rees et al., 2010, Kliment and Oury, 2011). However, it should be noted that not all the glycocalyx components are susceptible to I/R induced oxidation. SA, the cover of glycoproteins, instead serves as a scavenger for hydroxyl radicals. Differing from the protective role of superoxide dismutase, SA neutralizes hydroxyl radicals directly (Ogasawara et al., 2007).

1.4.3. Inflammatory stimuli

Disrupted glycocalyx contributes to inflammation by facilitating leukocyte adhesion. Conversely, the inflammatory response is also a cue for inducing the degradation of the glycocalyx, because the endothelium is exposed to an abnormally high concentration of cell-derived mediators and plasma-derived mediators (Lipowsky et al., 2011). Early studies reported that thrombin induced direct shedding of syndecan-1 through the activation of G protein-coupled receptors (Subramanian et al., 1997), while tumour necrosis factor-a (TNF-α) caused the shedding of the glycocalyx through the production of ROS and/or activating the cell surface-bound proteases (Henry and Duling, 2000). In recent years, the involvement of matrix metalloproteinases (MMPs) has been verified based on an experiment that the suppression of MMPs activity by doxycycline accentuated the leukocyte adhesion. MMPs, which are stored within the vesicles of phagocytes and endothelial cells, are robustly released under inflammatory stimuli (e.g., TNF-α). The newly-developed MMPs are prone to anchoring on the plasma membrane. The localization of MMPs enables them to cleave the entire syndecans ectodomain (Mulivor and Lipowsky, 2009, Lipowsky, 2012, Zeng et al., 2014) as well as the HA receptor, CD44 (Suenaga et al., 2005). Thus, the GAG chains are completely shed and leukocyte adhesion is enhanced. MMPs also bind to HS. The immobilization of MMPs on HS prevents the loss of secreted enzymes rather than performing cleavage on HS chains. (Yu and Woessner, 2000). In addition, neutrophil elastases (NEs) are released from the azurophilic granules of activated neutrophil granulocytes. NEs selectively cleave the HS (Key et al., 1992) through the interaction with sulphate groups of HS (Campbell and Owen, 2007).

In summary, the above pathological stimuli are not exclusive to any specific disease. They emerge simultaneously during the development and progression of vascular injury, and can induce single or multiple effectors (e.g. ROS, proteases) for disrupting the glycocalyx. Understanding the glycocalyx formation, as well as the mechanism underlying perturbation, enables us to develop therapeutic strategies for stabilizing the glycocalyx and restoring its functions. To date, a number of strategies have been proposed for protecting the glycocalyx (Kolarova et al., 2014). These include 1) the supplementing of exogenous GAGs; 2) the addition of ROS scavengers, 3) the addition of protease inhibitors; 5) proper control of atherogenic risk factor.

1.5. Electric field (EF)-directed endothelial cell migration

Membrane potential, stems from the concentration difference of ions between cells and micro-environment, and is modulated by the transport of ions through the semipermeable membrane. When tissue is intact, membrane potential is maintained uniform on every cell surface. No net electric potential difference occurs in this case. When tissue is injured, the membrane potential of the injured site drops. This alteration thereafter results in an electrical potential gradient which can produce an EF along the cell surface between injured and adjacent normal tissue (⩽1mm) (McCaig et al., 2005). The ensuing EF points towards the injury and has a potential to promote the reconstitution of tissue structure and function. Similar effects can be reproduced using external electrical stimulation, which helps us to uncover the mechanism underlying electrical signal transduction and further the application of EF in regeneration medicine.

In the vascular system, angiogenesis is the significant regenerative event that relies on endothelial cell migration. Conventionally, endothelial cell migration is driven by stimuli such as chemical gradient and shear stress. A number of studies have put forward the concept that endothelial cells also exhibited directional migration in response to an applied EF. For example, BAECs showed a significant cathodal migration within 30min under 200mV/mm (Li and Kolega, 2002). Human microvascular endothelial cells (HMECs) responded more slowly under the same EF strength (Bai et al., 2004), taking 5 hours to achieve a noticeable translocation towards cathode. Compared to the cathodal migration of HMECs, human macrovascular endothelial cells such as HUVECs migrated to the anode instead, although both were in a voltage-dependent manner (Bai et al., 2004, Zhao et al.,

2004). The EF strength used in these studies was within the range of endogenous EF in blood vessels (100mV/mm~400mV/mm) (Sawyer et al., 1966). But the reason for this different responsiveness was not clear at all. Moreover, it has been argued that EF is an overriding guidance cue that directs endothelial cell migration (Zhao, 2009).

1.6. Potential mechanism for EF-directed endothelial cell migration

Previous studies have demonstrated the involvement of EF in guiding endothelial cell migration. The next interesting question is how endothelial cells sense and transduce the EF signal. When endothelial cells are in stationary condition, they usually adhere to substratum and appear with a large and flat surface. Once cells start to move forward, membrane ruffling is released from substratum. When lamellipodium (also known as leading edge) comes into new contact with substratum, trailing edge of cell surface retracts passively. This structural remodeling, which depends on cytoskeleton reorganization, is thought to be the primary mechanism for EF-directed cell migration. Li and Kolega showed that F-actins accumulated to the leading side of the cells when BAECs moving towards cathode (Li and Kolega, 2002). It colocalized with the membrane protrusion which presented as an obvious lamellipodium in the cathode-facing side of the cells. This change was also applied to HUVECs moving to the anode. Moreover, Zhao et al. found that F-actins of endothelial cells realigned perpendicular to the EF vector with a long term EF exposure (e.g., 24h) (Zhao et al., 2004). Disassembly of F-actins had directional cell migration and reorientation totally suppressed. However, cell membrane is a lipid bilayer with high resistance to electrical current. It is unlikely that EF signal interacts with the

actin cytoskeleton directly and then induces reorganization. The F-actins in cell interior serve as terminal effectors for EF signal rather than sensors. There must be something effecting changes to the membrane to rectify the EF signal. Because few studies concentrate on the EF signal transduction in endothelial cells, considerable insight is gained from the responsiveness of other cell types.

1.6.1. Opening of gated Ca^{2+} channels

Cytoskeleton reorganization for cell migration requires increased intracellular Ca^{2+}. Transient Ca^{2+} elevation propagates from injured edge to the surviving cells both in epithelial cell and endothelial cell-based scratching models (Sammak et al., 1997, Klepeis et al., 2001). The elevation extent decreases with an increasing distance from injured edge. Meanwhile, an endogenous EF develops in scratching models and is involved in the cell migration (Zhao, 2009). The effective EF dropping on cell surface is stronger near injured edge but getting weak away from it. These consistent changes imply that Ca^{2+} oscillation is highly related to EF-directed cell migration. EF-induced Ca^{2+} oscillation has been extensively studied for a long time. Most studies shared an identical view that elevated Ca^{2+} was originated from extracellular Ca^{2+} (Cho et al., 1999, Cho et al., 2002, Sun and Cho, 2004). The reason why extracellular Ca^{2+} entered into cell interior varied in different studies. Some related this response to the changes of membrane potential. Normally, ions transport can reach an equilibrium in which cell exterior is positively charged relative to cell interior (also known as polarization). Membrane potential acquired from this relative static situation is called resting potential, which value is always negative (e.g., -70mV). Under direct current electrical stimulation, this membrane potential on the anode-facing

side of the cell becomes more negative while the opposite side is getting positive. The former response is called hyperpolarization and the latter called depolarization. As non-voltage-gated Ca^{2+} channels (e.g. leaky channel) is present in the cell membrane (Robinson, 1985), an enhanced driving force generated by hyperpolarization results in an increased Ca^{2+} influx on the anode-facing side of the cell. On the contrary, Ca^{2+} influx decreases due to a reduced driving force by depolarization on cathode-facing side of the cell. This is a passive influx pattern and suits to explain why cells moved towards anode. However, compared to passive Ca^{2+} entry, opening of voltage-gated Ca^{2+} channels (VGCC) depends on the depolarization of membrane potential. In this case, Ca^{2+} influx is much stronger on the cathode-facing side than on the anode-facing side, leading to EF-induced cathodal migration instead.

Several issues remain to be elucidated regarding to the opening of VGCC. 1) VGCC family is mainly divided into two subtypes. One is L-type channel whose opening relies on a higher voltage dropping (at least 60mV) across cell membrane. The other called T-type channel is susceptible to a low voltage (10mV is enough). The long axis of endothelial cells varies from 50μm to 100μm. When endogenous and exogenous EF (ranging from 10mV/mm to 200mV/mm) is applied, electrical potential exerting on cell membrane is no more than 20mV. Only the T-type channel is thus open in EF. Although Verapamil largely suppresses VGCC opening and then inhibits EF-induced cell migration, it is a general blocker which has no ability to distinguish L-type and T-type VGCC. Based on this uncertainty, we can't readily draw a conclusion that T-type channel is involved but L-type channel is negligible. 2) One VGCC contains four subunits——α1 subunits, α2/δ complex, β subunit and calmodulin. The voltage-sensing segments locates in each homologous domain

of α1 subunits but only segment 4 (S4) is the switch for channel opening. This S4 consists of basic residues bearing positive charges. When depolarization happens, extracellular environment is more negative relative to the cytoplasm. Resulting electrostatic force can pull those positively charged components out of cell membrane. This is confirmed by atomic force microscopy and immunofluorescence assay which showed that the opening of voltage-gated potassium channel and voltage-gated sodium channel depended on an outward movement of >2.5 and >7 amino acid residues, respectively (Yang et al., 1996, Mosbacher et al., 1998, Van Petegem and Minor, 2006). There is no doubt that VGCC shares similar mechanism and suits to explain why cells preferred moving towards cathode. However, it should be noted that some cell types such as HUVECs would rather move to the anode under the same EF strength. In this case, above interpretation looks contradicting because depolarization always occurs on the cathode-facing side of the cell.

Intrinsically, VGCC closes shortly by the neutralization of positive S4 in the cytoplasm side rather than the reversion of depolarized membrane potential. Whether prolonged EF (>30min) has a potential to sustain VGCC opening remain unknown. But intracellular Ca^{2+} replenished by endoplasmic reticulum (ER) has been shown to be associated with EF-induced motility. The release of internal stored Ca^{2+} is attributed to two reasons. 1) Intracellular Ca^{2+} increases to some extent through the opening of VGCC induced by EF. A slightly increased concentration provides a positive feedback signal for ER and then pushes ER to release more Ca^{2+}. 2) inositol trisphosphate (IP_3) pathway is independent of the VGCC but more important for the elevation of intracellular Ca^{2+}. This mainly require the dissociation of IP_3 from activated phospholipase C (PLC) on inner cell surface and the combination of IP3 with IP_3 receptor on ER membrane. Chao et al. revealed that

chondrocyte translocation was completely suppressed by pretreatment with U73122 (inactivation of PLC) and neomycin (inhibition of PLC-mediated hydrolysis) (Chao et al., 2000). These effects were later complemented by Khatib et al.'s study (Khatib et al., 2004) (Khatib et al., 2004), where the increase of intracellular Ca^{2+} was inhibited in osteoblasts treated with U73122 (not its analogue U73433).

In addition, stretch-activated cationic channel (SACC) is also involved in the regulation of extracellular Ca^{2+} entry. Traction force generated from cells is changed dynamically during EF-induced cell migration (Curtze et al., 2004). As there are correlation between stretch force and traction force, SACC is thought to be activated during this process. Direct evidence came from the blockage of SACC by Gd^{3+}. Sun and Cho depicted that Gd^{3+} significantly inhibited fibroblast migration and diffusion in 3D collagen gel model under EF (Sun and Cho, 2004). This effect was quite similar to the depletion of extracellular Ca^{2+}, suggesting that SACC also contributed to the EF-directed cell migration.

1.6.2. Redistribution of surface receptors

Zhao et al. demonstrated that surface receptors, such as epidermal growth factor receptor (EGFR), transforming growth factor β receptor and fibroblast growth factor receptor, redistributed when direct current EF induced epithelial cells move towards cathode (Zhao et al., 1999). EGFR showed an earlier (10min) and clearer cathode-side accumulation in applied EF ranging from 50 to 300mV/mm. It was suggested that the asymmetry of EGFR distribution predominated during EF-directed cell migration. Blocking ERK1/2 signal disrupted assembly of F-actins and then inhibited cathodal cell migration. Colocalization of

EGFR with ERK1/2 and F-actins on the cathode-facing site hinted that EGFR-ERK1/2-F-actins were the signal pathway for regulating cathodal cell migration. (Zhao et al., 2002) Moreover, Pu et al. found that epithelium-derived breast cancer cells preferred migrating to the anode under a similar EF strength (150mV/mm). Over-expression of EGFR enhanced the anodal cell migration while silencing of EGFR inhibited the directional migration (Pu et al., 2007). All these evidence suggests that EGFR is a sensor for EF-directed cell migration.

Surface receptors also act as sensory elements to receive extracellular chemical signals. As direct current potentially generates a chemical concentration gradient, it is argued that directional migration is due to a secondary response of chemotaxis. Cells show a preferential displacement to the position where ligands are at a higher concentration. To exclude this possibility, incorporation of flow into EF chamber has been used (Song et al., 2007). Chemical constituents driven by cyclic flow distribute evenly in the EF chamber. The asymmetrical accumulation of receptors still occurs and cells retain preferential movement in applied EF. EF-directed cell migration was independent of the chemotaxis. McCaig et al. thus concluded that EF-directed cell migration depended on spontaneous receptors redistribution while chemotaxis required ligands gradient (McCaig et al., 2005).

Apart from the perfusion of fluid, oscillatory EF is another efficient way to prevent production of chemical gradient. Cho et al. showed that transferrin receptors and low density lipoprotein receptors were distributed asymmetrically under 1Hz, 2300mV/mm EF strength for 15min exposure period (Cho et al., 1994). In a subsequent study, an index

called mean square displacement was determined and fitted assuming a combination of directed migration and random cell movement (Cho et al., 2000). This study indicated that 1 Hz, 200mV/mm EF biased macrophage migration after 1h exposure. It was highly related to the redistribution of β_2-integrin because microfilament was concentrated in podosomes at sites of contact. Inhibition of β_2-integrin (but not β_1-integrin) failed to induce net cell displacement.

1.6.3. Polarization of charged molecules

It is well accepted that the cell surface is usually negatively charged and is surrounded by equivalent cations to maintain electro-neutrality. When a directional EF is exerted, negatively charged cells will be driven towards the anode due to electrophoresis. Quite to the opposite, according to the electrostatic attraction between cations and cathode, the flow of cations toward the cathode forces negatively charged cells to move to the cathode. This process is called electro-osmosis. The cell moving direction depends on the balance between these two counteracting forces theoretically.

Previous studies (McLaughlin and Poo, 1981, Poo, 1981) demonstrated that surface charged molecules were accumulated on one side of the cell under electrical stimulation. The polarization of charged molecules on the cell surface has been once suggested to mediate EF-directed cell migration. Finkelstein et al. reported that when Hela cells were exposed to 600mV/mm for 1h, not only the cells migrated towards cathode, but also SA polarized to the cathode-facing side of the cell (Finkelstein et al., 2007). Hela cells moving towards cathode were largely suppressed following neuraminidase treatment. In the same

study, they conjugated the cell surface with positively charged avidin and found that the redistribution of SA still occurred but reversed to the anode-facing side. Surprisingly, Hela cells kept moving to the cathode. This inconsistent result appeared to be against the hypothesis that the polarization of charged molecules was essential for guiding cell movement. However, it should be noted that following coverage with excessive avidin, the original negative charges were overwhelmed and must have been changed from negative to positive. As avidin also participated in asymmetrical redistribution, it was likely that avidin polarization became the major cue to mediate cell movement. Cathodal cell migration was initiated due to the presence of surface charged molecules.

EF-directed cell migration is not a passive process dragged by electrostatic force on charged molecules. Based on the cytoskeleton reorganization during EF-induced cell migration, this process is active and involves the coordination between charged moiety and the underlying molecules. For example, SA overlaps with some surface receptors such as EGFR, it is likely that the polarization of SA is accompanied by an asymmetrical redistribution of these receptors. An ensuing stronger binding between receptors and their ligands on the leading side of the cell leads to continuous directional cell migration. In addition, some receptors without SA still bear negative charges (e.g. Concanavalin A (Con A) receptor, acetylcholine receptor). Fibroblasts moving towards cathode was also found to be mediated by cathodal redistribution of ConA receptor (Brown and Loew, 1994). SA here remained as a competitive charged constituent on the cell surface and influenced the movement of these receptors. McLaughlin and Poo showed that ConA receptor was reversed from cathodal-facing side to the anode-facing side of embryonic muscle cells by neuraminidase treatment when exposing to 10V/cm EF for 30min (McLaughlin and Poo,

1981). The researchers also demonstrated that these results were attributed to the changed zeta potential difference between these receptors and the adjacent cell surface. Zeta potential, which represented potential difference between bulk fluid away from particle and the stationary layer of fluid attached to the particle, became less negative on the adjacent cell surface than ConA receptor following neuraminidase treatment.

1.6.4. Determination of moving direction

The mechanism described above demonstrates the involvement of membrane-bound molecules in EF-directed cell migration. The exact mechanism that determines the moving direction had not been uncovered until two recent studies reported by Sato et al. and Ozkucur et al. Sato et al. genetically modified the guanylyl cyclases (GCase) in Dictyostelium cells and then applied 1000mV/mm for 20mins (Sato et al., 2009). They found that the catalytic domains of soluble GCase (sGCase) and phosphatidylinositol-3-OH kinases (PI3Ks) were responsible for the cathode-directed signaling whereas the N-terminal domain of sGCase determined the anode-directed signaling. In addition, normal cells with both two domains of sGCase preferred moving towards cathode, suggesting that the catalytic domain dominated the N-terminal domain in regular EF-directed cell migration. Accordingly, the study proposed that sGCase in response to the intracellular cyclic guanosine monophosphate (cGMP) levels determined the direction of cell migration (Fig 1-13): 1) at a high concentration of cGMP, cathode-directed signaling became dominant because of the activation of cGMP signaling and the suppression of N-terminal domain of sGCase. Hence cells displayed cathodal migration in applied EF; 2) a low concentration of cGMP inhibited the catalysis activity of sGCase and then released the

suppression of N-terminal domain. The anode-directed signaling was therefore switched on and guided cells moving towards anode.

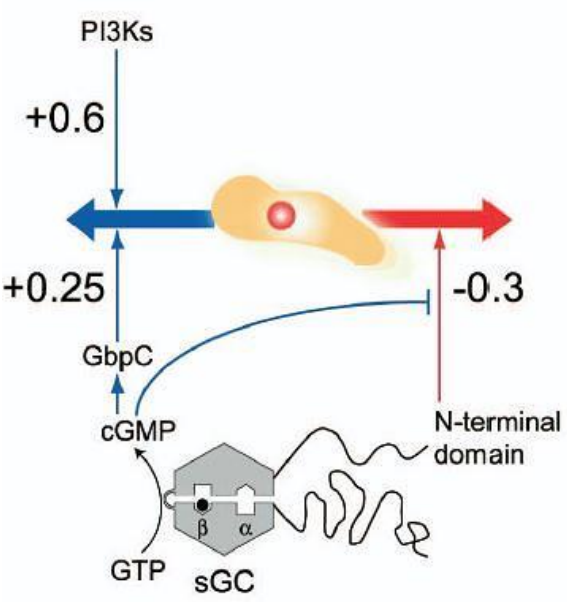

Figure 1.13 Multiple signalling pathways for electric field-directed cell migration.

The directedness of PI3Ks, GbpC, the N-terminal domain of sGCase were estimated to be 0.6, -0.25 and -0.3, respectively, where positive and negative values indicated the movement towards the cathode and anode, respectively. (Sato et al., 2009)

More recently, Ozkucur N et al. investigated ion transport proteins such as Na, K-ATPase (NaKA) and Na+/H+ exchanger isoforms (NHE3) in two types of osteoblasts (Ozkucur et al., 2011). They showed that inhibition of NaKA and NHE3 both attenuated the directedness in Calvaria (cathodal migration cells) and SaOS-2 (anodal migration cells) after 5h, 500mV/mm exposure. However, these two ion transport proteins functioned differently in response to EF. The relocation of NaKA to the leading edge resulted in a hyperpolarized cell membrane at the front and a depolarized membrane at the back. As this

phenomenon was observed on both Calvaria and SaOS-2 osteoblasts, it was suggested that NaKA served as a key to switch on the cell migration. On the other hand, the active NHE3, as well as the resulting elevation of pH level, was preferentially found at the leading edges of cathode-directed cells rather than anode-directed cells, indicating that the activation of NHE3 at the leading edges was the determinant of moving direction.

1.7. Aim and objectives

Although the functional importance of the glycocalyx is widely recognised, many issues remained to be elucidated. This PhD project aims to investigate the recovery and stability of the glycocalyx, and its role in electric field-directed cell migration *in vitro*.

The objectives of this project are set as follows.

- Investigate the role of seeding density and cell shape in glycocalyx recovery.

  The conditions for culturing endothelial cells *in vitro* are different from *in vivo* microenvironment. This difference easily results in an incomplete formation of the glycocalyx *in vitro*, thereby impacting on its functions *in vitro*. This part focuses on the recovery of the glycocalyx *in vitro*, in order to provide a better understanding of the glycocalyx formation. The observation of glycocalyx recovery is initiated after trypsinization. Different cell seeding densities are used and different cell shapes are confined. The glycocalyx is scanned in x-y-z mode by confocal microscope based on the labelling of SA. A convincing method is developed to quantify the glycocalyx.

- Explore the role of the actin cytoskeleton in stabilizing the glycocalyx.

  It is well accepted that the glycocalyx mediates reorganization of the actin cytoskeleton. No study has reported that how the actin cytoskeleton pays back the glycocalyx. The actin cytoskeleton provides physical support for the membrane and molecules anchored on it. It is unclear to what extent the actin cytoskeleton contributes to the stability of the glycocalyx. To probe into this issue, the actin cytoskeleton on monolayer cells is depolymerised by high and low concentration

cytochalasin D. The glycocalyx is scanned immediately after actin disruption. Additionally, a custom designed flow chamber is used and physiological shear stress is applied to the disrupted cells and non-disrupted cells, followed by the observation of F-actins, the glycocalyx and FAs.

- Probe the role of the glycocalyx in EF-guided cell migration.

  EF is a potential cue to direct endothelial cell migration. But the sensing and transduction mechanisms remain poorly understood. The glycocalyx possesses a bulk of negative charge and is responsible for the reorganisation of the actin cytoskeleton. It is likely that the glycocalyx is involved in EF-directed cell migration. To validate this hypothesis, a custom designed EF chamber is used and sparse cells migration in applied EF is videoed by time-lapse microscopy. Both neuraminidase-treated cells and non-treated cells are tracked. Migration index including translocation speed and directedness is determined. The glycocalyx, especially its spatial distribution, is analysed at the end of EF stimulation.

2. Materials and methods

2.1. Cell culture and treatment

Human umbilical vein endothelial cells (HUVECs) are commonly used in the research of vascular biology. As stated in chapter 1, the glycocalyx thickens with an increase in lumen diameter. The thickness of the glycocalyx in vein is greater than that in artery. Using umbilical vein-derived endothelial cells thus facilitate the visualization of the glycocalyx in our study. HUVECs purchased from ATCC were used before passage 12. Cells were grown in medium 199 supplemented with foetal bovine serum (FBS), β-endothelial cell growth factor, bovine neural extract, heparin, thymidine, penicillin and streptomycin. The recipe for complete endothelial cell growth medium is shown in the following tables.

Table 2-1 Preparation of endothelial cell growth factor (ECGF) supplement.

Products	Company	Catalog No.	Amount
β-endothelial cell growth factor	Sigma	E1388	25μg
Bovine neural extract	Sigma	E2759	75mg
Heparin	Sigma	H3149	25KU
Thymidine	Sigma	T1895	28.1mg
dH_2O	Millipore	-	40ml

The ECGF supplement was aliquot to 1ml per vial and stored in -80°C freezer.

Table 2-2 Preparation of complete endothelial cell growth medium.

	Products	Company	Catalog No.	Amount
Basic medium	Medium 199, HEPES	Invitrogen	22340/22350*	500ml
Antibiotics	Penicillin-streptomycin	Sigma	G1146	5ml
Extra nutrients	Foetal bovine serum	Sigma	F7524	56ml
	ECGF supplement	Sigma	-	1ml

**Two types of Medium199 were selected for different purposes of cell culture. Product 22340 was buffered with Sodium Bicarbonate ($NaHCO_3$) and required CO_2 for maintaining pH. However, the buffer system of Product 22350 was replaced with Sodium Phosphate dibasic (Na_2HPO_4-$7H_2O$) and Potassium Phosphate monobasic (KH_2PO_4), which are capable of maintaining pH in CO_2-free environment.*

Cells at a density of 3200 cells/cm^2 were plated in 25cm^2 flasks (NUNC, 136196) for seven-day culture. Confluent HUVECs were washed with Ca^{2+}-free phosphate-buffered saline (Invitrogen, 14190-169) and subsequently incubated with 1ml trypsin-EDTA solution (Sigma, T3924) for 5mins. Following on, 5ml 20% FBS was added for deactivating the trypsin. Detached cells were collected, washed and counted. Non-coating coverslips were used as substrate for subculture. Cell seeding density and culture time varied in terms of experiments. For cell density effect in chapter 3, HUVECs at a density of 500cells/cm^2 (low), 2500cells/cm^2 (moderate) and 10000cells/cm^2 (high) were cultured for a certain period of time. For chapter 4 and 5, even though same seeding density (2500cells/cm^2) was used, the cells were cultured for 7 days and 2 days, respectively, prior to the experiments.

Chemical treatments were required in some cases. HUVECs were incubated with 1U/ml neuraminidase (Sigma, N2876) for 1h for selectively removing the glycocalyx component. HUVECs were subjected to different concentration of cytochalasin D (Santa Cruz, 22144-77-0) for studying spatial-temporal depolymerisation of the actin cytoskeleton. More details are given in the corresponding chapters.

2.2. Micropatterning

The procedure of PMEDSAH brush (17±3nm) growth was performed according to Dr Julien Gautrot's instruction (Fig 2-1) (Gautrot et al., 2010b, Tan et al., 2013). Gold coated coverslips were deposited with ATRP initiator (5mM o-mercaptoundecylbromoisobutyrate) for 10s, printed with custom designed PDMS (Polydimethylsiloxane) stamp for 10s and then immersed in degassed MEDSAH monomer solution. Following 90mins polymerization, the modified coverslips were sequentially cleaned with brine (saturated sodium chloride solution), pure ethanol and water. Because PMEDSAH brush is protein resistant, HUVECs only spread and survive on brush-free islands. Circular and elliptical islands with similar surface areas were prepared for cell culture. To maximize the coverage of individual cells on single islands, a great amount of cells (15000cells/cm^2) were initially incubated for 2h and then gently washed. Cells remained adhering on the islands were further cultured for 24h.

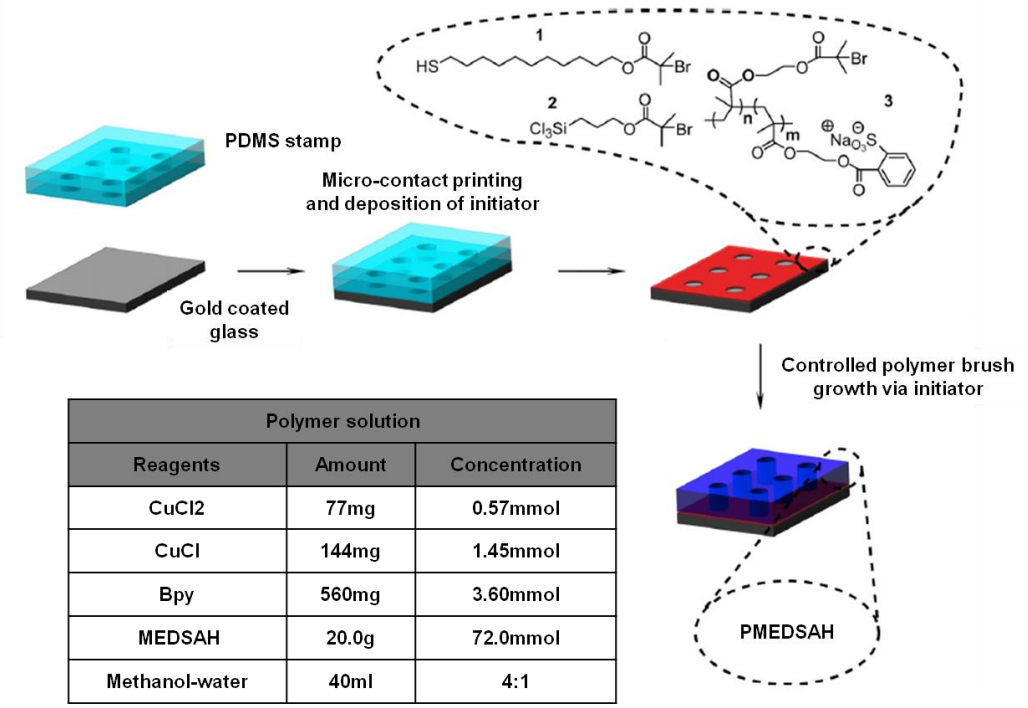

Polymer solution		
Reagents	Amount	Concentration
CuCl2	77mg	0.57mmol
CuCl	144mg	1.45mmol
Bpy	560mg	3.60mmol
MEDSAH	20.0g	72.0mmol
Methanol-water	40ml	4:1

Figure 2.1 Schematic drawing of PMEDSAH brush growth.

2.3. Apparatus assembly

2.3.1. Shear stress apparatus

Shear stress apparatus was composed of flow chamber system and fluid delivery system. Flow chamber system was manufactured according to the concept of two parallel plates system (Fig 2-2) (Bai and Wang, 2014, Yao et al., 2007). Upper PMMA plate was built with input and outlet connectors on each side while bottom PMMA plate was cut with a rectangular groove (48×18×0.13mm) on its surface. With two coverslips (24×18×0.13mm) fitting in the groove, the entire surface of the bottom plate remained level. A gasket ring with an inner dimension of 70×20×0.2mm was placed between these two plates for establishing a flow chamber. Leakage from the flow chamber was prevented by a tight clamp from two extra stainless plates.

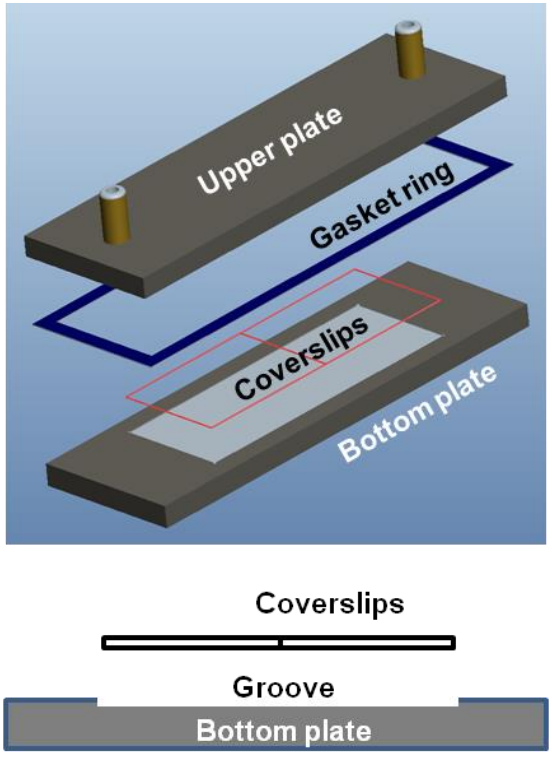

Figure 2.2 Schematic drawing of flow chamber system.

Fluid delivery system was set up as a closed loop by the use of two reservoirs and a peristaltic pump (Fig 2-3). Medium in a medium reservoir was pumped out into a cylinder reservoir at a constant rate. Due to equilibrium between influx and efflux, the volume of medium in the cylinder reservoir was constant, which resulted in a steady flow passing through the flow chamber. The medium was finally drained back to the media reservoir and recycled for the entire period of stimulation. Since the dimension of flow chamber was fixed, flow rate across the flow chamber was determined by the height of medium in the cylinder reservoir. Magnitude of laminar shear stress was calculated using following equation,

$$\tau = \frac{6\rho Q}{wh2} \qquad \text{[equ.1]}$$

Where τ is the shear stress, ρ is the viscosity (0.0084P), Q is the flow rate (0.25ml/s), w is the width (20mm) and h is the height (0.2mm).

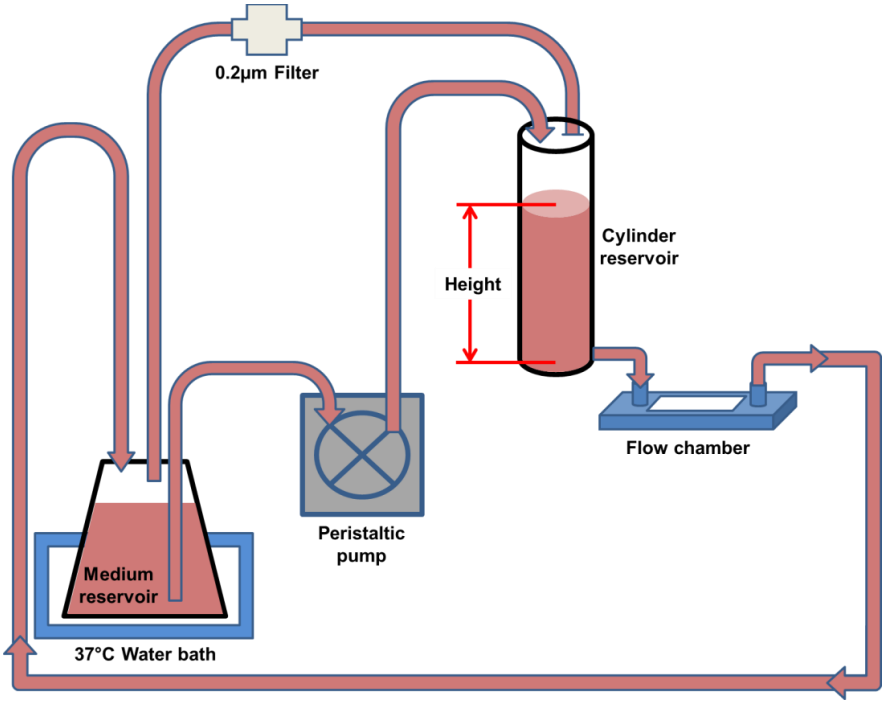

Figure 2.3 Schematic drawing of fluid delivery system.

Monolayer cells with or without treatment were exposed to shear stress of 15dyn/cm^2 for 24h. In addition, to maintain temperature and atmosphere, the medium reservoir was placed in a water bath and connected to the cylinder reservoir by the use of filter-connected tubing, which allowed constant and sterile airflow (Fig 2-4).

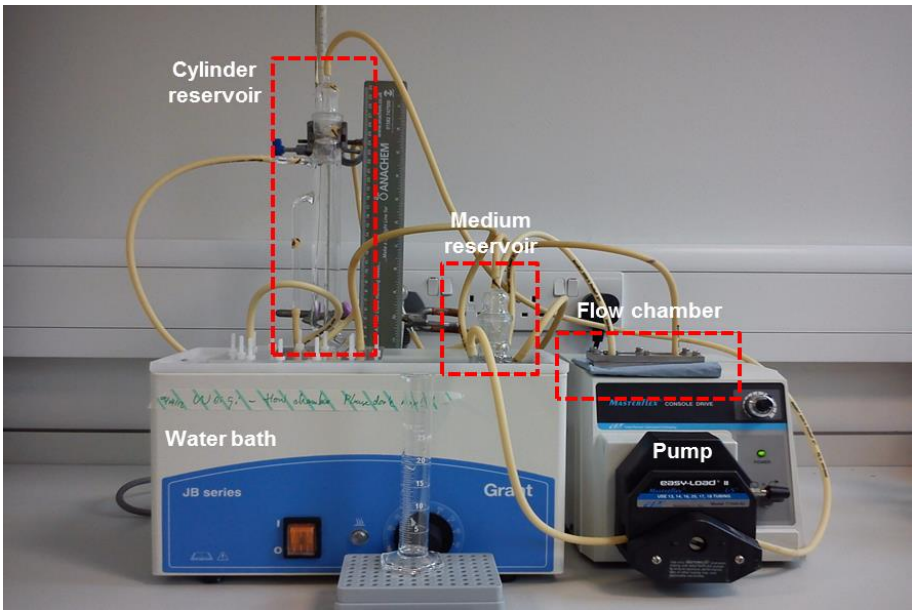

Figure 2.4 Fluid delivery system.

The materials used for assembling shear stress apparatus are listed in the following table.

Table 2-3 Materials used for assembling shear stress apparatus.

Products	Company	Catalog No.
Polymethylmethacrylate plate (PMMA plate)	Goodfellow	400-643-63
Cellulose acetate film (Gasket ring)	Goodfellow	138-038-81
Masterflex® variable-speed drive	Cole Parmer	77521-47
Masterflex® pump head	Cole Parmer	77200-50
Masterflex® platinum-cured silicone tubing (L/S 16)	Cole Parmer	06508-16
Glass reservoirs	QMUL	-

2.3.2. Electric field apparatus

Electric field apparatus was adapted from those reported previously (Fig 2-5) (Chao et al., 2000, Song et al., 2007). A piece of non-conductive PTFE plate was divided into 3 regions. Region in the middle of the plate was used as a culture zone while the two regions on each side were designed for electrolyte reservoirs. The middle region and two side regions were bridged together by using ABS moulds filled with 2% electrolyte-agar gel (Sigma, A1296). To construct a chamber for real time cell observation, a square window of 20×20mm was open at the bottom of the middle region, following by the placement of a coverslip (24×24×0.13mm). To prevent any leakage from the chamber, a hollow PTFE holder perfectly matched the chamber was placed on top of the coverslip, resulting in a clamp-like structure with the bottom of the middle region.

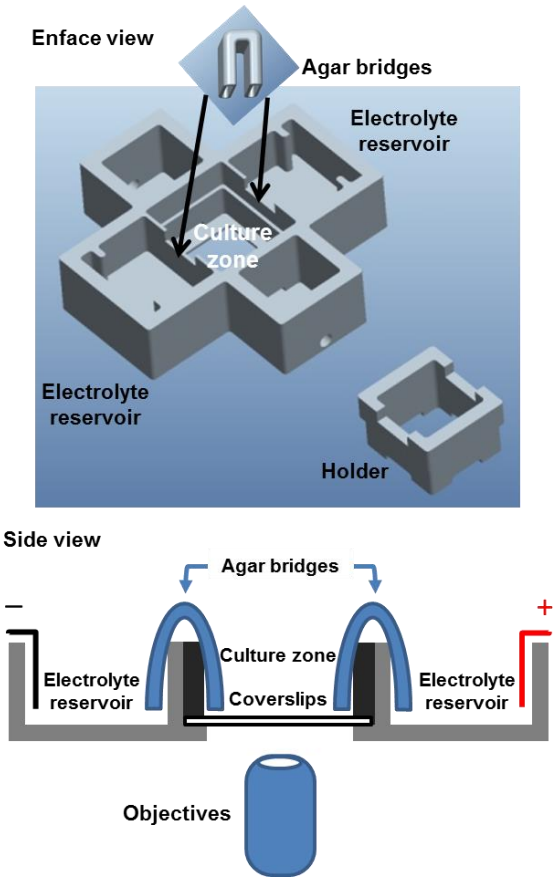

Figure 2.5 Schematic drawing of EF chamber.

Following on, a lid fitted with two platinum electrode wires was assembled with the chamber. Current generated by 10V power supply passed into the chamber through agar bridges. Sparse cells with or without treatment were continuously subjected to EF for 5h. EF ranging from 100 to 700mV/mm was tested. All EF experiments were carried out inside a microscope chamber, where constant temperature (37°C) was maintained at all times (Fig 2-6).

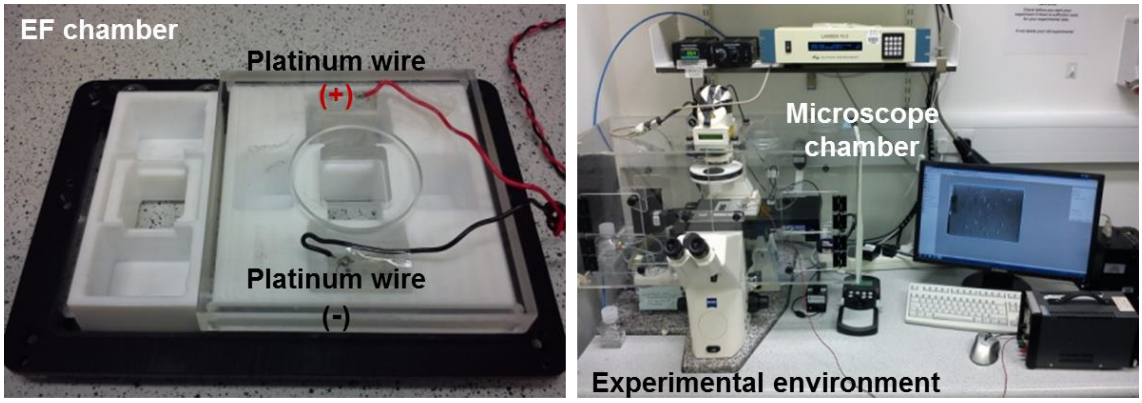

Figure 2.6 EF exposure system.

The materials used for assembling EF apparatus are listed in the following table.

Table 2-4 Materials used for assembling electric field apparatus.

Products	Company	Catalog No.
Polytetrafluoroethylene plate (PTFE plate)	RS	752-672
Acrylonitrile butadiene styrene (ABS)	RS	-
Platinum electrode wire (0.2mm thick)	Fisher Scientific	11503362
Stainless steel plates	QMUL	-
10V Power supply	QMUL	-

2.4. Immunostaining

2.4.1. Labelling of the glycocalyx

Two components of the glycocalyx are commonly used for visualizing the glycocalyx. One is sialic acid (SA) which selectively binds to wheat germ agglutinin (WGA) and the other is heparan sulphate (HS) which is only recognized by specific antibody. To exclusively label SA on the cell surface, the procedure reported previously was adapted (Bai and Wang, 2012, Barker et al., 2004). HUVECs were simultaneously incubated with 10μg/ml FITC-WGA and 10μM cell tracker red (CTR, cytoplasm indicator) in Hank's balanced salt solution (HBSS) at room temperature for 15mins. Following on, the cells were fixed with 4% paraformaldehyde (PFA) solution for 8mins and directly used for confocal scanning. Factors which affected the localization of SA are summarized in the following table.

Table 2-5 Factors affecting the labelling of the glycocalyx.

Factors	Conditions	Purposes
Temperature	Room temperature	Prevent uptake of FITC-WGA at 37°C
Incubation time	15mins	Prevent uptake of FITC-WGA from overtime incubation
Key step	Labelling before fixation*	Prevent permeation of FITC-WGA

**The molecular weight of FITC-WGA is only 38kD. When the cells are alive, intact cell membrane resists the permeation of FITC-WGA. Contrastingly, when the cells are fixed beforehand, small pores are easily formed on the cell membrane, which is large enough for FITC-WGA passing through. As a result, cytoplasmic SA and surface SA are both labelled.*

To label HS on the cell surface, HUVECs were fixed with 4% PFA solution and blocked with 1% bovine serum albumin (BSA) solution for 45mins. Following on, the cells were incubated with anti-heparan sulphate (10E4 epitope) primary antibody for 1h and stained with Cy3-AffiniPure goat anti-mouse IgM for 1h.

2.4.2. Staining of F-actins and focal adhesions

HUVECs were fixed with 4% PFA solution for 10mins and permeabilized with 0.1% Triton X-100 solution for 10mins prior to immunostaining. For visualization of the actin cytoskeleton, the cells were directly incubated with Rhodamine phalloidin in 1% BSA solution for 30mins. For visualization of focal adhesions (FAs), the cells were blocked with 1% BSA solution for 45mins, followed by incubation with anti-vinculin primary antibody for 1h and Alexa Fluor® 594 goat anti-mouse IgG (H+L) for 1h. Finally, the cells were counterstained with 4',6-Diamidino-2-Phenylindole (DAPI), mounted in ProLong® Gold reagent and scanned by confocal microscope within one week. Negative controls were carried out by omitting primary antibodies. Antibodies were diluted in 1% BSA solution. The chemicals used for immunostaining are listed in the following table.

Table 2-6 Chemicals used for immunostaining.

Products	Company	Catalog No.	Stock solution	Dilution
Dyes				
FITC-WGA	Sigma	L4895	1mg/ml	1:100
Rhodamine phalloidin	Sigma	R415	1000U/ml	1:200
DAPI	Invitrogen	D3571	5mg/ml	1:500
CellTracker Red	Invitrogen	C34552	10mM	1:1000
CellTrace FarRed	Invitrogen	C34553	10mM	1:1000
Antibodies				

Anti-vinculin (Gene ID 7414)	Sigma	V9264	1mg/ml	1:150
Alexa Fluor® 594 goat anti-mouse IgG (H+L)	Invitrogen	A11005	2mg/ml	1:400
Anti-heparan sulphate (10E4 epitope)	US biological	H1890	1mg/ml	1:50
Cy3-AffiniPure goat anti-mouse IgM	Jackson ImmunoResearch	115-165-075	1.3mg/ml	1:100
Other chemicals				
Hank's balanced salt solution	Invitrogen	14025-100	-	-
ProLong® Gold reagent	Invitrogen	P36930	-	-
Paraformaldehyde (PFA)	Sigma	16005	-	4%
Triton X-100	Sigma	T8787	-	0.1%
Bovine serum albumin (BSA)	Sigma	A2153	-	1%

2.5. Image acquisition and analysis

2.5.1. Cell migration analysis

A series of images were acquired at an interval of 10mins for 5h using a time-lapse microscope. Cell migration was quantified by manually tracking the centroid of cell nucleus in MTrack J, Image J (Meijering et al., 2012). Translocation speed was defined as the trajectory between starting and end position of a cell over this period. The significance of the mean direction was analysed using the Rayleigh test in Chemotaxis tool, Image J. Directedness was calculated according to sinθ (Fig 2-7), where the angle (θ) was formed between the displacement vector of a cell and a line drawn perpendicular to EF vector (Chao et al., 2000, Zhao et al., 2004). The directedness equalled to +1 [sin(90)] if the cell moved directly towards cathode. Contrarily, it changed to -1 [sin(-90)] if the cell moved directly towards anode. The directedness with a value of 0 [sin(0)] indicated that the cell moved perpendicularly to EF vector. Dying cells, dividing cells and cells from cluster were excluded from migration analysis.

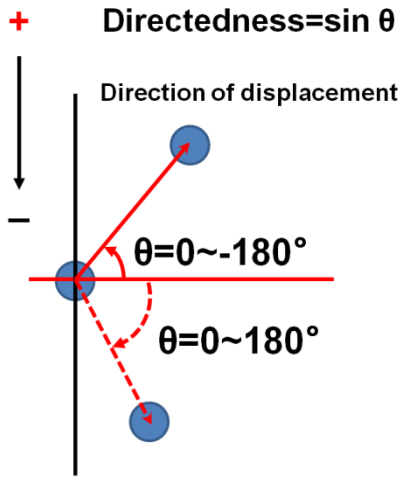

Figure 2.7 Definition of directedness.

2.5.2. Confocal image acquisition

The scales used for different microscopes are listed in the following table.

Table 2-7 Scales used for different microscopes.

Microscope	Brand	Objective	Format	Dimension (μm)	Pixel size (μm)
Inverted	Leica DMIL	10×	2592×1944	1029.39×772.05	0.4
Time-lapse	Zeiss Axiovert 200M	10×	1392×1040	1390.61×1038.96	1.0
Confocal	Leica TCS SP2	63×	1024×1024	238.10×238.10	0.23251

The power of 488nm argon laser, 543nm Helium/Neon laser and 633nm Helium/Neon laser was all set to 25%. Confocal images at a format of 1024×1024 were unidirectionally scanned at a speed of 400Hz. The AOBS power and PMT value of Gain/offset was adjusted for different channels. Pseudo-colour interface, where ‘bright orange’ referred to saturatation intensity and ‘green’ indicated intensity-free background, was always activated

for calibrating fluorescence intensity. To avoid cross-talk between two different fluorophores, sequential scanning mode was employed for multi-colour image acquisition. Image acquisition started from the basal cell surface and ended at the apical cell surface. Step size between each two sections was usually set as 0.3μm unless stated otherwise.

2.5.3. Glycocalyx quantification

A z-series stack of images was merged using maximum-intensity projection in Image J. Projected images were thresholded above the background intensity level. A cell and its cell body were separately outlined as regions of interest (ROIs) according to the labellings (Fig 2-8). The entire cell surface was visualized by FITC-WGA (green), while the cell body was tagged with CTR (red). In some cases, the appearance of CTR was too dispersed to distinguish the boundary of the cell body. The outline of the cell body in this instance was validated by checking the original stacked images.

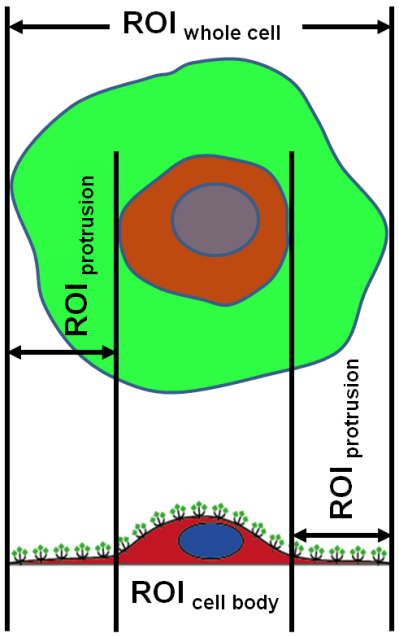

Figure 2.8 Definition of region of interests.

The surface area (A) of the entire cell and the cell body were directly measured by Image J. The area of cell protrusion was obtained by subtracting the area of the cell body from the area of the entire cell. Additionally, a surface area ratio was generated to compare the size difference between the cell body and the protrusion.

$$Surface\ area\ ratio = \frac{A_{cell\ body}}{A_{protrusion}} \qquad \text{[equ.2]}$$

Where the ratio < 1 indicated the protrusion was larger than the cell body, and vice versa.

To quantify the glycocalyx on the entire cell surface, mean fluorescence intensity (MFI) of ROI $_{\text{whole cell}}$ was measured. It was defined as the sum of fluorescence intensity (SFI) over all the pixels in ROI $_{\text{whole cell}}$. MFI acquired from the experimental group was normalized to the parallel control. To detail the spatial distribution of the glycocalyx, MFIs from ROI $_{\text{cell body}}$ and ROI $_{\text{protrusion}}$ were calculated. Similar to the calculation of cell surface area, MFI $_{\text{cell body}}$ was directly given, whereas the MFI of the protrusion was derived using the following equation (1μm^2 =18.52 pixels).

$$MFI_{protrusion} = \frac{SFI_{protrusion}}{All\ pixels_{protrusion}} = \frac{SFI_{whole\ cell} - SFI_{cell\ body}}{A_{protrusion} \times 18.52} \qquad \text{[equ.3]}$$

Following on, a spatial coverage ratio was created to clarify the differential coverage between the cell body and the protrusion.

$$Spatial\ coverage\ ratio = \frac{MFI_{cell\ body}}{MFI_{protrusion}} \qquad \text{[equ.4]}$$

Where the ratio < 1 indicated the glycocalyx was denser on the protrusion than on the cell body, and vice versa. When the ratio equalled to 1, the glycocalyx layer was perfectly uniform over the entire cell surface.

To validate the distribution of the glycocalyx on micropatterned cells, heatmap analysis was executed (Fig 2-9) (Tan et al., 2013). After z-axis projection of stacked images, individual cells on single islands were cropped using the same ROIs selection. Dying cells, non-spreading cells and cell cluster were all excluded (yellow box). The cropped cells (red box) were stacked together and projected once more using an average-intensity mode, where image intensity was shown as overall intensity averaged by the number of images. This image was finally plotted according to intensity gradient (0-255) using HeatMap Histogram, Image J, where red represented the maximum intensity, 255, while black referred to the minimum, 0.

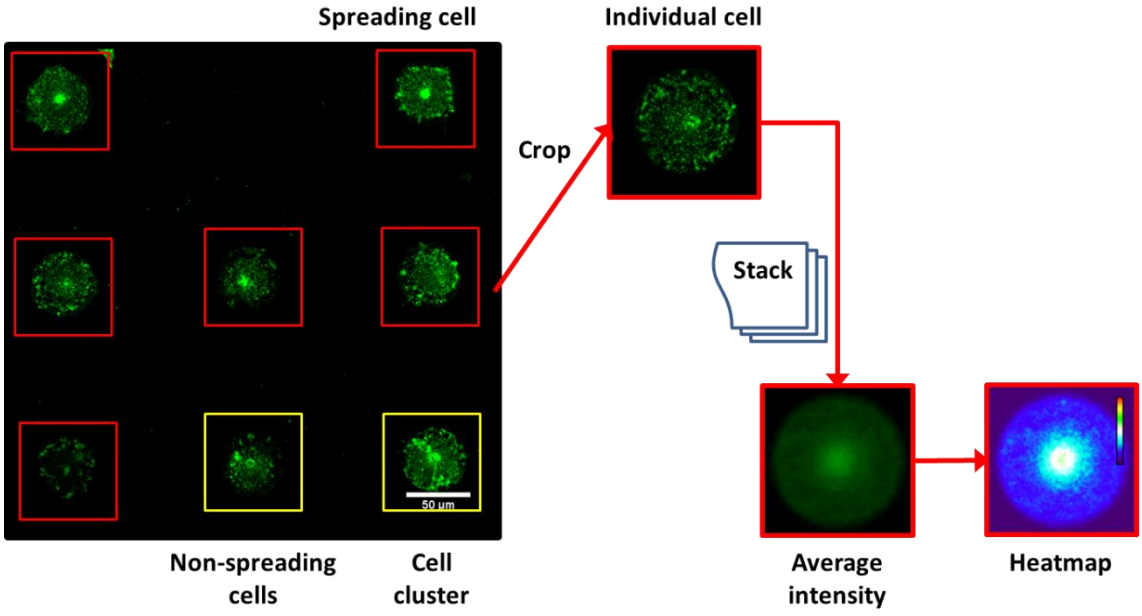

Figure 2.9 Schematic drawing of heatmap analysis.

2.5.4. F-actins quantification

F-actins were measured in two ways. One was line profile which was performed in Image J. Fluorescence intensity was determined by a straight line (50μm×0.23251μm) drawn across a bundle of F-actins within a cell (Acharya et al., 2008, Boudaoud et al., 2014). The other was FilaQuant, a newly-developed image processing tool for measuring ridges and filaments (Birkholz et al., 2010, Matschegewski et al., 2012). Projected images were cropped to individual cell per field in image J prior to inputting into FilaQuant. Actin filament usually consists of more than one line segment. Based on the principle of ridgeness measurement, every line segment (max width=0.23251μm) was tracked and joined to form a consecutive filament (Fig 2-10). To exclude immature filaments (filaments with short length) in the cell, minimum length of 4.65μm was predetermined according to repeated validations on original image. Ridge detector speed was optimized by setting iterations and vertex Laplacian threshold to 50 and -50, respectively. The number of filaments and their length were given at the end of analysis.

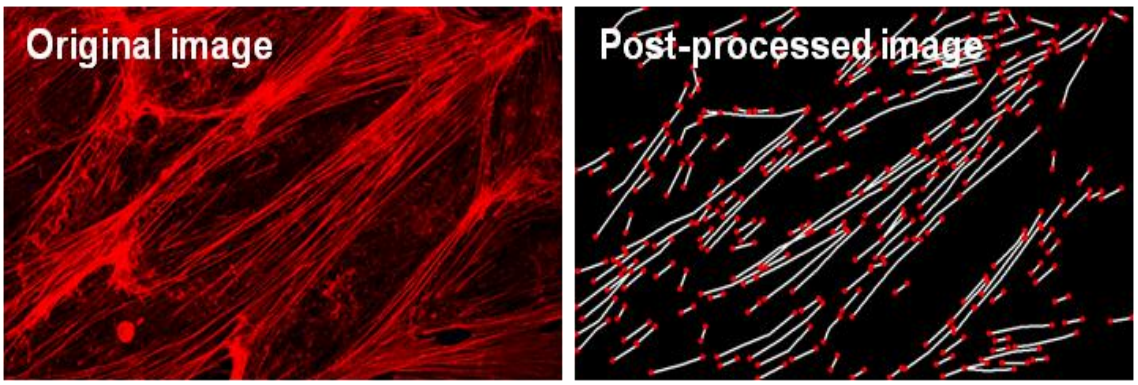

Figure 2.10 The outline of actin filament in FilaQuant.

2.5.5. Focal adhesions quantification

FAs were quantified using particles analysis, Image J (Fig 2-11) (Peacock et al., 2007, Tan et al., 2013). Stacked images with a step size of 0.115μm were projected to the XY plane and then thresholded by a high greyscale (threshold=155). Particles ranging from 0.5-10μm^2 were automatically tracked for each cell, followed by a manual validation on the particle shape and size. Particles localized on the cell boundary were excluded from counting because it was not able to distinguish which cells these particles belong to. To further analyse the distribution of FAs in the cell, a straight line was drawn from the centroid of cell nucleus to the centroid of FA. The location of FA was defined by the length of this line and the angle between this line and the shear stress vector. Parameters such as FA number, size, shape and distribution were provided at the end of analysis.

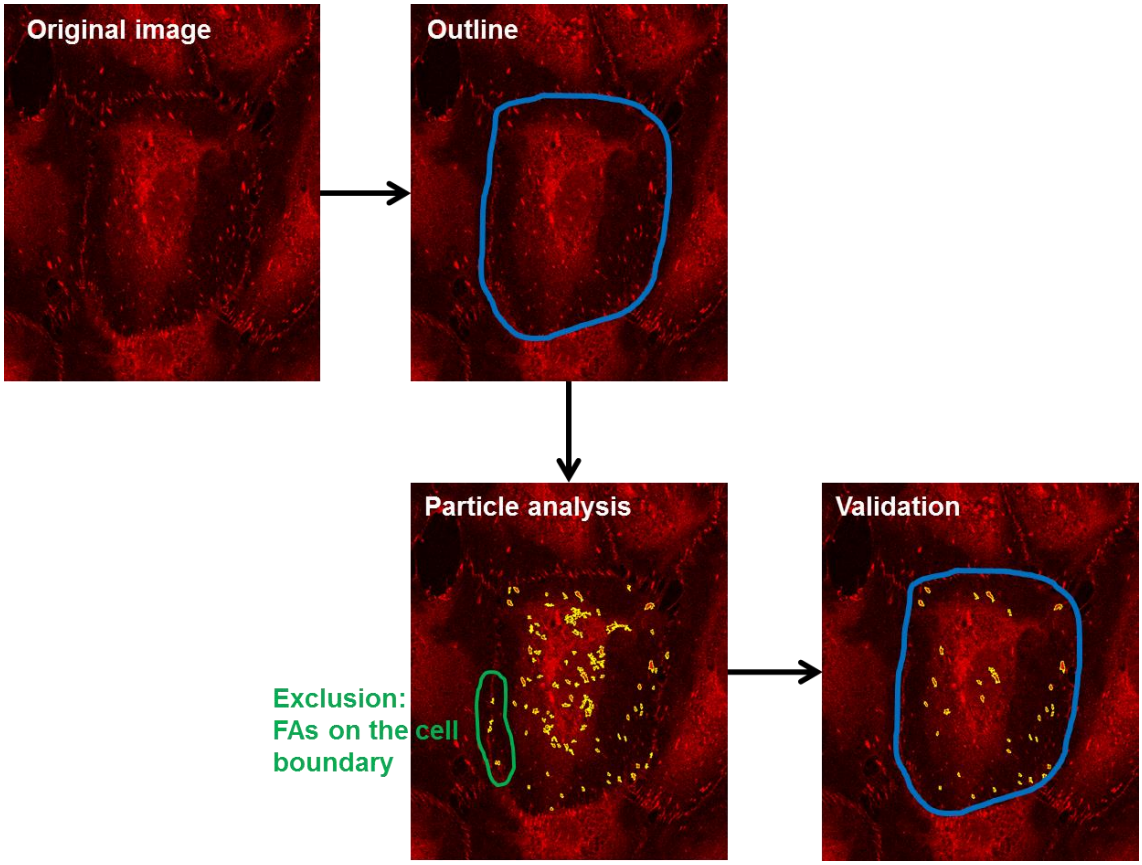

Figure 2.11 Schematic drawing of particle analysis.

2.6. Statistical analysis

All data was presented as mean±SE obtained from at least three independent experiments ($n \geq 3$). The cell number counted for each group varied and was stated in corresponding chapters. Statistical analysis was performed in Origin 8 software using one-way analysis of variance (ANOVA) with Bonferroni test (depending on Levene's statistic for homogeneity of variance) for multiple means comparisons, and nonparametric tests (Kruskal-Wallis ANOVA) for inhomogeneity of variance. Difference in means was considered significant if $p<0.05$.

3. Contribution of cell density and cell shape to the recovery of the glycocalyx

3.1. Introduction

The glycocalyx protrudes from the luminal surface of the endothelium. There are increasing studies on visualizing the glycocalyx *in vitro*. Potter and Damiano collected micro-PIV data from endothelialized microchannel and demonstrated that the hydrodynamic thickness of the glycocalyx was less than 0.05μm on cultured endothelial cells, which was at least 10 times smaller than the estimated thickness *in vivo* (Potter and Damiano, 2008, Potter et al., 2009) This was further supported by a EM study undertaken by Chappell et al., where the glycocalyx on cultured umbilical vein endothelial cells (29.4nm) was much thinner than that on umbilical vein endothelium (878nm) (Chappell et al., 2009c). Rapid freezing/freeze substitution transmission EM effectively preserves samples in hydrated configuration. By using this technique, Ebong et al. showed that the glycocalyx was surprisingly thick (≥5μm) on cultured endothelial cells (Ebong et al., 2011). The glycocalyx thickness obtained previously may be underestimated *in vitro*. It is essential, therefore to address the recovery of the glycocalyx *in vitro* before translating findings from *in vitro* model to the *in vivo* situation (Barakat, 2008, Potter and Damiano, 2008).

The conditions for culturing endothelial cells *in vitro* are different from *in vivo* microenvironment. These include enzymatic isolation from the tissue, the replacement of

artificial medium, trypsinization for cell harvesting and the absence of physiological flow. By labelling the glycocalyx with FITC-WGA, our group recently demonstrated that the development of the glycocalyx *in vitro* was time dependent (Bai and Wang, 2012). The recovery of the glycocalyx on HUVECs started from the edge of a cell and reached full coverage on the apical cell surface after two-week culture. The observation of glycocalyx recovery, however, began from sparse cell condition and ended at confluence. Cell-cell interaction during cell growth may alter cell configuration and behaviour (Friedl and Zallen, 2010). Considering the balance between cell proliferation, contact inhibition and glycocalyx synthesis, it will be interesting to investigate the effect of cell density on glycocalyx recovery *in vitro*. In addition, different shear stress profile regulated the formation of the glycocalyx *in vitro.* Endothelial cells bear less and uneven glycocalyx when subjected to low shear stress. (Koo et al., 2013). It is well known that the cells exposed to low shear stress become less elongated and revert to the cobblestone-like appearance as shown in static culture (Dai et al., 2004). It is not clear whether the changed morphology influences the recovery of the glycocalyx. Therefore, we aimed to explore the potential factors such as cell density and cell shape on the recovery of the glycocalyx *in vitro*.

To investigate the recovery of the endothelial glycocalyx, three questions are addressed in this chapter (Fig 3-1): 1) whether cell seeding density influences the recovery of the glycocalyx; 2) whether the glycocalyx is well-developed on confluent cells; 3) whether cell shape plays an important role in the recovery of the glycocalyx.

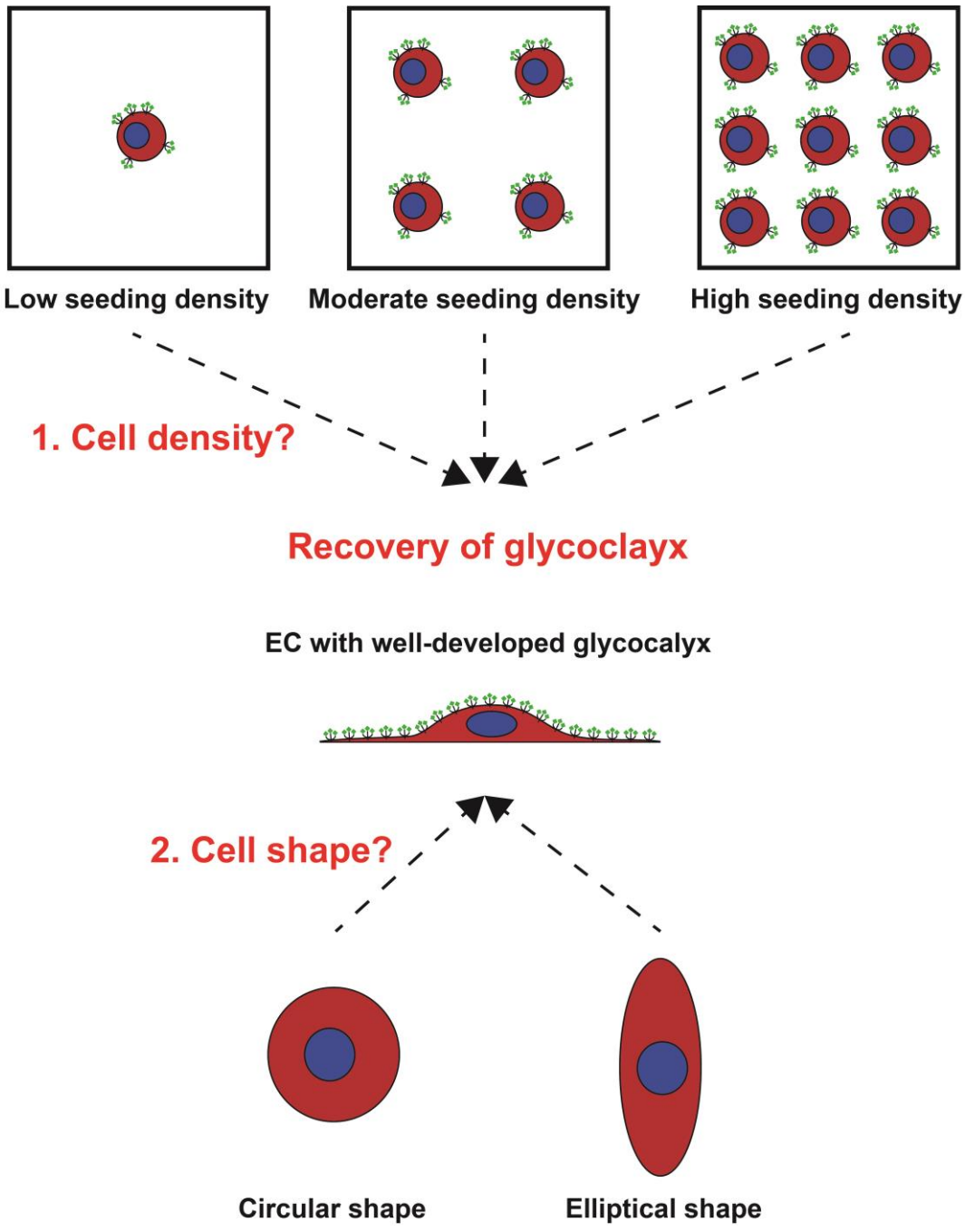

Figure 3.1 Diagram of contribution of cell density and cell shape to the recovery of the glycocalyx.

3.2. Methodology highlights

3.2.1. Cell seeding density

HUVECs harvested by trypsinization were seeded at a density of 500cells/cm^2 (low), 2500cells/cm^2 (moderate) and 10000cells/cm^2 (high) on non-coated coverslips (18×24cm) and cultured for a certain period of time as follows (Fig 3-2).

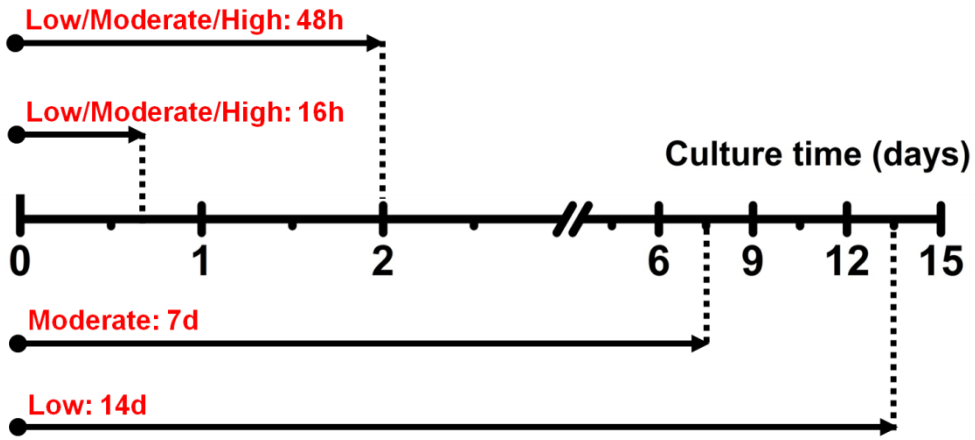

Figure 3.2 Culture time for different seeding densities.

Three cell states were established according to the seeding densities. Low cell density culture referred to as sparse cell condition that was short of cell-cell contacts, whereas high cell density culture resulted in cell confluence. Moderate cell density culture was set to bridge the low and high density cultures.

3.2.2. Cell shape

Circular and elliptical micropatterns with size at roughly 2000μm^2 were utilized. Circular micropattern was approximated to the shape of adherent cells under static culture, while

elliptical micropattern mimicked the endothelial cell shape under shear flow. Our previous study showed that endothelial cells were elongated at a long:short axis ratio of 3.14:1 following 24h and 1.5Pa shear stress stimulation. In the present study, the elliptical micropattern was customized with a large ratio of 5:1 to amplify the shape effect (Fig 3-3).

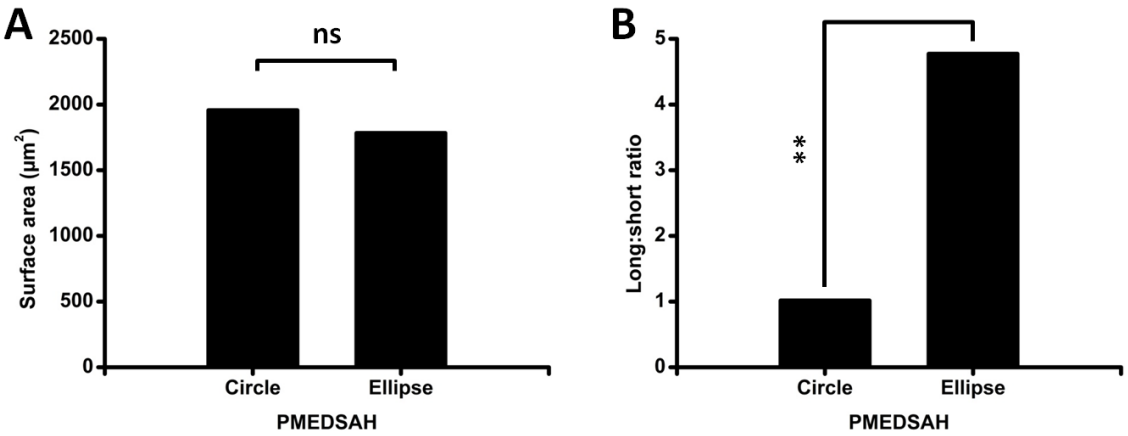

Figure 3.3 Characterization of PMEDSAH micropatterns.

Circular and elliptical micropatterns were confined at a similar surface area (A) and the elliptical micropattern was customized with a long:short axis ratio of 5:1 (B).

The micropatterns were cut and placed in 24-well plate prior to cell seeding. To maximize the coverage of individual cells on single micropatterns, HUVECs at a density of 15000cells/cm^2 were seeded and initially cultured for 2h, followed by the removal of excessive cells. The cells which remained attached to the micropatterns were continually cultured for 24h. The adherent cells at 2h and 24h were both collected for the labelling of the glycocalyx.

3.3. Results

3.3.1. Integrity of the glycocalyx was compromised by trypsinization

In normal cell passaging, enzymatic digestion such as trypsinization is commonly used for cell harvesting. Since the glycocalyx is a protein-anchored carbohydrate complex, it has the potential to compromise the integrity of the glycocalyx. To verify that the glycocalyx remained on the detached cells, we performed staining on suspension cells following trypsinization. As shown in Fig 3-4.B, the remainder of the glycocalyx did not layer around the cell surface. Instead, the glycocalyx appeared mainly as a large, dense aggregate or occasionally as scattered, smaller patches. The patterns shown on suspension cells indicated that the glycocalyx had been severely degraded.

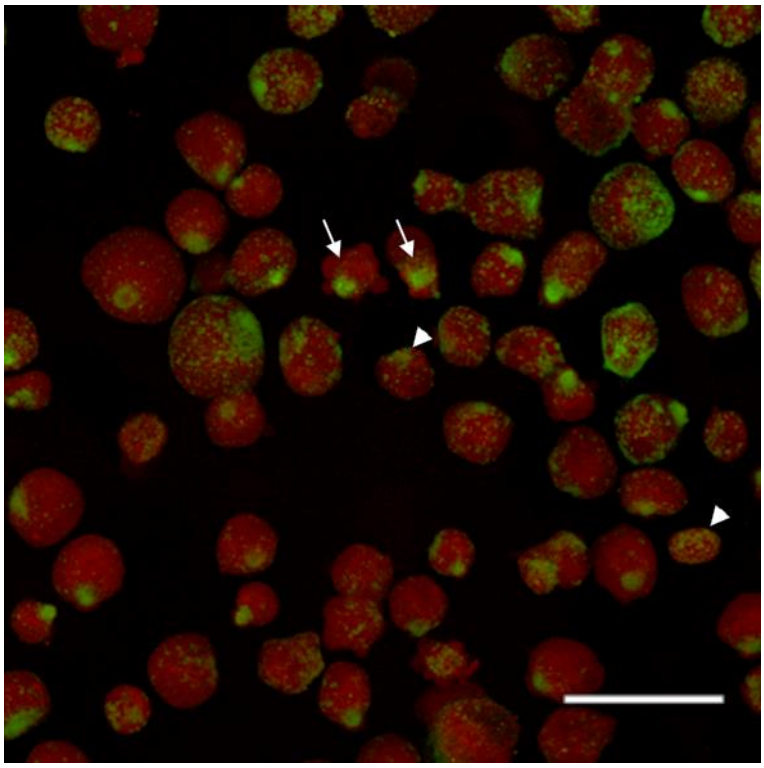

Figure 3.4 Remainder of the glycocalyx on trypsin-harvested suspension cells.

HUVECs were harvested by trypsinization. Suspension cells were stained with cell tracker red (red) and FITC-WGA (green). Images were merged to show the distribution of the remaining glycocalyx on suspension cells. The glycocalyx was severely damaged following trypsinization. Arrow indicates the dense aggregation of the glycocalyx. Arrowhead points to scattered patches. Scale bar = 50μm.

3.3.2. Higher cell density culture resulted in more rapid recovery of the glycocalyx

To investigate the effect of cell densities, 500cells/cm^2 (low), 2500cells/cm^2 (moderate) and 10000cells/cm^2 (high) were cultured. After 16h cultures, the glycocalyx aggregates were all dispersed on the cell surface in each group. The amount of the glycocalyx was small, so that a continuous, intensive layer of the glycocalyx could hardly be seen. In some cases, it was clear to see that the glycocalyx was relatively intensive on the cell protrusion compared to the cell body, suggesting that the recovery of the glycocalyx started from the cell periphery to the apex. Following 48h culture, vigorous recovery of the glycocalyx was achieved. The spatial distribution of developed glycocalyx varied in terms of seeding densities. Under low cell density culture (Fig 3-5.D), the glycocalyx was dominant on the cell protrusion. Contrarily, when a high density culture was employed, the recovery of the glycocalyx on the cell body was as robust as that on the protrusion and a clear, continuous glycocalyx layer was reformed on the entire cell surface (Fig 3-5.F). For the cells cultured at moderate density, the labelling pattern of the glycocalyx was close to that under high cell density culture.

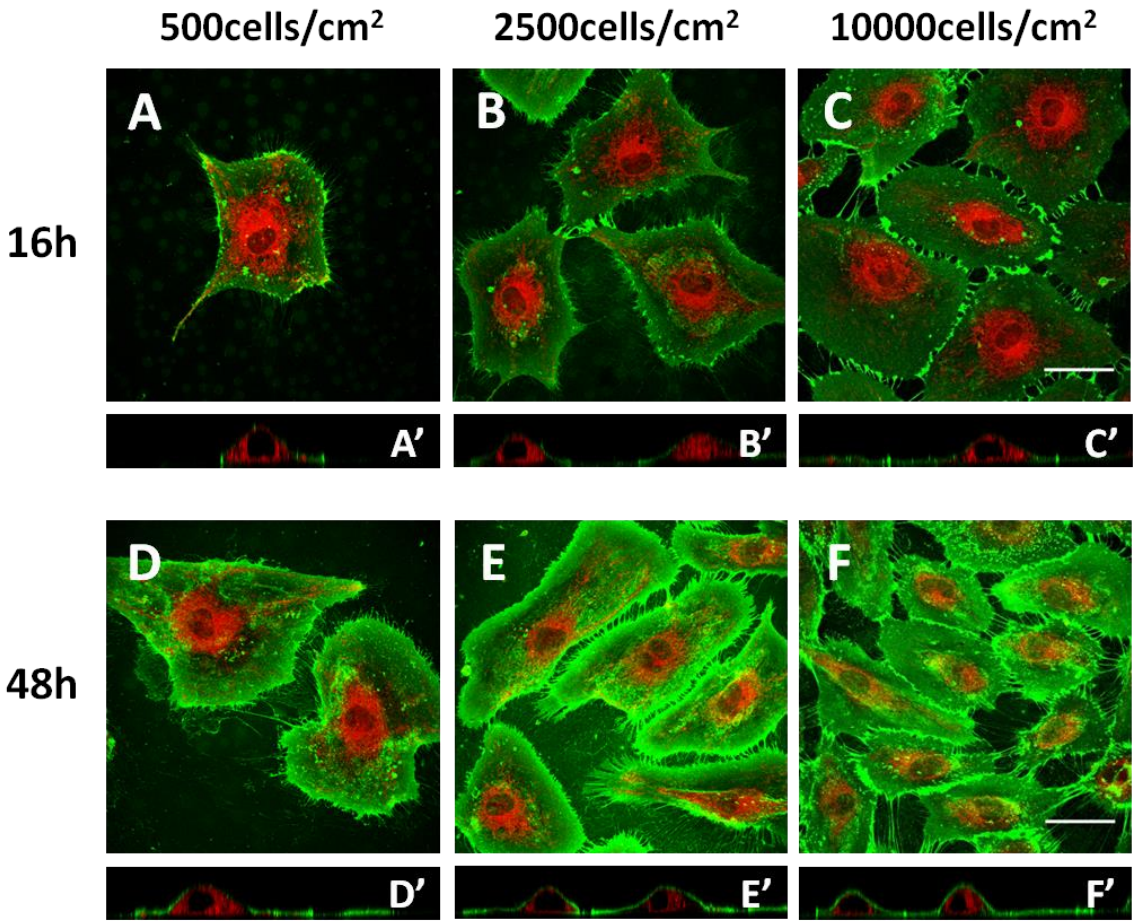

Figure 3.5 Recovery of the glycocalyx under different cell density cultures.

HUVECs with different seeding densities were cultured for 16h and 48h following trypsinization. A small amount of glycocalyx was recovered on the cell body for each group at 16h (A-C). (A) Density = 500cells/cm^2. (B) Density = 2500cells/cm^2. (C) Density = 10000cells/cm^2. The glycocalyx markedly recovered at 48h under moderate and high cell density culture (D-F). (D) Density = 500cells/cm^2. (E) Density = 2500cells/cm^2. (F) Density = 10000cells/cm^2. Scale bar = 50µm.

To quantify the total amount of the glycocalyx on the cell surface, the fluorescence intensity of the glycocalyx was measured. As shown in Fig 3-6.A, the intensities of the glycocalyx on the entire cell surface were significantly higher at 48h than at 16h for each pair of groups, indicating that the glycocalyx developed as time progressed. The intensities of the glycocalyx obtained from 48h were normalized compared to those from 16h and showed as intensity increments (Fig 3-6.B). The intensity of the glycocalyx under low cell density culture increased by 29.51±4.76% at 48h, whereas the increment was as high as 101.22±3.44% under high cell density culture. A remarkable increase of 57.90±3.26% was also found under moderate cell density culture. This increasing tendency suggested that higher cell density culture resulted in more rapid recovery of the glycocalyx. To distinguish the spatial development of glycocalyx, the entire cell surface was compartmentalized into the cell body and the protrusion. Changes in glycocalyx on the protrusion were proportional to those obtained from the entire cell surface. However, the recovery of the glycocalyx on the cell body varied. Under low cell density culture, the increase of 17.64±5.64% was insignificant, indicating that the glycocalyx recovered more slowly on the cell body. Contrarily, a larger increase was found under high cell density culture (cell body, 121.90±5.12% vs. 97.39±3.63% cell protrusion, $p<0.01$). This meant the recovery of the glycocalyx on the cell body had been additionally enhanced. The tendencies shown on the cell body and protrusion confirmed that the glycocalyx developed faster under higher cell density culture.

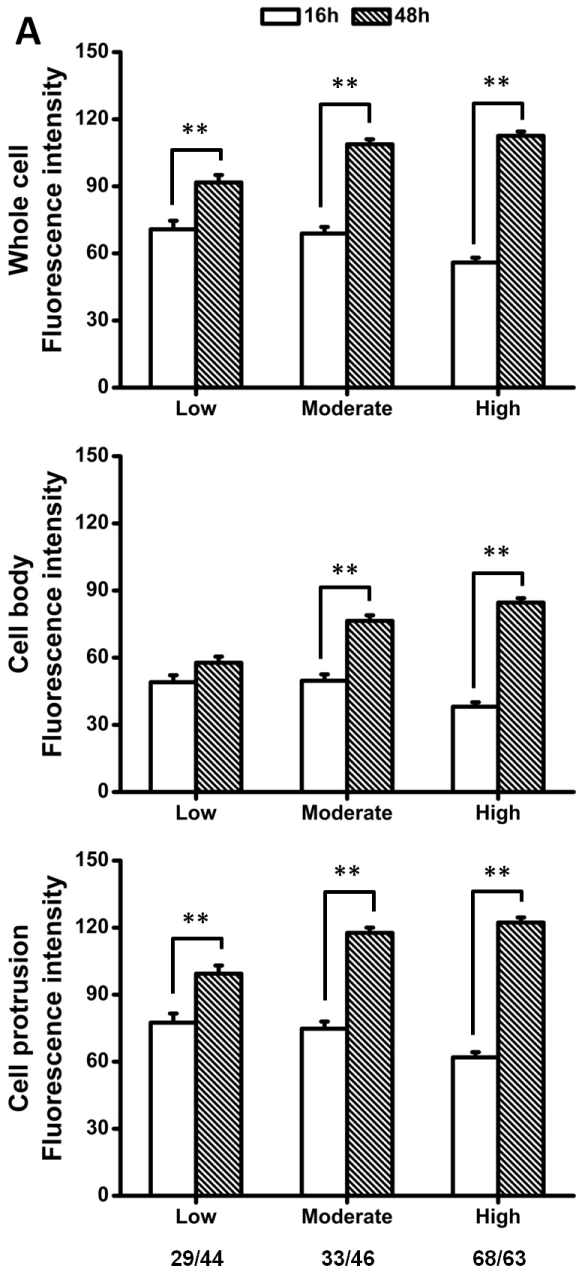

B

	Low	Moderate	High
Whole cell	29.51±4.76%	57.90±3.26%	101.22±3.44%
Cell body	17.64±5.64%	53.70±4.98%	121.90±5.12%**
Protrusion	28.22±4.71%	57.31±3.24%	97.39±3.63%

Figure 3.6 Higher cell density culture resulted in more rapid recovery of the glycocalyx.

Recovered glycocalyx was quantified at 16h and 48h by measuring fluorescence intensity. (A) The original intensity of the glycocalyx at each group. (B) Changes in the intensity of

*the glycocalyx from 16h to 48h. Higher cell density culture resulted in more rapid recovery of the glycocalyx on the entire cell surface. The recovery of the glycocalyx on the cell body was proportional to the change on the protrusion. Cell numbers tracked for each group were shown as N_{16h}/N_{48h}. *p<0.05, **p<0.01 when comparison was made between two parallel groups.*

In addition, the scaling of the fluorescence intensity showed that the labelling of the glycocalyx was always brighter on the protrusion than on the cell body. This was independent of culture time and cell seeding densities. Thus, to clarify the spatial distribution of glycocalyx, spatial coverage ratio was particularly calculated at 48h. Irrespective of cell density, spatial coverage ratio was always less than 1, supporting the fact that a larger amount of the glycocalyx covered the protrusion. Taking the cell density into consideration, we found that this ratio gradually increased alongside a higher cell density culture. Under low cell density culture, spatial coverage ratio was 0.58±0.019. The ratio further went up to 0.70±0.016 when a high cell density culture was employed. The numerical difference here was not large but nonetheless statistically significant. Accordingly, under low cell density culture, the glycocalyx tended to display as an unclear or non-continuous layer on the cell body, whereas the glycocalyx usually appeared as a uniform layer under high cell density culture. To further illustrate the potential mechanism for differential distribution, surface area ratio was also computed. Similarly, a surface area ratio less than 1 indicated that the protrusion accounted for a larger fraction of a whole cell. The ratio was as low as 0.24±0.012 under low cell density culture and increased to 0.37±0.017 under high cell density culture. Surface area ratio was well-correlated with the spatial coverage ratio, which in turn indicated that under low cell density culture, the

relatively small amount of glycocalyx covering the cell body could at least be partially attributed to the over-spreading protrusion. With an adequate retraction of cell protrusion, e.g., under high cell density culture, the recovery of the glycocalyx on the cell body was encouraged.

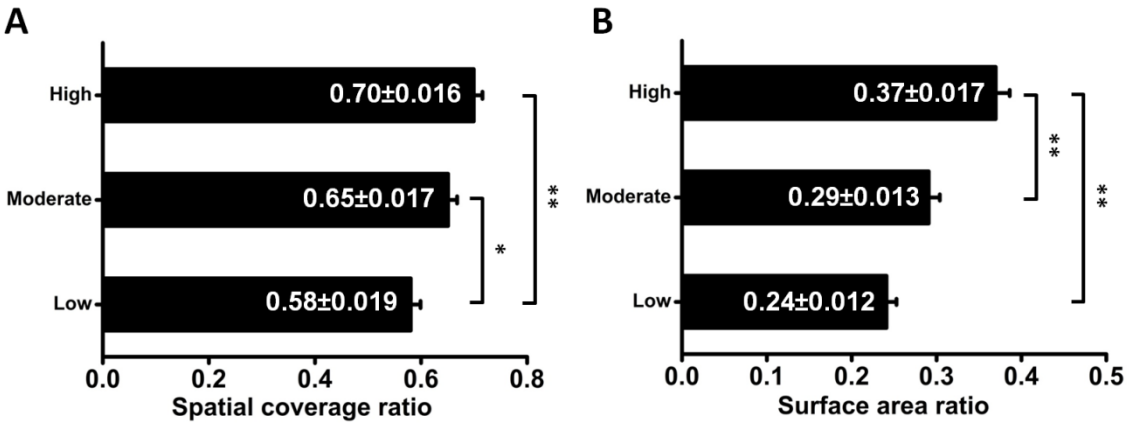

Figure 3.7 Higher cell density culture resulted in more uniform distribution of the glycocalyx.

*The spatial distribution of the glycocalyx at 48h was quantified through the use of spatial coverage ratio, which is defined as a ratio between the intensity of the glycocalyx on the cell body and the intensity on the protrusion. Higher cell density culture resulted in more uniform distribution of the glycocalyx (A). The spatial difference in glycocalyx distribution was positively correlated to the surface area difference between the cell body and the protrusion (B). *p<0.05, **p<0.01 when comparison was made between two parallel groups.*

3.3.3. The glycocalyx was well-developed on confluent cells

Given that a larger amount and better coverage of the glycocalyx were found at 48h under high cell density culture, we hypothesized that the glycocalyx was well-developed on confluent cells. The culture time for high, moderate and low cell density cultures were optimized to two days, seven days and 14 days for achieving cell confluence. Similar to two-day cultured cells, the cells grown for seven days and 14 days were covered with a distinct, continuous glycocalyx layer. The intensities of glycocalyx, particularly those obtained from the cell body, were similar to each other. Although significant differences were found on protrusion, these did not affect our conclusion because of the strong enough intensities of the glycocalyx and the clear glycocalyx layers shown in the confocal images. Moreover, we have shown that under low cell density culture, spatial coverage ratio increased from 0.58±0.019 at 48h to 0.71±0.015 at confluence. Surface area ratio reached up to 0.34±0.011. The cells from the other two groups shared a similar spatial coverage ratio and surface area ratio. Taken together, the data presented here prove our hypothesis that the glycocalyx was well-developed when culture time was prolonged for cell confluence.

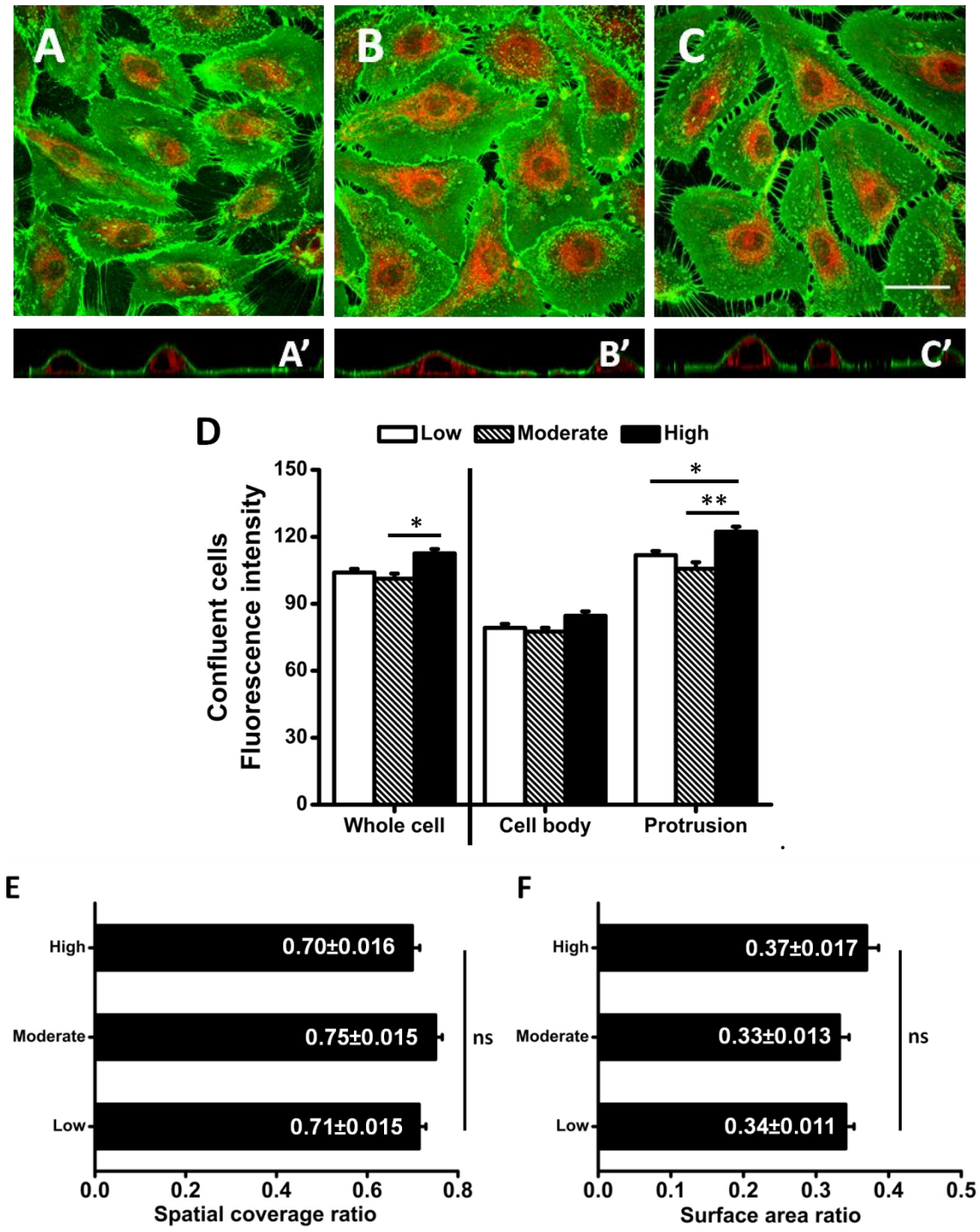

Figure 3.8 Glycocalyx was well-developed on confluent cells.

Cells with different seeding densities were continuously cultured for confluence. (A-C) Confluent cells from different groups exhibited uniform layers of the glycocalyx on the cell surface. (A) High density = 10000cells/cm^2. (B) Moderate density = 2500cells/cm^2. (C)

*Low density = 500cells/cm^2. Scale bar = 50μm. (D-F) Regardless of initial seeding densities, confluent cells from different groups shared the approximate intensity of the glycocalyx (C), spatial area ratio (E) and surface ratio (F). Cell numbers tracked for each group are 71 for 500cells/cm^2, 72 for 2500cells/cm^2, and 63 for 10000cells/cm^2. *p<0.05, **p<0.01 when comparison was made between each two groups.*

3.3.4. Cell shape played an important role in glycocalyx recovery

The effect of cell shape on glycocalyx recovery was investigated using a micropatterning technique. After a 2h subculture, the majority of the circular islands were covered by individual cells. Similar to the labelling pattern on suspended cells, the glycocalyx appeared as scattered patches on the cell surface. A large, dense patch was usually found on the central region of the cell surface, while a number of small patches were left on the rest of the cell surface. These individual cells remained attached to the islands for up to 24h of culture. The dense patch of glycocalyx was partially dispersed and the small patches became increasingly large, which eventually enabled the reformation of a continuous layer. Individual cells in maximum projection were stacked together and then projected once more using an average mode (Fig 3-9.E-F). This new projected image finally represented the mean intensity of the glycocalyx on individual cells and was plotted in the format of a heatmap. The heatmaps showed that the mean intensity of the glycocalyx was strikingly higher on the central region of the cell surface than on the cell periphery at a 2h subculture. As time progressed to 24h, the intensity of the glycocalyx on the cell periphery was also enhanced.

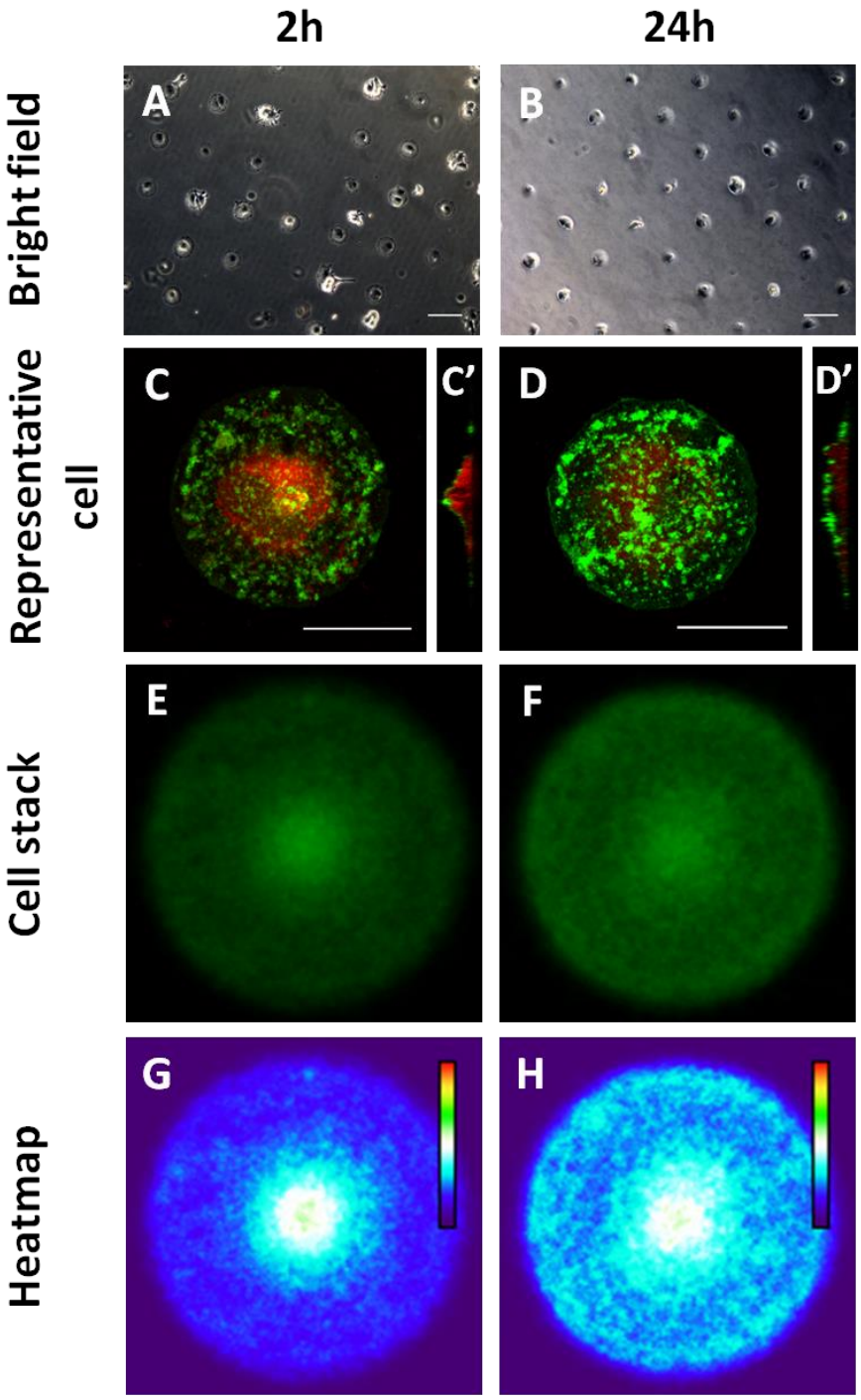

Figure 3.9 Recovery of the glycocalyx on a circular cell.

Individual cells adhering to circular micropatterns were cultured for 2h and 24h. (A, B) Bright field, scale bar = 100µm. (C, D) More glycocalyx was developed at 24h than at 2h. (E, F) All individual cells were stacked in average projection mode to show the mean

intensity of the glycocalyx on the cell surface. (G, H) The mean intensity of the glycocalyx was displayed in heatmap format. Scale bar = 25μm.

Similarly, elliptical islands were perfectly covered with individual cells at 2h. The pattern of the glycocalyx on the elongated cells, on the other hand, was completely different. Instead of a large patch aggregating on the cell surface, the glycocalyx patches distributed evenly on the entire cell surface. It was maintained when culture time proceeded for 24h. The coverage of the glycocalyx was further confirmed by heatmaps, where the mean intensity of the glycocalyx was relatively uniform throughout the entire culture period.

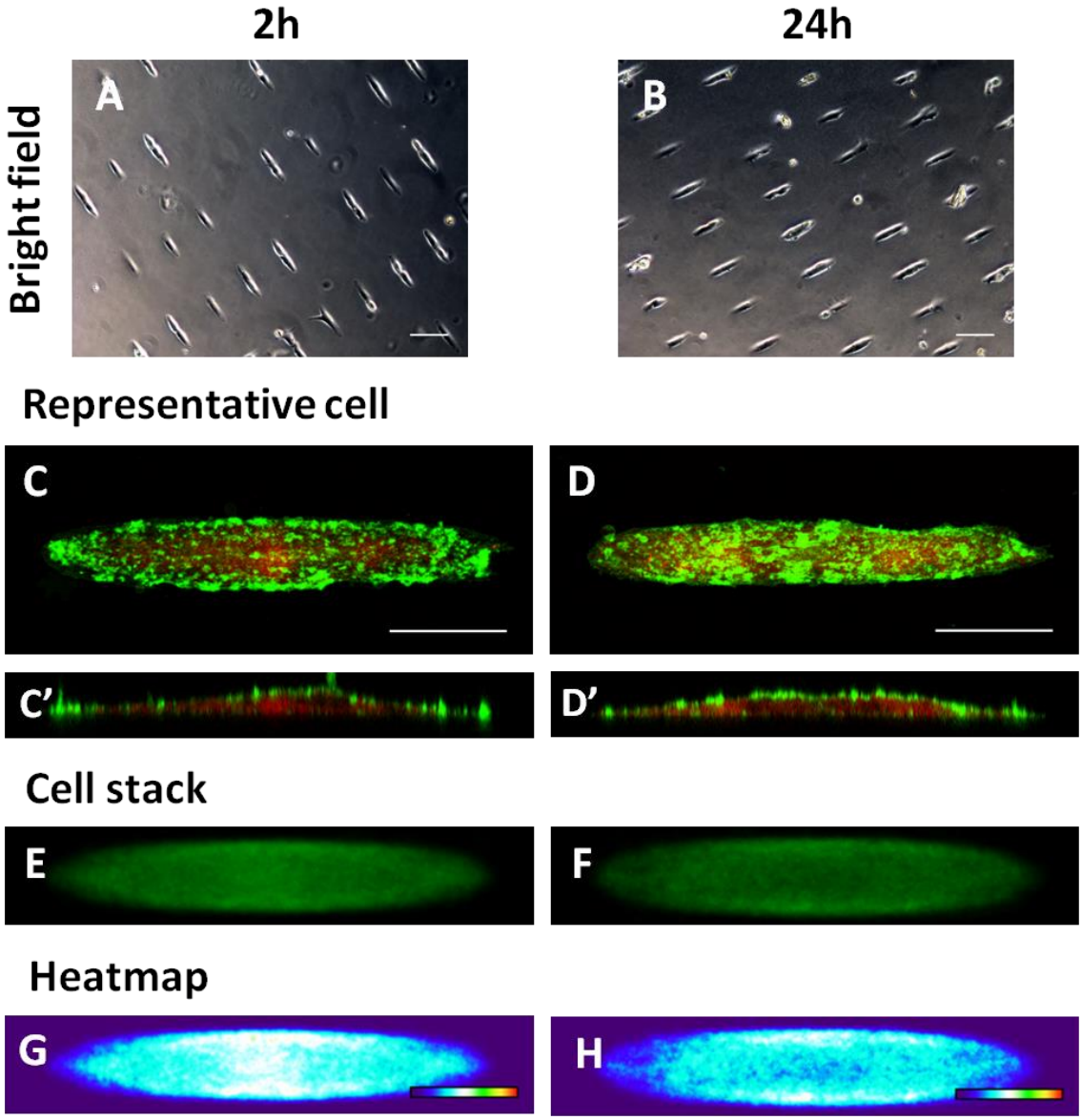

Figure 3.10 Recovery of the glycocalyx on an elliptical cell.

Individual cells adhering to elliptical micropatterns were cultured for 2h and 24h. (A, B) Bright field, scale bar = 100µm. (C, D) Well-developed glycocalyx is seen at both 2h and 24h. (E, F) All individual cells were stacked in an average projection mode to show the mean intensity of the glycocalyx on the cell surface. (G, H) The mean intensity of the glycocalyx was displayed in heatmap format. Scale bar = 25µm.

Finally, the differential recovery of the glycocalyx on circular cells and elliptical cells was quantified. For the circular cells, the mean intensity of the glycocalyx on the entire cell surface remarkably increased by 29.94±3.43% from 2h to 24h. However, the increase of the mean intensity for elliptical cells was negligible. This suggested that there was a further recovery of the glycocalyx on the surface of circular cells. Interestingly, a noticeable difference was found between circular cells and elliptical cells at 2h. Considering that the development of the glycocalyx was unlikely to start prior to cell reattachment, the stronger intensity measured on the elliptical cell surface was likely attributed to the faster dispersion of the residual glycocalyx. After 24 h cultures, the overall amount of the glycocalyx on circular and elliptical cells was equalized. Cell surface compartmentalization was also performed to distinguish the spatial recovery of the glycocalyx. For the cell body, there was an increase of 15.71±3.25% from 2h to 24h on circular cells. The glycocalyx was further recovered from the central region of the cell body to the rest of it. Contrarily, the intensity of the glycocalyx on elliptical cells was significantly reduced by 14.24±1.91%. The evident reduction on elliptical cells at 24h resulted from the faster dispersion of the glycocalyx at 2h, implying a negative feedback that regulates the over-crowded glycocalyx on the cell body. Although the order of magnitude of the intensity of the glycocalyx was much lower on the cell protrusion, the intensities of the glycocalyx on the protrusion of circular cells and elliptical cells were both enhanced as a result of the progression of culture time. In addition, the increase of the intensity of the glycocalyx on both cell protrusions was much larger than on the cell body (Fig 3-11.B). The glycocalyx was preferentially developed on regions short of the glycocalyx.

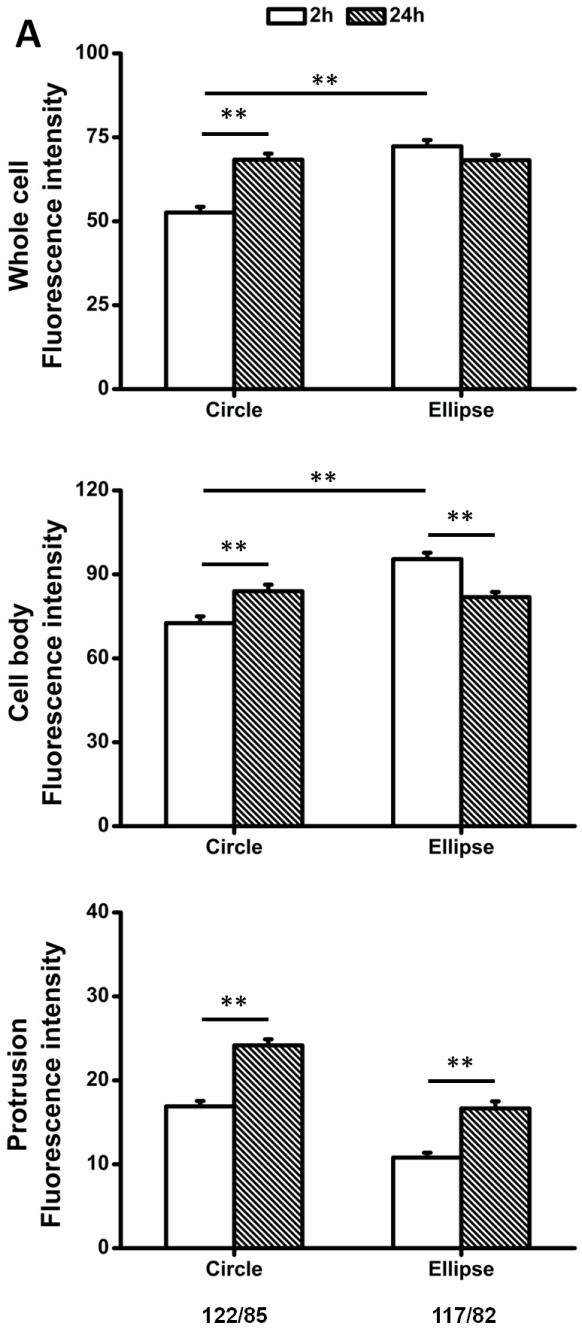

B

	Circle	Ellipse
Whole cell	29.94±3.43%	-5.68±2.16%
Cell body	15.71±3.25%	-14.24±1.91%
Protrusion	43.06±4.24%	54.13±7.85%

Figure 3.11 Elliptical cell shape led to more rapid recovery of the glycocalyx during the early stage of recovery.

*(A) The original intensity of the glycocalyx at each group. Elliptical cell shape led to more rapid recovery of the glycocalyx at 2h. (B) Changes in the intensity of the glycocalyx from 2h to 24h. Glycocalyx recovery on elliptical cell surface was saturated during this period. Cell numbers tracked for each group were shown as N_{2h}/N_{24h}. *p<0.05, **p<0.01 when comparison was made between two parallel groups.*

As previously described, the spatial coverage ratio was usually less than 1 under normal cell culture circumstances. However, this ratio was reversed on the micropatterned cells; here, the ratio was much greater than 1, suggesting that the distribution of the glycocalyx was more uneven on the cell surface. Although the ratios on both cell patterns decreased from 2h to 24h, the uneven distribution of glycocalyx still existed. A first glance at the decline of the spatial coverage ratio indicated that it was plausible that the recovery of glycocalyx occurred faster on the elliptical cells than on the circular cells. However, this discrepancy was clarified according to the surface area ratio. The cell attachment pattern varied according to cell shapes and the cells attached to the elliptical island with little protrusion, whereas the cells spread on the circular island with large protrusion. Accordingly, the surface area ratio of elliptical cells reached up to 1.96, but the ratio of circular cells was as low as 0.53. Since the ratio differed in the opposite direction, judging the recovery of glycocalyx according to the decline of spatial coverage ratio was inappropriate in this instance.

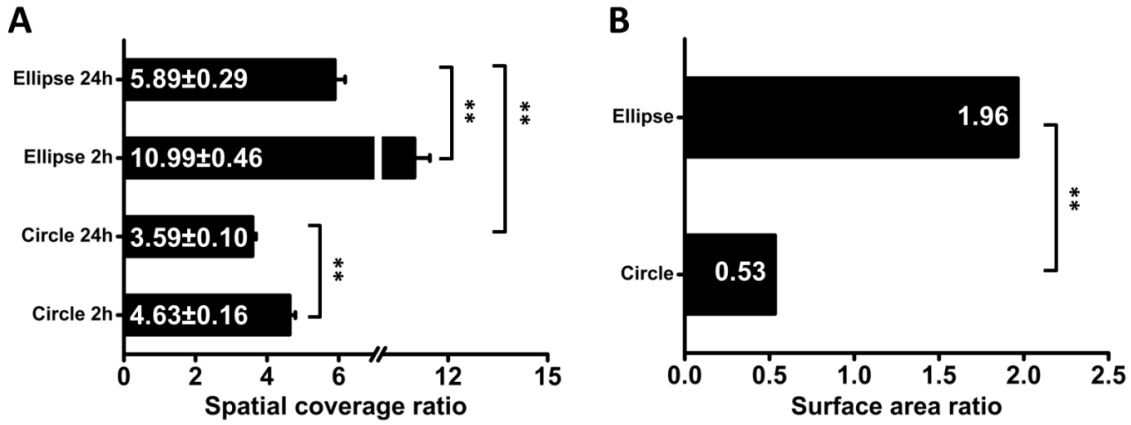

Figure 3.12 Elliptical cells exhibited smaller protrusion, leading to more glycocalyx recovered on the cell body.

*(A) Elliptical cell shape led to more glycocalyx recovered on the cell body, although the spatial coverage ratio reduced from 2h to 24h. (B) The spatial difference in glycocalyx distribution was attributed to the surface area difference between the cell body and the protrusion. The surface area ratio on time scale was not shown because micropatterned cells at 2h and 24h were outlined using the same ROIs. *p<0.05, **p<0.01 when comparison was made between two parallel groups.*

3.4. Discussion

In this study, our results showed that 1) the glycocalyx was severely damaged after trypsinization; 2) higher cell density culture resulted in more rapid recovery of the glycocalyx; 3) higher cell density culture resulted in more uniform distribution of the glycocalyx; 4) the glycocalyx was well-developed in confluent cells; 5) elliptical cell shape led to more rapid recovery of the glycocalyx during the early stage of recovery.

3.4.1. Visualization of glycocalyx components

The glycocalyx is an elaborate, carbohydrate-protein complex that lines the luminal surface of the endothelium. With the disclosure of glycocalyx compositions, the glycocalyx can be visualized by specific dyes that bind to one or more of its components. SA coats to the outmost end of the glycoproteins in the glycocalyx. SA contains carboxyl groups that render the glycocalyx with a bulk of negative charges in physiological pH. Visualization of the SA by confocal microscopy is in accordance with EM, where cationic molecules are usually applied for labelling the glycocalyx (Luft, 1966, Adamson and Clough, 1992). In the present study, we applied 10μg/ml FITC-WGA for 15mins to visualize the SA on the cell surface. We showed the presence of an intensive and evenly distributed layer covering the confluent HUVECs. The thickness of this layer was estimated to be 1~1.5μm. Our findings were consistent with those reported by Barker et al. (Barker et al., 2004), where a layer of glycocalyx was also observed on the primary HUVECs following incubation with 2μg/ml FITC-WGA for 30mins. The estimated thickness there reached up to 2.5±0.5μm, which was almost two times greater than ours. Considering the same cell type and similar labelling protocols we employed, the difference in dimension was likely due to the differential axial resolution in confocal microscopy. The axial resolution set in Barker et al.'s study was only 650nm, which was two-fold lower than that in our study (235.8nm). To our knowledge, a low z-axis resolution is usually accompanied with a smearing effect in the cross-sectional image, which blurs the layer boundary and then increases the thickness of the layer.

HS is the main constituent of the proteoglycans in the glycocalyx. Labelling of HS was of great interest to the researchers due to its crucial role in mechanotransduction. This label was preferentially used by Tarbell and his co-workers (Thi et al., 2004, Zeng et al., 2013). One of their early studies showed the development of the glycocalyx on rat fat-pad endothelial cells to be nutrient dependent. When the cells were cultured in DMEM only, the HS appeared as scattered patches on the cell surface. However, these patches were further enlarged and joined together as an intensive, continuous layer when 10% FBS was added. There was a 25% increase in the expression of HS. We also performed immunostaining so as to image the HS on HUVECs. Unexpectedly, as shown in the images in Fig 3-13, even though a higher concentration (1:50) of primary antibody was used, the HS was weakly labelled. Only a few scattered dots (arrows) appeared on the cell surface. This was independent of the nutrient (20% FBS), culture time, as well as the extent of cell confluence. In addition, the colocalization of HS and SA clearly showed SA to be dominant over HS. Our data demonstrated that only a small amount of HS was expressed on the surface of HUVECs and that this was structurally negligible compared to the SA. Thus, we chose SA as representative of the glycocalyx.

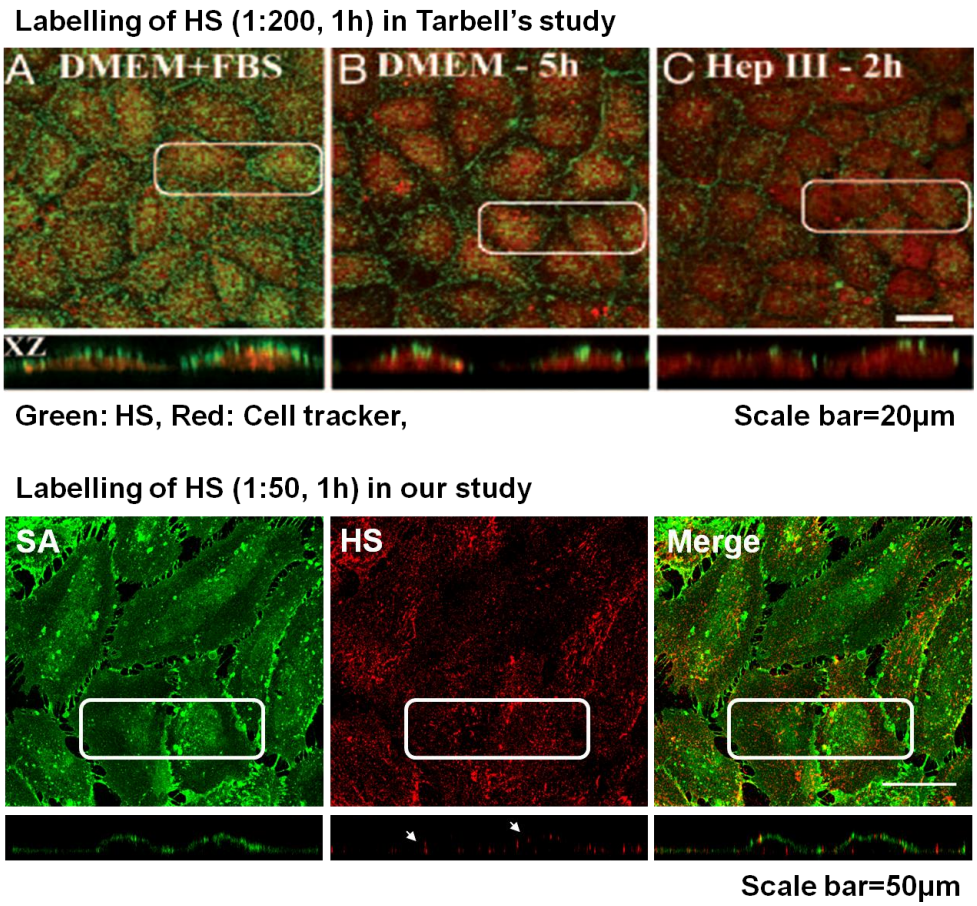

Figure 3.13 Labelling heparan sulphate on the surface of endothelial cells.

(Adapted from Thi et al., 2004)

3.4.2. Quantification of the glycocalyx

A number of methods have been developed for quantifying the glycocalyx in projected images (Barker et al., 2004, Zeng et al., 2012, Koo et al., 2013, Zeng et al., 2013). These parameters include the mean intensity and its derivatives such as coverage and thickness. The selection of parameters is determined by the pattern of immunostaining. For example, the labelling pattern of HS displayed as scattered patches with gaps. Coverage can reflect how dense the glycocalyx distributes on the cell surface; it is independent of the mean

intensity. Contrarily, the SA is labelled as a uniform layer on the cell surface. Even though the SA is exclusively degraded by the neuraminidase, a low intensity layer still remains based on the FITC-WGA staining. In this instance, coverage will be maintained at a high percentage. It is impracticable to discern the differential recovery of the glycocalyx. Thickness is another well-accepted parameter and the accuracy for measuring it depends highly on the intensity and the uniformity of the staining shown on the cross-sectional images. If intensity is low, thickness will be easily overestimated because of the smearing effect. If the layer is non-uniform (e.g., HS), thickness will be inaccurate due to the difference between well-developed region and the poorly-developed region of the glycocalyx. Accordingly, we stuck to the mean intensity, which referred to the total amount of the glycocalyx covered on the cell surface. We also performed normalization either to the control or the previous time point, which helped to eliminate errors between experimental groups. Furthermore, we compartmentalized cell surface into cell body and protrusion. By doing this, we provided information for the spatial distribution of the glycocalyx. This calculation was applied in our group to show the redistribution of the glycocalyx in shear flow (Bai and Wang, 2014). In addition to two-dimensional analysis, we also investigated the quantification in terms of three-dimensionality. This is an encouraging approach, as reconstructing the glycocalyx enables us to analyse the structure of the glycocalyx in terms of real cellular geometry. This work will be continued in combination with using the super resolution confocal microscope, which was recently newly equipped in our lab.

3.4.3. Recovery of the glycocalyx under different cell density cultures

Aspects of the glycocalyx coverage on endothelial cells *in vitro* are controversial. Chapell et al. (Chappell et al., 2009c) reported the glycocalyx visualized by EM to be much thinner on cultured HUVECs (29.4nm) than on umbilical vein endothelium (878nm). Particularly, the extent of cell confluence was considered for the first time *in vitro*. The cells cultured for six days were regarded as non-confluent cells, while those cultured for 12 days referred to fully confluent cells. The dimension of the glycocalyx was not changed at all. Both non-confluent and confluent cells displayed sparse glycocalyx layers on the surface. In contrast to the work of Chappell et al., we observed that there was differential recovery of the glycocalyx between non-confluent and confluent cells, based on the labelling of SA. The intensity increments from 16h to 48h at low, moderate and high density culture were calculated to be 29.51±4.76%, 57.90±3.26% and 101.22±3.44%, respectively. The difference in terms of glycocalyx coverage was further supported by the spatial coverage ratio at 48h, which was 0.58±0.019 for non-confluent cells, but reached up to 0.70±0.016 for confluent cells. This increasing tendency indicated that the higher the seeding density used, the faster the recovery of the glycocalyx was achieved.

The recovery of the glycocalyx is an outcome of the coordination between cell cycles and glycosylation. Cell cycles are serial, circulating events that require DNA duplication and numerous protein syntheses. On the other hand, glycosylation is an enzymatic process that modifies, transports and anchors glycans to membrane-bound proteins or lipids. Under non-confluent conditions, especially at sparse density, cellular energy is mainly spent on

cell cycles. The synthesis of DNA and protein is dominant, so that it drives cells towards proliferation. The interval between each cycle is shorter than the time required for sufficient glycosylation. Thus, the recovery of the glycocalyx is compromised. However, cell proliferation is gradually inhinited by cell contact inhibition. Biosynthetic activity for the progression of cell cycles is slowed down, whereas the glycosylation for constructing the glycocalyx is enhanced. When the confluence is fully established, cells enter the G0/G1 phase and remain quiescent. At this stage, robust glycosylation is maintained, which finally promotes the more rapid recovery of the glycocalyx on the cell surface. If the confluent cells are further cultured, the cells will squeeze. This not only activates cell apoptosis and detachment, but also suspends glycosylation. As a result, the equilibrium between development and digestion of the glycocalyx is broken and the well-developed glycocalyx turns towards shedding.

There is also the possibility that the recovery of the glycocalyx is closely related to cell spreading. Our speculation regarding this arises from the observation that cell size, especially the fraction of protrusion, gradually decreased from low cell density culture to high cell density culture. The inhibition of cell spreading induces a reduction in the cell stiffness (Stroka and Aranda-Espinoza, 2011). The change in cell stiffness in turn should impact on biosynthetic activities such as glycosylation. Accordingly, owing to the enlarged protrusion in non-confluent cells, an additional tension is applied to the cell surface. The “land” for growing the glycocalyx becomes stiffer so that either the anchorage of glycans to the developing glycocalyx is decreased, or the well-developed glycocalyx is shed. Contrastingly, when the cells become confluent, the spreading of protrusions is constrained. The tension exerted on the confluent cell surface is reduced, which is followed by a

softening of the “land” for growing the glycocalyx. Hence, the recovery of the glycocalyx is encouraged.

Although the recovery of the glycocalyx occurred relatively fast in high cell density culture, the spatial coverage ratio was only increased to 0.70±0.016. More glycocalyx was distributed on the protrusion; this was further supported by an experiment where different cell densities were cultured for confluence. We showed that after two, seven and 14 days, the spatial coverage ratio for high, moderate and low seeding density culture were saturated at a similar level of 0.7. Regarding the second mechanism proposed above, we believe that the spatial distribution of the glycocalyx at well-developed stage had also been determined by the size differences between the cell body and the protrusion. The surface area ratio was elevated as culture time progressed. However, a ratio remaining less than 1 indicated that the cell body region always remained smaller than the protrusion. The tension produced by the spreading of the protrusion can be decreased but cannot be ignored. Given that the protrusion remains in the same plane, whereas the cell body possesses a curving geometry, the cell body is more vulnerable to the applied force, so that the coverage of the glycocalyx is diminished.

3.4.4. Recovery of the glycocalyx on different micropatterned cells

Our emphasis on the recovery of the glycocalyx was initially based on the extent of cell confluence. Cultured cells normally spread either in an irregular or cobblestone-like pattern. In a natural microenvironment, endothelial cells are ceaselessly subjected to blood flow. Correspondingly, these cells are always elongated along the blood flow direction. Several

studies (Gouverneur et al., 2006b, Maroski et al., 2011, Henderson-Toth et al., 2012) have demonstrated the importance of shear stress on the regulation of glycocalyx expression. However, the relationship between cell morphology and the recovery of the glycocalyx remains poorly defined.

Micropatterning is an engineering technique that controls the crucial parameters of the cell microenvironment. Cells reshaped by micropatterning undergo a number of subcellular changes (Thery, 2010, Anderson and Hinds, 2011). It has been reported that gene/protein expression (e.g. vascular cell adhesion molecules and intercellular adhesion molecules) is diverse on micropatterned and non-micropatterned endothelial cells (Kato et al., 2001, Vartanian et al., 2010). Cytoskeletal elements anchored on the basal membrane (e.g. FAs) were also redistributed (Gautrot et al., 2010a, Kandere-Grzybowska et al., 2010). To our knowledge, using micropatterning for investigating the glycocalyx has not previously been described. Hence, we demonstrated for the first time the recovery of the glycocalyx on micropatterned cells.

In our work, we found that the glycocalyx dispersed faster on elongated cells following the initial culture. Once again, the differential recovery of the glycocalyx was likely due to cell spreading. The circular cells attached normally, so that the protrusion was larger than the cell body. Contrarily, the elongated cells spread through micropatterns mainly through the cell body. Little protrusion was formed on the cell periphery. This was consistent with findings obtained by Roca-Cusachs et al. (Roca-Cusachs et al., 2008), where micropattern with a surface area of 2500μm^2 and a shape factor of 6 was used. In that particular study,

the researchers demonstrated that cell elongation reduced cell stiffness and cell contractility, both of which reflected the reduction of cellular tension. Membrane tension has the ability to coordinate the processes involved in membrane deformations. It is speculated that the decreased membrane tension facilitated the rapid dispersion of the glycocalyx on the body of elongated cell. We also observed that the glycocalyx on the body of circular cell was significantly increased as time progressed, whereas the glycocalyx on the body of elongated cell was noticeably decreased. The intensity of the glycocalyx maintained at a relative high magnitude supported the notion that the glycocalyx on the body of elongated cell was already saturated after 2h dispersion. To maintain an adequate amount of glycocalyx on the cell surface, the development activity of the glycocalyx needed to be suspended and digestion activity was enhanced. This negative feedback loop thus cleaved excessive glycocalyx on the body of elongated cell. In addition, we did not employ shear flow in the current study. Our results demonstrated that cell morphology affected the recovery of the glycocalyx. How much it can potentially affect the coverage of the glycocalyx in shear flow is unknown. This unaddressed issue is of great interest to our group and will be further addressed in future work.

Altogether, we propose that the full recovery of the glycocalyx *in vitro* is achieved through two steps: dispersion from the residual glycocalyx and the development of the new glycocalyx. All these processes are at least partially determined by the extent of cell spreading, which involves the coordination of mechanical properties and glycosylation. Further research will be conducted on the effects of cell mechanics in order to combine biophysical properties and biochemical events across cells.

In conclusion, I have demonstrated that cell seeding density and cell shape both affect the recovery of the glycocalyx *in vitro*. In particular, elongated cell shape, which is conformed by a novel technology i.e. micropatterning, results in more rapid recovery of the glycocalyx. These findings further our knowledge of the glycocalyx formation. A better understanding of this process will lead to better approaches for restoring the glycocalyx in diseases.

4. Contribution of the actin cytoskeleton to the stability of the glycocalyx

4.1. Introduction

The endothelial glycocalyx continuously develops and sheds under physiological conditions. Over-shedding of the glycocalyx triggers endothelial dysfunction and eventually contributes to the occurrence and development of cardiovascular diseases (Reitsma et al., 2007, Weinbaum et al., 2007). Some pathological stimuli, including hypoxia, reperfusion following ischemia and inflammatory stimuli have been found to be involved in the perturbation of the glycocalyx. (Lipowsky et al., 2011, Annecke et al., 2011, Mulivor and Lipowsky, 2004). These stimuli provoke the degradation of the glycocalyx components by activating proteases and/or reactive oxygen species. Treatments of anti-thrombin and anti-oxidant counteract the abilities of proteases and reactive oxygen species, which in turn prevent the shedding of the glycocalyx under pathological conditions. (Chappell et al., 2009a, Chappell et al., 2009b, Mulivor and Lipowsky, 2009). It is believed that deepening the understanding of the stability of the glycocalyx will help to develop new therapeutic strategies against the shedding of the glycocalyx.

Structural connection between the glycocalyx and the actin cytoskeleton had not been recognized until the ultrastructure of the glycocalyx was demonstrated in 2001. The researchers proposed that the glycocalyx was anchored to the cortical actin filaments via a hexagonal arrangement (Squire et al., 2001). On the basis of this model, Weinbaum et al.

further suggested that core proteins arranged in the bush-like structures were ideal to act as mechanotransducers for converting shear stress from the edge of the glycocalyx to the actin cytoskeleton (Weinbaum et al., 2003). If the integrity of the glycocalyx is compromised, the adaption of the actin cytoskeleton to shear stress is suppressed (Ebong et al., 2014, Thi et al., 2004). To date, the research has been focused on the mechanical transduction from the glycocalyx to the actin cytoskeleton. No study has reported that how the actin cytoskeleton contributes to the glycocalyx. The actin cytoskeleton provides physical support to the cell membrane. Whether actin depolymerisation has the potential to destabilize the glycocalyx is poorly understood. Therefore, we aim to investigate the contribution of the actin cytoskeleton to the stability of the endothelial glycocalyx *in vitro*.

To probe the stability of the endothelial glycocalyx, four questions are addressed in this chapter (Fig 4-1): 1) whether glycocalyx shedding occurs when the actin cytoskeleton is rapidly depolymerised; 2) whether glycocalyx shedding occurs following persistent actin depolymerisation; 3) whether glycocalyx shedding occurs in the presence of shear stress; 4) correlation between the shedding of the glycocalyx and the disassembly of focal adhesions.

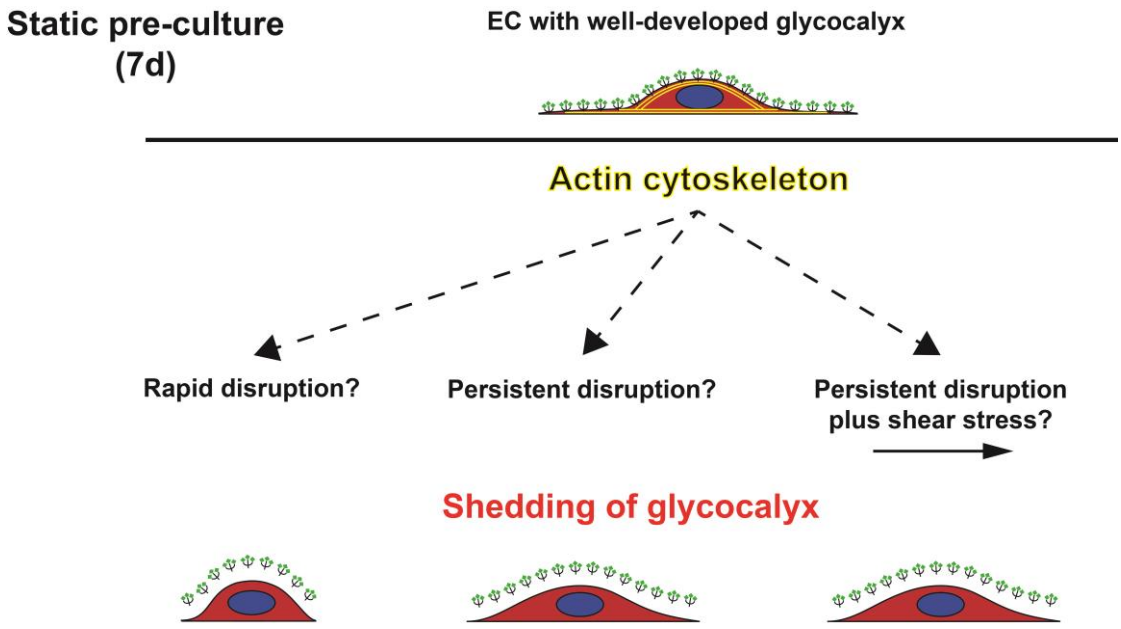

Figure 4.1 Diagram of possible contribution of the actin cytoskeleton to the stability of the glycocalyx.

4.2. Methodology highlights

4.2.1. Pre-culture time

In chapter 3, we demonstrated that the glycocalyx was well-developed on confluent cells. We also found that two-week culture (low cell density) and two-day culture (high cell density) were not ideal for obtaining a perfect cell monolayer. When low cell density culture was used, cells proliferated and then aggregated to a cluster, which resulted in non-uniform distribution of cells in the monolayer. For high cell density culture, culture time was too short so that cell-cell adhesion was not tightly formed. In addition, over-confluent cells were discarded. The cells under this condition were squeezed rather than well-spreading, leading to a weak cell attachment to the substrate. As a result, these cells were more vulnerable, so that confused the actual effect from actin-destabilizing agent.

Accordingly, HUVECs at a density of 2500cells/cm^2 were cultured for 1 week prior to drug treatment.

4.2.2. Cytochalasin D treatment

The role of the actin cytoskeleton in the stability of the glycocalyx was investigated using cytochalasin D (CD). CD is an actin-targeting drug that promotes actin depolymerisation. CD concentration ranging from 250nM to 2000nM was tested for verifying dose- and time-dependent effects. To maintain actin depolymerisation during shear stress stimulation, confluent cells were incubated with 250nM CD for 1h and then subjected to shear stress, concurrent with 30nM CD.

4.2.3. Labelling of the glycocalyx

As stated before, the glycocalyx was labelled prior to cell fixation. This protocol prevented the formation of small pores on the cell surface, so that inhibited the permeation of FITC-WGA. However, actin depolymerisation was reversible when CD medium was discarded. Performing the labelling prior to the fixation affected cell morphology and the coverage of the glycocalyx. Accordingly, slight fixation for 3mins was executed prior to the labelling of the glycocalyx, which helped to slow down actin repolymerization without influence on the cell membrane. Following on, slightly-fixed cells were labelled according to the procedure stated before.

4.3. Results

4.3.1. Glycocalyx was preserved after rapid actin depolymerisation

The extent of rapid actin depolymerisation induced by CD was investigated prior to assessing the stability of the glycocalyx. As shown in Fig 4-2.A-C, after 10min incubation, F-actins in endothelial cells were partially depolymerised by 500nM CD and completely depolymerised by 1000nM CD. The line profiles of F-actins (Fig 4-2.B''-C'') show that the intensities of remaining F-actins were weaker at 1000nM CD than at 500nM CD, suggesting that 1000nM CD was optimal for completely depolymerizing the actin cytoskeleton. In addition to actin depolymerisation, cell morphology changed. The cells kept spreading and partially connecting to one another when subjected to 500nM CD, whereas the cells treated with 1000nM CD apparently retracted, leaving few contacts available to their neighbours. With the increase of CD concentration or incubation time, cell rounding easily occurred and caused cell detachment. When 1000nM CD was replaced with a fresh CD-free medium, F-actins were repolymerized within 10mins. Although repolymerization of actin filaments was observed to cover the cells, F-actin staining was much more intensive at the junctional regions of cells, suggesting that actin repolymerization had been initiated from the cell periphery to the centroid of the cell. Following 60mins refreshment, F-actins far away from the junctional regions were further polymerized and recovered to a pre-treated level, which was confirmed by the increase of F-actin intensities in line profiles from 10min to 60min recovery. All of the above results verified that the disruption of the actin cytoskeleton was reversible. Cells were able to fully respread through the repolymerization of F-actins.

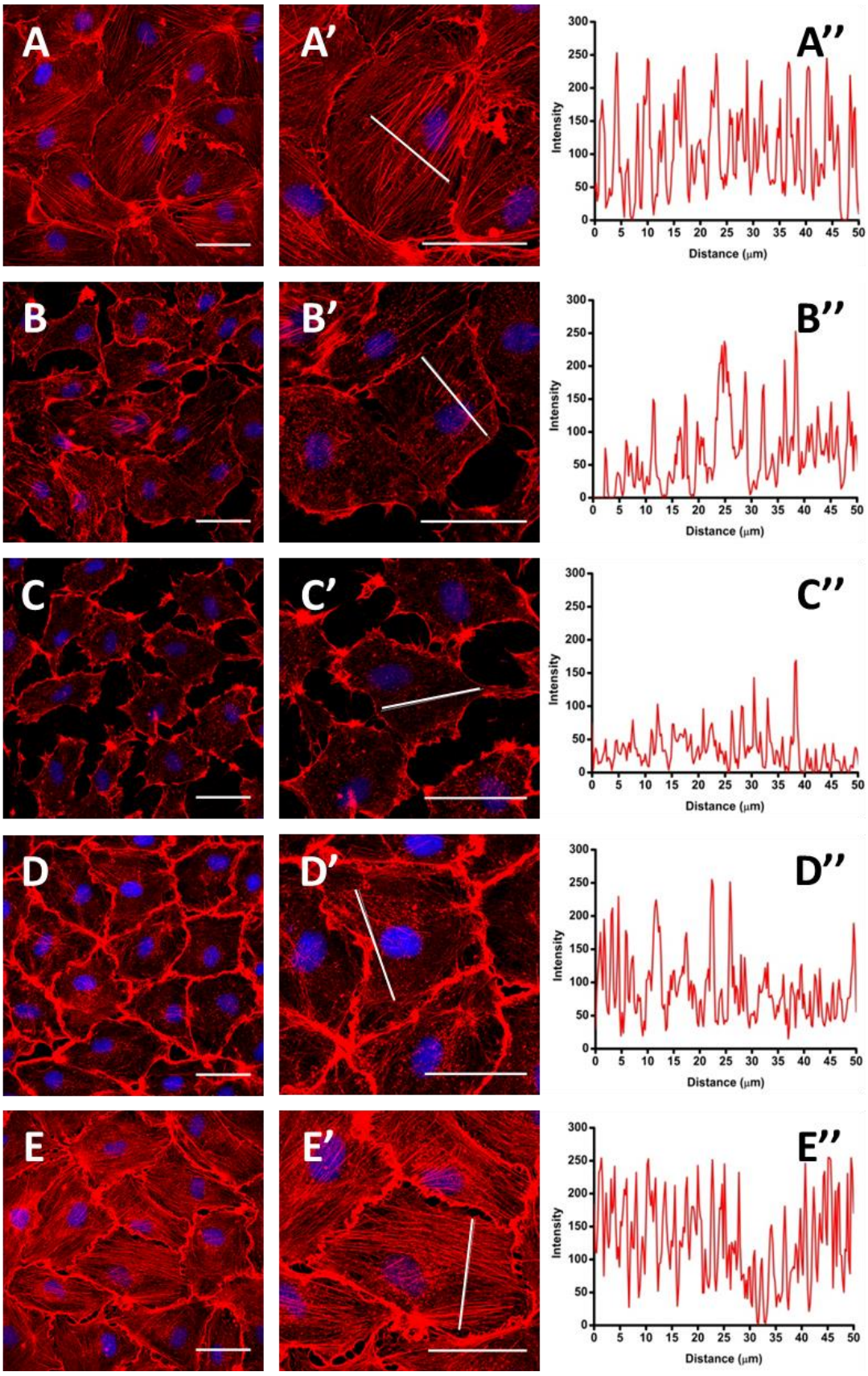

Figure 4.2 CD at high concentration rapidly depolymerised the actin cytoskeleton.

Confluent cells were subjected to a medium with different concentrations of CD for 10mins. The actin cytoskeleton was partially depolymerised by 500nM (B) and completely depolymerised by 1000nM (C). After rapid depolymerisation by 1000nM CD, the medium was replaced with a CD-free medium for actin repolymerization. The actin cytoskeleton was partially recovered at 10mins (D) and fully recovered at 60mins (E). Scale bar = 50μm. A line was drawn across F-actins at representative cell (A'-E') and plotted as intensity profile (A''-E'').

To further quantify F-actins after depolymerisation and repolymerization, the number of F-actin filaments was counted using FilaQuant (Fig 4-3.A). The filament number was 75.86±5.14/cell prior to CD treatment and decreased to 63.63±5.03/cell at 500nM CD, followed by a further two-fold reduction at 1000nM CD (31.37±2.03/cell). Following replacement with a fresh CD-free medium, the filament number was recovered twice at 10min recovery (59.14±3.07/cell) and reached 71.67±4.61/cell at 60mins. The change of filament number was positively correlated to the change of basal cell surface area, which is a common indicator for cell spreading (Fig 4-3.B). The basal surface area dropped from 4214.24±89.51μm^2 to 3288.25±60.82μm^2 at 500nM CD, followed by a further reduction of 2043.70±54.01μm^2 at 1000nM CD. After discarding the CD-free medium, the basal surface area immediately shifted back to 3418.03±47.96μm^2 within 10mins. The cells kept on spreading until the actin cytoskeleton had been fully repolymerized. The final cell surface area returned to 4382.36±73.56μm^2.

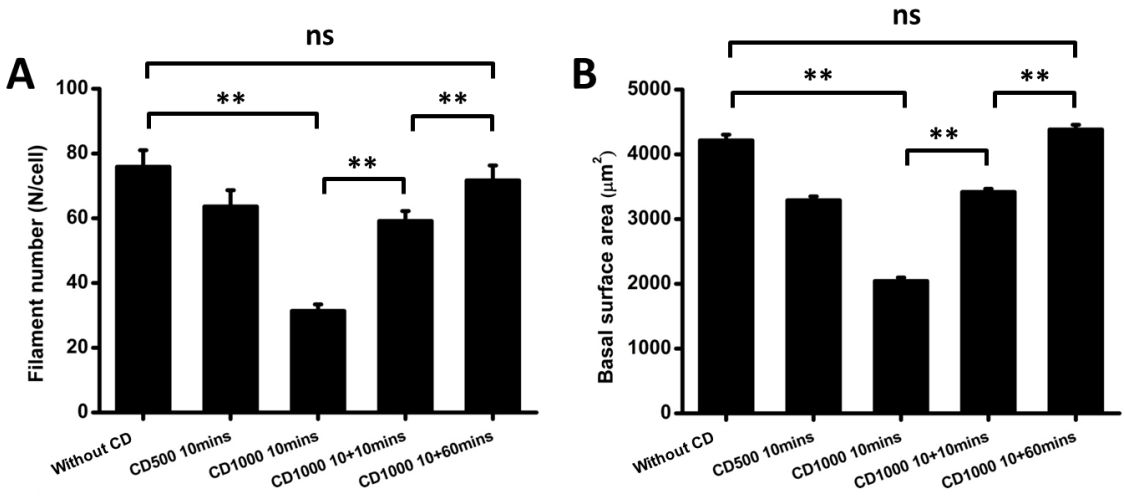

Figure 4.3 Rapid actin depolymerisation resulted in severe cell retraction.

*Actin depolymerisation was quantified by measuring the actin filament number. Filament number decreased when the actin cytoskeleton was disrupted and rebound following the removal of CD (A). Filament number was positively correlated to the basal surface area (B). Cell numbers tracked for each group were 32 for before CD, 24 for 500nM CD, 27 for 1000nM CD, 35 for 1000nM CD plus 10mins recovery, and 30 for 1000nM CD plus 60mins recovery. *p<0.05, **p<0.01 when comparison was made between each two groups.*

Following on, the shedding of the glycocalyx on actin-depolymerised cells was evaluated. For cells without CD treatment (Fig 4-4.A), the well-developed glycocalyx was shown as a continuous layer covering the cell surface. After robustly disrupting the actin cytoskeleton for 10mins, this layer was preserved on retracting cells rather than shed (Fig 4-4.B), suggesting that the glycocalyx was stable even if the actin cytoskeleton was lost. Since disruption of the actin cytoskeleton was reversible, the glycocalyx was also examined when the actin cytoskeleton was repolymerized. As shown in Fig 4-4.C, the cells

respreading for 10mins still showed a well-preserved glycocalyx layer on the cell surface. Glycocalyx coverage was retained when recovery time increased to 60mins. To quantify changes in the glycocalyx on the cell surface, fluorescence intensities measured on actin-depolymerised and actin-repolymerized cells were normalized to the intensity of same day control. For the entire cell surface, the intensity of the glycocalyx slightly increased after rapid actin depolymerisation. However, no significance was found when it was compared to the control and other groups, confirming that the glycocalyx was well-preserved after rapid actin depolymerisation and repolymerization. In addition, the entire cell surface had been compartmentalized. The intensities of the glycocalyx on the cell body shared similar changes to those observed on the cell protrusion, both of which were consistent with the changes obtained from the entire cell surface.

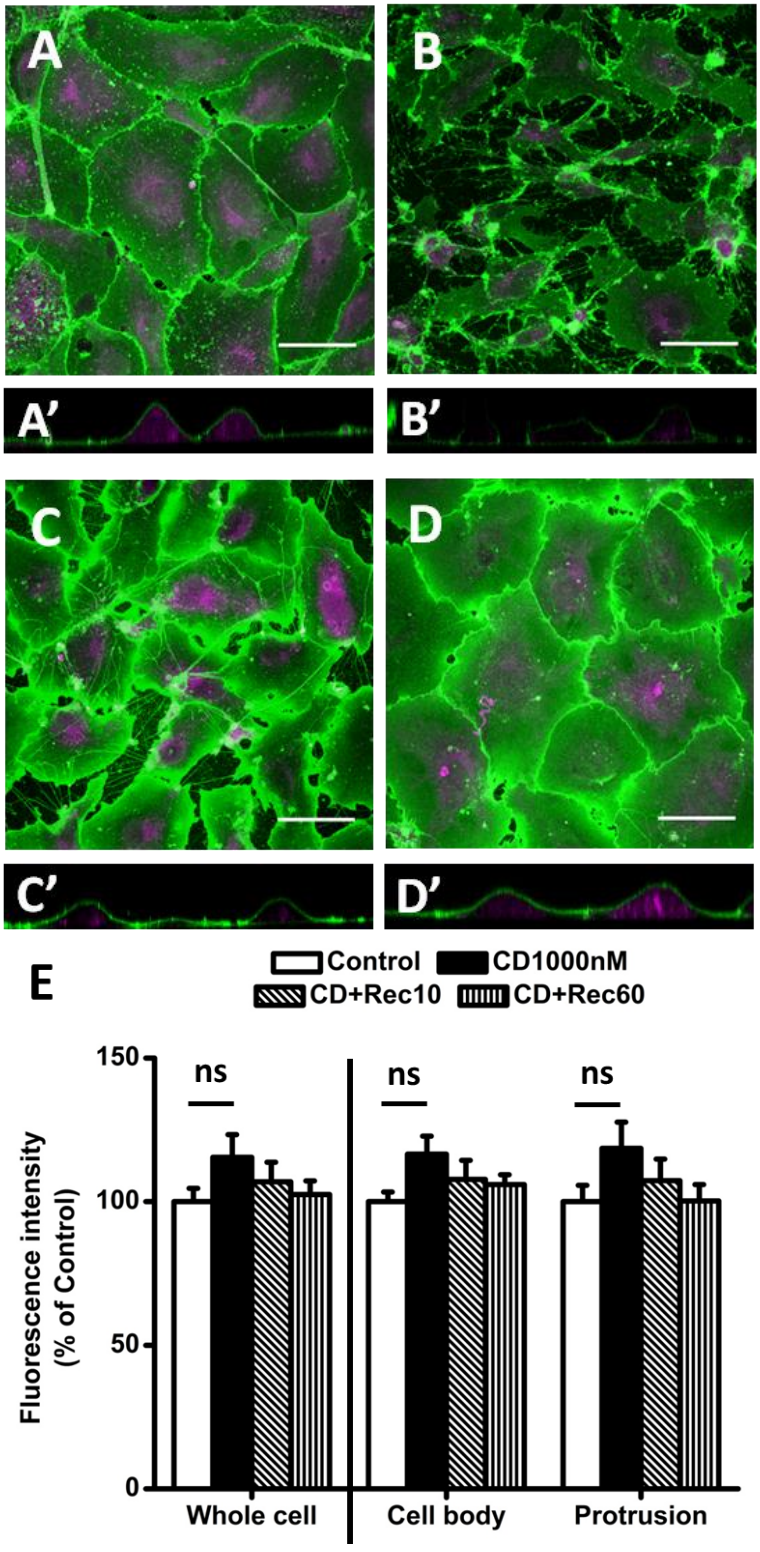

Figure 4.4 Glycocalyx was preserved after rapid actin depolymerisation.

Cells without (A) and with (B) rapid actin depolymerisation were covered with a uniform glycocalyx layer. This was sustained after partial (C) and complete (D) actin

*repolymerization. Scale bar = 50μm. The intensities of the glycocalyx remained insignificantly changed with respect to the control (without CD) (E). Cell numbers tracked for each group were 31 for the control, 26 for 1000nM CD, 24 for CD plus 10mins recovery, and 26 for CD plus 60mins recovery. *p<0.05, **p<0.01 when compared with the control.*

4.3.2. Glycocalyx was preserved after persistent actin depolymerisation

Cell detachment at 500nM CD and 1000nM CD was easily induced as incubation time increased. In order to address the issue of cell detachment during prolonged actin disruption, we studied the disruption effect at a lower CD concentration. As shown in Fig 4-5.A, F-actins were significantly depolymerised when cells were subjected to 250nM CD for 1h. However, owing to incomplete disassembly of the actin cytoskeleton, a great number of punctate actin polymers remained in the cytoplasm. The intensities of the line profile remained at a relatively high level and a number of short filamentous-like structures were detectible in the cells (53.04±3.55/cell). When the incubation time of 250nM CD was prolonged for 24h, F-actins and the punctate polymers (except those enriched in the junctional area) were lost (Fig 4-5.B). The intensities of the line profile dropping down suggested that F-actins had been completely broken apart. The actin filament number was dramatically reduced from 53.04±3.55/cell at 1h to 28.78±1.37/cell at 24h. Nonetheless, the basal surface area only decreased to 3336.08±61.13μm^2 at 1h and no further reduction of the basal surface area was detected at 24h. Cell spreading was sustained for a long period without the support of the actin cytoskeleton.

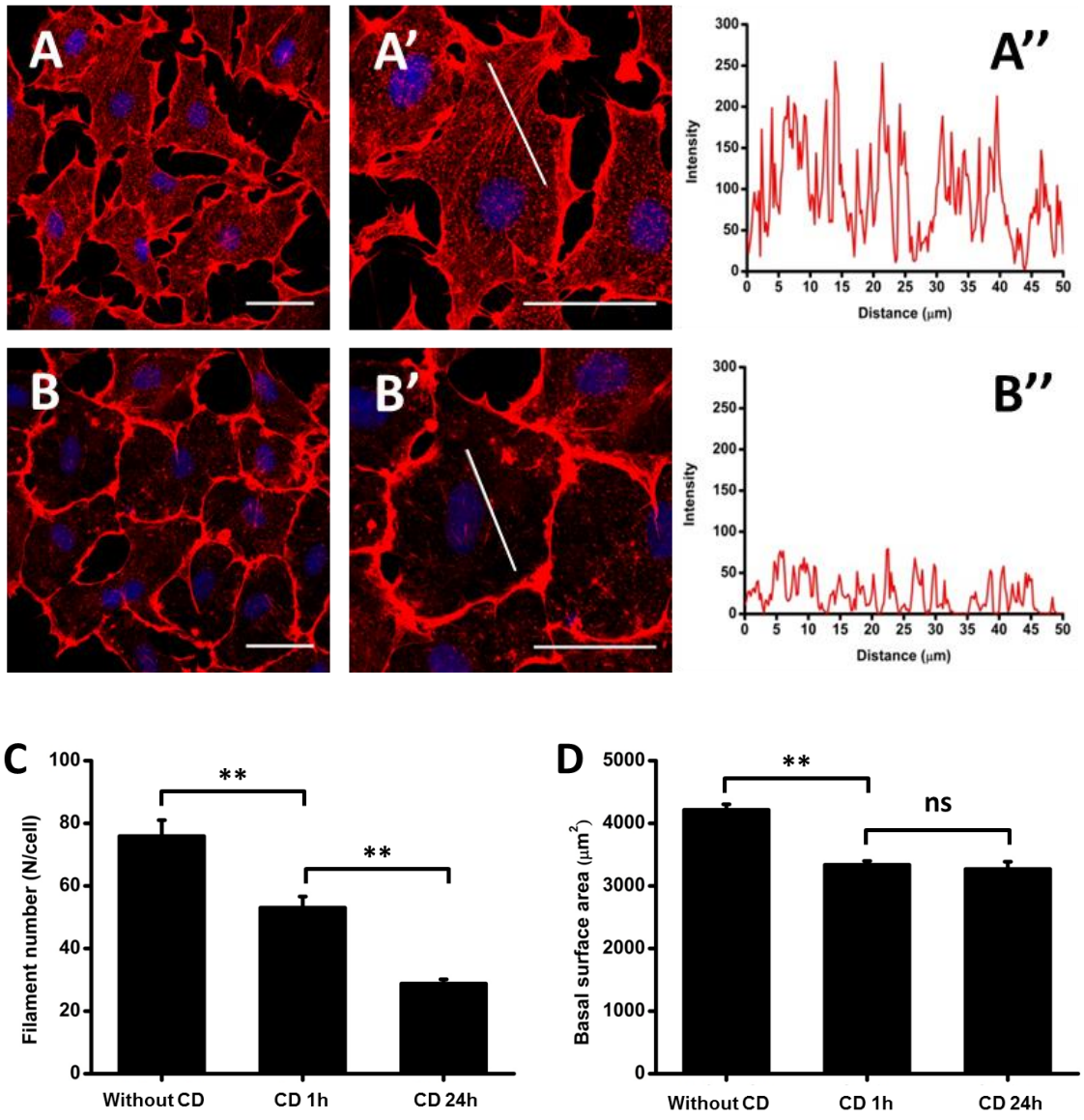

Figure 4.5 CD at low concentration continuously depolymerised the actin cytoskeleton.

*Confluent cells were subjected to 250nM CD for 1h (A) and 24h (B). Scale bar = 50μm. A line was drawn across the representative cell at each group (A'-B') and plotted as intensity profile (A''-B''). Filament number decreased with the increase of CD exposure time (C). Persistent actin depolymerisation in a low concentration of CD led to slight cell retraction (D). Cell numbers tracked for each group were 27 for 1h CD treatment and 37 for 24h CD treatment. *p<0.05, **p<0.01 when the comparison was made between two groups.*

The shedding of the glycocalyx on actin-depolymerised cells was investigated at the end of CD treatment. As shown in Fig 4-6.A, the glycocalyx was preserved as a continuous layer on the cell surface. This was further confirmed by changes in fluorescence intensity, which differed insignificantly from the control. Together with the results gained from rapid actin depolymerisation, our study indicated that under static conditions, the stability of the glycocalyx was independent of the actin cytoskeleton.

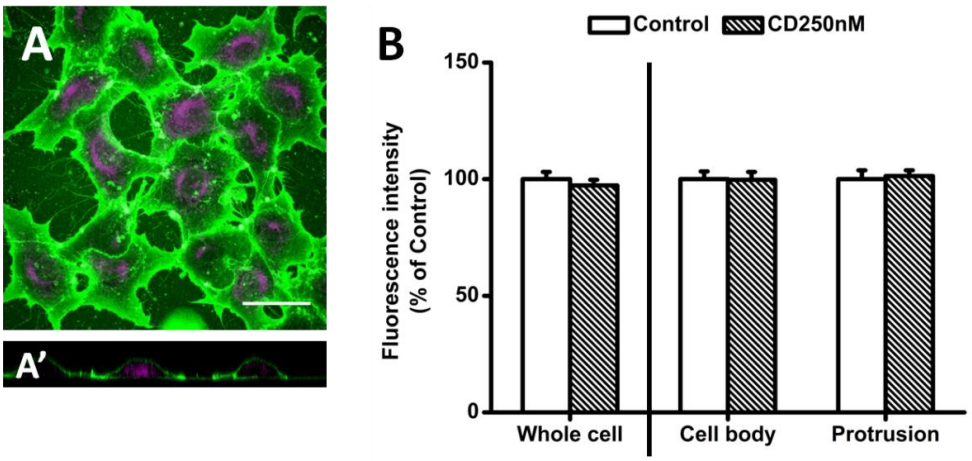

Figure 4.6 Glycocalyx was preserved after persistent actin depolymerisation.

*Cells with 24h persistent actin depolymerisation still presented a uniform glycocalyx layer (A). Scale bar = 50μm. No significant change was detected in the intensities of the glycocalyx (B). Cell numbers tracked for each group were 26 for the control and 33 for 250nM CD, *p<0.05, **p<0.01 when compared with the control.*

4.3.3. Glycocalyx on actin-depolymerised cells was shed in the presence of shear stress

The actin cytoskeleton was further evaluated by exposing it to 1.5Pa laminar shear stress (SS) concurrently with or without CD for 24h. F-actins in normal cells relocated to the cell periphery and realigned parallel to the flow direction (Fig 4-7.A). Correspondingly, the cells were strikingly elongated and reoriented parallel to the flow direction. For CD treatment, cells were pre-treated with 250nM CD for 1h and subsequently subjected to the circulating medium with CD. As previously noted, cells slightly retracted at 250nM CD after 24h static culture. However, they only survived and remained adherent in applied SS when 30nM CD was employed. Other cells subjected to a higher concentration of CD were easily washed away by the continuous laminar flow. In actin-depolymerised cells, reorganization of the actin cytoskeleton to the applied SS was abolished (Fig 4-7.B). The actin cytoskeleton was still in an entirely disrupted state, which led to a significant reduction of intensities in the line profile. As a result, cell elongation and cell alignment was absent. In particular, the following four groups (static cultured cells, SS exposed cells, CD treated cells and CD+SS treated cells) were quantitatively compared. In SS exposed cells, there was a further increase in filament number (static, 75.86±5.14/cell vs. SS, 88.81±4.43/cell, $p<0.01$) and basal surface area (static, 4124.08±110.74μm^2 vs. SS, 4619.15±161.81 μm^2, $p<0.01$). Contrarily, CD treated cells and CD+SS treated cells both showed a diminished number of filaments (CD, 23.25±1.46/cell vs. CD+SS, 29.57±1.97/cell, $p>0.05$) and basal surface area. Moreover, there was a two-fold reduction of basal surface area in CD+SS treated cells (CD, 3136.08±129.43 μm^2 vs. CD+SS, 1268.73±64.22μm^2, $p<0.01$), indicating that cells with actin depolymerisation were suffering an additional retracting force from the applied SS.

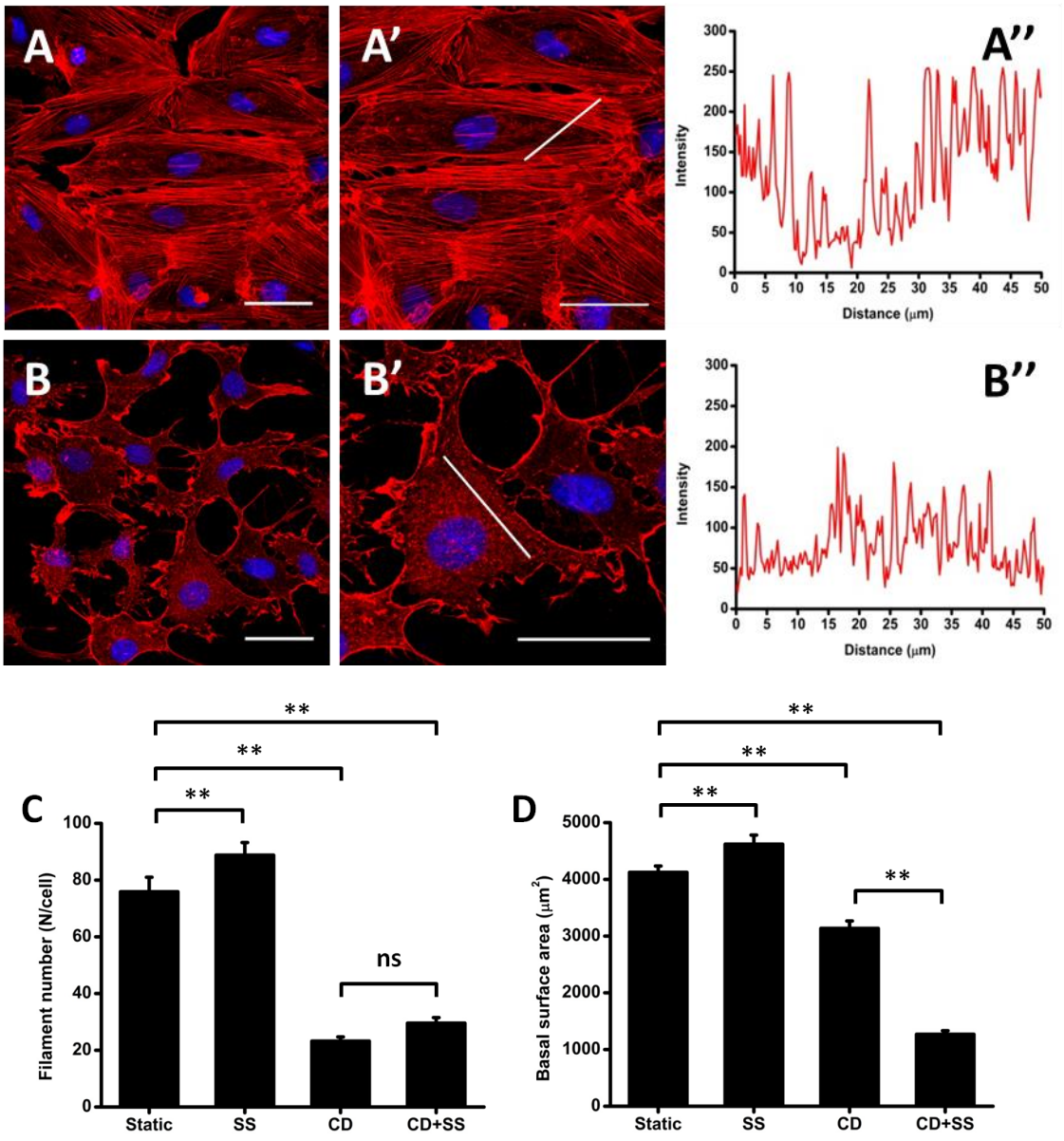

Figure 4.7 CD at low concentration continuously depolymerised the actin cytoskeleton in the presence of shear stress.

Cells were pre-treated with 250nM CD for 1h and subsequently subjected to 1.5Pa SS concurrent with 30nM CD for 24h. Normal cells exposed to SS only were used as a control. The actin cytoskeleton on normal cells was reorganized under SS, leading to cell realignment parallel to the flow direction (A). In the presence of CD, the actin cytoskeleton was continuously depolymerised and failed to reorient the cells. (B). Scale bar = 50μm. A

*line was drawn across the representative cell at each group (A'-B') and plotted as intensity profile (A''-B''). The filament number decreased in actin-depolymerised cells regardless of SS (C). Further retraction was, however, detected in actin-depolymerised cells under SS (D). Cell numbers tracked for each group were 32 for static culture, 48 for SS exposure, 32 for CD treatment, and 51 for CD treatment plus SS exposure. *p<0.05, **p<0.01 when comparison was made between two groups.*

Two additional groups were established to validate the shedding of the glycocalyx in actin-depolymerised cells. Firstly, the glycocalyx on normal cells was analysed following SS stimulation. The glycocalyx on elongated cells was seen to polymerize to the downstream of the laminar flow. The changes in fluorescence intensity on the entire cell surface were insignificant compared to the control. After surface compartmentalization, the intensity of the glycocalyx on cell bodies was similar to one another, whereas the intensity of the glycocalyx significantly decreased on the protrusion. The reason for this reduction was unclear but the data still excluded the possibility of SS-induced severe shedding of the glycocalyx on actin-preserved cells. Secondly, to distinguish the shedding state of the glycocalyx from the intact glycocalyx, neuraminidase (Neu) was employed to cleave SA during the stimulation. In brief, normal cells was pre-treated with 1U/ml Neu and then exposed to SS concurrent with 0.2U/ml Neu. As shown in Fig 4-8.C, the cells remained elongated in response to the applied SS. The labelling at the regions of cell-cell junctions was intensive, whereas the glycocalyx on the cell surface could barely be observed. This cleavage effect was mainly attributed to the differences in the molecular weight of FITC-WGA (38kD) and Neu (>50kD). Given that molecules smaller than 50kD were allowed to pass through the cell-cell junctions, Neu was filtered and exclusively cleaved SA on the

cell surface. Despite this, the fluorescence intensity of the glycocalyx on the entire cell surface dramatically declined by 70% (the junctional regions were not outlined as part of the cell protrusion). A similar reduction was found on the cell body and the protrusion, suggesting that the effect of Neu had been evenly applied to the cell surface. Following on, the shedding of the glycocalyx on actin-depolymerised cells was evaluated in applied SS. In the presence of CD, the glycocalyx layer on the cell surface was strikingly shed by appling SS. Only a few patches were left on the cell surface. The intensity of the glycocalyx on the entire cell surface dropped by 45% compared to other groups. Taken together, these effects enabled us to demonstrate that the actin cytoskeleton was essential for maintaining the stability of the glycocalyx under physiological SS.

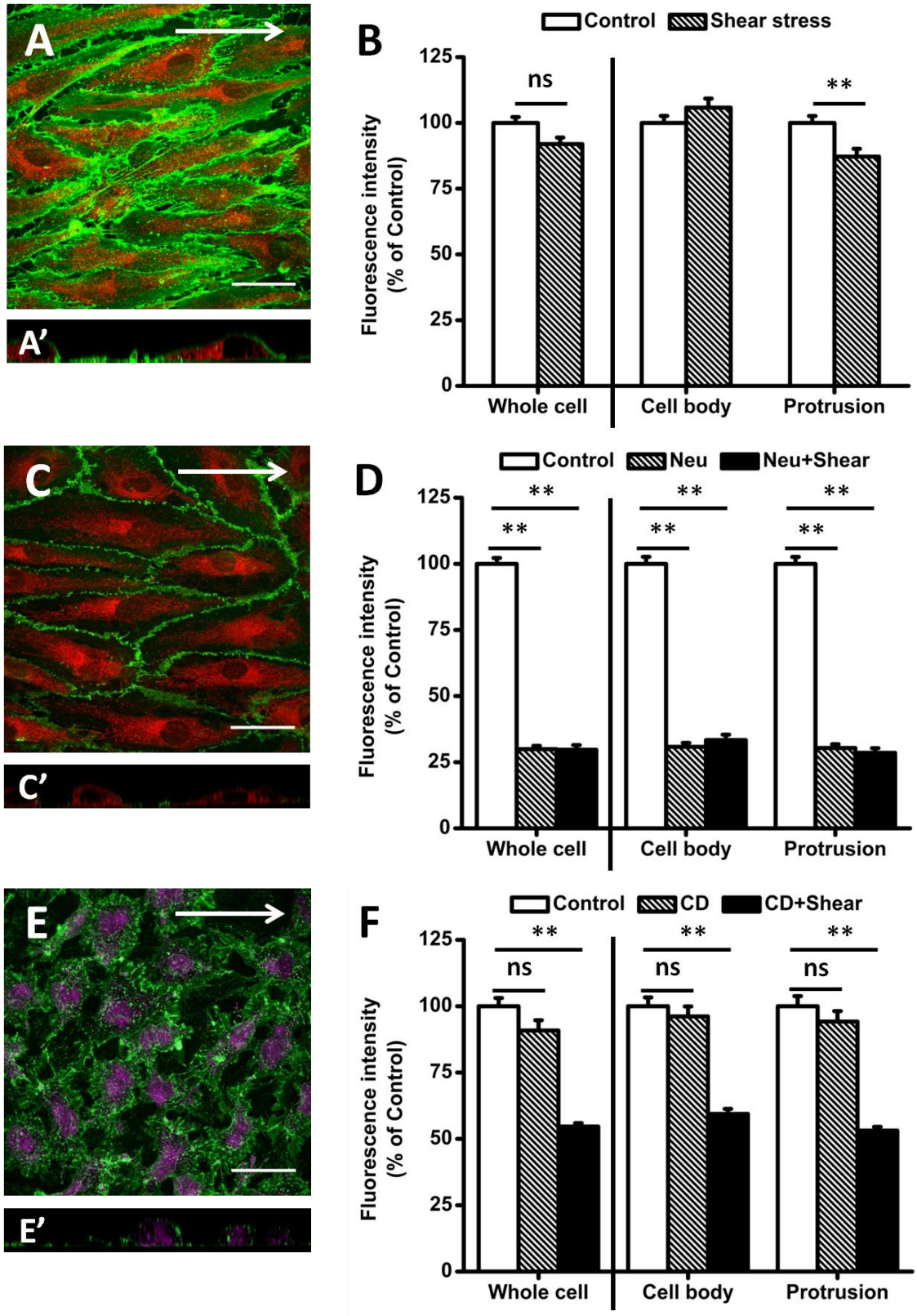

Figure 4.8 Glycocalyx on actin-depolymerised cells was shed in the presence of shear stress.

(A-B) The glycocalyx on normal cells was seen to shift to the downstream of the cell surface following 24h and 1.5Pa SS stimulation (A). This was not attributed to the shedding of the glycocalyx because the intensity of the glycocalyx remained insignificantly changed with respect to the control (B). Cell numbers tracked for each group were 45 for the control and 46 for SS.

(C-D) Glycocalyx component SA was continuously removed by Neu in the absence and the presence (C) of SS for 24h, in order to set a positive control for the shedding experiment. Cell numbers tracked for each group were 45 for the control, 35 for Neu and 55 for Neu+SS.

*(E-F) With actin depolymerisation, significant shedding of the glycocalyx from the luminal surface of the cell was observed at the end of SS stimulation (E). This was confirmed by a remarkable reduction in the intensity of the glycocalyx (F). Cell numbers tracked for each group were 26 for the control, 31 for CD and 62 for CD+SS. *p<0.05, **p<0.01 when compared with the control. Arrow indicates the flow direction. Scale bar=50μm.*

4.3.4. Correlation between shedding of the glycocalyx and disassembly of focal adhesions

To correlate the shedding of the glycocalyx to the disassembly of focal adhesions (FAs), FA was analysed by labelling one of its key components i.e., vinculin. In general, FAs in static cultured cells were labelled as small particles (0.5~5μm^2) and were mainly localized around the cell periphery (Fig 4-9.A-B). Most of FAs were lost when cells were subjected to CD (Fig 4-9.C-D). We then quantified the number of FAs, their size and their morphology. Following 24h SS stimulation, not only did the number of FAs significantly

increase to 24.63±1.20/cell, but the size of FAs was also augmented from 1.40±0.04μm^2 to 1.87±0.04μm^2. The increasing number and size of FAs eventually led to a larger fraction (approximately 1%) of FAs on the basal surface area, suggesting that cell attachment to the substrate was strengthened by applied SS. In addition, FAs were further stretched in response to SS, which was indicated by a long:short axis ratio of 3.38±0.05. Although the size of FAs remained similar in CD treated cells and CD+SS treated cells, the number of FAs was greatly reduced in the presence of SS (CD, 5.79±0.58/cell vs. CD+SS, 1.04±0.26/cell, p<0.01). The fraction of remaining FAs on the basal cell area was thus as small as 0.1~0.2%. Moreover, the remainder of FAs in CD treated cells maintained an elliptical shape (CD, 2.47±0.06), whereas FAs in CD+SS treated cells transformed into a circle-like shape (Static, 2.54±004 vs. CD+SS, 1.70±0.07 p<0.01). Taken together, this information implied that the failure of FA adaption to SS facilitated the shedding of the glycocalyx in applied SS.

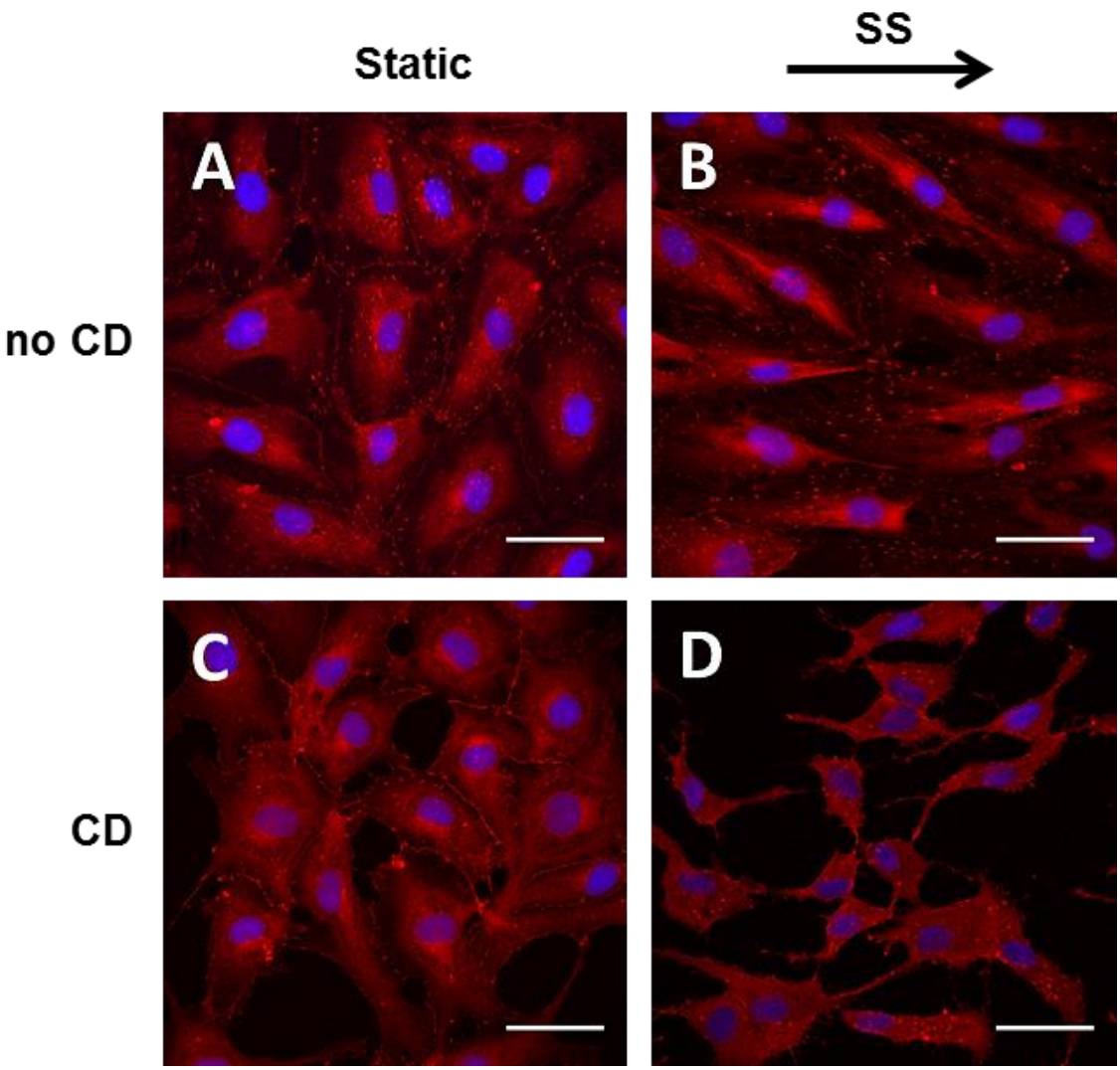
Static
SS
A
B
C
D
no CD
CD

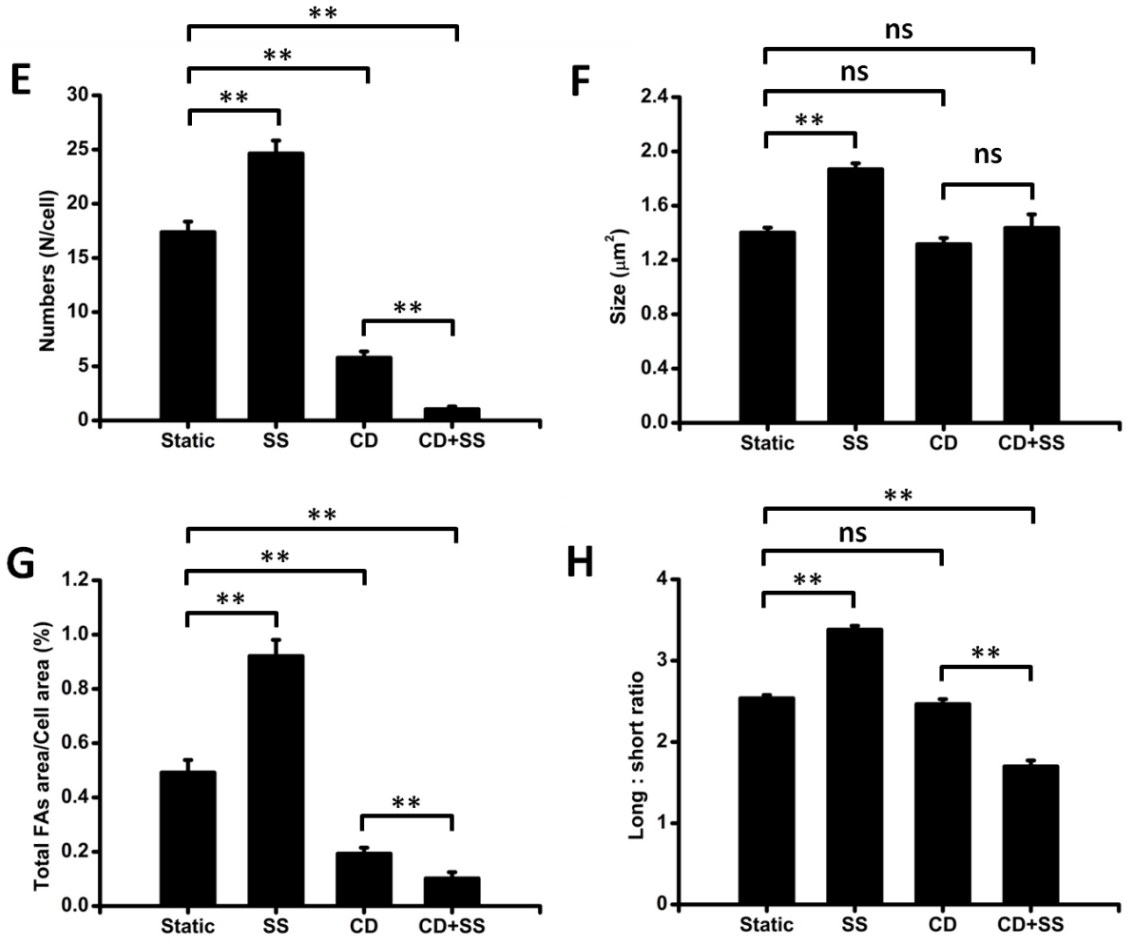

Figure 4.9 Assembly and disassembly of focal adhesions.

*FAs were investigated before and after 24h persistent actin depolymerisation, either in the absence or the presence of SS. (A) Static culture. (B) SS exposure. (C) CD treatment. (D) CD treatment plus SS exposure. Scale bar = 50μm. FAs were quantified in terms of number (E), size (F), area fraction (G) and shape (H). The assembly of FAs in normal cells was enhanced by SS, whereas the assembly of FAs in actin-depolymerised cells were more severely suppressed in the presence of SS. Cell numbers tracked for each group were 56 for static culture, 52 for SS exposure, 61 for CD treatment, and 54 for CD treatment plus SS exposure. *p<0.05, **p<0.01 when comparison was made between two groups.*

Finally, the distribution of FAs was plotted to correlate the redistribution of the glycocalyx in applied SS. As shown in Fig 4-10.A, FAs (black dots) in static cultured cells were evenly distributed in a circular ring-like pattern around the cell nucleus. Consistent with the cellular morphological changes in applied SS, this circular pattern was changed to an ellipse. More importantly, the distribution of FAs was biased by the applied SS, leaving a larger number of FAs (red dots) on the left of the circle. Given that the flow direction pointed from left to right, more FAs were accumulated to the upstream side of the cells. This contrasted with the redistribution of the glycocalyx, which was preferentially located on the downstream side of the cells (Fig 4-8.A). A model was further illustrated in the discussion. Contrastingly, the remaining FAs in CD treated cells circled around the nucleus. Since the number of FAs was so small, it was difficult to determine whether SS had effect on the distribution pattern of FAs in actin-depolymerised cells (Fig 4-10.B).

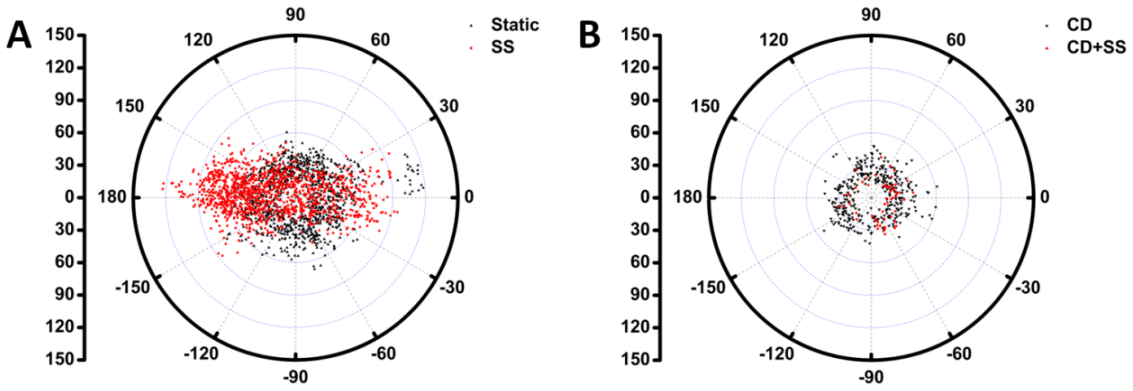

Figure 4.10 Redistribution of focal adhesions after shear stress exposure.

The distribution of FAs was further plotted prior to (black) and following SS exposure (red). FAs distributed randomly in the absence of SS, but were polarized to the upstream of the cell surface under SS (A). Regardless of SS, the remaining FAs in CD treated cells still circled around the nucleus (B).

4.4. Discussion

In this study, our results showed that 1) the glycocalyx was preserved after rapid actin depolymerisation; 2) the glycocalyx was preserved after persistent actin depolymerisation; 3) the glycocalyx on actin-depolymerised cells was shed in the presence of shear flow; 4) the shedding of the glycocalyx was related to the disassembly of FAs.

4.4.1. Assembly and disassembly of the actin cytoskeleton in endothelial cells

Actin exists in the forms of G-actin (monomer) and F-actin (polymer) in cytosol. With optimal ionic strength, the globular G-actin assembles into filamentous F-actin from the barbed end of existing actin. This process is accompanied by ATP hydrolysis, which intrinsically impacts on the kinetics of actin polymerization. Capping or severing the barbed end facilitates the disassembly of actin filaments. At the opposite end, i.e., pointed end, actin subunits tend to depolymerize, which maintains the equilibrium between the assembly and disassembly of actin filaments (Lodish. et al., 2000). To study the importance of actin cytoskeleton integrity for cellular and sub-cellular activities, depolymerizing F-actins are required. All microfilament-destabilizing agents, cytochalasins are the most effective. Not only do they inhibit the assembly of actin subunits at the barbed ends by capping them, they also sever actin filaments and sequester monomers and dimmers (Cooper, 1987). In our study, cytochalasin D (CD) was used for destabilizing the actin filaments in a statically cultured endothelial monolayer (Schliwa, 1982, Yahara et al., 1982) and two states of disruption were established. One of these states was rapid disruption accompanied by extensive cell retraction (Control,

4214.24±89.51μm^2 vs. 1000nM CD, 2043.70±54.01μm^2, p<0.01). Under microscopic observation, F-actin spreading over the cell body was completely diminished. Incubation time was set as 10mins to prevent further rounding up of cells and detachment. The second state was persistent disruption with a minor influence on cell morphology (250nM CD, 3268.50±116.40μm^2). Loss of spanning F-actins was observed over the entire 24h exposure of 250nM CD.

The line profile was employed as a manual approach for numerically analysing the section of filaments. It showed that the intensities of F-actins in representative cell dropped down to the base line when CD concentration was increased up to 1000nM, confirming that the rapid disruption of F-actins had been achieved. On the other hand, a dramatic reduction of intensity profile was observed at 250nM, when incubation time was extended to 24h. Actin disruption was sustained without the cost of having to round up cells. We also employed an automatic processing tool, FilaQuant, which had recently been developed by Matschegewski et al. (Matschegewski et al., 2012). This tool tracked the filaments on the basis of ridgeness measurement and provided quantitative information such as the number of filaments contained in the cells (Table 4-1). However, due to the patterns labelled by phalloidin, the filament number needed to be carefully interpreted. The staining patterns included highly-polymerized structures such as central spanning filaments (CSF) and dense peripheral actin band (DPAB) (Wong and Gotlieb, 1986, Wong and Gotlieb, 1990), less-polymerized structures such as actin asters (AA) (Verkhovsky et al., 1997), and depolymerised structures such as punctate F-actins (pFA) (Kantak et al., 1993). In an intact cell monolayer, filament number was predominated by CSF and DPAB. When CD was applied, these two structures were diminished or entirely lost. In turn, AA and pFA

replaced normal filaments in the body and pFA also accumulated to the cell border due to the folding of the membrane protrusion. The scattered, central AA and pFA were short enough to be excluded by the length threshold in counting. However, the border areas enriched with pFA mimicked filamentous structure. These fake filaments were intensive and linear, so that they were included in the tracking measures of FilaQuant. As a result, even though the actin cytoskeleton was completely disrupted, the remaining filament number was still counted to be greater than zero. In other words, FilaQuant was not able to distinguish the actin filaments from those areas enriched with pFA. Despite this limitation, our results showed that the number of filaments on normal cells was 75.86±5.14. This showed a dramatic decline to 31.37±2.03 and 28.78±1.37 when rapid disruption and persistent disruption were performed respectively. This significant reduction was consistent with the findings of line profiles, both of which adequately represented the changes in actin filaments during disruption.

Table 4-1 Comparison between line profile and FilaQuant.

	Line profile (plotted by Image J)	**FilaQuant**
Processing type	Manual	Automatic
Tracking algorithm	Linear	Ridgeness
ROI selection	Line across/along filaments	The whole cell
Outputs	Intensity	Number, Length & orientation
Averaging data points	No	Yes

The disruption of the actin cytoskeleton by CD was reversible. Following the rapid disruption model, we observed that most of the newly repolymerized F-actins emerged in the form of DPAB at the early stage of repolymerization. In particular, the repolymerization of DPAB at the junctions occurred much faster than that of CSF. This responsiveness was attributed to the following two reasons. Firstly, DPAB was thin bundles in the periphery while CSF stood for the thick bundles in the centre. The bundle with a smaller diameter contributed to a faster repolymerization rate. Secondly, after rapid disruption, some punctate F-actins remained on the cell border. When the cytoskeleton undergoes repolymerization, these remaining actins on adjacent cells quickly fused together and were incorporated to the newly-repolymerized circumferential filaments, which finally facilitated the formation of mature cell-cell junctions. This process was also observed in the normal growth of cell populations, where sub-confluent cells became confluent. (Yonemura et al., 1995, Zhang et al., 2005). Owing to the rapid reconstruction of DPAB, the number of filaments was recovered to 59.14±3.07 at 10mins following drug removal. With the time increase, abundant CSF was repolymerized, which eventually dominated the filament when taken together with DPAB. Full restoration of the filament number to the control level at 1h suggested that the actin cytoskeleton had been completely rebuilt.

4.4.2. Reorganization of the actin cytoskeleton in response to shear stress

Endothelial cells are ceaselessly subjected to a variety of shear flow levels within blood vessels. Patterns of flow are dependent on the types of blood vessel, as well as the region

of blood vessels (e.g., unbranched region, bifurcation and stenosed region). By designing flow chambers with specific geometries, an increasing number of patterns can be reproduced *in vitro*. A flow chamber with steady laminar flow has been the most widely-studied model to date. Applying laminar flow in vitro enables us to study the biological events that occur on endothelial cells *in vivo*. In response to laminar SS, endothelial cells align parallel to the SS vector and execute elongation. This adaptation to flow contributes to the reduction of shear gradients along endothelial cell surface and requires the reorganization of the actin cytoskeleton. Ookawa et al. (Ookawa et al., 1992) first correlated cell alignment and F-actin alignment at a time scale of 24h. The randomly distributed F-actins were initially reoriented to the direction of flow at 3h after the onset of flow (20dyn/cm^2). They also demonstrated that filament bundles were formed in the central region of cell at this early stage and then dispersed to the periphery as time progressed. In line with this research and others, we showed that both CSF-dominant and DPB-dominant cells were found within a static culture. However, after 24h SS stimulation, the F-actins in most of the cells were preferentially relocated to the cell periphery and reoriented to the flow direction. Moreover, we showed that the filament number counted in shear-exposed cells was further increased by 17%, reaching as high as 88.81±4.43. One of the possibilities for this increased filament number was that actin assembly was continued in shear-exposed cells (Noria et al., 2004). Free G-actins further assembled into either end of the pre-existing filaments for coordinating the morphological changes occurring due to SS stimulation (15dyn/cm^2). Not only highly polymerized filaments were extended, but those short filaments were also directly lengthened or joined with other adjacent short filaments. Given that the counting threshold of filament length was set as 4.65μm in

FilaQuant, an additional number of filaments will enter the counting domain after shear stress stimulation.

In addition to the filament extension, filament turnover is another factor that affects filament number counting. Osborn et al. (Osborn et al., 2006) illustrated for the first time that filament turnover rate was evidently increased at 1h following the onset of laminar flow (12dyn/cm^2). With an elevated turnover rate, the polymer fraction was decreased in shear-exposed cells, suggesting that there was a net depolymerisation for the actin cytoskeleton at the early stage of stimulation (<6h). Based on this postulation, we assumed that a well-polymerized filament could be divided into several parts at the early stage. With the reorientation completed, the shorter filaments were realigned and then lengthened separately. As a result, the parental filament was substituted with the newly repolymerized filaments, which was believed to increase filament counting at the end of 24h stimulation. Unlike the early phase of stimulation, the adaption of the actin cytoskeleton to SS was already completed at 24h. Turnover rate was reversed to the pre-stimulated level (Osborn et al., 2006). To sustain the elongated cell shape, the resulting increase of polymer fraction should involve the adequate extension of filaments. As anticipated, we were able to show that in the histogram where the frequency distribution of filament length had been plotted, a clear shift had taken place from a range of 0~10μm to that of 10~60μm (Fig 4-11). The percentage of filament numbers at the range of 10~60μm at shear-exposed cells was elevated to 41%, which in turn led to an increase in median filament length over statically cultured cells. All of these observations were consistent with the case where turnover rate was slower in confluent endothelial cells than those at the adjacent wounding edge (McGrath et al., 2000). The endothelial cells with less remodelling of the actin

cytoskeleton contained more polymerized filaments, either in an increased number or length.

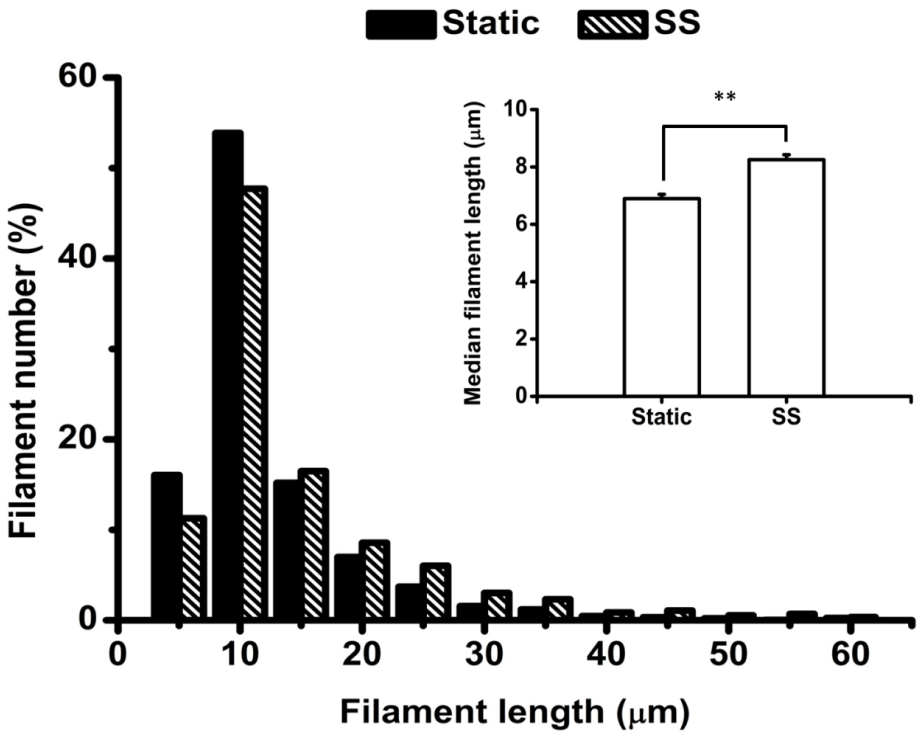

Length range	Static	SS
0~10μm	69.93%	58.99%
10~60μm	30.07%	41.00%

Figure 4.11 Filament length in shear stress-exposed cells.

4.4.3. Actin cytoskeleton is not related to the stability of the glycocalyx under static conditions

The glycocalyx is dynamically synthesized and degraded. This not only maintains a constant amount of the glycocalyx on the cell surface, but also facilitates its reorganization in response to stimuli. However, the structural stability of well-developed glycocalyx is not very well understood. The focus of current studies instead draws on the interaction of the

glycocalyx components. Based on the notion that the glycocalyx is formed as an interconnected-gel like structure by GAGs, Zeng et al. first demonstrated the contribution of individual GAGs to the structural stability of the glycocalyx (Zeng et al., 2012). They showed that the removal of HS, CS and HA alone did not collapse any remaining GAGs. The interaction of GAGs is not required for stabilizing the glycocalyx. In addition to GAGs, the glycocalyx contains short chain glycan-based structures in the form of glycoproteins (Fig 4-12). The interaction between GAGs and glycoproteins has also been depicted in some reports (Haldenby et al., 1994, Barker et al., 2004, Reitsma et al., 2011). Particularly, Barker et al. (Barker et al., 2004) showed that FITC-WGA intensity was reduced to 21±8%, 29±3% and 13±5% after a 60min incubation of heparitinase, hyaluronidase and chondroitinase ABC, respectively. The collapse of GAGs appeared to affect the stability of glycoproteins. However, this was not the case, due to the cross-reactivity of WGA. WGA mainly binds to the sialyl residues on glycoproteins but still has an affinity for N-acetyl-D-glucosamine (GlcNAc). GlcNAc is one of the constituents in HS and HA. The reduction of FITC-WGA intensity by heparitinase and hyaluronidase treatments in Barker et al.'s study (Barker et al., 2004) was attributed to the cleavage of GlcNAc, rather than the collapse of glycoproteins. Even though GlcNAc does not exist in CS, the reduction of FITC-WGA intensity by chondroitinase ABC treatment was small. Collectively, the effect of disrupted GAGs on glycoproteins was negligible, indicating that the structural stability of the glycocalyx was not maintained via the interaction between glycocalyx components. The glycocalyx is likely stabilized by anchoring to the membrane.

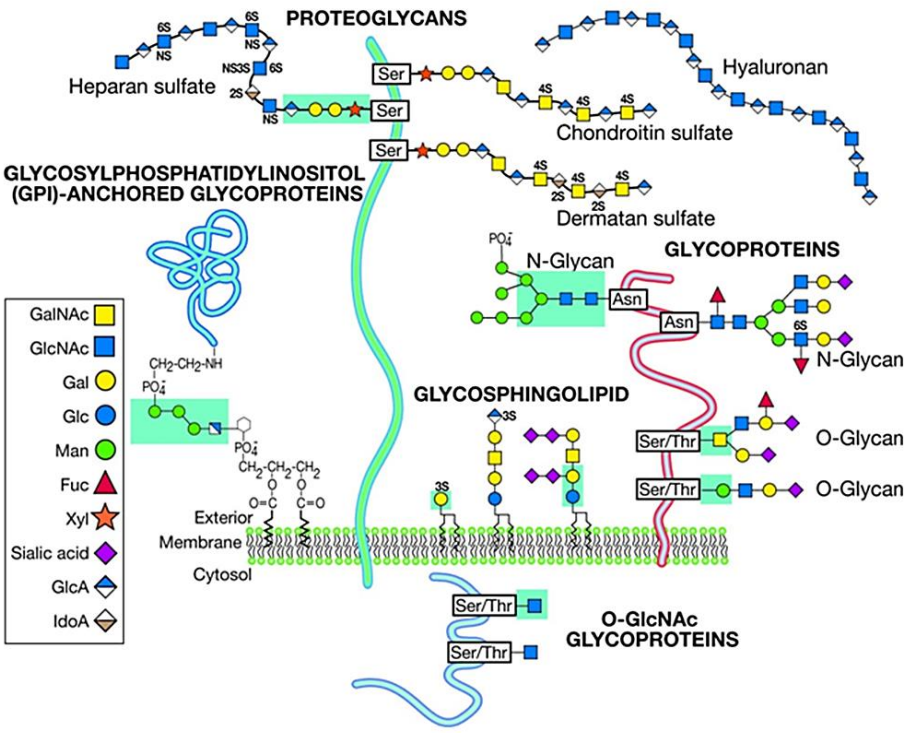

Figure 4.12 Classification of glycocalyx components.

(Varki et al., 2009)

It is widely believed that the actin cytoskeleton provides support for the membrane and molecules anchored on it. However, no study has experimentally verified to what extent the actin cytoskeleton contributes to the stability of the glycocalyx. In the present study, the seven-day cultured cell monolayer, which possessed sufficiently well-developed glycocalyx, was used for studying CD effects on the collapse of the glycocalyx. We observed that the average intensity of the glycocalyx was insignificantly increased by 15.42±7.92% at rapid disruption and -2.69±2.41% at persistent disruption, indicating that the glycocalyx was well-preserved. The stability of the glycocalyx was maintained independently of the actin cytoskeleton. The effects of CD were reversible when the cells were refreshed with a CD-free medium. The glycocalyx was further evaluated on cells that

recovered from rapid disruption. We found that the intensity of the glycocalyx fluctuated at a small increment of 6.91±6.78% at partial cell recovery and 2.46±4.77% at full cell recovery. The well-preserved glycocalyx on retracted cells were stable after cell re-spreading. Rapid disruption followed by repolymerization exerted a reciprocal force on the cell membrane. The vibration of the cell membrane was here intrinsically reflected by changes in membrane tension. Since the glycocalyx was preserved during cell retraction and cell spreading, our results suggested that neither the loss of the actin cytoskeleton nor the derived changes in membrane tension were sufficient to compromise the stability of the glycocalyx under static conditions.

4.4.4. Actin cytoskeleton is required for the stability of the glycocalyx under flow conditions

The glycocalyx is the outermost part of the endothelium and is in direct contact with blood flow. Investigating the contribution of the actin cytoskeleton to the stability of the glycocalyx in shear flow is of great importance. We showed that on normal cells, the average intensity of glycocalyx remained at the static level following 24h stimulation. No net collapse of the glycocalyx occurred. This was in line with results recently demonstrated by Tarbell's group, where there was no reduction in mean intensity and coverage on bovine aortic endothelial cells (BAECs) at 24h (Zeng and Tarbell, 2014). However, the redistribution pattern of the glycocalyx remained inconsistent. In that particular study, the researchers developed a new scattering distribution method for discerning the spatial distribution of the glycocalyx. The normalized intensity of the glycocalyx on the centroid was decreased, whereas the intensity on the boundary was increased at an early stage of

30mins. Since no alteration was found for the mean intensity over the entire surface, the researchers declared that the asymmetric coverage of the glycocalyx was attributed to its movement to the downstream of the cells. Interestingly, the redistribution of the glycocalyx was not maintained over the entire period of stimulation. Instead, it returned to the static level at 24h, likely due to the enhanced biosynthetic activity induced by the shear flow. Contrarily, we observed that the glycocalyx was clearly polarized to the downstream of well-elongated cells at 24h. Similarly, Yao et al. (Yao et al., 2007) showed that more glycocalyx was detected on the cell periphery of BAECs after 24h shear flow, suggesting that the glycocalyx preferred relocating from the central region of the cell to the junctional regions. Despite this discrepancy, the glycocalyx was believed to serve as an adaptor for reducing the shear gradients on the cell surface, especially on the centre region of the cell.

We further presented findings concerning the stability of the glycocalyx on actin-disrupted cells in shear flow. Normal cells were pre-treated with 250nM CD for 1h and then subjected to shear flow for 24h in circulating medium with 30nM CD. We found that the glycocalyx had apparently been damaged due to loss of the actin cytoskeleton. The reduction in intensity confirmed that the stability of the glycocalyx had been compromised. The integrity of the actin cytoskeleton was especially required for stabilizing the glycocalyx in shear flow. Since we did not observe the coverage of the glycocalyx at the time scale, it was not clear when the shedding of the glycocalyx was initiated and whether the glycocalyx could be completely shed with an increase in time. Similar results have never been described until recently. Zeng and Tarbell reported that disrupting the actin cytoskeleton by 40nM CD did not influence the amount and distribution of glycocalyx under static condition or through 30mins shear stimulation (Zeng and Tarbell, 2014).

However, the recovery of the glycocalyx at 24h was completely abolished. The glycocalyx remained located to the cell periphery, which was similar to the pattern at 30mins. Thus, the researchers concluded that the clustering of the glycocalyx at the downstream at 30mins occurred independently of the actin cytoskeleton, whereas the recovery of the glycocalyx at 24h depended on the reorganization of the actin cytoskeleton. They emphasized the adaptive remodelling of the glycocalyx to SS, which was different from what we have underlined in the present study.

In addition, we observed that the actin-disrupted cells had apparently been retracted in shear flow. This was another difference in the present study from the results of Zeng and Tarbell's report (Zeng and Tarbell, 2014), where the cells remained confluent in the circulating medium with 40nM CD over the entire stimulation period. Since we used a similar CD concentration to maintain the disrupted state of the actin cytoskeleton, the difference in confluence was mainly due to the different vascular cell type that we used. The rat fat pad endothelial cells (RFPECs) used in Zeng and Tarbell's study were isolated from rat epididymal fat pad capillaries. There are few central filament bundles but strong expression of VE-cadherin in capillary endothelial cells (Strauss et al., 1987, Herwig et al., 2008). VE-cadherin-mediated intercellular adhesion, rather than the central filament bundles and the associated focal adhesions, is likely predominant in the maintenance of capillary endothelial cell monolayer. Thus, RFPEC monolayer was less vulnerable to CD and remained confluent even after a disruption of central filament bundles. Contrarily, VE-cadherin is less expressed, while a greater amount of central filament bundles is assembled in venous endothelial cells (Strauss et al., 1987, Herwig et al., 2008). Loss of these bundles results in cell retraction and then easily breaks cell-cell adhesion, particularly under flow

conditions where an extra force is applied to the endothelial cells. As a result, severe cell retraction was found in actin-disrupted HUVECs in the present study.

Cell retraction is the outcome of actin depolymerisation; this process is generally accompanied by the disassembly of FAs. We found that under static culture, FAs on actin-disrupted cells were dramatically decreased in number and in their general size. There was a further disassembly of FAs in shear flow, indicating that the FAs were almost completely degraded. The effect of FAs on the stability of the glycocalyx was not considered in the present study. We were unsure whether the failure of FA formation alone was sufficient for encouraging the shedding of the glycocalyx. In spite of this, our results still indicated that the shedding of the glycocalyx in shear flow was related to the disassembly of FAs.

4.4.5. A model illustrating the contribution of the actin cytoskeleton to the stability of the glycocalyx

Our hypothesis concerning the contribution of the actin cytoskeleton to the stability of the glycocalyx is illustrated as a mooring model and shown in Figure 4-13. In this model, the entire endothelial cell is considered as a region of 'sea', in which the apical surface refers to the water surface while the basal surface refers to the bottom. The glycocalyx is compared to a boat floating on the water surface. To moor the boat on this region, the anchors, here represented by FAs, are normally dropped down to the bottom via their connection with chains, in this instance represented by actin filaments (Fig 4-13.A). Even though the boat is not equipped with chains or anchors, the displacement of the boat is still negligible owing to the calm sea (Fig 4-13.C). Correspondingly, the glycocalyx remains

stable on the cell surface when the actin filaments are depolymerised under static culture. Contrastingly, the boat becomes unsteady when the sea transits from a calm state to a violent state. When the boat is anchored on the violent sea, unidirectional sea waves have the potential to dislodge the boat. Due to the linkage between the chains and the anchors, the force exerted by the sea wave is counteracted by the dragging force derived from the anchors. Since the net force is prone to be greater than zero, the boat still has a tendency to displace forward (Fig 4-13.B). This is similar to the case where static culture is shifted to SS exposure. The glycocalyx tends to redistribute to the downstream of the cell surface, while FAs preferentially accumulate to the upstream. In addition, for some reason (e.g. rusting), the chains are easily broken apart, so that the anchors are disconnected from the boat. Without any binding to the bottom of the sea, the boat is entirely subjected to the driving force of the wave. The displacement of the boat can be significant, causing it to be dislodged from this region. Even worse, the boat can be destroyed by the wave (Fig 4-13.D). Accordingly, the glycocalyx sheds off the cell surface when the actin filaments are disrupted in shear flow.

Despite this, it should be noticed that the "violent sea" here is referred to as steady laminar shear flow. This model only applies to the conditions where a physiological shear stress develops. It is uncertain whether it could explain how the actin cytoskeleton contributes to the stability of the glycocalyx under abnormal flow conditions (e.g. low and oscillatory flow). To expand this model, incorporating different flow patterns is required in the future work.

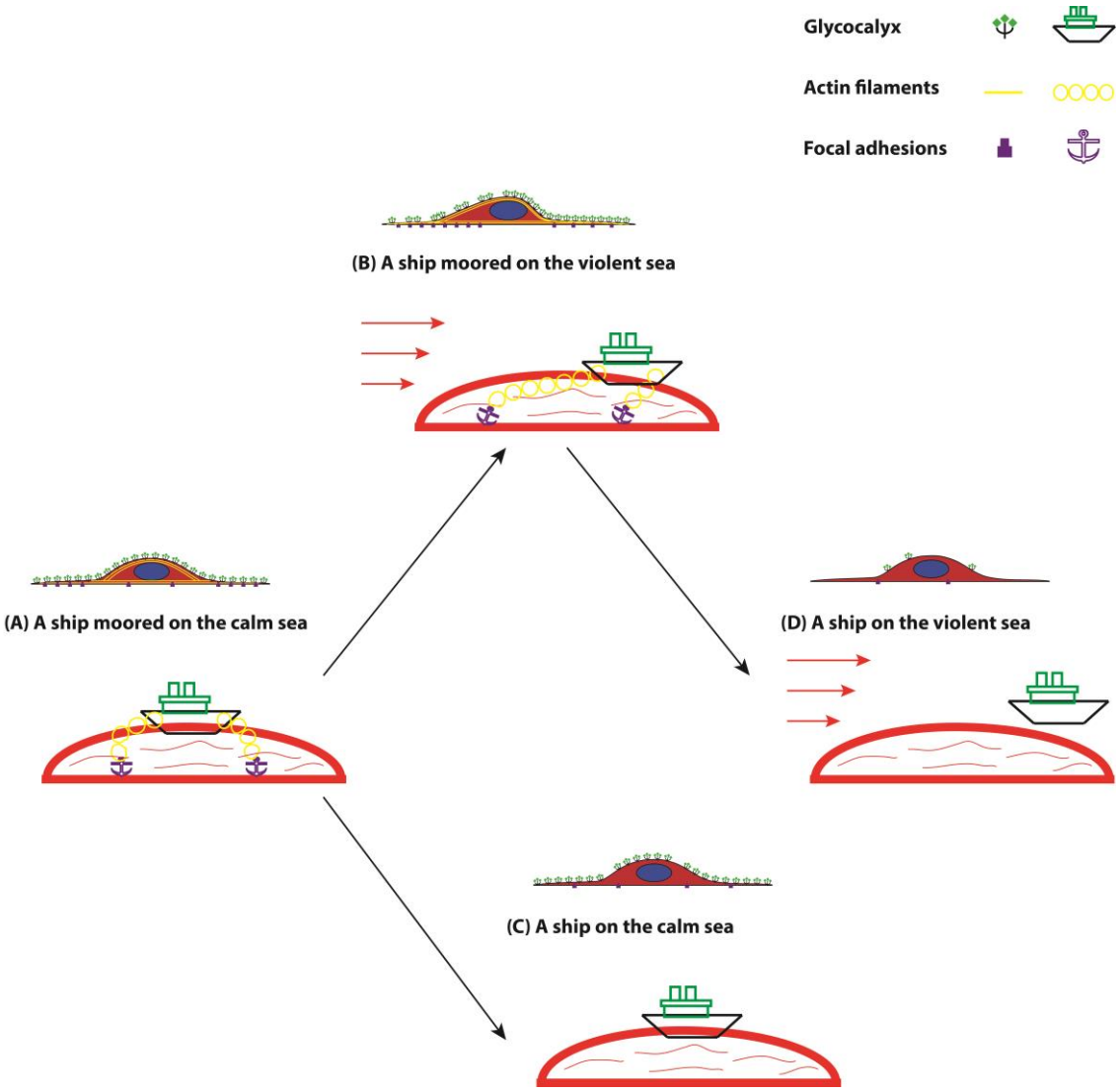

Figure 4.13 A model illustrating the contribution of the actin cytoskeleton to the stability of the glycocalyx.

In conclusion, I have demonstrated an important role of the actin cytoskeleton in stabilizing the endothelial glycocalyx. Neither the loss of the actin cytoskeleton nor the derived changes in cell morphology sufficiently compromises the integrity of the glycocalyx under static conditions. However, the actin cytoskeleton functions as a crucial element for the stabilization of the glycocalyx in the presence of steady laminar shear

stress. All these findings deepen our understanding in the structural stability of the endothelial glycocalyx and will help to develop new strategies to prevent shedding of the glycocalyx in diseases.

5. Contribution of the glycocalyx to EF-directed endothelial cell migration

5.1. Introduction

Endothelial cell migration is an essential step for angiogenesis. It is dynamically driven by various stimuli such as chemical gradient and shear stress (Li et al., 2005, Lamalice et al., 2007). Little attention has been given to the transendothelial potential (TEP), which varies over a range of 100mV~400mV in different types of blood vessels (Sawyer et al., 1966). Disruption of TEP instantaneously results in a steep and lateral voltage gradient close to the disrupted region (≤1mm) (McCaig et al., 2005). The resulting endogenous electric field (EF, 100~400mV/mm) has the potential to promote the reconstitution of tissue structure and the restoration of corresponding function. Similar effects are reproduced by exogenous electrical stimulation, which has once been considered as an approach to study endothelial cell migration. Li and Kolega showed that bovine aortic endothelial cells migrated rapidly toward the cathode within 30mins at 200mV/mm (Li and Kolega, 2002). By applying similar field strength, Zhao and his co-workers demonstrated that HUVECs performed anodal cell migration in 5h while HMECs exhibited cathodal cell migration (Bai et al., 2004, Zhao et al., 2004). Despite the discrepancy in moving direction, they all agreed that reorganization of the actin cytoskeleton was involved in EF-directed endothelial cell migration. However, since then, studies of the EF-directed endothelial cell migration have not continued. The sensing and transduction mechanism of EF-directed endothelial cell migration remains poorly understood.

EF-directed cell migration has been described in variable cell types such as fibroblasts, keratinocytes, stem cells and even cancer cells (Onuma and Hui, 1988, Brown and Loew, 1994, Nishimura et al., 1996, Djamgoz et al., 2001, Pu et al., 2007, Zhang et al., 2011, Zhao et al., 2011). Early studies suggested that 'the redistribution of receptors on the membrane surface' (Zhao et al., 1999, Zhao et al., 2002) and 'the transient opening of ion channels' (Onuma and Hui, 1988, Djamgoz et al., 2001) determined the direction of cell migration in applied EF. Alternate mechanisms involving 'cGMP signalling' (Sato et al., 2009), 'ion transporter' (Ozkucur et al., 2011) and 'epithelial sodium channel' (Yang et al., 2013) have been recently proposed as switches of EF-directed cell migration. Above potential mechanism may apply to EF-directed endothelial cell migration, but we are more interested in the brush-like structure namely the glycocalyx on the endothelial cell surface (Weinbaum et al., 2007). Due to the negatively charged network, the glycocalyx adjusts streaming potentials on the blood vessels via balancing the ion distribution from the edge of the glycocalyx to cell membrane. (Mestel et al., 1998). The glycocalyx also experiences mechanical force derived from the EF. It has been theoretically verified that the transduction of EF into cell interior was implemented via the mechanical torque exerting on the glycocalyx (Hart, 2008). In addition, the glycocalyx acts as a mechano-sensor and -transducer for shear stress. The adaptive remodelling of the glycocalyx induces cell migration and alignment via the reorganization of the actin cytoskeleton (Thi et al., 2004, Yao et al., 2007, Ebong et al., 2014, Zeng and Tarbell, 2014). To our knowledge, whether the endothelial glycocalyx is involved in EF-directed endothelial cell migration has not been studied. Answering this question will provide new insights into the endothelial cell migration and the related angiogenesis. Therefore, we aim to investigate the role of the endothelial glycocalyx in EF-directed cell migration *in vitro*.

To identify the role of the endothelial glycocalyx, three questions are addressed in this chapter (Fig 5-1). 1) How endothelial cells migrate in applied EF when cells are well preserved with developed glycocalyx? 2) How endothelial cells migrate in applied EF if the glycocalyx is removed? 3) Whether the polarization of the endothelial glycocalyx participates in the EF directed cell migration?

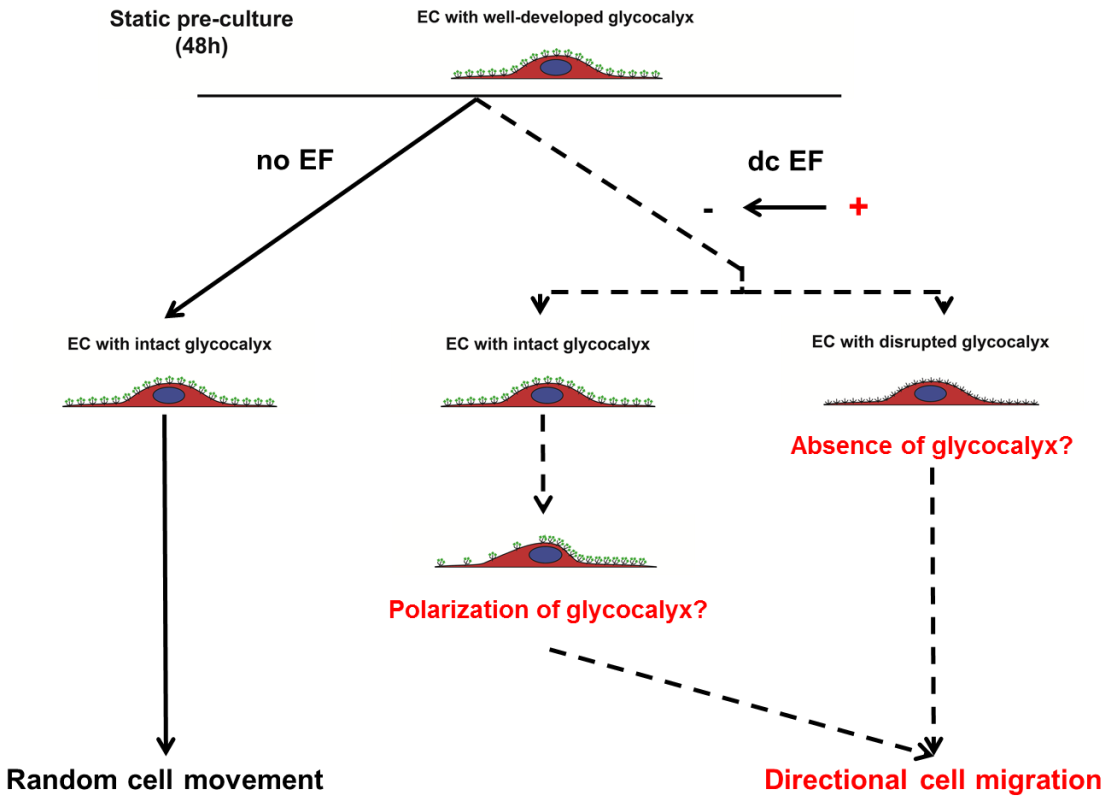

Figure 5.1 Diagram of contribution of the glycocalyx to EF-directed cell migration.

5.2. Methodology highlights

5.2.1. Pre-culture time

HUVECs at a sparse density are commonly pre-cultured for 6~24h prior to the onset of EF. Sparse cell density prevents cell migration from contact inhibition, whilst short term pre-culture avoids cell division and the formation of cell clusters during the stimulation. The aim of our study is to verify the role of the glycocalyx on the cell surface. In addition to these general concerns for cell migration, the recovery time and amount of the glycocalyx has a great impact on the accuracy of our results. As described in chapter 3, a small amount of glycocalyx was recovered on the endothelial cell surface after 24h culture. Low cell density culture may favour cell division and migration at the cost of deceleration of glycocalyx recovery within 48h. Even though pre-culture time can be extended for the recovery of the glycocalyx, more and more cells will undergo division and eventually increase cell-cell contacts and hinder cell movement. Contrarily, high cell density culture facilitates the recovery of the glycocalyx within 48h but certainly inhibits cell migration. To make a compromise, HUVECs at a moderate density of 2500cells/cm^2 were pre-cultured for 48h prior to the onset of EF. There were a few cell-cell contacts under this condition, whilst the glycocalyx was sufficiently recovered.

5.2.2. EF Exposure time

Exposure time for generating observable directional cell migration varies from 1h to 6h. Some cell types such as fibroblast, cancer cells respond quickly and display preferential migration within 1h. Others like macrovascular cells appear to be insensitive in sensing EF signal. These cells require a longer time period (≥2h) to execute obvious directional

migration. In addition, electrolysis potentially affects the exposure time. Heavy electrolysis, which was indicated by the changed colour and the turbidity of medium, occurred after 5h stimulation in our study and others (Song et al., 2007). Hence, HUVECs were continuously stimulated for 5h.

5.2.3. Neuraminidase treatment

The role of the glycocalyx in EF-directed cell migration was investigated using neuraminidase (Neu). Neu is a non-proteolytic enzyme that exclusively cleaves SA from the glycocalyx. HUVECs were pre-incubated with 1U/ml Neu for 1h prior to the onset of EF. During the stimulation, 0.2U/ml Neu was maintained in culture medium. Thus, not only the developed SA, but also the newly developing SA was completely removed.

5.2.4. Cell tracking

Images collected at an interval of 10mins were stacked for cell tracking. Some have argued that tracking cell centroid is the best way for assessing cell migration while others preferred using cell nucleus. In some cases, lamellipodia and filopodia were also used for cell tracking. In the present study, the tracking preference was made according to the following consideration. Cell migration depends on the equilibrium between leading edge and trailing edge. Extension of membrane protrusion alone doesn’t mean real movement of a whole cell. The cell body, especially the cell nucleus, can remain still when the cell protrusion spreads and retracts within a certain range. Unlike flexible cell protrusion, the shape of cell nucleus remains less deformed under two-dimensional cell migration. Symmetrical circle and ellipse makes the tracking of nucleus centre more easily. The

centroid of cell body is not accurately judged because the shape and size of cell body are more changeable. Judging the centre of mass only by eyes is less accurate. Altogether, the nucleus centre was manually tracked over the entire period of stimulation.

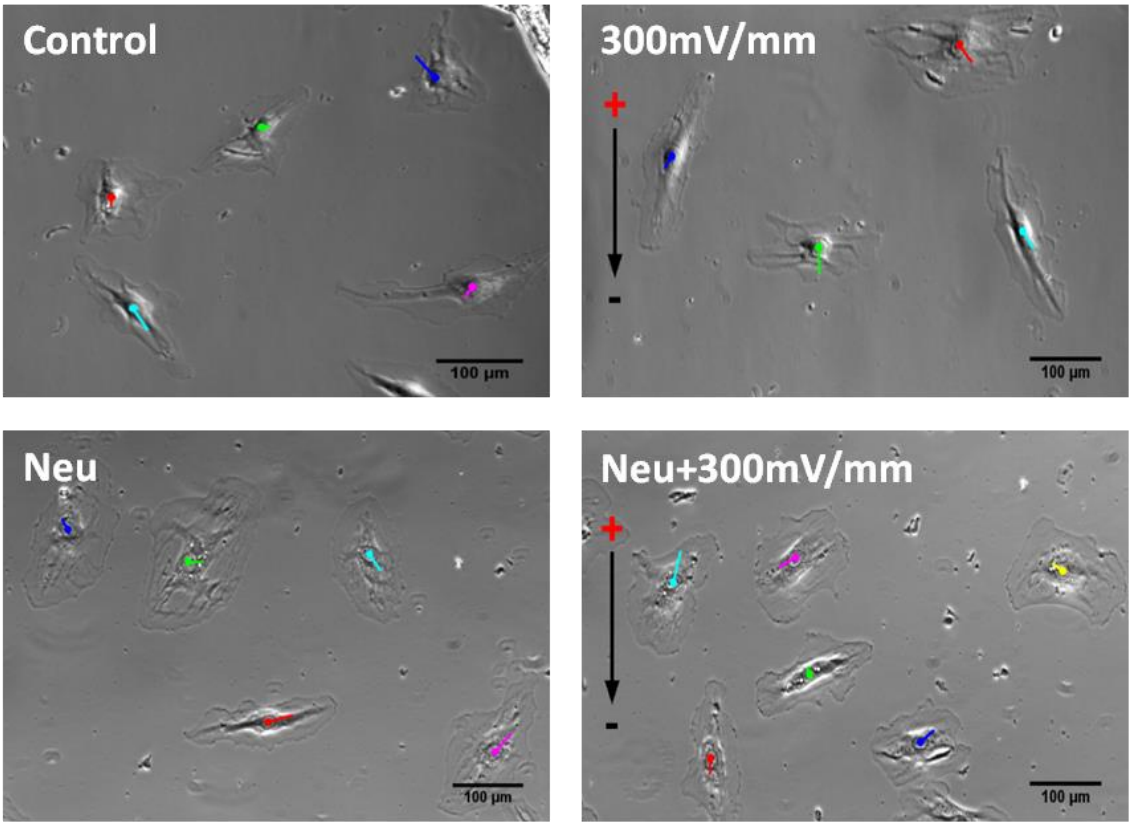

Figure 5.2 Representative images before and after EF stimulation.

Colour oval arrows refer to cell displacement and moving direction at the end of 5h, 300mV/mm stimulation. The tail of the arrow indicates the initial position of nucleus centroid, while the head represents the position at the end of 5h stimulation. Oval arrows in the upper right image points to the anode side, whereas others point randomly. Control: no Neu and no EF. Scale bar = 100µm.

5.3. Results

5.3.1. EF remarkably enhanced endothelial cell migration

Cells with and without EF stimulation were simultaneously tracked using time-lapse microscopy. As shown in Fig 5-3.A, the cells responded quickly when the field strength of 100mV/mm was applied for 1h, showing a much greater speed in comparison to the control. This speed was maintained over the entire period of the stimulation. Similarly, the migration speed was significantly elevated by 300mV/mm (Fig 5-3.B). Even though the speed appeared to gradually decrease alongside the increasing exposure time, the decreasing trend was parallel to the changes in the control, indicating that the reduction of speed was irrelevant to the field strength and the exposure time. In addition, cells were subjected to the field strength up to 500mV/mm (Fig 5-3.C). At first glance, the increase of migration speed at 500mV/mm was higher than those of 100mV/mm and 300mV/mm. Due to the relatively high speed in the corresponding control, it is inappropriate to draw the conclusion that EF-stimulated migration was voltage dependent.

To exclude the bias of cell passages and the performance of time during the experiments, normalized migration speed, which is defined as the speed of the stimulation group normalized by that of the corresponding control, was used for comparing the different field strengths over 5h stimulation. Compared to the control, there was a significant increase of migration speed in all stimulation groups, confirming that endothelial cell migration had been significantly sped up in applied EF. However, when the field strength was increased from 100mV/mm to 500mV/mm, the increase of the speed fluctuated narrowly around 40%, suggesting that EF-stimulated migration was voltage independent.

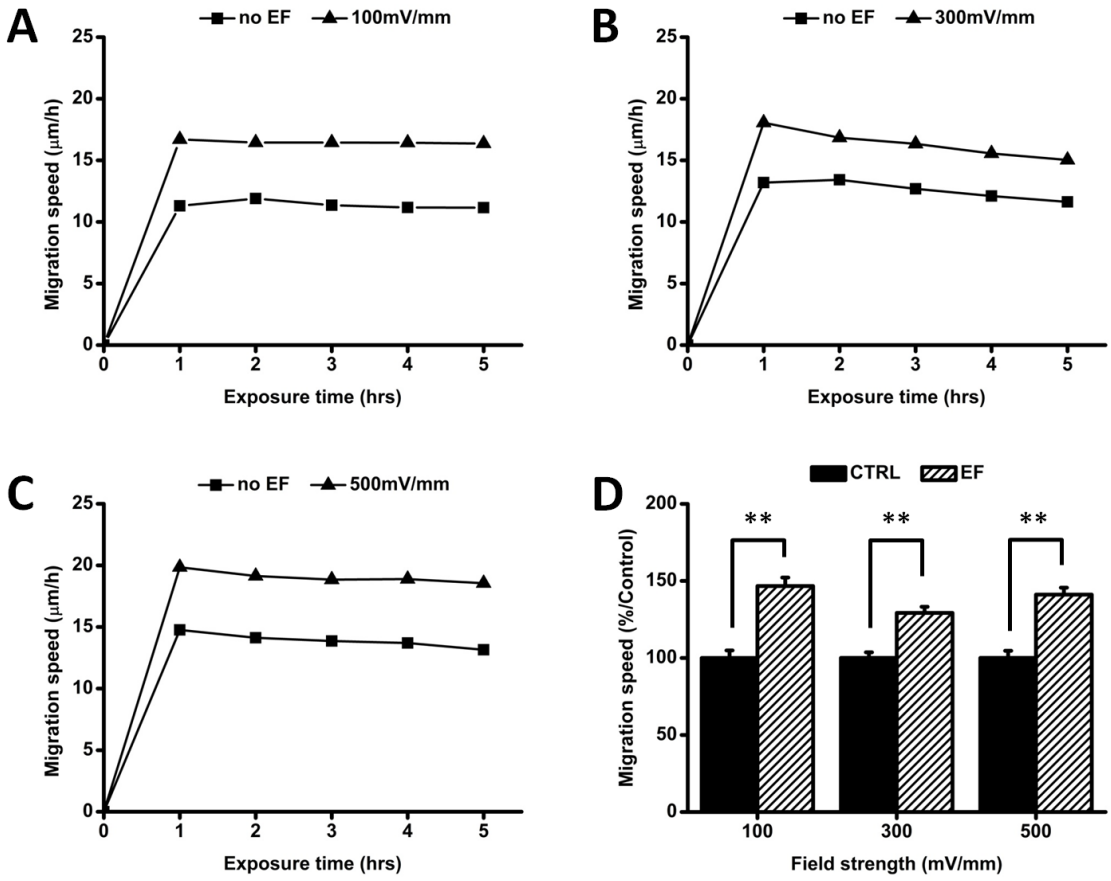

Figure 5.3 EF remarkably enhanced endothelial cell migration.

*Endothelial cell migration was recorded at intervals of 10mins for 5h using a time-lapse microscope. EF remarkably enhanced cell migration over the entire period of stimulation. (A) 100mV/mm. (B) 300mV/mm. (C) 500mV/mm. (D) The increase of migration speed over 5h was independent of EF strength. Cell numbers tracked for individual field strength and the corresponding control were 68 and 62 for 100mV/mm, 72 and 82 for 300mV/mm, and 68 and 53 for 500mV/mm. *P<0.05, **P<0.01 when compared with the control.*

5.3.2. EF guided endothelial cells migrate towards anode

To elucidate how endothelial cells moved in applied EF, trajectories with marked ends were plotted for each cell in a normalized scatter graph, where cell points all started from the origin of coordinate and ended in different quadrants. The upper two quadrants referred to the anode side and the lower quadrants to the cathode side. As shown in the control (Fig 5-4.A), the numbers of end points distributing evenly to each quadrant, indicating that endothelial cells moved randomly during static culture. This was further confirmed by the Rayleigh test, where *p* value equalled 0.5509. A biased distribution of cell points was not found until the field strength was increased to 300mV/mm, where the *p* value of the Rayleigh test dropped down to 0.0117. The cell points shifting to the upper two quadrants suggested that endothelial cell migration in applied EF was anodal preferential. When the field strength was additionally enhanced to 500mV/mm, further anodal migration was not observed. Instead, the Rayleigh test indicated that the biased cell migration was reversed to random movement in applied EF (Rayleigh test, p=0.1029).

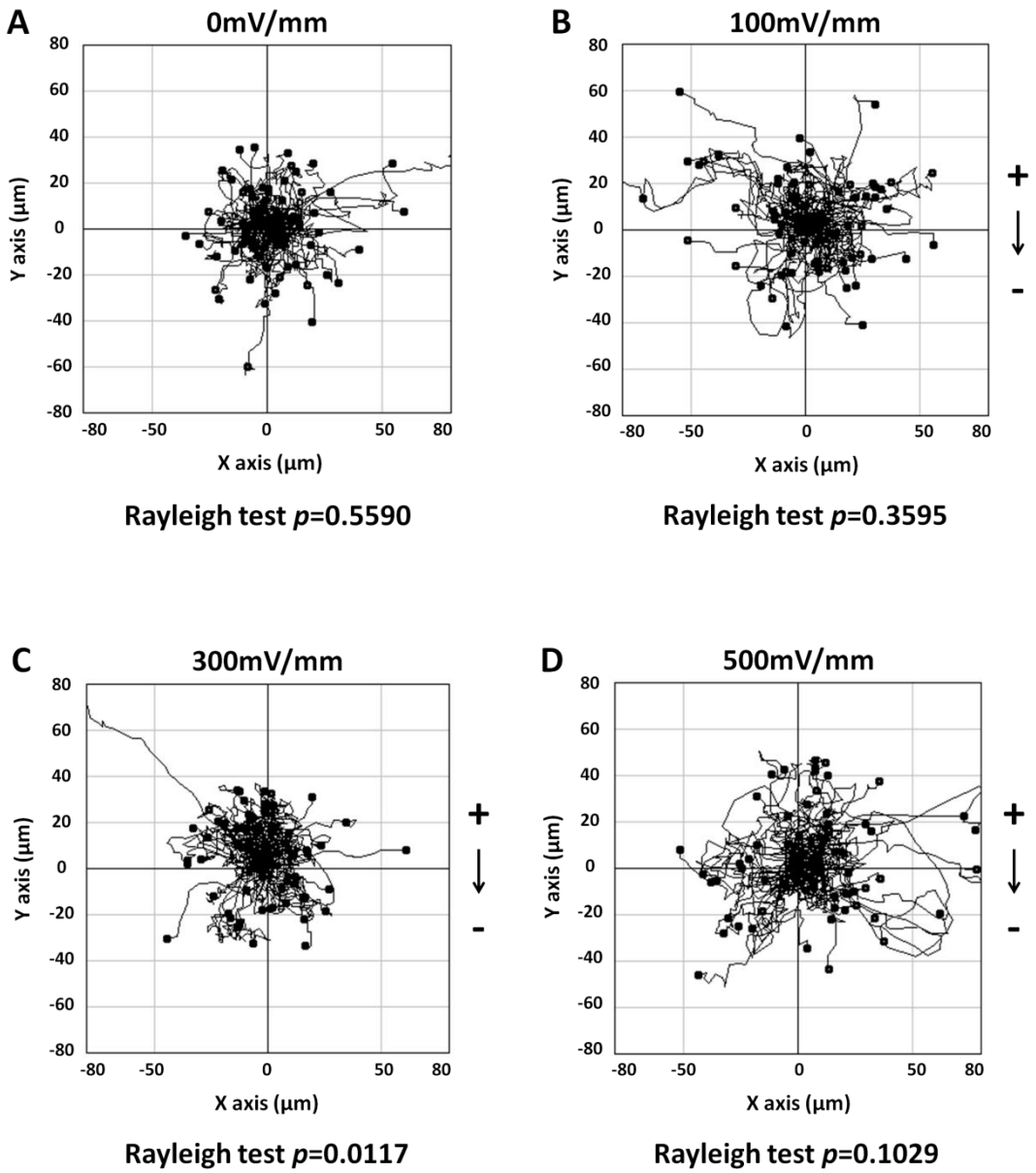

Figure 5.4 Trajectories of endothelial cells in applied EF.

The trajectory of each endothelial cell was plotted in normalized scattered graph, followed by a randomness detection using the Rayleigh test. The trajectories were ended with a solid circle. The 'less than 0.05' p value of the Rayleigh test indicated bias cell migration.

To further quantify biased cell migration, the directedness index (sinθ) was calculated. This was determined by the angle formed between the displacement vector and the line drawn perpendicular to the EF vector. Values changing from 0 to -1 indicated that the cells switched from random movement to straight anodal movement. As shown in Fig 5-5.A, the directedness slightly changed to -0.133±0.093 when the field strength of 100mV/mm was applied for 5h. This negative value was significantly increased when the field strength was enhanced to 300mV/mm (-0.241±0.083, $p<0.01$ vs. control), followed by a slight reduction at a field strength of 500mV/mm (-0.184±0.091, $p<0.05$ vs. control). Taken together, the above data demonstrated that the cells initiated anodal migration at the threshold of 100mV/mm and saturated at 300mV/mm. The following weaker response at 500mV/mm mainly resulted from the electrolysis occurring at higher voltage stimulation, where the guided signal was easily disturbed by side effects. In addition to the field strength effect, the time effect on directional cell migration was specifically studied at the field strength of 300mV/mm (Fig 5-5.B). The directedness of -0.473±0.063 showed that the anodal cell migration was more robust at 1h. It was not clear why a decreasing tendency of directedness occurred over the exposure time. One explanation may be that electrolysis took place immediately after the onset of EF, which counteracted the EF cues alongside the increase in time. Another explanation may be that a false robust response had been induced at an early stage due to equilibrium not having been achieved. Irrespective of the exposure time, the directedness was still greater than that of the control, verifying that endothelial cells performed anodal cell migration in applied EF.

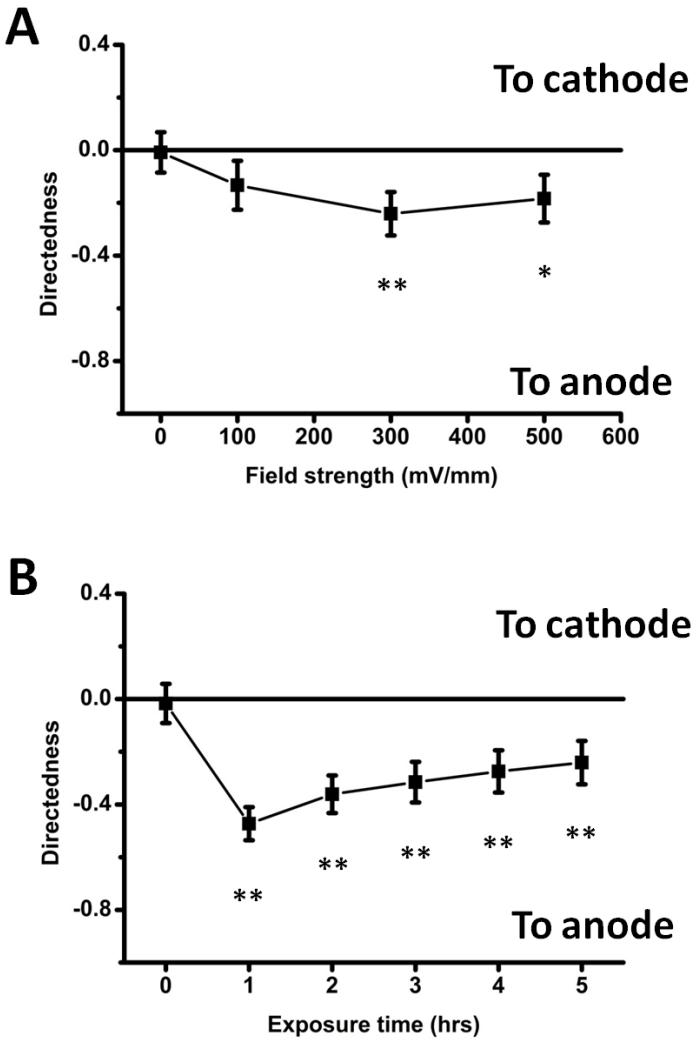

Figure 5.5 EF guided endothelial cells migrate towards anode.

*The direction of cell migration was quantified using directedness [sin (θ)], where the angle (θ) was formed between the cell displacement vector and a line drawn perpendicular to the EF vector. EF guided endothelial cells towards anode in a voltage-dependent mode (A). The time course of directedness at 300mV/mm was particularly marked. Directedness decreased with the increase of EF exposure time (B). Cell numbers tracked for each group were 62 for 0mV/mm, 68 for 100mV/mm, 72 for 300mV/mm, and 68 for 500mV/mm. *P<0.05, **P<0.01 when compared with the control.*

5.3.3. Enzymatic removal of the glycocalyx inhibited EF-enhanced cell migration

Before testing the role of the glycocalyx on EF-induced endothelial cell migration, removal of glycocalyx component was verified using confocal imaging. HUVECs were pre-incubated in a culture medium with 1U/ml Neu for 1h before subjecting them to EF and then exposed to a fresh medium with 0.2U/ml Neu throughout the stimulation period. The former step helped to remove all well-developed SA on the cell surface, while the latter further cleaved SA newly formed during the experiment. The representative images of cross sections showed that only a small amount of SA remained on top of the cytoplasm after 1h Neu pre-incubation (Fig 5-7.B'). The SA was not restored due to the additional exposure of Neu during the stimulation (Fig 5-7.C'). Removal efficiency was also confirmed by the measurement of fluorescence intensity (Fig 5-7.D). The intensity of the glycocalyx was dramatically decreased by 65% following 1h Neu pre-incubation (1h pre'Neu). Further reduction or recovery of glycocalyx intensity was not found after 5h additional exposure of Neu (5h add'Neu), confirming that SA was minimized over the entire period of the stimulation. Since WGA has cross-reactivity with N-acetyl-D-glucosamine, it is unlikely that the fluorescence intensity can drop down to 0. Additionally, to discover whether Neu can influence cell migration, endothelial cells with and without 5h Neu treatment were tracked (Fig 5-7.E). There was a slight decrease in migration speed from 11.42±0.34μm/h to 10.34±0.38μm/h. The difference was insignificant, so that the treatment of Neu did not disturb endothelial cell migration.

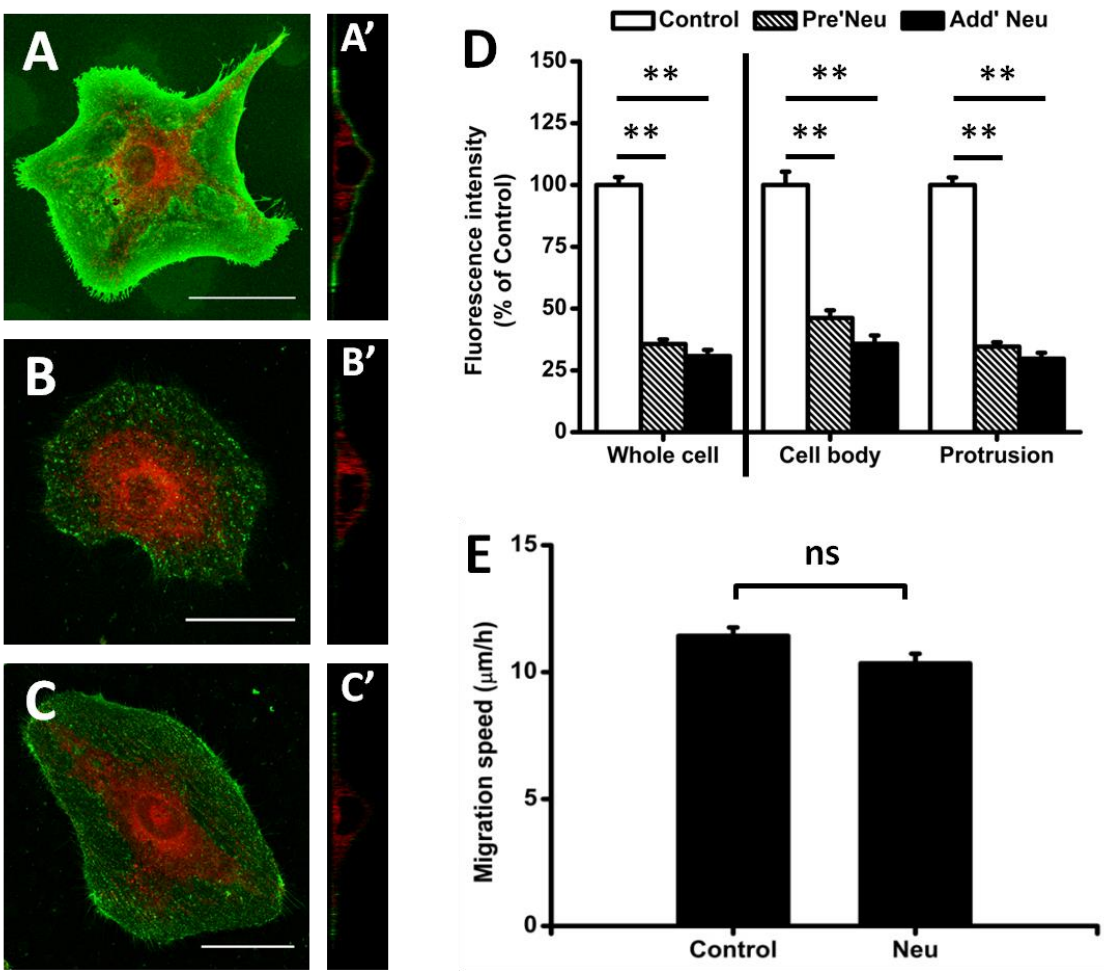

Figure 5.6 Enzymatic removal of the glycocalyx did not influence endothelial cell migration.

*Cells were pre-incubated with 1U/ml Neu for 1h and then incubated with 0.2U/ml Neu for an additional 5h. Following Neu cleavage, the glycocalyx layer was absent on the cell surface (B, C). (A) Without Neu. (B) Pre-incubation with 1U/ml Neu for 1h. (C) Pre-incubation plus 0.2U/ml Neu for 5h. Scale bar = 50μm. (D) The intensity of the glycocalyx on Neu-treated cells dropped in comparison to the control. (E) Removal of the glycocalyx by 5h Neu did not influence endothelial cell migration. Cell numbers tracked for each group were 16 for Without Neu, 19 for pre-Neu, 20 for add-Neu. *P<0.05, **P<0.01 when compared with the control.*

The migration speed of treated cells and non-treated cells were particularly compared in applied EF. The speed of treated cells strikingly decreased over the entire period of different EF stimulation. Cell movement was sustained at a speed of around 10μm/h, which was close to that of normal cells. The migration speed was then normalized to that of the corresponding non-treated cells over 5h EF exposure. The normalized speed significantly dropped by 30% at 100mV/mm. The decrease was maintained even if the field strength was enhanced up to 500mV/mm, indicating that EF-stimulated cell migration was suppressed by the treatment of Neu.

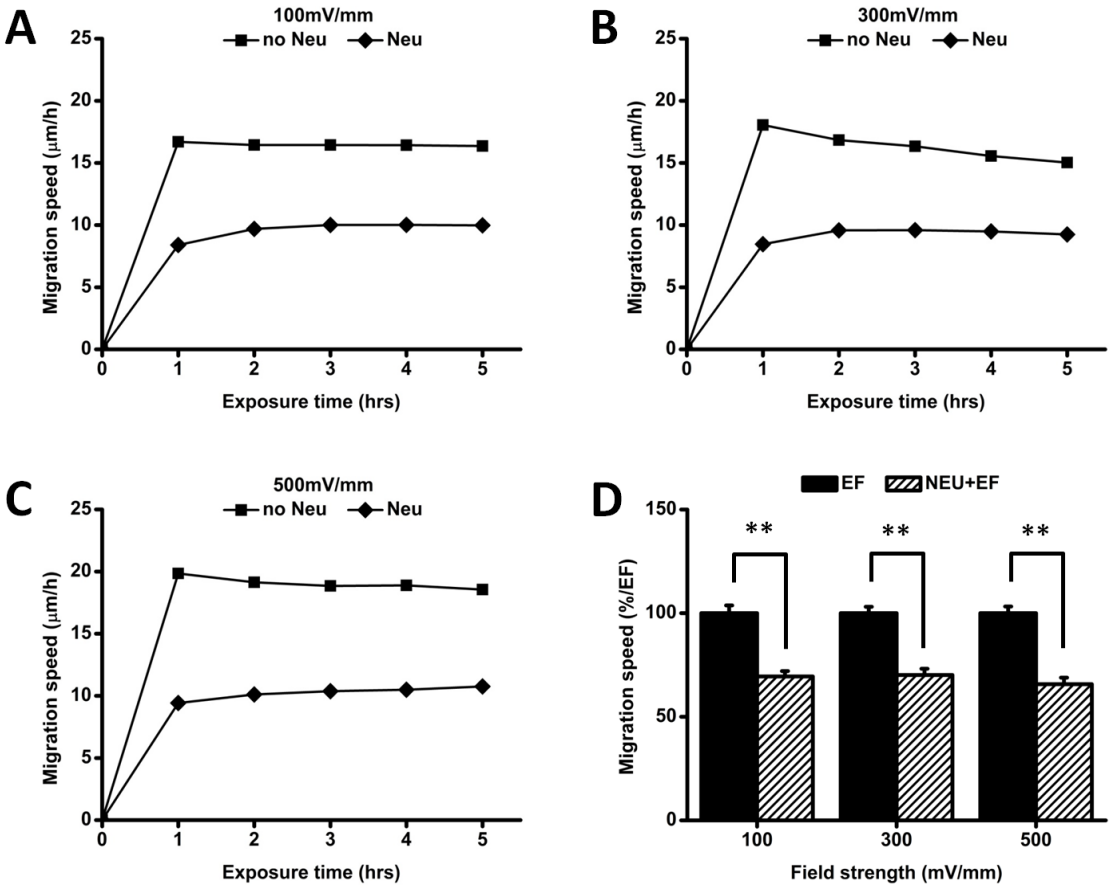

Figure 5.7 Enzymatic removal of the glycocalyx inhibited EF-enhanced cell migration.

Cells were pre-incubated with 1U/ml Neu for 1h and then exposed to EF, concurrent with 0.2U/ml Neu for an additional 5h. Removal of the glycocalyx by Neu inhibited EF-

*enhanced cell migration at all times. (A) 100mV/mm. (B) 300mV/mm. (C) 500mV/mm. (D) The decrease of migration speed over 5h. Cell numbers tracked for EF alone and EF plus Neu were 68 and 46 for 100mV/mm, 72 and 93 for 300mV/mm, and 68 and 62 for 500mV/mm. *P<0.05, **P<0.01 when compared with EF only.*

5.3.4. Enzymatic removal of the glycocalyx abolished anodal cell migration in applied EF

The trajectories of cell migration in applied EF were investigated following the removal of glycocalyx components. The trajectories with random distribution in terms of end points showed that only cells treated with Neu migrated randomly. No biased distribution was observed in treated cells when EF ranging from 100mV/mm to 500mV/mm was applied for 5h (Fig 5-9.B-D). The Rayleigh tests suggested that anodal cell migration in applied EF was suppressed by Neu treatment.

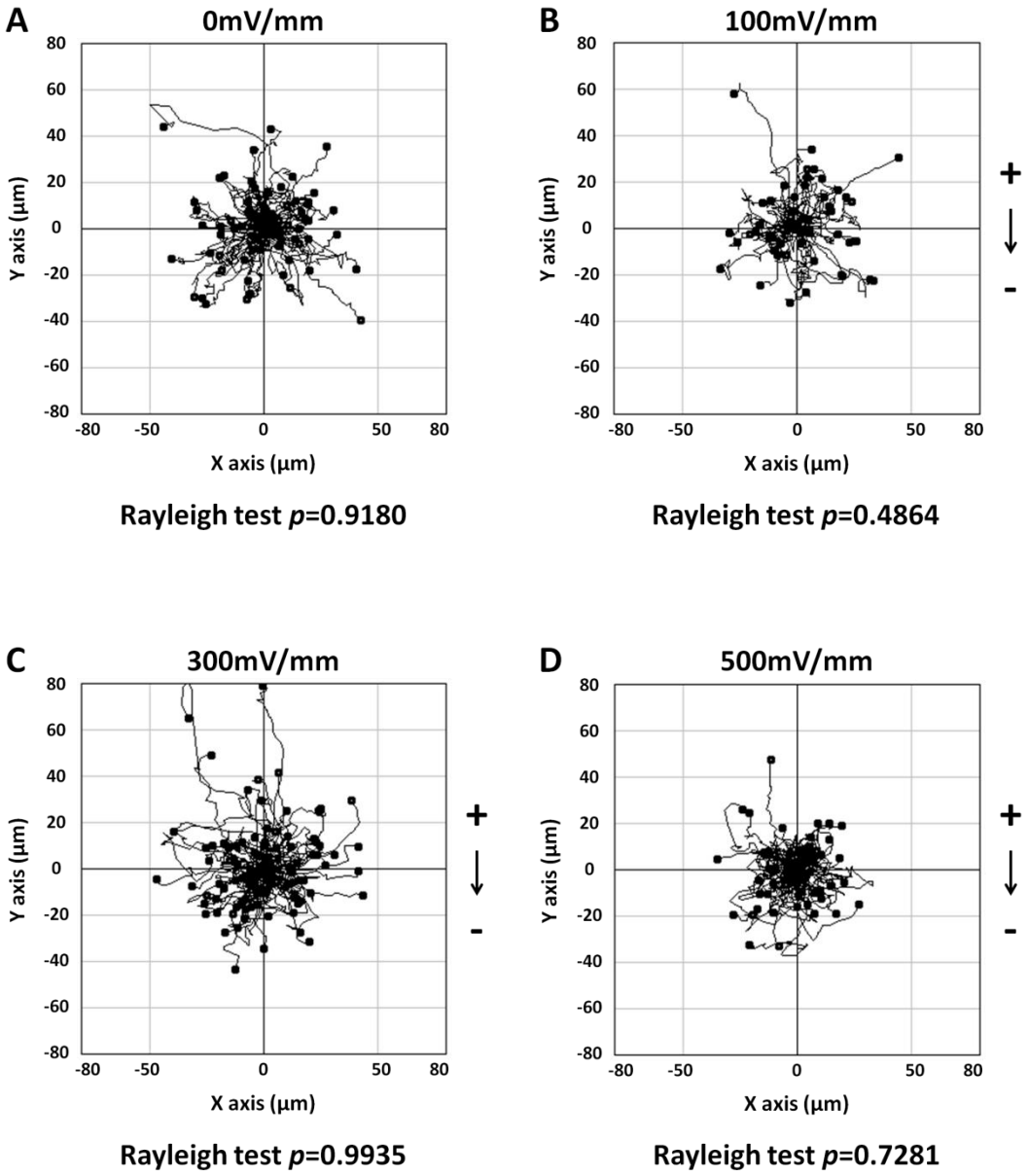

Figure 5.8 Trajectories of neuraminidase-treated cells in applied EF.

The 'greater than 005' p value of the Rayleigh test indicated random cell movement.

The inhibition of anodal cell migration was further quantified using directedness. As shown in Fig 5-9.A, the average directedness of treated cells always fluctuated around 0 when the field strength was enhanced from 0mV/mm to 500mV/mm, confirming that anodal cell migration in applied EF had been reversed to the random movement. The

maintenance of directedness at the base line over time (Fig 5-9.B) demonstrated that the abolishment of anodal cell migration was sustained for as long as cells were subjected to Neu.

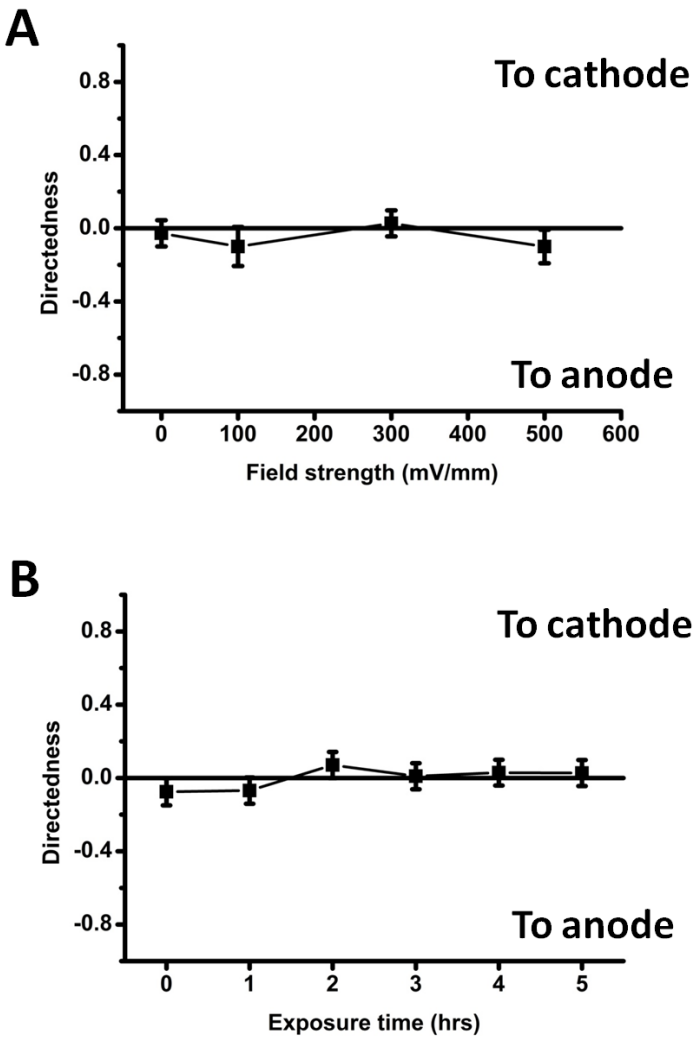

Figure 5.9 Enzymatic removal of the glycocalyx abolished anodal cell migration.

*Removal of the glycocalyx by Neu completely abolished anodal cell migration in applied EF (A). The time course of directedness at 300mV/mm in particular was extracted. Directedness remained close to 0 at all times (B). Cell numbers tracked for each group were 79 for 0mV/mm, 46 for 100mV/mm, 93 for 300mV/mm, 62 for 500mV/mm. *P<0.05, **P<0.01 when compared with Neu control.*

5.3.5. Anodal cell migration was not related to the polarization of the glycocalyx

To further elucidate how the glycocalyx contributes to directional cell migration, the distribution of the glycocalyx on the cell surface was evaluated after 5h and 300mV/mm stimulation. Compared to the control, EF-exposed cells still showed uniform distribution of the glycocalyx on the protrusion as well as on the cell body (Fig 5-10.B'). The fluorescence intensity of the glycocalyx in the XY plane did not differ significantly from that of the control (Fig 5-10.E), implying that no damage had been done to the glycocalyx during EF stimulation. Additionally, the intensity profiles of the glycocalyx in XY and YZ planes were plotted using heatmaps, where purple refers to an intensity-free background and red represents saturation intensity. Colour remaining at a similar level on the cell surface (Fig 5-10.D') confirmed that the glycocalyx had not been polarized to the anodal side of the cell surface.

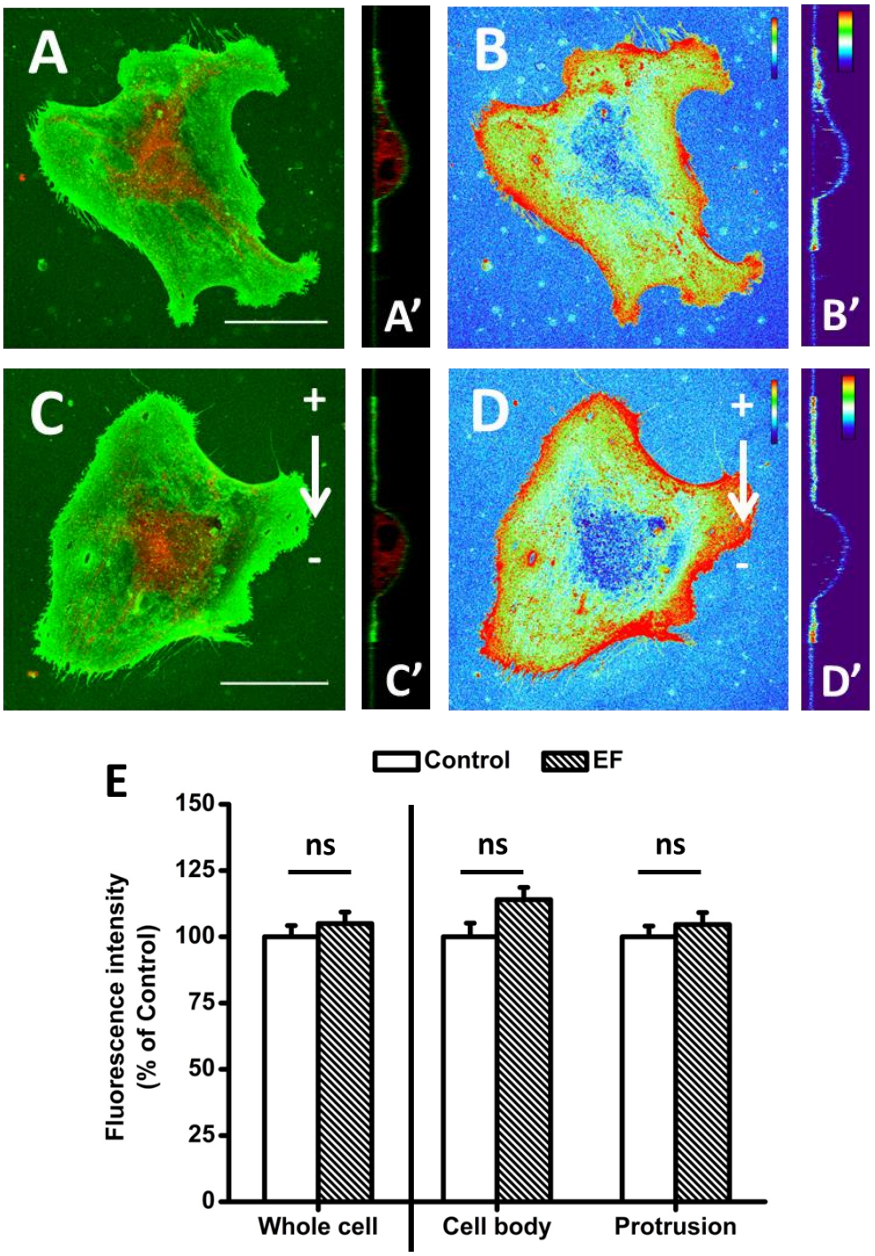

Figure 5.10 Anodal cell migration was not related to the polarization of the glycocalyx on the cell surface.

The distribution of the glycocalyx was quantified using heatmap analysis before and after 5h at 300mV/mm stimulation. No polarization of the glycocalyx was observed after EF stimulation. (A, B) without EF. (C, D) with EF. Scale bar = 50μm. The intensity of the glycocalyx remained unchanged before and after stimulation (E). Cell numbers tracked for

*each group were 16 for the control, 16 for EF. *P<0.05, **P<0.01 when compared with the control.*

5.4. Discussion

In this study, our results showed that 1) EF remarkably enhanced endothelial cell migration; 2) EF guided endothelial cells towards anode; 3) Removal of the glycocalyx inhibited EF-enhanced cell migration; 4) Removal of the glycocalyx abolished anodal cell migration in applied EF; 5) Anodal cell migration was not related to the polarization of the glycocalyx on the cell surface.

5.4.1. Involvement of the glycocalyx in EF-stimulated endothelial cell migration

Endothelial cells undergo persistent, spontaneous migration prior to cell division and contact inhibition. It is a dynamic, coordinated process that includes the protrusion of the leading edge, the formation of new adhesions at the front, the contraction of the endothelial cell body and the release of developed adhesions at the rear (Fig 5-11.A) (Lamalice et al., 2007). This can be remodelled by external chemical and physical cues. Compared to the haemodynamic forces that endothelial cells naturally experience, the significance of EF in endothelial cell migration has not been given much attention. The effect of EF stimulated endothelial cell migration is uncertain. By tracking the cell nucleus, Zhao et al. demonstrated that the migration speed of HUVECs remained at 1-2μm/h prior to and after 150mV/mm stimulation (Zhao et al., 2004). In the same year, the researchers drew a map

for vascular cell migration by using translocation rate instead of migration speed (Bai et al., 2004). The rate of HUVECs shown in this instance was enhanced in voltage dependent mode, where a steep increase from 1μm/h to 5μm/h was found at 50mV/mm and a plateau (7μm/h) was approached at 200mV/mm. In our study, the absolute values (>10μm/h) in each group were much greater than those in Zhao et al.'s reports. The migration speed of cells in applied EF was prominently increased, but the normalized speed for different field strengths indicated that the increase of migration speed was independent of the magnitude of applied EF.

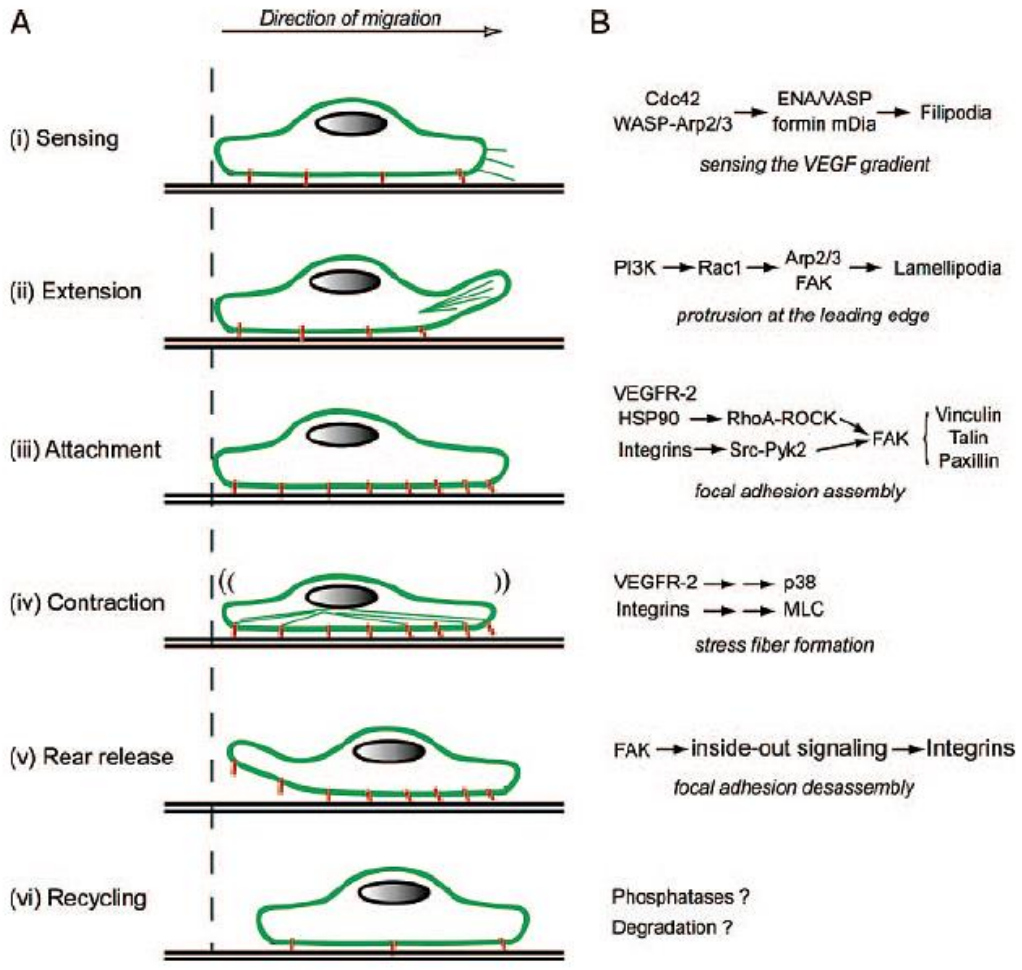

Figure 5.11 Steps for endothelial cell migration.

(Lamalice et al., 2007)

Spontaneous cell migration is an integrated molecular process that involves the activation of Cdc42/Rac at the leading edge, intracellular catalysis from PI3K signalling and coordination of Rho A from the front to the rear of the cell. (Vicente-Manzanares et al., 2005, Lamalice et al., 2007). Similarly, EF alters cell movement through the same elements. For instance, Chao et al. demonstrated that blocking Ca^{2+} entry into the chondrocytes decreased cell migration through the inactivation of the inositol phospholipid pathway (Chao et al., 2000). Zhao et al. reported that genetic disruption of PI3K-γ in keratinocytes largely inhibited cell motility in applied EF (Zhao et al., 2006), whilst the inhibition of Cdc42/GSK-3β signalling significantly reduced the migration speed of CHO cells (Cao et al., 2011). Since both types of movement rely on similar migratory mechanics, the inhibition effects on EF-stimulated cell migration are confusing. It is difficult to tell whether it is an actual effect on EF stimulated migration or false effect occurring due to the affected spontaneous migration. In our study, this concern was largely excluded. By applying Neu treatment prior to and during the entire period of stimulation, the SA on both well-developed and developing glycocalyx was exclusively removed from the endothelial cell surface. Although the migration speed of treated cells was slightly decreased (10.34±0.38μm/h) compared to the control (11.42±0.34μm/h), the difference was insignificant, indicating that spontaneous cell migration had not been disturbed. More importantly, the increase in migration speed in cells subjected to the EF was largely inhibited. The suppression of cell migration wasn't restored, even when the time and field strength increased. Treated cells maintained spontaneous cell migration rather than remaining static throughout the stimulation. In other words, EF-accelerated endothelial cell migration requires the sensation of SAs on the glycocalyx.

5.4.2. EF-directed anodal migration in endothelial cells

Apart from the translocation speed, transition from random movement to directional migration in endothelial cells is an important motility, which is regulated by external cues. It emerges in a variety of mechanisms such as chemotaxis (directional migration stimulated by a gradient of soluble chemoattractants), haptotaxis (directional migration induced by a gradient of substrate-bound chemoattractants), mechanotaxis (directional migration in response to the haemodynamic forces) and electrotaxis (directional migration driven by a gradient of electrical potential). To date, electrotaxis is the least studied effect among these. Increasing evidence regarding electrotaxis will help to highlight the importance of directional cell migration in angiogenesis. In the present study, endothelial cells in applied EF moved preferentially to the anode compared to the cells without stimulation. There was a steep increase of directedness starting from 100mV/mm to 300mV/mm (-0.241±0.083 at 5h), which was followed by a gradual decrease at 500mV/mm (-0.184±0.091 at 5h). This change was consistent with changes reported previously (Bai et al., 2004, Zhao et al., 2004). It was shown that HUVECs responded to the EF at a threshold of 150mV/mm. The directedness was maintained at roughly -0.25, between 150mV/mm to 300mV/mm and then dramatically decreased at 400mV/mm. Our results and previous studies collectively indicated that anodal migration was inhibited when cells were over-stimulated.

Moving direction of cells varies according to cell types, as does the magnitude of directedness. The magnitude of directedness may be related to the coordination of membrane protrusion. The electrotaxis is generally classified into two types (Table 5-1). Cells that responds strikingly and/or quickly within a certain period of stimulation are

defined as strong responding cells (absolute directedness>0.5). These include fibroblasts, keratinocytes and cancer cells (Brown and Loew, 1994, Nishimura et al., 1996, Djamgoz et al., 2001). Cells that react weakly and slowly throughout stimulation, such as vascular cells, epithelial cells and embryonic stem cells (Zhao et al., 1996, Zhao et al., 1999, Wang et al., 2000, Bai et al., 2004, Zhang et al., 2011) are classed as weak responding cells (absolute directedness≤0.5). According to this classification, we should notice that strong responding cells are fibroblast-like cells that share a spindle shape with the less-extended membrane protrusion. Strong responding cells' bodies are more easily synchronized when the peripheral membranes protrude. The entire cell is capable of moving directly along the EF vector (Finkelstein et al., 2004). On the other hand, weak responding cells (except SMCs) normally contain large lamellipodium and appear epithelial-like. The signal transduced from the cell body to the membrane protrusion can be time consuming and divergent. In addition, the well-spread lamellipodium generally hinders spontaneous cell migration due to the relatively firm cell attachment to the substrate. As a result, the magnitude of directedness in applied EF is easily compromised.

Table 5-1 Classification of directional cell migration in applied EF.

Strong responding cells			Weak responding cells		
Cell type	**Directedness**	**Time**	**Cell type**	**Directedness**	**Time**
Dictyostelium cells (Sato et al., 2009)	0.88±0.02	0.5h	**HMECs (Bai et al., 2004)**	0.35±0.08	5h
Keratinocytes (Nishimura et al., 1996)	0.81±0.03	2.5h	**HUVECs (Zhao et al., 2004)**	-0.149±0.08	5h
Fibroblasts (Brown et al., 2004)	0.73±0.05	1h	**Aorta SMCs (Bai et al., 2004)**	-0.35±0.05	5h
Prostate cancer cells *(Highly invasive)* (Djamgoz et al., 2001)	0.82±0.01	6h	**Prostate cancer cells *(Less invasive)* (Djamgoz et al., 2001)**	-0.34±0.01	6h
Chondrocytes (Chao et al., 2000)	0.94±0.83	2h	**Lens epithelial cells (Wang et al., 2000)**	0.35±0.07	5h
MSCs (Zhao et al., 2011)	-0.54±0.04	2h	**Corneal epithelial cells (Zhao et al., 1999)**	0.31±0.09	5h
iPS cells (Zhang et al., 2011)	-0.70±0.08	1h	**Embryonic stem cells (Zhang et al., 2011)**	0.14±0.12	3h
Fibroblast-like cells			**Epithelial-like cells**		

The occurrence of chemotaxis was not experimentally excluded in the present study. Due to the electrophoresis effect, a concentration gradient of growth factors likely occurred due to the applied EF. In particular, VEGFs, the most abundant and highly endothelial cell-specific ligands in the medium were driven to the cathode side, owing to its isoelectric point of 8.5 (medium pH=7.4). If chemotaxis occurred, HUVECs should have moved to the cathode where positively charged VEGFs had accumulated. However, our study, as well as Bai et al.'s report (Bai et al., 2004), demonstrated that HUVECs preferred moving to the anode rather than the cathode. It was unlikely that electric cues directed cell migration through the gradient of VEGFs. To completely rule out chemotaxis in response

to growth factors, it is important to introduce a flow chamber that can dispel the accumulation of VEGF.

5.4.3. Contribution of the glycocalyx to EF-directed endothelial cell migration

Intracellular signalling pathways like PI3K and Rho GTPases trigger a cascade of downstream events and thereafter mediate the electrotaxis in endothelial cells (Zhao et al., 2004). For this study, we focused on an extracellular complex, namely the glycocalyx coated on the apical surface of endothelial cells. This layer varies from 100 nm to several μm in thickness and is composed of a network of proteoglycans and glycoproteins. Of all the glycocalyx components, the termination of SA on the mature chains of the glycocalyx is uniquely representative of the coverage of the glycocalyx. The link with carboxyl groups imbues the glycocalyx with a bulk of negative charges, raising the possibility that the glycocalyx might have a big impact on electrotaxis. Based on the labelling of SA, we have verified that the glycocalyx was sufficiently recovered on the cell surface prior to stimulation. This type of cell was “electrophoretically” moved to the anode when subjected to the EF. Contrastingly, this anodal migration was completely suppressed in the Neu-treated cells. The above results supported our main hypothesis that anodal cell migration can be attributed to the coverage of charged glycocalyx on the endothelial cell surface. Although sulphate groups such as HS also contribute to networks of negative charges, they were hardly found on the HUVECs surface using immunofluorescence. The impact of HS on electrotaxis was negligible.

Whether the magnitude of directedness has been determined by the amount of the glycocalyx on the cell surface was uncertain. The averaged directedness indicated that the cells preferred moving towards the anode. However, as shown in the frequency distribution of directedness, a small portion of cells still executed weakly anodal or even cathodal migration (Fig 5-12). The estimation of coverage and amount of the glycocalyx were all based on FITC-WGA labelling prior to stimulation. WGA is small molecule that can be easily taken by live cells following over-time incubation. Performing real time observation of the glycocalyx in combination with cell migration proved impracticable. It was uncertain whether moving cells with small negative or positive value of directedness should be attributed to the insufficient recovery of the glycocalyx. For the same reason, whether cells with greater negative values were to be attributed to the large amount of glycocalyx was also unclear. Despite the limitations listed above, our results still strongly support the hypothesis that the glycocalyx is responsible for anodal cell migration *in vitro*. Finding a practical way to establish the relationship between directedness and the amount of the glycocalyx will add further value to our conclusion.

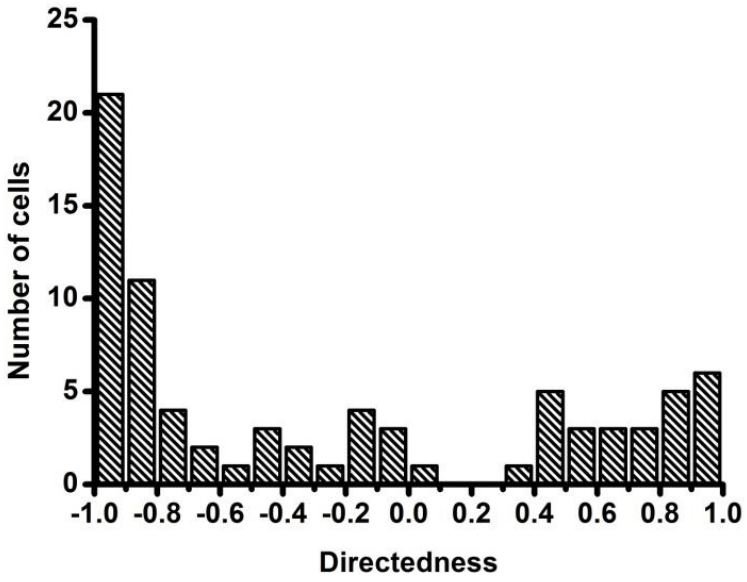

Figure 5.12 Frequency distribution of directedness in 5h, 300mV/mm EF.

The spatial polarization of molecules or organelles is another potential mechanism involved in electrotaxis. In the early 1980s, McLaughin and Poo found that concanavalin A receptors were capable of moving towards the cathode side of muscle cells in applied EF (McLaughlin and Poo, 1981). Following on, Zhao et al. demonstrated that more functional molecules such as EGF and TGF receptors accumulated on the cathode side of epithelial cells (Zhao et al., 1999). Asymmetrical redistribution of EGF receptors was particularly involved in cathodal cell migration. However, the importance of the polarization of charged surface proteins on HeLa cells was disputed in terms of determining electrotaxis (Finkelstein et al., 2007). Given that the redistribution of surface molecules is less identified in endothelial cells, it is worth considering whether the polarization of the glycocalyx participates in anodal cell migration. According to the cross-sectional images and heatmaps in Fig 5-10, the glycocalyx was distributed evenly on the apical surface prior to the onset of EF. Following 5h stimulation, polarization of glycocalyx to either side of the cell surface was barely present, excluding the postulation that EF initiated anodal migration by driving the glycocalyx to the anode side of the cell.

Nonetheless, the following can be used to explain the failure to verify the polarization of the glycocalyx: 1) the glycocalyx anchors on the surface membrane via the actin cytoskeleton. Actin filaments assemble in various forms. During electrotaxis, the reorganized actin cytoskeleton mainly refers to the actin filament bundles on the basal membrane, rather than the actin filament network at the cortex. The cortical actins remain relatively stable, so that they stabilize the membrane and the embedded glycocalyx at all times. The displacement of the glycocalyx is accordingly constrained; 2) an electromechanical model has recently been proposed as a transduction mechanism for applied EF (Fig 5-13.A) (Hart, 2008, Hart, 2010). By using alternating current EF, the

researchers described that an electrical force was exerted on the glycocalyx and then transmitted into the cell interior via the actin cytoskeleton. Regarding the calculation, other forces derived from the surrounding environment were also considered. These included drag forces induced by the medium and the restoring force of the membrane. Due to the counteraction between each type of force, the net force exerted on the glycocalyx was negligible (Fig 5-13.B) and consequently, the glycocalyx remained relatively static. This model also works for direct current EF (Hart et al., 2013). Direct current EF exerts a constant torque on the glycocalyx that is transmitted as a constant force on the cytoskeleton. The forces acting on the glycocalyx are similarly counteracted, which in turn helps to explain why polarization of the glycocalyx was not necessary for signal transduction in the present study; 3) the electrical force acting on the glycocalyx may induce bending instead of polarization and angular displacement. However, in our study, the visualization of the glycocalyx was achieved by using a confocal microscope. Considering the dimension of the glycocalyx proposed by Squire et al. (Squire et al., 2001), the scanning format of 0.232μm×0.232μm×0.3μm (lateral resolution=139.4nm, axial resolution=235.8nm) did not provide a high enough resolution for observing the ultrastructure of the glycocalyx (20nm for core protein spacing and 100nm for intercluster spacing). In other words, the bending amplitude can be omitted due to the limited resolution and magnification properties of the confocal microscope. The fluorescent-labelled glycocalyx is always displayed as a continuous and dense layer.

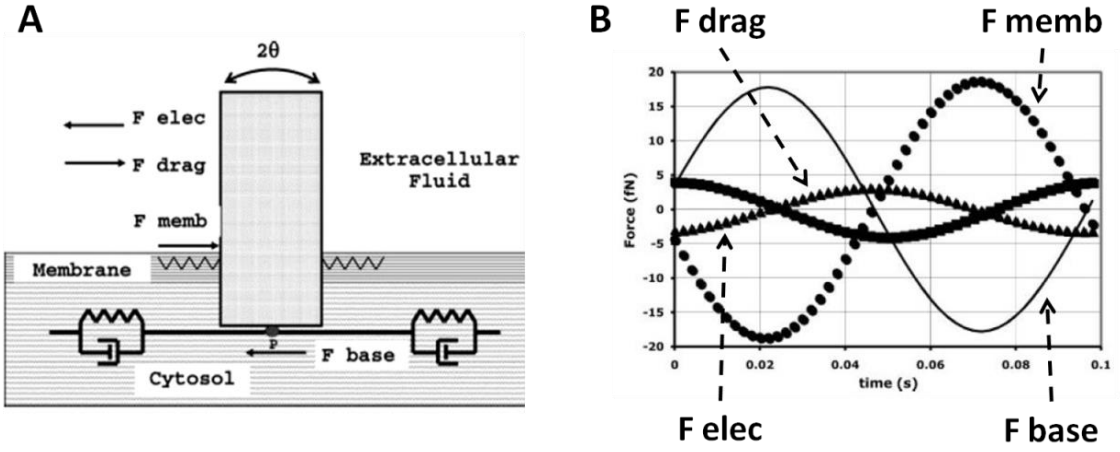

Figure 5.13 An electromechanical model for glycocalyx vibration.

(Adapted from Hart, 2010)

5.4.4. Other glycocalyx-coupled mechanisms in EF-directed endothelial cell migration

The mechanisms that link the glycocalyx and electrotaxis include more than simply spatial polarization and mechanical transduction. Increasing evidence suggests that the opening of sodium channels acts as a potential coupling event. The involvement of voltage-gated sodium channel (VGSC) in electrotaxis has been found in highly metastatic cancer cells. Blockage of VGSC with tetrodotoxin suppresses cathodal cell migration, while veratridine enhances it by persistently activating VGSC (Djamgoz et al., 2001). VGSC is composed of a pore-like α subunit and several β subunits. They are both terminated with SA and modulated by SA in a similar manner. SA binds to α subunit trigger channel gating at lower depolarized potentials and the fully sialylated β subunit induces a shift of channel gating in the hyperpolarized direction (Johnson et al., 2004). As a result, entry of Na^+ into the cells will easily occur in response to the next depolarization pulse. The expression of

VGSC is also found in endothelial cells. Unlike the low importance of voltage-gated calcium channels on Ca^{2+} entry into endothelial cells, the activity of VGSC on Na^{+} entry mediates multiple angiogenic functions including endothelial cell migration (Andrikopoulos et al., 2011). With the coverage of the glycocalyx, the membrane potential of endothelial cells is maintained at a relative hyperpolarized level. The applied EF easily triggers membrane depolarization and in turn, facilitates the entry of Na^{+}, eventually leading to anodal cell migration.

Apart from the VGSC, sodium channels insensitive to the voltage also contribute to electrotaxis. The epithelial sodium channel (ENaC) is highly expressed in different types of epithelium and mediates the homeostasis of Na^{+} transport and water balance between the cell and the microenvironment. The involvement of ENaC in directional cell migration is detected not only in the closure of wound healing (endogenous EF), but also in applied EF (Exogenous EF). Genetic depletion or pharmacologic blockade of ENaC abolishes cathodal migration in keratinocytes, whereas over-expression or persistent opening of ENaC further increases the magnitude of electrotaxis. (Chifflet et al., 2005, Del Monaco et al., 2009, Yang et al., 2013). The ENaC is not restricted to the epithelium. A number of other cell types such as endothelial cells express ENaC. The coverage of the glycocalyx over ENaC maintains limited Na^{+} entry into endothelial cells (Fig 5-14) (Warnock et al., 2014). If the glycocalyx is deranged or cleaved, more ENaCs are exposed and the entry of Na^{+} is increased. This excessive Na^{+} compels polymerization of G-actin to F-actin and thereafter maintains endothelial cells in a stiffened state. This contrasts to the actin dynamic in electrotaxis and may be the reason why anodal cell migration shifts back to

random movement. Assuming the activity of ENaC is enhanced in response to the EF, the glycocalyx may function as an inhibiting factor for Na^+ homeostasis in electrotaxis.

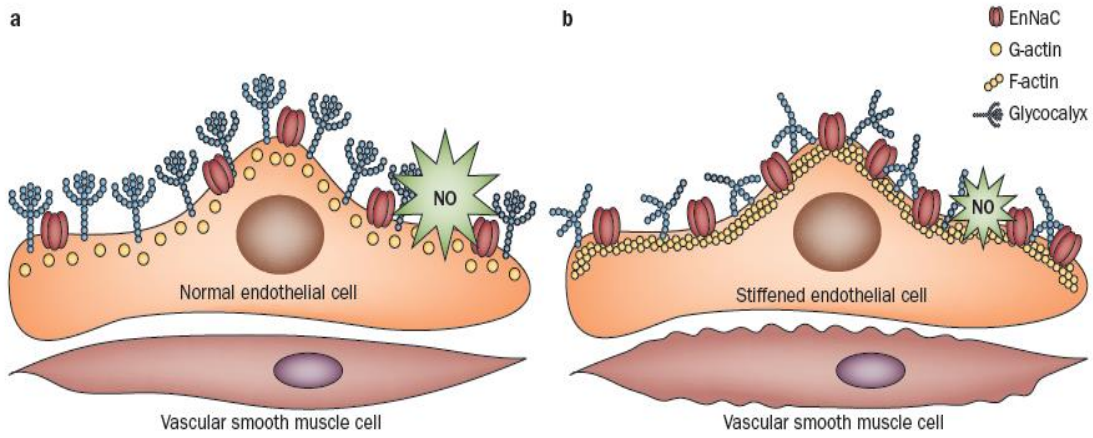

Figure 5.14 A model for EnNaC-dependent transition.

(Warnock et al., 2014)

5.4.5. Pathophysiological implications

Angiogenesis plays an indispensable role in tissue development, wound healing, as well as tumour growth and metastasis. Both endogenous EF and exogenous EF are involved in the regulation of angiogenesis. (1) ***Therapeutic angiogenesis.*** EF-guided angiogenesis was a non-molecular and non-invasive strategy first proposed by Kanno et al. in 1999 (Kanno et al., 1999). Since then, advances have been made in the field of its effectiveness and the disclosure of participating cellular events (Amaral et al., 2000, Ebina et al., 2002, Hudlicka et al., 2002, Milkiewicz et al., 2005). However, the progression was far from what had been expected due to poorly understood molecular mechanisms. Applying EF for therapeutic angiogenesis was controversial and had been underestimated, especially compared to the molecular therapy such as vascular endothelial growth factor delivery. The introduction of the endothelial glycocalyx offers a novel signaling pathway for

electrotaxis in endothelial cells. It particularly provides an alternative to the commonly accepted mechanisms involved in EF-guided angiogenesis, which will render EF a more convincing approach toward achieving therapeutic angiogenesis. (2) ***Anti-angiogenesis.*** Apart from therapeutic angiogenesis, anti-angiogenesis is of great interest to clinicians. This area of research holds particular promise for the treatment of tumour growth and metastasis (Farnsworth et al., 2014). Blood vessels developing in the tumour are subjected to endogenous EF. It is unlikely that we can electrically reverse the directional movement of endothelial cells in the tumour. Instead, we are able to target the endothelial glycocalyx as a novel approach for facilitating anti-angiogenic therapy. By disrupting the endothelial glycocalyx, cellular sensing ability to the endogenous EF is disturbed. The suppression of electrotaxis in endothelial cells could in turn weaken the EF-guided angiogenesis in the tumour.

In conclusion, I have demonstrated an indispensable role of the endothelial glycocalyx in EF-directed cell migration. The anodal cell migration in an applied EF is attributed to the presence of endothelial glycocalyx, but not related to the polarization of the glycocalyx on the membrane. All these data provide new insights into the vasculoprotective properties of the glycocalyx. As directional cell migration is an essential step in angiogenesis, these results also suggest an alternative mechanism for EF-guided angiogenesis and vascular regeneration.

6. Summary and future work

The endothelial glycocalyx, an interface between the endothelium and blood flow, plays a pivotal role in maintaining vascular homeostasis. It serves as a barrier to prevent the interaction between blood cells/plasma proteins and the endothelium. It also acts as mechano -sensor and -transducer to modulate vasodilatation. Damage to the glycocalyx causes vascular pathological changes and in turn contributes to the development of cardiovascular diseases such as atherosclerosis. To date, the metabolism and the vasculoprotective properties of the glycocalyx are not fully understood. In this thesis, I have demonstrated factors impacting on the recovery and stability of the glycocalyx, and the important role of the glycocalyx in EF-directed cell migration *in vitro.*

Original contribution

- ✓ Although the difference in the glycocalyx thickness between natural endothelium and cultured endothelial cells is widely recognised, the factors involved are not fully understood. In chapter 3, I have demonstrated for the first time that cell shape is of great importance to the recovery of the glycocalyx. This finding leads to a better understanding of the glycocalyx formation. As such, it may promote the development of new approaches to restore the glycocalyx in diseases.

- ✓ The actin cytoskeleton provides support for the membrane and molecules anchored on it. However, no study has experimentally verified to what extent the actin cytoskeleton contributes to the stability of the glycocalyx. In chapter 4, I have demonstrated for the first time that the actin cytoskeleton plays an important role in

stabilizing the glycocalyx under laminar flow conditions. This finding contributes to the knowledge of the structural stability of the glycocalyx and thereafter will help to develop new strategy against the shedding of the glycocalyx in diseases.

- ✓ It has been shown that EF guides endothelial cell migration. However, the underlying mechanism is poorly understood. Whether the glycocalyx is involved in EF-directed endothelial cell migration has not been studied. In chapter 5, I have demonstrated for the first time that the glycocalyx is indispensable for the directional cell migration in an applied EF. This finding not only highlights the functional importance of the glycocalyx in endothelial behaviours, but also provides new insights into the field of EF-guided angiogenesis.

Contribution of cell density and cell shape to the recovery of the glycocalyx following trypsinization.

The glycocalyx is severely damaged following trypsinization, leaving a dense aggregate on the cell surface. The increase of the intensity of the glycocalyx from 16h to 48h is calculated for assessing the recovery rate of the glycocalyx. Higher cell density results in more rapid recovery of the glycocalyx within 48h. Regardless of the initial seeding densities, the glycocalyx is well-developed on confluent cells. Moreover, an index i.e., spatial coverage ratio, is used for quantifying the spatial distribution of the glycocalyx. This ratio increases as cell seeding densities increase and reaches maximum when cells become confluent, indicating that higher cell density culture results in more uniform distribution of the glycocalyx on the cell surface.

High cell density culture is characterized by the presence of cell-cell contacts. The degree of cell-cell contacts is negatively correlated with cell stiffness (Stroka and Aranda-Espinoza, 2011). Changes of cell stiffness may alter cell behaviours such as biosynthesis of the glycocalyx. However, cell culture with different densities is not a precise control for the cell stiffness. Whether cell stiffness is causally involved in the recovery of the glycocalyx remains to be elucidated. Manipulation of cell stiffness by changing substrate rigidity may provide a solution to this problem (Tee et al., 2011). Furthermore, the glycocalyx is dynamically developed and degraded. It is unclear whether the alteration of cell stiffness can lead to shedding of the glycocalyx. One prerequisite for proving this is to preserve the well-developed glycocalyx prior to the alteration of cell stiffness. Temperature-responsive cell culture surface may make it possible to prevent the degradation of the glycocalyx due to its non-enzymatic digestion technology. Temperature-responsive cell culture surface is fabricated with an immobilized polymer layer i.e., poly(N-isopropylacrylamide). This layer is hydrophobic at 37°C, allowing cells to attach and grow, and becomes very hydrophilic when the temperature of the culture is reduced to below 32°C, resulting in the release of adherent cells. By using this technique, single cells or monolayer cells can be harvested and transferred without damage to the cell surface proteins. Further research will focus on these techniques and carefully correlate cell stiffness and the coverage of the glycocalyx.

I use micropatterning to demonstrate for the first time that cell shape plays an important role in the recovery of the glycocalyx. The glycocalyx is recovered faster on elliptical cells than on circular cells at the early stage of recovery (2h). The recovery of the glycocalyx on both cells is approximated at 24h. Nevertheless, the observation of the glycocalyx recovery

ends at 24h. This is because micropatterned cells undergo division following 24h culture. Majority of the micropatterns are instead covered with two or more cells, which in turn compromises the effects of cell shape on the recovery of the glycocalyx. It is unclear whether there is further recovery of the glycocalyx over 24h. To extend the observation of the glycocalyx recovery, application of cell proliferation inhibitors (e.g., mitomycin C) is necessary.

A conventional confocal microscope (Leica TCS SP2) was used for the observation of the glycocalyx in this thesis. This confocal microscope provides a lateral resolution of 139.4nm and an axial resolution of 235.8nm, and makes it possible to detect an intensive, continuous layer of the glycocalyx on the entire cell surface. However, the glycocalyx is visualized as a brush-like layer. The core protein spacing is estimated to be 20nm, while the inter-cluster spacing is 100nm. The resolution provided by the conventional confocal microscope is not sufficient to reveal the ultrastructure of the glycocalyx. A super-resolution microscope, which can give up to twice the resolution of a conventional confocal microscope, may allow us to see the arrangement of the glycocalyx. A super-resolution microscope (ZEISS ELYRA PS.1) has recently been installed in the Institute of Bioengineering, QMUL. Employing the super-resolution microscope in the observation of the glycocalyx will improve the accuracy of the measurement of glycocalyx coverage and thickness.

Contribution of the actin cytoskeleton to the stability of the glycocalyx under static and shear flow conditions.

Actin depolymerisation is quantified by measuring the number of actin filaments. Both 10min rapid depolymerisation and 24h persistent depolymerisation result in 2.5-fold decreases in the filament number. Cells are largely retracted after 10mins actin depolymerisation but the glycocalyx is still preserved on the cell surface. Contrastingly, cell morphology is maintained and the glycocalyx is well-preserved after 24h actin depolymerisation. These observations indicate that under static conditions, the stability of the glycocalyx does not rely on the actin polymerization. However, in the presence of shear stress, the glycocalyx is shed off and FAs are completely disassembled when the actin cytoskeleton is persistently depolymerised. Collectively, I propose a mooring model to illustrate that the glycocalyx in shear flow is stabilized by the anchorage of FAs to substrate via the link of F-actins.

With intact actin cytoskeleton, the glycocalyx is seen to polarize to the downstream of elongated cells following 24h, 1.5Pa shear stress stimulation. This adaptive remodelling of the glycocalyx helps to reduce the shear stress gradient exerted on the cell membrane. No study has experimentally ruled out that the redistribution of the glycocalyx may occur as a secondary response to shear stress-induced cell elongation. One possible approach to clarifying this is to employ elliptical micropattern. I have demonstrated in chapter 3 that the intensities of the glycocalyx on elongated cells and circular cells are similar at the end of 24h culture. No significant redistribution of the glycocalyx is observed, suggesting that cell elongation has no effect on the redistribution of the glycocalyx. For further research,

elliptically-micropatterned cells will be subjected to the shear flow for validating the direct role of shear stress in glycocalyx redistribution.

Shedding of the glycocalyx in this part is observed based on the labelling of FITC-WGA. This in particular refers to the shedding of glycoproteins in shear flow. Proteoglycans are other important components that anchor to the actin cytoskeleton. For example, syndecan-1 mediates mechanical transduction from HS to the actin cytoskeleton, leading to reorganization of a cell in shear flow. Even though there is recent research concerning the structural stability of proteoglycans, the results show that GAG components (HS, CS and HA) are independent of one another (Zeng et al., 2012). Further research can look into the recovery of proteoglycans and the contribution of the actin cytoskeleton to the stability of proteoglycans.

Contribution of the glycocalyx to EF-directed endothelial cell migration.

EF ranging from 100mV/mm to 500mV/mm enhances endothelial cell migration in a voltage-independent manner. EF guides endothelial cells to migrate towards the anode. An index namely directedness is used for evaluating the extent of anodal cell migration. The directedness increases as the increase of EF strength, indicating that EF-guided cell migration is voltage-dependent. However, both responses are abolished after the enzymatic removal of the glycocalyx, indicating that EF-directed endothelial cell migration requires the presence of the glycocalyx. It should be noted that this EF study is performed in the absence of shear flow. Applying shear flow not only helps to eliminate the chemotaxis induced by EF, but also reproduces a fluidic environment as in blood vessel. A few studies

have utilized flowing medium to dispel the chemical gradients occurring in applied EF. The predetermined flow rate is so low that the derived shear stress is much less than physiological shear stress (Song et al., 2007). It is unclear whether incorporation of physiological shear stress with EF can produce synergistic effect on directional endothelial cell migration. Moreover, the direction of physiological shear flow may not be in accordance with EF vector *in situ*. Which is the prioritising cue in endothelial cell migration in this instance needs to be clarified. On the other hand, even distribution of the glycocalyx is observed at the end of 5h EF stimulation, suggesting that polarization of the glycocalyx is not related to EF-guided cell migration. Further research can investigate the signal transduction of the glycocalyx in EF-directed cell migration. Answering this question will further our understanding in the function of the glycocalyx and its role in vascular regeneration.

7. Reference

ACHARYA, P. S., MAJUMDAR, S., JACOB, M., HAYDEN, J., MRASS, P., WENINGER, W., ASSOIAN, R. K. & PURE, E. 2008. Fibroblast migration is mediated by CD44-dependent TGF beta activation. *Journal of Cell Science,* 121**,** 1393-1402.

ADAMSON, R. H. & CLOUGH, G. 1992. Plasma proteins modify the endothelial cell glycocalyx of frog mesenteric microvessels. *J Physiol,* 445**,** 473-86.

ALGENSTAEDT, P., SCHAEFER, C., BIERMANN, T., HAMANN, A., SCHWARZLOH, B., GRETEN, H., RUTHER, W. & HANSEN-ALGENSTAEDT, N. 2003. Microvascular alterations in diabetic mice correlate with level of hyperglycemia. *Diabetes,* 52**,** 542-9.

AMARAL, S. L., LINDERMAN, J. R. & GREENE, A. S. 2000. Angiogenesis induced by electrical stimulation is mediated by angiotensin II and VEGF. *Faseb Journal,* 14**,** A34-A34.

ANDERSON, D. E. & HINDS, M. T. 2011. Endothelial cell micropatterning: methods, effects, and applications. *Ann Biomed Eng,* 39**,** 2329-45.

ANDRIKOPOULOS, P., FRASER, S. P., PATTERSON, L., AHMAD, Z., BURCU, H., OTTAVIANI, D., DISS, J. K., BOX, C., ECCLES, S. A. & DJAMGOZ, M. B. 2011. Angiogenic functions of voltage-gated Na+ Channels in human endothelial cells: modulation of vascular endothelial growth factor (VEGF) signaling. *J Biol Chem,* 286**,** 16846-60.

ANNECKE, T., FISCHER, J., HARTMANN, H., TSCHOEP, J., REHM, M., CONZEN, P., SOMMERHOFF, C. P. & BECKER, B. F. 2011. Shedding of the coronary endothelial glycocalyx: effects of hypoxia/reoxygenation vs ischaemia/reperfusion. *Br J Anaesth,* 107**,** 679-86.

ARISAKA, T., MITSUMATA, M., KAWASUMI, M., TOHJIMA, T., HIROSE, S. & YOSHIDA, Y. 1995. Effects of shear stress on glycosaminoglycan synthesis in vascular endothelial cells. *Ann N Y Acad Sci,* 748**,** 543-54.

BAI, H., MCCAIG, C. D., FORRESTER, J. V. & ZHAO, M. 2004. DC electric fields induce distinct preangiogenic responses in microvascular and macrovascular cells. *Arterioscler Thromb Vasc Biol,* 24**,** 1234-9.

BAI, K. & WANG, W. 2012. Spatio-temporal development of the endothelial glycocalyx layer and its mechanical property in vitro. *Journal of the Royal Society Interface,* 9**,** 2290-2298.

BAI, K. & WANG, W. 2014. Shear stress-induced redistribution of the glycocalyx on endothelial cells in vitro. *Biomech Model Mechanobiol,* 13**,** 303-11.

BARAKAT, A. I. 2008. Dragging along - The Glycocalyx and vascular endothelial cell mechanotransduction. *Circulation Research,* 102**,** 747-748.

BARKEFORS, I., AIDUN, C. K. & ULRIKA EGERTSDOTTER, E. M. 2007. Effect of fluid shear stress on endocytosis of heparan sulfate and low-density lipoproteins. *J Biomed Biotechnol,* 2007**,** 65136.

BARKER, A. L., KONOPATSKAYA, O., NEAL, C. R., MACPHERSON, J. V., WHATMORE, J. L., WINLOVE, C. P., UNWIN, P. R. & SHORE, A. C. 2004. Observation and characterisation of the glycocalyx of viable human endothelial cells using confocal laser scanning microscopy. *Physical Chemistry Chemical Physics,* 6**,** 1006-1011.

BAUMGARTNER, W., HINTERDORFER, P., NESS, W., RAAB, A., VESTWEBER, D., SCHINDLER, H. & DRENCKHAHN, D. 2000. Cadherin interaction probed by atomic force microscopy. *Proc Natl Acad Sci U S A,* 97**,** 4005-10.

BERESEWICZ, A., CZARNOWSKA, E. & MACZEWSKI, M. 1998. Ischemic preconditioning and superoxide dismutase protect against endothelial dysfunction and endothelium glycocalyx disruption in the postischemic guinea-pig hearts. *Mol Cell Biochem,* 186**,** 87-97.

BERNFIELD, M., GOTTE, M., PARK, P. W., REIZES, O., FITZGERALD, M. L., LINCECUM, J. & ZAKO, M. 1999. Functions of cell surface heparan sulfate proteoglycans. *Annu Rev Biochem,* 68**,** 729-77.

BIRKHOLZ, H., MATSCHEGEWSKI, C., NEBE, J. B. & ENGEL, K. 2010. Quantification of Actin Filament Organization by Estimating Graph Structures in Confocal Microscopic Images. *World Congress on Medical Physics and Biomedical Engineering, Vol 25, Pt 4: Image Processing, Biosignal Processing, Modelling and Simulation, Biomechanics,* 25**,** 1932-1935.

BORN, G. V. & PALINSKI, W. 1985. Unusually high concentrations of sialic acids on the surface of vascular endothelia. *Br J Exp Pathol,* 66**,** 543-9.

BOUDAOUD, A., BURIAN, A., BOROWSKA-WYKRET, D., UYTTEWAAL, M., WRZALIK, R., KWIATKOWSKA, D. & HAMANT, O. 2014. FibrilTool, an ImageJ plug-in to quantify fibrillar structures in raw microscopy images. *Nature Protocols,* 9**,** 457-463.

BRISKIN, M. J., MCEVOY, L. M. & BUTCHER, E. C. 1993. MAdCAM-1 has homology to immunoglobulin and mucin-like adhesion receptors and to IgA1. *Nature,* 363**,** 461-4.

BROWN, M. J. & LOEW, L. M. 1994. Electric Field-Directed Fibroblast Locomotion Involves Cell-Surface Molecular Reorganization and Is Calcium-Independent. *Journal of Cell Biology,* 127**,** 117-128.

CAMPBELL, E. J. & OWEN, C. A. 2007. The sulfate groups of chondroitin sulfate- and heparan sulfate-containing proteoglycans in neutrophil plasma membranes are novel binding sites for human leukocyte elastase and cathepsin G. *J Biol Chem,* 282**,** 14645-54.

CAO, L., PU, J. & ZHAO, M. 2011. GSK-3 beta is essential for physiological electric field-directed Golgi polarization and optimal electrotaxis. *Cellular and Molecular Life Sciences,* 68**,** 3081-3093.

CARNEY, S. (ed.) 1986. *Proteoglycans,* IRL: Oxford.

CHAO, P. H., ROY, R., MAUCK, R. L., LIU, W., VALHMU, W. B. & HUNG, C. T. 2000. Chondrocyte translocation response to direct current electric fields. *J Biomech Eng,* 122**,** 261-7.

CHAPPELL, D., HOFMANN-KIEFER, K., JACOB, M., REHM, M., BRIEGEL, J., WELSCH, U., CONZEN, P. & BECKER, B. F. 2009a. TNF-alpha induced shedding of the endothelial glycocalyx is prevented by hydrocortisone and antithrombin. *Basic Res Cardiol,* 104**,** 78-89.

CHAPPELL, D., JACOB, M., HOFMANN-KIEFER, K., REHM, M., WELSCH, U., CONZEN, P. & BECKER, B. F. 2009b. Antithrombin reduces shedding of the endothelial glycocalyx following ischaemia/reperfusion. *Cardiovasc Res,* 83**,** 388-96.

CHAPPELL, D., JACOB, M., PAUL, O., REHM, M., WELSCH, U., STOECKELHUBER, M., CONZEN, P. & BECKER, B. F. 2009c. The glycocalyx of the human umbilical vein endothelial cell: an impressive structure ex vivo but not in culture. *Circ Res,* 104**,** 1313-7.

CHIFFLET, S., HERNANDEZ, J. A. & GRASSO, S. 2005. A possible role for membrane depolarization in epithelial wound healing. *Am J Physiol Cell Physiol,* 288**,** C1420-30.

CHO, M. R., MARLER, J. P., THATTE, H. S. & GOLAN, D. E. 2002. Control of calcium entry in human fibroblasts by frequency-dependent electrical stimulation. *Front Biosci,* 7**,** a1-8.

CHO, M. R., THATTE, H. S., LEE, R. C. & GOLAN, D. E. 1994. Induced redistribution of cell surface receptors by alternating current electric fields. *Faseb Journal,* 8**,** 771-6.

CHO, M. R., THATTE, H. S., LEE, R. C. & GOLAN, D. E. 2000. Integrin-dependent human macrophage migration induced by oscillatory electrical stimulation. *Ann Biomed Eng,* 28**,** 234-43.

CHO, M. R., THATTE, H. S., SILVIA, M. T. & GOLAN, D. E. 1999. Transmembrane calcium influx induced by ac electric fields. *Faseb Journal,* 13**,** 677-83.

CONSTANTINESCU, A. A., VINK, H. & SPAAN, J. A. 2003. Endothelial cell glycocalyx modulates immobilization of leukocytes at the endothelial surface. *Arterioscler Thromb Vasc Biol,* 23**,** 1541-7.

COOPER, J. A. 1987. Effects of cytochalasin and phalloidin on actin. *J Cell Biol,* 105**,** 1473-8.

CURTZE, S., DEMBO, M., MIRON, M. & JONES, D. B. 2004. Dynamic changes in traction forces with DC electric field in osteoblast-like cells. *Journal of Cell Science,* 117**,** 2721-9.

DAI, G., KAAZEMPUR-MOFRAD, M. R., NATARAJAN, S., ZHANG, Y., VAUGHN, S., BLACKMAN, B. R., KAMM, R. D., GARCIA-CARDENA, G. & GIMBRONE, M. A., JR. 2004. Distinct endothelial phenotypes evoked by arterial waveforms derived from atherosclerosis-susceptible and -resistant regions of human vasculature. *Proc Natl Acad Sci U S A,* 101**,** 14871-6.

DAVIES, P. F. 1995. Flow-mediated endothelial mechanotransduction. *Physiol Rev,* 75**,** 519-60.

DEL MONACO, S. M., MARINO, G. I., ASSEF, Y. A., DAMIANO, A. E. & KOTSIAS, B. A. 2009. Cell migration in BeWo cells and the role of epithelial sodium channels. *J Membr Biol,* 232**,** 1-13.

DJAMGOZ, M. B. A., MYCIELSKA, M., MADEJA, Z., FRASER, S. P. & KOROHODA, W. 2001. Directional movement of rat prostate cancer cells in direct-current electric field: involvement of voltagegated Na+ channel activity. *Journal of Cell Science,* 114**,** 2697-705.

DU, X. L., EDELSTEIN, D., DIMMELER, S., JU, Q., SUI, C. & BROWNLEE, M. 2001. Hyperglycemia inhibits endothelial nitric oxide synthase activity by posttranslational modification at the Akt site. *J Clin Invest,* 108**,** 1341-8.

EBINA, T., HOSHI, N., KOBAYASHI, M., KAWAMURA, K., NANJO, H., SUGITA, A., SUGIYAMA, T., MASUDA, H. & XU, C. 2002. Physiological angiogenesis in electrically stimulated skeletal muscle in rabbits: characterization of capillary sprouting by ultrastructural 3-D reconstruction study. *Pathol Int,* 52**,** 702-12.

EBONG, E. E., LOPEZ-QUINTERO, S. V., RIZZO, V., SPRAY, D. C. & TARBELL, J. M. 2014. Shear-induced endothelial NOS activation and remodeling via heparan sulfate, glypican-1, and syndecan-1. *Integr Biol (Camb),* 6**,** 338-47.

EBONG, E. E., MACALUSO, F. P., SPRAY, D. C. & TARBELL, J. M. 2011. Imaging the endothelial glycocalyx in vitro by rapid freezing/freeze substitution transmission electron microscopy. *Arterioscler Thromb Vasc Biol,* 31**,** 1908-15.

FARNSWORTH, R. H., LACKMANN, M., ACHEN, M. G. & STACKER, S. A. 2014. Vascular remodeling in cancer. *Oncogene,* 33**,** 3496-505.

FINKELSTEIN, E., CHANG, W., CHAO, P. H. G., GRUBER, D., MINDEN, A., HUNG, C. T. & BULINSKI, J. C. 2004. Roles of microtubules, cell polarity and adhesion in electric-field-mediated motility of 3T3 fibroblasts. *Journal of Cell Science,* 117**,** 1533-1545.

FINKELSTEIN, E. I., CHAO, P. H., HUNG, C. T. & BULINSKI, J. C. 2007. Electric field-induced polarization of charged cell surface proteins does not determine the direction of galvanotaxis. *Cell Motil Cytoskeleton,* 64**,** 833-46.

FLORIAN, J. A., KOSKY, J. R., AINSLIE, K., PANG, Z., DULL, R. O. & TARBELL, J. M. 2003. Heparan sulfate proteoglycan is a mechanosensor on endothelial cells. *Circ Res,* 93**,** e136-42.

FRANSSON, L. A., BELTING, M., CHENG, F., JONSSON, M., MANI, K. & SANDGREN, S. 2004. Novel aspects of glypican glycobiology. *Cell Mol Life Sci,* 61**,** 1016-24.

FRIEDL, P. & ZALLEN, J. A. 2010. Dynamics of cell-cell and cell-matrix interactions in morphogenesis, regeneration and cancer. *Curr Opin Cell Biol,* 22**,** 557-9.

FUX, L., ILAN, N., SANDERSON, R. D. & VLODAVSKY, I. 2009. Heparanase: busy at the cell surface. *Trends Biochem Sci,* 34**,** 511-9.

GAO, L. & LIPOWSKY, H. H. 2010. Composition of the endothelial glycocalyx and its relation to its thickness and diffusion of small solutes. *Microvasc Res,* 80**,** 394-401.

GAUTROT, J. E., TRAPPMANN, B., OCEGUERA-YANEZ, F., CONNELLY, J., HE, X., WATT, F. M. & HUCK, W. T. 2010a. Exploiting the superior protein resistance of polymer brushes to control single cell adhesion and polarisation at the micron scale. *Biomaterials,* 31**,** 5030-41.

GAUTROT, J. E., TRAPPMANN, B., OCEGUERA-YANEZ, F., CONNELLY, J., HE, X. M., WATT, F. M. & HUCK, W. T. S. 2010b. Exploiting the superior protein resistance of polymer brushes to control single cell adhesion and polarisation at the micron scale. *Biomaterials,* 31**,** 5030-5041.

GIANTSOS-ADAMS, K. M., KOO, A. J., SONG, S., SAKAI, J., SANKARAN, J., SHIN, J. H., GARCIA-CARDENA, G. & DEWEY, C. F., JR. 2013. Heparan Sulfate Regrowth Profiles Under Laminar Shear Flow Following Enzymatic Degradation. *Cell Mol Bioeng,* 6**,** 160-174.

GOLIGORSKY, M. S., LI, H., BRODSKY, S. & CHEN, J. 2002. Relationships between caveolae and eNOS: everything in proximity and the proximity of everything. *Am J Physiol Renal Physiol,* 283**,** F1-10.

GOROG, P. & BORN, G. V. 1982. Increased uptake of circulating low-density lipoproteins and fibrinogen by arterial walls after removal of sialic acids from their endothelial surface. *Br J Exp Pathol,* 63**,** 447-51.

GOROG, P. & BORN, G. V. 1983. Uneven distribution of sialic acids on the luminal surface of aortic endothelium. *Br J Exp Pathol,* 64**,** 418-24.

GOUVERNEUR, M., BERG, B., NIEUWDORP, M., STROES, E. & VINK, H. 2006a. Vasculoprotective properties of the endothelial glycocalyx: effects of fluid shear stress. *J Intern Med,* 259**,** 393-400.

GOUVERNEUR, M., SPAAN, J. A., PANNEKOEK, H., FONTIJN, R. D. & VINK, H. 2006b. Fluid shear stress stimulates incorporation of hyaluronan into endothelial cell glycocalyx. *Am J Physiol Heart Circ Physiol,* 290**,** H458-2.

HALDENBY, K. A., CHAPPELL, D. C., WINLOVE, C. P., PARKER, K. H. & FIRTH, J. A. 1994. Focal and regional variations in the composition of the glycocalyx of large vessel endothelium. *J Vasc Res,* 31**,** 2-9.

HAMAI, A., HASHIMOTO, N., MOCHIZUKI, H., KATO, F., MAKIGUCHI, Y., HORIE, K. & SUZUKI, S. 1997. Two distinct chondroitin sulfate ABC lyases. An endoeliminase yielding tetrasaccharides and an exoeliminase preferentially acting on oligosaccharides. *J Biol Chem,* 272**,** 9123-30.

HANDEL, T. M., JOHNSON, Z., CROWN, S. E., LAU, E. K. & PROUDFOOT, A. E. 2005. Regulation of protein function by glycosaminoglycans--as exemplified by chemokines. *Annu Rev Biochem,* 74**,** 385-410.

HART, F. X. 2008. The mechanical transduction of physiological strength electric fields. *Bioelectromagnetics,* 29**,** 447-55.

HART, F. X. 2010. Cytoskeletal forces produced by extremely low-frequency electric fields acting on extracellular glycoproteins. *Bioelectromagnetics,* 31**,** 77-84.

HART, F. X., LAIRD, M., RIDING, A. & PULLAR, C. E. 2013. Keratinocyte galvanotaxis in combined DC and AC electric fields supports an electromechanical transduction sensing mechanism. *Bioelectromagnetics,* 34**,** 85-94.

HAYASHIDA, K., PARKS, W. C. & PARK, P. W. 2009. Syndecan-1 shedding facilitates the resolution of neutrophilic inflammation by removing sequestered CXC chemokines. *Blood,* 114**,** 3033-43.

HECKER, M., MULSCH, A., BASSENGE, E. & BUSSE, R. 1993. Vasoconstriction and increased flow: two principal mechanisms of shear stress-dependent endothelial autacoid release. *Am J Physiol,* 265**,** H828-33.

HENDERSON-TOTH, C. E., JAHNSEN, E. D., JAMARANI, R., AL-ROUBAIE, S. & JONES, E. A. V. 2012. The glycocalyx is present as soon as blood flow is initiated and is required for normal vascular development. *Developmental Biology,* 369**,** 330-339.

HENRY, C. B. & DULING, B. R. 1999. Permeation of the luminal capillary glycocalyx is determined by hyaluronan. *Am J Physiol,* 277**,** H508-14.

HENRY, C. B. & DULING, B. R. 2000. TNF-alpha increases entry of macromolecules into luminal endothelial cell glycocalyx. *Am J Physiol Heart Circ Physiol,* 279**,** H2815-23.

HERWIG, M. C., MULLER, K. M. & MULLER, A. M. 2008. Endothelial VE-cadherin expression in human lungs. *Pathol Res Pract,* 204**,** 725-30.

HU, X. & WEINBAUM, S. 1999. A new view of Starling's hypothesis at the microstructural level. *Microvasc Res,* 58**,** 281-304.

HUDLICKA, O., MILKIEWICZ, M., COTTER, M. A. & BROWN, M. D. 2002. Hypoxia and expression of VEGF-A protein in relation to capillary growth in electrically stimulated rat and rabbit skeletal muscles. *Experimental Physiology,* 87**,** 373-381.

IHRCKE, N. S., WRENSHALL, L. E., LINDMAN, B. J. & PLATT, J. L. 1993. Role of heparan sulfate in immune system-blood vessel interactions. *Immunol Today,* 14**,** 500-5.

IOZZO, R. V. 1994. Perlecan: a gem of a proteoglycan. *Matrix Biol,* 14**,** 203-8.

JOHNSON, D., MONTPETIT, M. L., STOCKER, P. J. & BENNETT, E. S. 2004. The sialic acid component of the beta1 subunit modulates voltage-gated sodium channel function. *J Biol Chem,* 279**,** 44303-10.

KANDERE-GRZYBOWSKA, K., SOH, S., MAHMUD, G., KOMAROVA, Y., PILANS, D. & GRZYBOWSKI, B. A. 2010. Short-term molecular polarization of cells on symmetric and asymmetric micropatterns. *Soft Matter,* 6**,** 3257-3268.

KANNO, S., ODA, N., ABE, M., SAITO, S., HORI, K., HANDA, Y., TABAYASHI, K. & SATO, Y. 1999. Establishment of a simple and practical procedure applicable to therapeutic angiogenesis. *Circulation,* 99**,** 2682-7.

KANTAK, S. S., DIGLIO, C. A. & ONODA, J. M. 1993. Low dose radiation-induced endothelial cell retraction. *Int J Radiat Biol,* 64**,** 319-28.

KATO, S., ANDO, J. & MATSUDA, T. 2001. MRNA expression on shape-engineered endothelial cells: adhesion molecules ICAM-1 and VCAM-1. *J Biomed Mater Res,* 54**,** 366-72.

KELLY, R., RUANE-O'HORA, T., NOBLE, M. I., DRAKE-HOLLAND, A. J. & SNOW, H. M. 2006. Differential inhibition by hyperglycaemia of shear stress- but not acetylcholine-mediated dilatation in the iliac artery of the anaesthetized pig. *J Physiol,* 573**,** 133-45.

KENNETT, E. C. & DAVIES, M. J. 2007. Degradation of matrix glycosaminoglycans by peroxynitrite/peroxynitrous acid: evidence for a hydroxyl-radical-like mechanism. *Free Radic Biol Med,* 42**,** 1278-89.

KENNETT, E. C. & DAVIES, M. J. 2009. Glycosaminoglycans are fragmented by hydroxyl, carbonate, and nitrogen dioxide radicals in a site-selective manner: implications for peroxynitrite-mediated damage at sites of inflammation. *Free Radic Biol Med,* 47**,** 389-400.

KENNETT, E. C., REES, M. D., MALLE, E., HAMMER, A., WHITELOCK, J. M. & DAVIES, M. J. 2010. Peroxynitrite modifies the structure and function of the extracellular matrix proteoglycan perlecan by reaction with both the protein core and the heparan sulfate chains. *Free Radic Biol Med,* 49**,** 282-93.

KEY, N. S., PLATT, J. L. & VERCELLOTTI, G. M. 1992. Vascular endothelial cell proteoglycans are susceptible to cleavage by neutrophils. *Arterioscler Thromb,* 12**,** 836-42.

KHATIB, L., GOLAN, D. E. & CHO, M. 2004. Physiologic electrical stimulation provokes intracellular calcium increase mediated by phospholipase C activation in human osteoblasts. *Faseb Journal,* 18**,** 1903-5.

KLEPEIS, V. E., CORNELL-BELL, A. & TRINKAUS-RANDALL, V. 2001. Growth factors but not gap junctions play a role in injury-induced Ca2+ waves in epithelial cells. *Journal of Cell Science,* 114**,** 4185-95.

KLIMENT, C. R., ENGLERT, J. M., GOCHUICO, B. R., YU, G., KAMINSKI, N., ROSAS, I. & OURY, T. D. 2009. Oxidative stress alters syndecan-1 distribution in lungs with pulmonary fibrosis. *J Biol Chem,* 284**,** 3537-45.

KLIMENT, C. R. & OURY, T. D. 2011. Extracellular superoxide dismutase protects cardiovascular syndecan-1 from oxidative shedding. *Free Radic Biol Med,* 50**,** 1075-80.

KOLAROVA, H., AMBRUZOVA, B., SVIHALKOVA SINDLEROVA, L., KLINKE, A. & KUBALA, L. 2014. Modulation of endothelial glycocalyx structure under inflammatory conditions. *Mediators Inflamm,* 2014**,** 694312.

KOO, A., DEWEY, C. F., JR. & GARCIA-CARDENA, G. 2013. Hemodynamic shear stress characteristic of atherosclerosis-resistant regions promotes glycocalyx formation in cultured endothelial cells. *Am J Physiol Cell Physiol,* 304**,** C137-46.

KUME, T. 2010. Specification of arterial, venous, and lymphatic endothelial cells during embryonic development. *Histol Histopathol,* 25**,** 637-46.

LAMALICE, L., LE BOEUF, F. & HUOT, J. 2007. Endothelial cell migration during angiogenesis. *Circ Res,* 100**,** 782-94.

LEVICK, J. R. 1991. Capillary filtration-absorption balance reconsidered in light of dynamic extravascular factors. *Exp Physiol,* 76**,** 825-57.

LI, S., HUANG, N. F. & HSU, S. 2005. Mechanotransduction in endothelial cell migration. *J Cell Biochem,* 96**,** 1110-26.

LI, X. & KOLEGA, J. 2002. Effects of direct current electric fields on cell migration and actin filament distribution in bovine vascular endothelial cells. *J Vasc Res,* 39**,** 391-404.

LIPOWSKY, H. H. 2012. The endothelial glycocalyx as a barrier to leukocyte adhesion and its mediation by extracellular proteases. *Ann Biomed Eng,* 40**,** 840-8.

LIPOWSKY, H. H., GAO, L. & LESCANIC, A. 2011. Shedding of the endothelial glycocalyx in arterioles, capillaries, and venules and its effect on capillary hemodynamics during inflammation. *Am J Physiol Heart Circ Physiol,* 301**,** H2235-45.

LODISH., H., BERK., A., ZIPURSKY., S. L., MATSUDAIRA., P., BALTIMORE., D. & DARNELL., J. (eds.) 2000. *Molecular Cell Biology. 4th edition. Section 18.1, The Actin Cytoskeleton,* New York: W. H. Freeman.

LOPES, C. C., DIETRICH, C. P. & NADER, H. B. 2006. Specific structural features of syndecans and heparan sulfate chains are needed for cell signaling. *Braz J Med Biol Res,* 39**,** 157-67.

LOPEZ-QUINTERO, S. V., CANCEL, L. M., PIERIDES, A., ANTONETTI, D., SPRAY, D. C. & TARBELL, J. M. 2013. High glucose attenuates shear-induced changes in endothelial hydraulic conductivity by degrading the glycocalyx. *PLoS One,* 8**,** e78954.

LORTAT-JACOB, H., GROSDIDIER, A. & IMBERTY, A. 2002. Structural diversity of heparan sulfate binding domains in chemokines. *Proc Natl Acad Sci U S A,* 99**,** 1229-34.

LUFT, J. H. 1966. Fine structures of capillary and endocapillary layer as revealed by ruthenium red. *Fed Proc,* 25**,** 1773-83.

MANDAL, C. 1990. Sialic acid binding lectins. *Experientia,* 46**,** 433-41.

MAROSKI, J., VORDERWULBECKE, B. J., FIEDOROWICZ, K., DA SILVA-AZEVEDO, L., SIEGEL, G., MARKI, A., PRIES, A. R. & ZAKRZEWICZ, A. 2011. Shear stress increases endothelial hyaluronan synthase 2 and hyaluronan synthesis especially in regard to an atheroprotective flow profile. *Exp Physiol,* 96**,** 977-86.

MATSCHEGEWSKI, C., STAEHLKE, S., BIRKHOLZ, H., LANGE, R., BECK, U., ENGEL, K. & NEBE, J. B. 2012. Automatic Actin Filament Quantification of Osteoblasts and Their Morphometric Analysis on Microtextured Silicon-Titanium Arrays. *Materials,* 5**,** 1176-1195.

MCCAIG, C. D., RAJNICEK, A. M., SONG, B. & ZHAO, M. 2005. Controlling cell behavior electrically: current views and future potential. *Physiol Rev,* 85**,** 943-78.

MCGRATH, J. L., OSBORN, E. A., TARDY, Y. S., DEWEY, C. F., JR. & HARTWIG, J. H. 2000. Regulation of the actin cycle in vivo by actin filament severing. *Proc Natl Acad Sci U S A,* 97**,** 6532-7.

MCLAUGHLIN, S. & POO, M. M. 1981. The role of electro-osmosis in the electric-field-induced movement of charged macromolecules on the surfaces of cells. *Biophys J,* 34**,** 85-93.

MEGENS, R. T., REITSMA, S., SCHIFFERS, P. H., HILGERS, R. H., DE MEY, J. G., SLAAF, D. W., OUDE EGBRINK, M. G. & VAN ZANDVOORT, M. A. 2007. Two-photon microscopy of vital murine elastic and muscular arteries. Combined structural and functional imaging with subcellular resolution. *J Vasc Res,* 44**,** 87-98.

MEIJERING, E., DZYUBACHYK, O. & SMAL, I. 2012. Methods for Cell and Particle Tracking. *Imaging and Spectroscopic Analysis of Living Cells: Optical and Spectroscopic Techniques,* 504**,** 183-200.

MESTEL, A. J., MOKADY, A. J., PARKER, K. H. & WINLOVE, C. P. 1998. Effects of the glycocalyx on the electrophoretic mobility of red cells and on streaming potentials in blood vessels: predictions of a structurally-based model. *Biorheology,* 35**,** 365-81.

MEYER, K., HOBBY, G. L., CHAFFEE, E. & DAWSON, M. H. 1940. The Hydrolysis of Hyaluronic Acid by Bacterial Enzymes. *J Exp Med,* 71**,** 137-46.

MICHEL, C. C. 1997. Starling: the formulation of his hypothesis of microvascular fluid exchange and its significance after 100 years. *Exp Physiol,* 82**,** 1-30.

MILKIEWICZ, M., HUDLICKA, O., BROWN, M. D. & SILGRAM, H. 2005. Nitric oxide, VEGF, and VEGFR-2: interactions in activity-induced angiogenesis in rat skeletal

muscle. *American Journal of Physiology-Heart and Circulatory Physiology,* 289**,** H336-H343.

MOCHIZUKI, S., VINK, H., HIRAMATSU, O., KAJITA, T., SHIGETO, F., SPAAN, J. A. & KAJIYA, F. 2003. Role of hyaluronic acid glycosaminoglycans in shear-induced endothelium-derived nitric oxide release. *Am J Physiol Heart Circ Physiol,* 285**,** H722-6.

MONTREUIL, J., BOUQUELET, S., DEBRAY, H., FOURNET, B., SPIK, G. & STRECKER, G. (eds.) 1986. *Glycoproteins,* IRL: Oxford.

MOON, J. J., MATSUMOTO, M., PATEL, S., LEE, L., GUAN, J. L. & LI, S. 2005. Role of cell surface heparan sulfate proteoglycans in endothelial cell migration and mechanotransduction. *J Cell Physiol,* 203**,** 166-76.

MORIGI, M., ANGIOLETTI, S., IMBERTI, B., DONADELLI, R., MICHELETTI, G., FIGLIUZZI, M., REMUZZI, A., ZOJA, C. & REMUZZI, G. 1998. Leukocyte-endothelial interaction is augmented by high glucose concentrations and hyperglycemia in a NF-kB-dependent fashion. *J Clin Invest,* 101**,** 1905-15.

MOSBACHER, J., LANGER, M., HORBER, J. K. & SACHS, F. 1998. Voltage-dependent membrane displacements measured by atomic force microscopy. *J Gen Physiol,* 111**,** 65-74.

MULIVOR, A. W. & LIPOWSKY, H. H. 2002. Role of glycocalyx in leukocyte-endothelial cell adhesion. *Am J Physiol Heart Circ Physiol,* 283**,** H1282-91.

MULIVOR, A. W. & LIPOWSKY, H. H. 2004. Inflammation- and ischemia-induced shedding of venular glycocalyx. *Am J Physiol Heart Circ Physiol,* 286**,** H1672-80.

MULIVOR, A. W. & LIPOWSKY, H. H. 2009. Inhibition of glycan shedding and leukocyte-endothelial adhesion in postcapillary venules by suppression of matrixmetalloprotease activity with doxycycline. *Microcirculation,* 16**,** 657-66.

MURESAN, V., IWANIJ, V., SMITH, Z. D. & JAMIESON, J. D. 1982. Purification and use of limulin: a sialic acid-specific lectin. *J Histochem Cytochem,* 30**,** 938-46.

NADER, H. B., PORCIONATTO, M. A., TERSARIOL, I. L., PINHAL, M. A., OLIVEIRA, F. W., MORAES, C. T. & DIETRICH, C. P. 1990. Purification and substrate specificity of heparitinase I and heparitinase II from Flavobacterium heparinum. Analyses of the heparin and heparan sulfate degradation products by 13C NMR spectroscopy. *J Biol Chem,* 265**,** 16807-13.

NANDI, A., ESTESS, P. & SIEGELMAN, M. H. 2000. Hyaluronan anchoring and regulation on the surface of vascular endothelial cells is mediated through the functionally active form of CD44. *J Biol Chem,* 275**,** 14939-48.

NIEUWDORP, M., MOOIJ, H. L., KROON, J., ATASEVER, B., SPAAN, J. A., INCE, C., HOLLEMAN, F., DIAMANT, M., HEINE, R. J., HOEKSTRA, J. B., KASTELEIN, J. J., STROES, E. S. & VINK, H. 2006a. Endothelial glycocalyx damage coincides with microalbuminuria in type 1 diabetes. *Diabetes,* 55**,** 1127-32.

NIEUWDORP, M., VAN HAEFTEN, T. W., GOUVERNEUR, M. C., MOOIJ, H. L., VAN LIESHOUT, M. H., LEVI, M., MEIJERS, J. C., HOLLEMAN, F., HOEKSTRA, J. B., VINK, H., KASTELEIN, J. J. & STROES, E. S. 2006b. Loss of endothelial glycocalyx during acute hyperglycemia coincides with endothelial dysfunction and coagulation activation in vivo. *Diabetes,* 55**,** 480-6.

NISHIMURA, K. Y., ISSEROFF, R. R. & NUCCITELLI, R. 1996. Human keratinocytes migrate to the negative pole in direct current electric fields comparable to those measured in mammalian wounds. *Journal of Cell Science,* 109**,** 199-207.

NORIA, S., XU, F., MCCUE, S., JONES, M., GOTLIEB, A. I. & LANGILLE, B. L. 2004. Assembly and reorientation of stress fibers drives morphological changes to endothelial cells exposed to shear stress. *Am J Pathol,* 164**,** 1211-23.

NORVELL, S. M., PONIK, S. M., BOWEN, D. K., GERARD, R. & PAVALKO, F. M. 2004. Fluid shear stress induction of COX-2 protein and prostaglandin release in cultured MC3T3-E1 osteoblasts does not require intact microfilaments or microtubules. *J Appl Physiol (1985),* 96**,** 957-66.

OGASAWARA, Y., NAMAI, T., YOSHINO, F., LEE, M. C. & ISHII, K. 2007. Sialic acid is an essential moiety of mucin as a hydroxyl radical scavenger. *FEBS Lett,* 581**,** 2473-7.

ONUMA, E. K. & HUI, S. W. 1988. Electric field-directed cell shape changes, displacement, and cytoskeletal reorganization are calcium dependent. *J Cell Biol,* 106**,** 2067-75.

OOHIRA, A., WIGHT, T. N. & BORNSTEIN, P. 1983. Sulfated proteoglycans synthesized by vascular endothelial cells in culture. *J Biol Chem,* 258**,** 2014-21.

OOKAWA, K., SATO, M. & OHSHIMA, N. 1992. Changes in the microstructure of cultured porcine aortic endothelial cells in the early stage after applying a fluid-imposed shear stress. *J Biomech,* 25**,** 1321-8.

OSBORN, E. A., RABODZEY, A., DEWEY, C. F., JR. & HARTWIG, J. H. 2006. Endothelial actin cytoskeleton remodeling during mechanostimulation with fluid shear stress. *Am J Physiol Cell Physiol,* 290**,** C444-52.

OZKUCUR, N., PERIKE, S., SHARMA, P. & FUNK, R. H. W. 2011. Persistent directional cell migration requires ion transport proteins as direction sensors and membrane potential differences in order to maintain directedness. *Bmc Cell Biology,* 12.

PAHAKIS, M. Y., KOSKY, J. R., DULL, R. O. & TARBELL, J. M. 2007. The role of endothelial glycocalyx components in mechanotransduction of fluid shear stress. *Biochem Biophys Res Commun,* 355**,** 228-33.

PARISH, C. R. 2006. The role of heparan sulphate in inflammation. *Nat Rev Immunol,* 6**,** 633-43.

PATEL, K. D., NOLLERT, M. U. & MCEVER, R. P. 1995. P-selectin must extend a sufficient length from the plasma membrane to mediate rolling of neutrophils. *J Cell Biol,* 131**,** 1893-902.

PEACOCK, J. G., MILLER, A. L., BRADLEY, W. D., RODRIGUEZ, O. C., WEBB, D. J. & KOLESKE, A. J. 2007. The abl-related gene tyrosine kinase acts through p190RhoGAP to inhibit actomyosin Contractility and regulate focal adhesion dynamics upon adhesion to fibronectin. *Molecular Biology of the Cell,* 18**,** 3860-3872.

PERRIN, R. M., HARPER, S. J. & BATES, D. O. 2007. A role for the endothelial glycocalyx in regulating microvascular permeability in diabetes mellitus. *Cell Biochem Biophys,* 49**,** 65-72.

PETERS, B. P., EBISU, S., GOLDSTEIN, I. J. & FLASHNER, M. 1979. Interaction of wheat germ agglutinin with sialic acid. *Biochemistry,* 18**,** 5505-11.

PLATTS, S. H. & DULING, B. R. 2004. Adenosine A3 receptor activation modulates the capillary endothelial glycocalyx. *Circ Res,* 94**,** 77-82.

PLATTS, S. H., LINDEN, J. & DULING, B. R. 2003. Rapid modification of the glycocalyx caused by ischemia-reperfusion is inhibited by adenosine A2A receptor activation. *Am J Physiol Heart Circ Physiol,* 284**,** H2360-7.

POHL, U., HERLAN, K., HUANG, A. & BASSENGE, E. 1991. EDRF-mediated shear-induced dilation opposes myogenic vasoconstriction in small rabbit arteries. *Am J Physiol,* 261**,** H2016-23.

PONIK, S. M. & PAVALKO, F. M. 2004. Formation of focal adhesions on fibronectin promotes fluid shear stress induction of COX-2 and PGE2 release in MC3T3-E1 osteoblasts. *J Appl Physiol (1985),* 97**,** 135-42.

POO, M. 1981. In situ electrophoresis of membrane components. *Annu Rev Biophys Bioeng,* 10**,** 245-76.

POTTER, D. R. & DAMIANO, E. R. 2008. The hydrodynamically relevant endothelial cell glycocalyx observed in vivo is absent in vitro. *Circ Res,* 102**,** 770-6.

POTTER, D. R., JIANG, J. & DAMIANO, E. R. 2009. The recovery time course of the endothelial cell glycocalyx in vivo and its implications in vitro. *Circ Res,* 104**,** 1318-25.

PU, J., MCCAIG, C. D., CAO, L., ZHAO, Z. Q., SEGALL, J. E. & ZHAO, M. 2007. EGF receptor signalling is essential for electric-field-directed migration of breast cancer cells. *Journal of Cell Science,* 120**,** 3395-3403.

RAPRAEGER, A., JALKANEN, M., ENDO, E., KODA, J. & BERNFIELD, M. 1985. The cell surface proteoglycan from mouse mammary epithelial cells bears chondroitin sulfate and heparan sulfate glycosaminoglycans. *J Biol Chem,* 260**,** 11046-52.

REES, M. D., WHITELOCK, J. M., MALLE, E., CHUANG, C. Y., IOZZO, R. V., NILASAROYA, A. & DAVIES, M. J. 2010. Myeloperoxidase-derived oxidants

selectively disrupt the protein core of the heparan sulfate proteoglycan perlecan. *Matrix Biol,* 29**,** 63-73.

REHM, M., BRUEGGER, D., CHRIST, F., CONZEN, P., THIEL, M., JACOB, M., CHAPPELL, D., STOECKELHUBER, M., WELSCH, U., REICHART, B., PETER, K. & BECKER, B. F. 2007. Shedding of the endothelial glycocalyx in patients undergoing major vascular surgery with global and regional ischemia. *Circulation,* 116**,** 1896-906.

REITSMA, S., OUDE EGBRINK, M. G., VINK, H., VAN DEN BERG, B. M., PASSOS, V. L., ENGELS, W., SLAAF, D. W. & VAN ZANDVOORT, M. A. 2011. Endothelial glycocalyx structure in the intact carotid artery: a two-photon laser scanning microscopy study. *J Vasc Res,* 48**,** 297-306.

REITSMA, S., SLAAF, D. W., VINK, H., VAN ZANDVOORT, M. A. & OUDE EGBRINK, M. G. 2007. The endothelial glycocalyx: composition, functions, and visualization. *Pflugers Arch,* 454**,** 345-59.

ROBINSON, K. R. 1985. The responses of cells to electrical fields: a review. *J Cell Biol,* 101**,** 2023-7.

ROCA-CUSACHS, P., ALCARAZ, J., SUNYER, R., SAMITIER, J., FARRE, R. & NAVAJAS, D. 2008. Micropatterning of single endothelial cell shape reveals a tight coupling between nuclear volume in G1 and proliferation. *Biophys J,* 94**,** 4984-95.

RUBIO-GAYOSSO, I., PLATTS, S. H. & DULING, B. R. 2006. Reactive oxygen species mediate modification of glycocalyx during ischemia-reperfusion injury. *Am J Physiol Heart Circ Physiol,* 290**,** H2247-56.

SAMMAK, P. J., HINMAN, L. E., TRAN, P. O., SJAASTAD, M. D. & MACHEN, T. E. 1997. How do injured cells communicate with the surviving cell monolayer? *Journal of Cell Science,* 110 (Pt 4)**,** 465-75.

SASAKI, K., OKOUCHI, Y., ROTHKOTTER, H. J. & PABST, R. 1998. Three-dimensional distribution of intercellular adhesion molecule-1 on lymphocytes in the high endothelial venule analyzed by backscatter electron imaging. *Acta Anat (Basel),* 162**,** 33-9.

SATCHER, R. L., JR., BUSSOLARI, S. R., GIMBRONE, M. A., JR. & DEWEY, C. F., JR. 1992. The distribution of fluid forces on model arterial endothelium using computational fluid dynamics. *J Biomech Eng,* 114**,** 309-16.

SATO, M. J., KUWAYAMA, H., VAN EGMOND, W. N., TAKAYAMA, A. L., TAKAGI, H., VAN HAASTERT, P. J., YANAGIDA, T. & UEDA, M. 2009. Switching direction in electric-signal-induced cell migration by cyclic guanosine monophosphate and phosphatidylinositol signaling. *Proc Natl Acad Sci U S A,* 106**,** 6667-72.

SAVERY, M. D. & DAMIANO, E. R. 2008. The endothelial glycocalyx is hydrodynamically relevant in arterioles throughout the cardiac cycle. *Biophys J,* 95**,** 1439-47.

SAWYER, P. N., HIMMELFARB, E., LUSTRIN, I. & ZISKIND, H. 1966. Measurement of streaming potentials of mammalian blood vessels, aorta and vena cava, in vivo. *Biophys J,* 6**,** 641-51.

SCHAUER, R. 2000. Achievements and challenges of sialic acid research. *Glycoconj J,* 17**,** 485-99.

SCHLIWA, M. 1982. Action of cytochalasin D on cytoskeletal networks. *J Cell Biol,* 92**,** 79-91.

SCHMIDT, E. P., YANG, Y., JANSSEN, W. J., GANDJEVA, A., PEREZ, M. J., BARTHEL, L., ZEMANS, R. L., BOWMAN, J. C., KOYANAGI, D. E., YUNT, Z. X., SMITH, L. P., CHENG, S. S., OVERDIER, K. H., THOMPSON, K. R., GERACI, M. W., DOUGLAS, I. S., PEARSE, D. B. & TUDER, R. M. 2012. The pulmonary endothelial glycocalyx regulates neutrophil adhesion and lung injury during experimental sepsis. *Nat Med,* 18**,** 1217-23.

SCOTT, J. E. 1989. Secondary structures in hyaluronan solutions: chemical and biological implications. *Ciba Found Symp,* 143**,** 6-15; discussion 15-20, 281-5.

SECOMB, T. W., HSU, R. & PRIES, A. R. 2001. Effect of the endothelial surface layer on transmission of fluid shear stress to endothelial cells. *Biorheology,* 38**,** 143-50.

SHAUL, P. W. 2002. Regulation of endothelial nitric oxide synthase: location, location, location. *Annu Rev Physiol,* 64**,** 749-74.

SIMIONESCU, N., SIMIONESCU, M. & PALADE, G. E. 1981. Differentiated microdomains on the luminal surface of the capillary endothelium. I. Preferential distribution of anionic sites. *J Cell Biol,* 90**,** 605-13.

SMITH, M. L., LONG, D. S., DAMIANO, E. R. & LEY, K. 2003. Near-wall micro-PIV reveals a hydrodynamically relevant endothelial surface layer in venules in vivo. *Biophys J,* 85**,** 637-45.

SONG, B., GU, Y., PU, J., REID, B., ZHAO, Z. & ZHAO, M. 2007. Application of direct current electric fields to cells and tissues in vitro and modulation of wound electric field in vivo. *Nat Protoc,* 2**,** 1479-89.

SQUIRE, J. M., CHEW, M., NNEJI, G., NEAL, C., BARRY, J. & MICHEL, C. 2001. Quasi-periodic substructure in the microvessel endothelial glycocalyx: a possible explanation for molecular filtering? *J Struct Biol,* 136**,** 239-55.

STARLING, E. H. 1896. On the Absorption of Fluids from the Connective Tissue Spaces. *J Physiol,* 19**,** 312-26.

STRAUSS, B. I., LANGILLE, B. L. & GOTLIEB, A. I. 1987. In situ localization of F-actin microfilaments in the vasculature of the porcine retina. *Exp Eye Res,* 45**,** 533-44.

STROKA, K. M. & ARANDA-ESPINOZA, H. 2011. Effects of Morphology vs. Cell-Cell Interactions on Endothelial Cell Stiffness. *Cell Mol Bioeng,* 4**,** 9-27.

SUBRAMANIAN, S. V., FITZGERALD, M. L. & BERNFIELD, M. 1997. Regulated shedding of syndecan-1 and -4 ectodomains by thrombin and growth factor receptor activation. *J Biol Chem,* 272**,** 14713-20.

SUENAGA, N., MORI, H., ITOH, Y. & SEIKI, M. 2005. CD44 binding through the hemopexin-like domain is critical for its shedding by membrane-type 1 matrix metalloproteinase. *Oncogene,* 24**,** 859-68.

SUN, S. & CHO, M. 2004. Human fibroblast migration in three-dimensional collagen gel in response to noninvasive electrical stimulus. II. Identification of electrocoupling molecular mechanisms. *Tissue Eng,* 10**,** 1558-65.

SWIFT, M. R. & WEINSTEIN, B. M. 2009. Arterial-venous specification during development. *Circ Res,* 104**,** 576-88.

TAN, K. Y., LIN, H., RAMSTEDT, M., WATT, F. M., HUCK, W. T. S. & GAUTROT, J. E. 2013. Decoupling geometrical and chemical cues directing epidermal stem cell fate on polymer brush-based cell micro-patterns. *Integrative Biology,* 5**,** 899-910.

TARBELL, J. M. & PAHAKIS, M. Y. 2006. Mechanotransduction and the glycocalyx. *J Intern Med,* 259**,** 339-50.

TEE, S. Y., FU, J., CHEN, C. S. & JANMEY, P. A. 2011. Cell shape and substrate rigidity both regulate cell stiffness. *Biophys J,* 100**,** L25-7.

THERY, M. 2010. Micropatterning as a tool to decipher cell morphogenesis and functions. *J Cell Sci,* 123**,** 4201-13.

THI, M. M., TARBELL, J. M., WEINBAUM, S. & SPRAY, D. C. 2004. The role of the glycocalyx in reorganization of the actin cytoskeleton under fluid shear stress: a "bumper-car" model. *Proc Natl Acad Sci U S A,* 101**,** 16483-8.

UEDA, A., SHIMOMURA, M., IKEDA, M., YAMAGUCHI, R. & TANISHITA, K. 2004. Effect of glycocalyx on shear-dependent albumin uptake in endothelial cells. *Am J Physiol Heart Circ Physiol,* 287**,** H2287-94.

USHIYAMA, S., LAUE, T. M., MOORE, K. L., ERICKSON, H. P. & MCEVER, R. P. 1993. Structural and functional characterization of monomeric soluble P-selectin and comparison with membrane P-selectin. *J Biol Chem,* 268**,** 15229-37.

VAN DEN BERG, B. M., SPAAN, J. A., ROLF, T. M. & VINK, H. 2006. Atherogenic region and diet diminish glycocalyx dimension and increase intima-to-media ratios at murine carotid artery bifurcation. *Am J Physiol Heart Circ Physiol,* 290**,** H915-20.

VAN DEN BERG, B. M., SPAAN, J. A. & VINK, H. 2009. Impaired glycocalyx barrier properties contribute to enhanced intimal low-density lipoprotein accumulation at the carotid artery bifurcation in mice. *Pflugers Arch,* 457**,** 1199-206.

VAN GOLEN, R. F., VAN GULIK, T. M. & HEGER, M. 2012. Mechanistic overview of reactive species-induced degradation of the endothelial glycocalyx during hepatic ischemia/reperfusion injury. *Free Radic Biol Med,* 52**,** 1382-402.

VAN HAAREN, P. M., VANBAVEL, E., VINK, H. & SPAAN, J. A. 2003. Localization of the permeability barrier to solutes in isolated arteries by confocal microscopy. *Am J Physiol Heart Circ Physiol,* 285**,** H2848-56.

VAN HAAREN, P. M., VANBAVEL, E., VINK, H. & SPAAN, J. A. 2005. Charge modification of the endothelial surface layer modulates the permeability barrier of isolated rat mesenteric small arteries. *Am J Physiol Heart Circ Physiol,* 289**,** H2503-7.

VAN PETEGEM, F. & MINOR, D. L., JR. 2006. The structural biology of voltage-gated calcium channel function and regulation. *Biochem Soc Trans,* 34**,** 887-93.

VARKI, A., CUMMINGS, R. & ESKO, J. (eds.) 2009. *Sialic Acids*: Cold Spring Harbor Laboratories Press.

VARKI, N. M. & VARKI, A. 2007. Diversity in cell surface sialic acid presentations: implications for biology and disease. *Lab Invest,* 87**,** 851-7.

VARTANIAN, K. B., BERNY, M. A., MCCARTY, O. J., HANSON, S. R. & HINDS, M. T. 2010. Cytoskeletal structure regulates endothelial cell immunogenicity independent of fluid shear stress. *Am J Physiol Cell Physiol,* 298**,** C333-41.

VERKHOVSKY, A. B., SVITKINA, T. M. & BORISY, G. G. 1997. Polarity sorting of actin filaments in cytochalasin-treated fibroblasts. *J Cell Sci,* 110 (Pt 15)**,** 1693-704.

VICENTE-MANZANARES, M., WEBB, D. J. & HORWITZ, A. R. 2005. Cell migration at a glance. *Journal of Cell Science,* 118.

VINK, H., CONSTANTINESCU, A. A. & SPAAN, J. A. 2000. Oxidized lipoproteins degrade the endothelial surface layer : implications for platelet-endothelial cell adhesion. *Circulation,* 101**,** 1500-2.

VINK, H. & DULING, B. R. 2000. Capillary endothelial surface layer selectively reduces plasma solute distribution volume. *Am J Physiol Heart Circ Physiol,* 278**,** H285-9.

VOGL-WILLIS, C. A. & EDWARDS, I. J. 2004. High-glucose-induced structural changes in the heparan sulfate proteoglycan, perlecan, of cultured human aortic endothelial cells. *Biochim Biophys Acta,* 1672**,** 36-45.

VOYVODIC, P. L., MIN, D., LIU, R., WILLIAMS, E., CHITALIA, V., DUNN, A. K. & BAKER, A. B. 2014. Loss of syndecan-1 induces a pro-inflammatory phenotype in endothelial cells with a dysregulated response to atheroprotective flow. *J Biol Chem,* 289**,** 9547-59.

WALSH, C. T. (ed.) 2006. *Posttranslational Modification of Proteins: Expanding Nature's Inventory*: Roberts and Company Publishers.

WANG, E., ZHAO, M., FORRESTER, J. V. & CD, M. C. 2000. Re-orientation and faster, directed migration of lens epithelial cells in a physiological electric field. *Exp Eye Res,* 71**,** 91-8.

WANG, F., WANG, Y., KIM, M. S., PUTHANVEETIL, P., GHOSH, S., LUCIANI, D. S., JOHNSON, J. D., ABRAHANI, A. & RODRIGUES, B. 2010. Glucose-induced endothelial heparanase secretion requires cortical and stress actin reorganization. *Cardiovasc Res,* 87**,** 127-36.

WANG, L., FUSTER, M., SRIRAMARAO, P. & ESKO, J. D. 2005. Endothelial heparan sulfate deficiency impairs L-selectin- and chemokine-mediated neutrophil trafficking during inflammatory responses. *Nat Immunol,* 6**,** 902-10.

WARNOCK, D. G., KUSCHE-VIHROG, K., TARJUS, A., SHENG, S., OBERLEITHNER, H., KLEYMAN, T. R. & JAISSER, F. 2014. Blood pressure and amiloride-sensitive sodium channels in vascular and renal cells. *Nat Rev Nephrol,* 10**,** 146-57.

WEIGEL, P. H., HASCALL, V. C. & TAMMI, M. 1997. Hyaluronan synthases. *J Biol Chem,* 272**,** 13997-4000.

WEINBAUM, S. 1998. 1997 Whitaker Distinguished Lecture: Models to solve mysteries in biomechanics at the cellular level; a new view of fiber matrix layers. *Ann Biomed Eng,* 26**,** 627-43.

WEINBAUM, S., TARBELL, J. M. & DAMIANO, E. R. 2007. The structure and function of the endothelial glycocalyx layer. *Annu Rev Biomed Eng,* 9**,** 121-67.

WEINBAUM, S., ZHANG, X., HAN, Y., VINK, H. & COWIN, S. C. 2003. Mechanotransduction and flow across the endothelial glycocalyx. *Proc Natl Acad Sci U S A,* 100**,** 7988-95.

WEKSBERG, R., SQUIRE, J. A. & TEMPLETON, D. M. 1996. Glypicans: a growing trend. *Nat Genet,* 12**,** 225-7.

WIEDEMAN, M. P. 1963. Dimensions of blood vessels from distributing artery to collecting vein. *Circ Res,* 12**,** 375-8.

WONG, M. K. & GOTLIEB, A. I. 1986. Endothelial cell monolayer integrity. I. Characterization of dense peripheral band of microfilaments. *Arteriosclerosis,* 6**,** 212-9.

WONG, M. K. & GOTLIEB, A. I. 1990. Endothelial monolayer integrity. Perturbation of F-actin filaments and the dense peripheral band-vinculin network. *Arteriosclerosis,* 10**,** 76-84.

YAHARA, I., HARADA, F., SEKITA, S., YOSHIHIRA, K. & NATORI, S. 1982. Correlation between Effects of 24 Different Cytochalasins on Cellular Structures and Cellular Events and Those on Actin Invitro. *Journal of Cell Biology,* 92**,** 69-78.

YAMAGATA, T., SAITO, H., HABUCHI, O. & SUZUKI, S. 1968. Purification and properties of bacterial chondroitinases and chondrosulfatases. *J Biol Chem,* 243**,** 1523-35.

YANG, H. Y., CHARLES, R. P., HUMMLER, E., BAINES, D. L. & ISSEROFF, R. R. 2013. The epithelial sodium channel mediates the directionality of galvanotaxis in human keratinocytes. *Journal of Cell Science,* 126**,** 1942-1951.

YANG, N., GEORGE, A. L., JR. & HORN, R. 1996. Molecular basis of charge movement in voltage-gated sodium channels. *Neuron,* 16**,** 113-22.

YAO, Y., RABODZEY, A. & DEWEY, C. F., JR. 2007. Glycocalyx modulates the motility and proliferative response of vascular endothelium to fluid shear stress. *Am J Physiol Heart Circ Physiol,* 293**,** H1023-30.

YEN, W. Y., CAI, B., ZENG, M., TARBELL, J. M. & FU, B. M. 2012. Quantification of the endothelial surface glycocalyx on rat and mouse blood vessels. *Microvasc Res,* 83**,** 337-46.

YONEMURA, S., ITOH, M., NAGAFUCHI, A. & TSUKITA, S. 1995. Cell-to-cell adherens junction formation and actin filament organization: similarities and differences between non-polarized fibroblasts and polarized epithelial cells. *J Cell Sci,* 108 (Pt 1)**,** 127-42.

YU, W. H. & WOESSNER, J. F., JR. 2000. Heparan sulfate proteoglycans as extracellular docking molecules for matrilysin (matrix metalloproteinase 7). *J Biol Chem,* 275**,** 4183-91.

ZENG, Y., ADAMSON, R. H., CURRY, F. R. & TARBELL, J. M. 2014. Sphingosine-1-phosphate protects endothelial glycocalyx by inhibiting syndecan-1 shedding. *Am J Physiol Heart Circ Physiol,* 306**,** H363-72.

ZENG, Y., EBONG, E. E., FU, B. M. & TARBELL, J. M. 2012. The structural stability of the endothelial glycocalyx after enzymatic removal of glycosaminoglycans. *PLoS One,* 7**,** e43168.

ZENG, Y. & TARBELL, J. M. 2014. The adaptive remodeling of endothelial glycocalyx in response to fluid shear stress. *PLoS One,* 9**,** e86249.

ZENG, Y., WATERS, M., ANDREWS, A., HONARMANDI, P., EBONG, E. E., RIZZO, V. & TARBELL, J. M. 2013. Fluid shear stress induces the clustering of heparan sulfate via mobility of glypican-1 in lipid rafts. *Am J Physiol Heart Circ Physiol,* 305**,** H811-20.

ZHANG, J., CALAFIORE, M., ZENG, Q., ZHANG, X., HUANG, Y., LI, R. A., DENG, W. & ZHAO, M. 2011. Electrically guiding migration of human induced pluripotent stem cells. *Stem Cell Rev,* 7**,** 987-96.

ZHANG, J. K., BETSON, M., ERASMUS, J., ZEIKOS, K., BAILLY, M., CRAMER, L. P. & BRAGA, V. M. M. 2005. Actin at cell-cell junctions is composed of two dynamic and functional populations. *Journal of Cell Science,* 118**,** 5549-5562.

ZHAO, M. 2009. Electrical fields in wound healing-An overriding signal that directs cell migration. *Semin Cell Dev Biol,* 20**,** 674-82.

ZHAO, M., AGIUSFERNANDEZ, A., FORRESTER, J. V. & MCCAIG, C. D. 1996. Orientation and directed migration of cultured corneal epithelial cells in small electric fields are serum dependent. *Journal of Cell Science,* 109**,** 1405-1414.

ZHAO, M., BAI, H., WANG, E., FORRESTER, J. V. & MCCAIG, C. D. 2004. Electrical stimulation directly induces pre-angiogenic responses in vascular endothelial cells by signaling through VEGF receptors. *Journal of Cell Science,* 117**,** 397-405.

ZHAO, M., DICK, A., FORRESTER, J. V. & MCCAIG, C. D. 1999. Electric field-directed cell motility involves up-regulated expression and asymmetric redistribution of the epidermal growth factor receptors and is enhanced by fibronectin and laminin. *Molecular Biology of the Cell,* 10**,** 1259-1276.

ZHAO, M., PU, J., FORRESTER, J. V. & MCCAIG, C. D. 2002. Membrane lipids, EGF receptors, and intracellular signals colocalize and are polarized in epithelial cells moving directionally in a physiological electric field. *Faseb Journal,* 16**,** 857-+.

ZHAO, M., SONG, B., PU, J., WADA, T., REID, B., TAI, G. P., WANG, F., GUO, A. H., WALCZYSKO, P., GU, Y., SASAKI, T., SUZUKI, A., FORRESTER, J. V., BOURNE, H. R., DEVREOTES, P. N., MCCAIG, C. D. & PENNINGER, J. M. 2006. Electrical signals control wound healing through phosphatidylinositol-3-OH kinase-gamma and PTEN. *Nature,* 442**,** 457-460.

ZHAO, Y., CHIEN, S. & WEINBAUM, S. 2001. Dynamic contact forces on leukocyte microvilli and their penetration of the endothelial glycocalyx. *Biophys J,* 80**,** 1124-40.

ZHAO, Z., WATT, C., KARYSTINOU, A., ROELOFS, A. J., MCCAIG, C. D., GIBSON, I. R. & DE BARI, C. 2011. Directed migration of human bone marrow mesenchymal stem cells in a physiological direct current electric field. *Eur Cell Mater,* 22**,** 344-58.

ZUURBIER, C. J., DEMIRCI, C., KOEMAN, A., VINK, H. & INCE, C. 2005. Short-term hyperglycemia increases endothelial glycocalyx permeability and acutely decreases lineal density of capillaries with flowing red blood cells. *J Appl Physiol (1985),* 99**,** 1471-6.